

Advances in Science, Technology & Innovation
IEREK Interdisciplinary Series for Sustainable Development



Santanu Banerjee · Reza Barati
Shirish Patil *Editors*

Advances in Petroleum Engineering and Petroleum Geochemistry

Proceedings of the 1st Springer Conference of the
Arabian Journal of Geosciences (CAJG-1), Tunisia 2018

Advances in Science, Technology & Innovation

IEREK Interdisciplinary Series for Sustainable Development

Editorial Board Members

Anna Laura Pisello, Department of Engineering, University of Perugia, Italy
Dean Hawkes, Cardiff University, UK
Hocine Bougdah, University for the Creative Arts, Farnham, UK
Federica Rosso, Sapienza University of Rome, Rome, Italy
Hassan Abdalla, University of East London, London, UK
Sofia-Natalia Boemi, Aristotle University of Thessaloniki, Greece
Nabil Mohareb, Beirut Arab University, Beirut, Lebanon
Saleh Mesbah Elkaffas, Arab Academy for Science, Technology, Egypt
Emmanuel Bozonnet, University of la Rochelle, La Rochelle, France
Gloria Pignatta, University of Perugia, Italy
Yasser Mahgoub, Qatar University, Qatar
Luciano De Bonis, University of Molise, Italy
Stella Kostopoulou, Regional and Tourism Development, University of Thessaloniki, Thessaloniki, Greece
Biswajeet Pradhan, Faculty of Engineering and IT, University of Technology Sydney, Sydney, Australia
Md. Abdul Mannan, Universiti Malaysia Sarawak, Malaysia
Chaham Alalouch, Sultan Qaboos University, Muscat, Oman
Iman O. Gawad, Helwan University, Egypt

Series Editor

Mourad Amer, Enrichment and Knowledge Exchange, International Experts for Research, Cairo, Egypt

Advances in Science, Technology & Innovation (ASTI) is a series of peer-reviewed books based on the best studies on emerging research that redefines existing disciplinary boundaries in science, technology and innovation (STI) in order to develop integrated concepts for sustainable development. The series is mainly based on the best research papers from various IEREK and other international conferences, and is intended to promote the creation and development of viable solutions for a sustainable future and a positive societal transformation with the help of integrated and innovative science-based approaches. Offering interdisciplinary coverage, the series presents innovative approaches and highlights how they can best support both the economic and sustainable development for the welfare of all societies. In particular, the series includes conceptual and empirical contributions from different interrelated fields of science, technology and innovation that focus on providing practical solutions to ensure food, water and energy security. It also presents new case studies offering concrete examples of how to resolve sustainable urbanization and environmental issues. The series is addressed to professionals in research and teaching, consultancies and industry, and government and international organizations. Published in collaboration with IEREK, the ASTI series will acquaint readers with essential new studies in STI for sustainable development.

More information about this series at <http://www.springer.com/series/15883>

Santanu Banerjee • Reza Barati
Shirish Patil
Editors

Advances in Petroleum Engineering and Petroleum Geochemistry

Proceedings of the 1st Springer Conference
of the Arabian Journal of Geosciences
(CAJG-1), Tunisia 2018



Editors

Santanu Banerjee
Department of Earth Sciences
Indian Institute of Technology Bombay
Mumbai, India

Shirish Patil
King Fahd University of Petroleum &
Minerals
Dhahran, Saudi Arabia

Reza Barati
The University of Kansas
Lawrence, KS, USA

ISSN 2522-8714 ISSN 2522-8722 (electronic)
Advances in Science, Technology & Innovation
IEREK Interdisciplinary Series for Sustainable Development
ISBN 978-3-030-01577-0 ISBN 978-3-030-01578-7 (eBook)
<https://doi.org/10.1007/978-3-030-01578-7>

Library of Congress Control Number: 2018959252

© Springer Nature Switzerland AG 2019

This work is subject to copyright. All rights are reserved by the Publisher, whether the whole or part of the material is concerned, specifically the rights of translation, reprinting, reuse of illustrations, recitation, broadcasting, reproduction on microfilms or in any other physical way, and transmission or information storage and retrieval, electronic adaptation, computer software, or by similar or dissimilar methodology now known or hereafter developed.

The use of general descriptive names, registered names, trademarks, service marks, etc. in this publication does not imply, even in the absence of a specific statement, that such names are exempt from the relevant protective laws and regulations and therefore free for general use.

The publisher, the authors and the editors are safe to assume that the advice and information in this book are believed to be true and accurate at the date of publication. Neither the publisher nor the authors or the editors give a warranty, express or implied, with respect to the material contained herein or for any errors or omissions that may have been made. The publisher remains neutral with regard to jurisdictional claims in published maps and institutional affiliations.

This Springer imprint is published by the registered company Springer Nature Switzerland AG
The registered company address is: Gewerbestrasse 11, 6330 Cham, Switzerland

Preface

In recent years, the oil and gas industry has been facing major challenges related to highly volatile prices, global demand, and environmental issues. The industry is forced to adopt strategies to optimize the performance of reservoirs, reducing the production and development costs for sustainable operations and environmental monitoring. Petroleum engineering has undergone a major technological revolution with the adoption of advanced computational facilities at every stage of the exploration and development processes. Growing energy demand and stringent environmental monitoring pose major challenges to the E & P industry for enhancing recovery from old fields and monitoring produced water. Although conventional fossil fuel remains the main source of energy, more and more funds are being allocated to explore nonconventional hydrocarbon sources and green energy. A right mix of conventional and unconventional hydrocarbons should meet the global demand of hydrocarbon for the next several decades. The petroleum industry remains the backbone of the Middle East's economic development. The Middle East and North Africa (MENA) region accounts for more than 50% of the world's hydrocarbon reserves. Despite being the largest oil and gas producer of the world, the MENA countries face routine problems regarding petroleum engineering, reservoir modeling, and production optimization.

This volume of Proceedings includes selected papers accepted for presentations during the 1st Springer Conference of the Arabian Journal of Geosciences (CAJG-1), Tunisia 2018. This book presents a collection of papers on new methods in petroleum engineering, petrophysics, petroleum geochemistry, and petroleum system modeling by researchers primarily from the MENA region. This volume contains topics related mainly to formation evaluation, enhanced oil recovery, petroleum system modeling, source rock analysis, hydrocarbon exploration, and nonconventional energy resources. A few papers discuss the environmental impact of hydrocarbon production and management of hydrocarbon development and production business. Data and discussions presented in this volume highlight major issues in petroleum industries concerning the improvement of hydrocarbon recovery and reservoir engineering pertaining to the development of old fields and petroleum system modeling and exploration methods for finding new fields. Various case studies of this book provide the latest methods in petroleum exploration and production business.

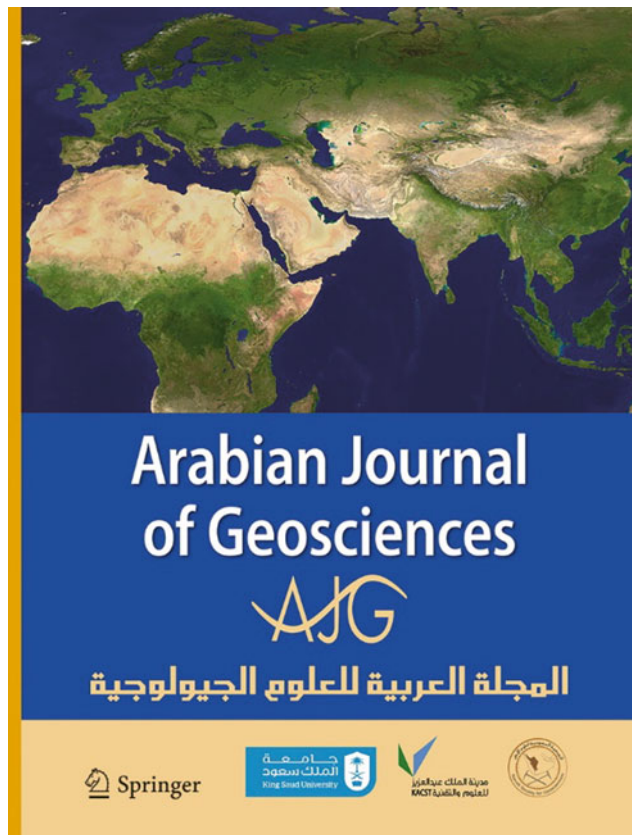
Mumbai, India
Lawrence, USA
Dhahran, Saudi Arabia
July 2018

Santanu Banerjee
Reza Barati
Shirish Patil

Acknowledgements

Our appreciation is extended to the authors of the papers for their hard and diligent work in producing high-quality contributions. We would like to thank the reviewers of the papers for their in-depth reviews and great efforts in improving the quality of the papers. Also, thanks are extended to Amjad Kallel who supervised and handled the evaluation process, to Sahbi Moalla who handled the submission and evaluation system for the ten conference proceedings volumes, and to the publishing staff of Springer headed by Nabil Khélifi, Senior Editor for their efforts and contributions in completing this conference proceedings volume. All the above-mentioned efforts were very important in making this book a success.

About the 1st Springer Conference of the Arabian Journal of Geosciences (CAJG-1), Tunisia 2018



The *Arabian Journal of Geosciences* (AJG) is a Springer journal publishing original articles on the entire range of Earth sciences in partnership with the Saudi Society for Geosciences. The journal focuses on, but not limited to, research themes which have regional significance to the Middle East, the Euro-Mediterranean, Africa, and Asia. The journal receives on average 2000 submissions a year and accepts around 500 papers for publication in its 24 annual issues (acceptance rate 25%). It enjoys the participation of an editorial team of 100 international associate editors who generously help in evaluating and selecting the best papers.

In 2008, Prof. Abdullah Al-Amri, in close partnership with Springer, founded the Arabian Journal of Geosciences (AJGS). In this year, the journal celebrates its tenth anniversary. On this occasion and to mark this event, the Founder and Editor-in-Chief of the AJGS Prof. Al-Amri organized in close collaboration with Springer the 1st Conference of the Arabian Journal of Geosciences (1st CAJG) in Hammamet, Tunisia, from November 12 to 15, 2018 (www.cajg.org).

The conference was an occasion to endorse the journal's long-held reputation for bringing together leading authors from the Middle East, the Euro-Mediterranean, Africa, and Asia who work at the wide-ranging fields of Earth sciences. The conference covered all cross-cutting themes of Geosciences and focused principally on the following ten tracks:

- Track 1. Climate, paleoclimate and paleoenvironmental changes
- Track 2. Geoinformatics, remote sensing, geodesy
- Track 3. Geoenvironmental engineering, geomechanics and geotechnics, geohazards
- Track 4. Geography, geoecology, geoarcheology, geotourism
- Track 5. Geophysics, seismology
- Track 6. Hydrology, hydrogeology, hydrochemistry
- Track 7. Mineralogy, geochemistry, petrology and volcanology
- Track 8. Petroleum engineering and petroleum geochemistry
- Track 9. Sedimentology, stratigraphy, palaeontology, geomorphology, pedology
- Track 10. Structural/petroleum/mining geology, geodynamics, marine geology

The dynamic four-day conference provided more than 450 attendees with opportunities to share their latest unpublished findings and learn the newest geoscience studies. The event also allowed attendees to meet and discuss with the journal's editors and reviewers.

More than 950 short contributing papers to the conference were submitted by authors from more than 70 countries. After a pre-conference peer review process by more than 500 reviewers, 700 papers were accepted. These papers were published as chapters in the conference proceedings by Springer.

The conference proceedings consist of ten edited volumes, each edited by the following group of *Arabian Journal of Geosciences* (AJGS) editors and other guest editors:

Volume 1. Patterns and Mechanisms of Climate, Paleoclimate, and Paleoenvironmental Changes from Low-Latitude Regions

Zhihua Zhang (AJGS Editor): Beijing Normal University, Beijing, China

Nabil Khélifi (AJGS Editor): Earth Sciences Editorial Department, Springer, Heidelberg, Germany

Abdelkader Mezghani (Guest Editor): Norwegian Meteorological Institute, Norway

Essam Heggy (Guest Editor): University of Southern California and Jet Propulsion Laboratory, Caltech, USA

Volume 2. Advances in Remote Sensing and Geo Informatics Applications

Hesham M. El-Askary (Guest Editor): Schmid College of Science and Technology at Chapman University, USA

Saro Lee (AJGS Editor): Korea Institute of Geoscience and Mineral Resources, Daejeon, South Korea

Essam Heggy (Guest Editor): University of Southern California and Jet Propulsion Laboratory, Caltech, USA

Biswajeet Pradhan (AJGS Editor): University of Technology Sydney, Sydney, Australia

Volume 3. Recent Advances in Geo-Environmental Engineering, Geomechanics and Geotechnics, and Geohazards

Amjad Kallel (AJGS Editor): ENIS, University of Sfax, Tunisia

Zeynal Abiddin Erguler (AJGS Editor): Dumlupınar University, Kutahya, Turkey

Zhen-Dong Cui (AJGS Editor): China University of Mining and Technology, Xuzhou, Jiangsu, China

Ali Karrech (AJGS Editor): The University of Western Australia, Australia

Murat Karakus (AJGS Editor): University of Adelaide, Australia

Pinnaduwa Kulatilake (AJGS Editor): Department of Materials Science and Engineering, The University of Arizona, USA
Sanjay Kumar Shukla (AJGS Editor): School of Engineering, Edith Cowan University, Perth, Australia

Volume 4. Exploring the Nexus of Geoecology, Geography, Geoarcheology and Geotourism: Advances and Applications for Sustainable Development in Environmental Sciences and Agroforestry Research

Haroun Chenchouni (AJGS Editor): University of Tebessa, Algeria
Ezzoura Errami (Guest Editor): Chouaïb Doukkali University, El Jadida, Morocco
Fernando Rocha (Guest Editor): University of Aveiro, Portugal
Luisa Sabato (AJGS Editor): Università degli Studi di Bari “Aldo Moro”, Bari, Italy

Volume 5. On Significant Applications of Geophysical Methods

Narasimman Sundararajan (AJGS Editor): Sultan Qaboos University, Muscat, Oman
Mehdi Eshagh (AJGS Editor): University West, Trollhättan, Sweden
Hakim Saibi (AJGS Editor): United Arab Emirates University, Al-Ain, Abu Dhabi, UAE
Mustapha Meghraoui (AJGS Editor): Université de Strasbourg, Strasbourg, France
Mansour Al-Garni (AJGS Editor): King Abdulaziz University, Jeddah, Saudi Arabia
Bernard Giroux (AJGS Editor): Centre Eau Terre Environnement, Québec, Canada

Volume 6. Advances in Sustainable and Environmental Hydrology, Hydrogeology, Hydrochemistry and Water Resources

Helder I. Chaminé (AJGS Editor): School of Engineering (ISEP), Polytechnic of Porto, Portugal
Maurizio Barbieri (AJGS Editor): University of Rome La Sapienza, Italy
Ozgur Kisi (AJGS Editor): Ilia State University, Tbilisi, Georgia
Mingjie Chen (AJGS Editor): Sultan Qaboos University, Muscat, Oman
Broder J. Merkel (AJGS Editor): TU Bergakademie Freiberg, Freiberg, Germany

Volume 7. Petrogenesis and Exploration of the Earth’s Interior

Domenico Doronzo (AJGS Editor): Consejo Superior de Investigaciones Científicas, Spain
Emanuela Schingaro (AJGS Editor): Università degli Studi di Bari Aldo Moro–UniBa, Italy
John S. Armstrong-Altrin (AJGS Editor): The National Autonomous University of Mexico, Mexico
Basem Zoheir (Guest Editor): Benha University, Egypt and University of Kiel, Germany

Volume 8. Advances in Petroleum Engineering and Petroleum Geochemistry

Santanu Banerjee (AJGS Editor): Indian Institute of Technology Bombay, Mumbai, India
Reza Barati (AJGS Editor): The University of Kansas, Lawrence, KS, USA
Shirish Patil (Guest Editor): Saudi Aramco and King Fahd University of Petroleum and Minerals, Dhahran, Saudi Arabia

Volume 9. Paleobiodiversity and Tectono-Sedimentary Records in the Mediterranean Tethys and Related Eastern Areas

Mabrouk Boughdiri (AJGS Editor): University of Carthage, Amilcar, Tunisia
Beatriz Bádenas (AJGS Editor): University of Zaragoza, Zaragoza, Spain
Paul Selden (AJGS Editor): University of Kansas, Lawrence, KS, USA
Etienne Jaillard (Guest Editor): University of Grenoble Alpes, France
Peter Bengtson (AJGS Editor): University of Heidelberg, Heidelberg, Germany
Bruno R. C. Granier (AJGS Editor): University of Bretagne Occidentale, Brest, France

**Volume 10. The Structural Geology Contribution to the Africa-Eurasia Geology:
Basement and Reservoir Structure, Ore Mineralisation and Tectonic Modelling**

Federico Rossetti (Guest Editor): Università Roma Tre, Roma, Italy

Ana Crespo Blanc (Guest Editor): University of Granada, Spain

Federica Riguzzi (Guest Editor): National Institute of Geophysics and Volcanology, Roma, Italy

Estelle Leroux (Guest Editor): IFREMER, Unité Géosciences Marines, Plouzané, France

Kosmas Pavlopoulos (Guest Editor): Sorbonne University Abu Dhabi, Abu Dhabi, UAE

Olivier Bellier (Guest Editor): CEREGE, Aix-en-Provence, France

Vasilios Kapsimalis (Guest Editor): Institute of Oceanography, Hellenic Centre for Marine Research, Anavyssos, Greece

About the Conference Steering Committee

General Chair



Abdullah Al-Amri: Founder and Editor-in-Chief of AJGS,
King Saud University, Saudi Arabia

Conference Supervisor



Nabil Khélifi: Senior Publishing Editor, Springer Middle East
and North African Program Springer, a part of Springer Nature,
Heidelberg, Germany

Scientific Committee Chair

François Roure: Guest of Editorial Board of AJGS, IFP—
Energies Nouvelles, France



Walter D. Mooney: Guest of Editorial Board of AJGS, US
Geological Survey Western Region, USA

Local Organization Chair

Mabrouk Boughdiri: Associate Editor of AJGS, University of
Carthage, Bizerte, Tunisia

Evaluation Chair



Amjad Kallel: Assistant Editor of AJGS, ENIS, University of Sfax, Tunisia

Publication Chair



Biswajeet Pradhan: Associate Editor of AJGS, University of Technology Sydney, Sydney, Australia



Essam Heggy: Guest of Editorial Board of AJGS, University of Southern California and Jet Propulsion Laboratory, Caltech, USA

Program Chair

Hakim Saibi: Associate Editor/Assistant Editor of AJGS,
United Arab Emirates University, Al-Ain, Abu Dhabi, UAE



Domenico Doronzo: Associate Editor/Assistant Editor of
AJGS, Consejo Superior de Investigaciones Cientificas, Spain

Communication Chair

Mohamed Ksibi: Guest of Editorial Board of AJGS, ISBS,
University of Sfax, Tunisia

English Language Advisory Committee

Abdelmajid Dammak: ENIS, University of Sfax, Tunisia
Chokri Khalaf: FMS, University of Sfax, Tunisia
Dhouha Mabrouk: FLSHS, University of Sfax, Tunisia
Mohamed Elbahi: ENIS, University of Sfax, Tunisia
Sami Shami: ENIS, University of Sfax, Tunisia
Yasmine Basha: FLSHS, University of Sfax, Tunisia

Conference Manager



Mohamed Sahbi Moalla: Coordinator of AJGS, ISET,
University of Sfax, Tunisia

Contents

Part I Keynote

Use of Artificial Intelligence in Determining the Location of Infill Wells in Hydrocarbon Exploration and Production Activities	3
Turgay Ertekin and Qian Sun	

Part II Advances in Petrophysical Characterization of Reservoir Rocks

Rock Typing: Reservoir Permeability Calculation Using Discrete Rock Typing Methods (DRT): Case Study from the Algerian B-H Oil Field Reservoir	9
Houssem Eddine Belhouchet and Mohamed Elsaïd Benzagouta	
A Fast and Less Expensive Test to Determine Permeability-Related Parameters on Well's Drilled Cuttings.....	13
Marco Ludovico-Marques	

The Method of Analytic Calculation of Initial and Ultimate Pressure Gradients to Flow for Low-Permeability Reservoirs	17
Oksana Shevchenko and Vladimir Astafev	

Development of an Empirical Model for Predicting the Cation Exchange Capacity of Shaly Sandstones Using Complex Dielectric Permittivity Measurements	21
Ali A. Garrouch	

Back Propagation and Hidden Weight Optimization Algorithms Neural Network for Permeability Estimation from Well-Logs Data in Shaly Sandstone Petroleum Reservoirs: Application to Algerian Sahara.....	25
Leila Aliouane, Sid-Ali Ouafeul, and Amar Boudella	

Experimental Relationship Between Confining Pressure, Fluid Flowrates, Flow Time Period and Temperature on Effective Permeability to Water in High Porous Sandstone	29
Thomas Adebayo and Marie Lordinon	

Petrophysical Properties Modeling Using the Geostatistical Approach: Case Study of Barito Basin, Indonesia	33
Abdul Haris, Brianto Adhie Setya Wardhana, Grace Stephani Titaley, and Agus Riyanto	

Part III Enhanced Oil Recovery Methods

Considerable Influence of Reservoir Properties on the Production Flow Rate During Low Salinity Water Flooding.....	41
Afshin Davarpanah	

Experimental Investigation of Low and High Salinity Water Injection Simulation and Their Comparison with Pure Water Injection to Determine Optimum Salinity.....	45
Afshin Davarpanah	
Experimental Investigation of the Performance of Low Salinity Water Flooding at High Temperature.....	47
Hasan N. Al-Saedi and Ralph E. Flori	
Effect of Rising Reservoir Temperature on Production of High-Viscosity Oil.....	51
Vladimir Astafev, Valeria Olkhovskaya, Sergey Gubanov, Kirill Ovchinnikov, and Victor Konovalov	
Effect of CO₂-Oil Contact Time on the Swelling Factor and Viscosity of Paraffinic Oil at Reservoir Temperature	55
Muslim Abdurrahman, Asep Kurnia Permadi, Wisup Bae, Shabrina Sri Riswati, Rochvi Agus Dewantoro, Ivan Efriza, and Adi Novriansyah	
Mechanistic Simulation of Foam Injection in the Sandstone Oilfield to Optimize the Oil Recovery Enhancement.....	59
Afshin Davarpanah	
Nanoparticle-Stabilized CO₂ Foam Flooding.....	61
Feng Guo and Saman A. Aryana	
Foam Flooding in a Heterogeneous Porous Medium.....	65
Feng Guo and Saman A. Aryana	
Synergetic Effect of SLS Surfactant of Bagasse on Enhanced Oil Recovery	69
Rini Setiati, Septoratno Siregar, Taufan Marhaendrajana, and Deana Wahyuningrum	
A Microfluidic Study of Immiscible Drainage Two-Phase Flow Regimes in Porous Media	73
Feng Guo and Saman A. Aryana	
Creation of Saturation Maps from Two-Phase Flow Experiments in Microfluidic Devices	77
Yuhang Wang and Saman A. Aryana	
Nonequilibrium Effects in Immiscible Two-Phase Flow	81
Yuhang Wang and Saman A. Aryana	
Part IV Advances in Petroleum Exploration and Management	
Gravity Changes, Earthquakes and Oil Field (Italy).....	87
Valentino Straser and Mario Campion	
Significance of Microbial Anomalies in Identifying the Hydrocarbon Prospects in Parts of a Petroliferous Region [Tunisia]	91
Mohamed Seddik Mahmoud Bougi, Jawhar Gharbi, Syrine Baklouti, Mohamed Abdul Rasheed, P. L. Srinivasa Rao, Syed Zaheer Hasan, and Mohamed Ksibi	
Conductivity and Temperature Corrections in the Djelfara Basin (Tunisia): Impact of the Basin Heat Flow Reconstructions	97
Insaf Mraidi, Amina Mabrouk El Asmi, and Ahmed Skanji	
Fault-Controlled on Hydrocarbon Migration and Accumulation of Baodao Northern Slope in the Qiongdongnan Basin, South China Sea	101
Xinshun Zhang, Hongju Zheng, and Congsheng Bian	

A Visual Investigation of Different Pollutants on the Rheological Properties of Sodium/Potassium Formate Fluids.....	105
Afshin Davarpanah	
The Integration of the Two Key Levers for the Success of a Company	107
Rima Derradji and Rachida Hamzi	
Quantitative and Qualitative Characterization of Oil Field Produced Water of Upper Assam Basin (India)	113
Debasish Konwar, Subrata Borgohain Gogoi, Joyshree Barman, and Monem Kallel	
Analyses and Treatment of Oil Field Formation Water of Upper Assam Basin (India)	117
Tapan Jyoti Gogoi and Subrata Borgohain Gogoi	
Experimental Analysis and Cement Slurries Properties Evaluation Using Novel Additives	121
Masoud Rashidi, Biltayib Misbah Biltayib, and Adel Asadi	
Part V Evaluation of Hydrocarbon Source Potential and Petroleum System Modeling	
Petrographical Features of Organic Matter from Upper Jurassic Naokelekan Formation, Kurdistan-Iraq: A Study on Regional Thermal Maturity Trends	127
Rzger A. Abdula, Kamal Kolo, Victoria Raftopoulou, Polla Khanaqa, and Stavros Kalaitzidis	
Visual Kerogen Typing: A Case Study of the Northern Song Hong Basin (Vietnam).....	131
Quan Vo Thi Hai and Giao Pham Huy	
Characterization of Potential Source Rock Intervals of Late Mesozoic to Cenozoic Age in the On- and Offshore Area of Cyprus and Their Impact on Petroleum Systems in the Eastern Mediterranean Sea	135
Sebastian Grohmann, Maria Fernanda Romero-Sarmiento, Fadi Henri Nader, Francois Baudin, and Ralf Little	
Source Rocks and Hydrocarbon Accumulation Characteristics of Upper Cretaceous to Paleogene in the Northern Kaikang Trough, Muglad Basin, Sudan	139
Congsheng Bian, Youliang Feng, Jun Li, Xuexian Zhou, Yongxin Li, and Xinshun Zhang	
Ech Cheid Salt Structure and Its Influence on the Maturity of the Bahloul Fr Source Rock	143
Mohamed Malek Khenissi, Mohamed Montassar Ben Slama, Amina Mabrouk El Asmi, Anis Mohamed Belhadj, and Moncef Saidi	
Geochemical Characterization of the Permian Series and Associated Oil Indices in the Jeffara Area: Origin of Hydrocarbon and 1D Thermal Maturity Modeling.....	147
Khawla Ouerghi, Amina Mabrouk El Asmi, Anis Bel Haj Mohamed, and Moncef Saidi	
Geopetrology Evaluation of the Ordovician and Triassic Reservoirs in the Southern Part of Chotts Area (Southern Tunisia) and Maturity Modeling.....	153
Safa Kraouia, Amina Mabrouk El Asmi, Abdelhamid Ben Salem, and Moncef Saidi	

Hydrocarbon Source Rocks within the Western Flank of the South Caspian Basin (Azerbaijan): Geochemical Study and Petroleum System Modeling 157
Shalala Huseynova

Organic Source Input, Thermal Maturity and Paleodepositional Conditions of Imo Formation in the Anambra Basin, Nigeria 161
Mutiu A. Adeleye and Damilola A. Daramola

Biodegradation of Hopanes, Steranes and Tricyclic Terpanes in Heavy Oils 165
Yang Li, Xiangchun Chang, Jinliang Zhang, and Youde Xu

Detailed Hydrocarbon Analysis of Reservoir Fluids of Some Oil Fields of Upper Assam Basin (India) 169
Joyshree Barman, Subrata Borgohain Gogoi, and Debasish Konwar

Geochemical Assessment of the Telisa Shale Gas Reservoir: A Case Study from the South Sumatra Basin, Indonesia 175
Abdul Haris, Aldo Hutagalung, and Agus Riyanto

Part VI Non-Conventional Energy Resources

Utilization of Abandoned Oil and Gas Wells for Geothermal Energy Production in Pakistan 181
Asif Mehmood, Jun Yao, Dong Yan Fan, Kelvin Bongole, and Ubedullah Ansari

Determination of Deliverability Equation and IPR for Siba Gas Condensate Reservoir in (Iraq)—Case Study 185
Ghazwan Noori Saad Jreou

Stimulation-Based Recovery Enhancement Feedback of Oil-Rim Reservoirs 189
Afshin Davarpanah

Electrochemical Studies of Porphyrin and Its Metal Complexes 193
Bechki Lazhar, Kadri Mohamed, and Lanez Touhami

About the Editors



Dr. Santanu Banerjee is a Professor at the Department of Earth Sciences, Indian Institute of Technology, Bombay. He obtained his Ph.D. from Jadavpur University, Kolkata, in 1997. Santanu does research in sedimentology and petroleum geology. His research areas cover sedimentary facies and basin analysis, microbially induced sedimentary structures, sequence stratigraphy of Vindhyan and Kutch basins, recent sedimentary environments around the Gulf of Cambay for outcrop analogs of subsurface reservoirs, provenance and tectonic settings, Glauconite formation in sequence stratigraphic contexts, and Jurassic black shale in Kutch. He is the Associate Editor in Chief of the Journal of Palaeogeography. He is a member of the editorial board of the Arabian Journal of Geosciences and Journal of the Geological Society of India. He is the Vice-President of the Indian Association of Sedimentologists. He has supervised many research projects sponsored by Government agencies and oil companies.



Dr. Reza Barati is an Associate Professor of Petroleum Engineering at the University of Kansas (KU). He earned his Ph.D. in Chemical and Petroleum Engineering at KU in 2010, and worked for the Enhanced Oil Recovery Institute (EORI) in Wyoming before joining KU as a faculty member in 2012. In addition to his academic career, Barati has extensively worked on several industry and state-funded projects as a consultant. He has also worked as a visiting researcher with Schlumberger, Halliburton, and Kinder Morgan for nearly 2 years. Barati has authored or co-authored more than 40 technical papers. He has received several SPE awards including the 2012 Petroleum Engineering Junior Faculty Research Initiation Award, the 2015 SPE Faculty Innovative Teaching Award, and the 2017 SPE Reservoir Evaluation & Engineering Technical Editor Award for outstanding service. His research areas include enhanced water-flooding through modification of injection brine, CO₂ EOR-mobility control, waterless/foam fracturing, EOR for shale oil, characterization of tight oil and gas reservoirs, and improvement of hydraulic fracturing fluids and proppants.



Dr. Shirish Patil In 1987, Shirish joined the newly established Petroleum Development Laboratory at the University of Alaska Fairbanks (UAF) as a Research Associate. He was instrumental in designing the research laboratories and overseeing the graduate research. He joined the Petroleum Engineering department as a faculty member in 1991 and rose through the ranks to Full Professor in 2007. Shirish served as the Director of the Petroleum Development Laboratory from 2006 to 2016. He, then, joined the College of Petroleum Engineering and Geosciences, King Fahd University of Petroleum and Minerals, Saudi Arabia, in September 2016, as the Saudi Aramco Chair Professor of Petroleum Engineering.

Shirish has served in numerous capacities the professional Society of Petroleum Engineers (SPE), American Association of Drilling Engineers (AADE) and the Accreditation Board for Engineering and Technology (ABET). Shirish has also served as the UAF Faculty Senate President and Chair of the University of Alaska system-wide Faculty Alliance, representing all three university campuses, as well as seven rural satellite campuses. Shirish is as an Associate Editor of the Arabian Journal of Science and Engineering (AJSE) and member of the editorial board of the Journal of Petroleum and Environmental Biotechnology (JPETB) and the International Journal of Petroleum Engineering (IJPE). Currently, he is the SPE Commissioner on the Engineering Accreditation Commission (EAC) of ABET.

Part I
Keynote



Use of Artificial Intelligence in Determining the Location of Infill Wells in Hydrocarbon Exploration and Production Activities

Turgay Ertekin and Qian Sun

Abstract

Among all of the energy resources, oil is the most widely used primary energy source. Oil reservoirs need to be characterized accurately for effective field development purposes. Typically, available field data in the reservoir characterization stage may include seismic surveys, well logs, core analysis data and field production history. One of the challenges for reservoir engineers is to utilize various types of data collected in different scopes to characterize the reservoir and propose optimized development strategies. Numerical reservoir simulation is one of the most broadly implemented approaches to quantitatively evaluate a field development plan. However, establishing a decent reservoir simulation model requires rigorous conversions from the raw field data to structural maps and spatial petrophysical property distributions as input parameters. History matching needs to be carried out to tune the property distributions to match numerical model predictions to field histories. The conventional reservoir characterization and field development workflow could be time and labor intensive. This keynote lecture presents the development of artificial-neural-network based expert systems which effectively correlate seismic survey data, well log data and field production history. When compared against the conventional reservoir characterization and field development optimization protocols, the developed expert system can provide much more rapid predictions than conventional reservoir simulators.

Keywords

Artificial neural network • Infill drilling • Reservoir characterization • Sweet-spot identification • Reservoir management

1 Introduction

The bursting developments of big data and soft computing technologies introduce innovative insights into the petroleum and natural gas industry. Artificial Neural Network (ANN) methodology is considered to be a powerful data-driven approach for its fast-computational speed and strong generalization capabilities. ANN has been broadly employed as a robust alternative approach to overcome the following difficulties that are faced in high-fidelity reservoir simulation studies and other conventional reservoir engineering tools:

1. The process of converting the raw field data including seismic data, well logs, core data, laboratory fluid sample measurements to input data for high-fidelity simulation models can be laborious and time intensive and may introduce significant uncertainties (scaling-up issues).
2. Establishing a decent reservoir simulation model requires tuning of a number of parameters. For instance, a grid block sensitivity analysis needs to be conducted to eliminate the effect of grid size on the simulation results. To make a meaningful prediction, the spatial reservoir properties need to be tuned to match the history by a history-matching study (inverse simulation). Both grid sensitivity analysis and history-matching workflows may require a large number of simulation runs to be conducted, but results will still have a good degree of uncertainty.
3. As more complex physical, thermodynamical and chemical phenomena if they are understood correctly and then incorporated into the governing equations, the computational overhead of the numerical simulation rapidly rises, potentially making the simulation study prohibitively time and energy intensive.

Within the petroleum industry, research interests have considerably increased for developing ANN models to solve reservoir engineering problems, especially when the existing

T. Ertekin (✉) · Q. Sun
The Pennsylvania State University, University Park,
PA 16802, USA
e-mail: eur@psu.edu

complex relationships are vaguely understood. ANN models act as robust multi-dimensional predictors and classification tools in solving reservoir engineering problems. Training ANN models utilizes synthetic data generated from high fidelity simulation models, real data collected from field operations or laboratory data measured as part of experimental investigations. Such knowledgebase can be categorized into three critical elements that are involved in reservoir engineering studies: reservoir rock/fluid properties, engineering design parameters and nature of the field response data. A subset of data needs to be isolated from training data for a blind testing purpose. A developed ANN model needs to be validated by comparing the predictions against the actual data of the blind testing dataset. As new data become available, ANN model can be re-trained using the enriched training data to improve the generalization capability.

Training an expert ANN model is challenging because the available field data can be limited, which can make the pattern indistinct for ANN models to learn. Moreover, the scope of the problem could be large, especially when the seismic attributes and well log signatures are included as inputs or outputs. Therefore, the size of weight matrices connecting the hidden layers of the ANN model could be extremely large, which in turn increase the computational overhead of training. Therefore, a robust ANN model with optimized architecture needs to be developed.

The prediction performance of an artificial neural network model strongly depends on the network architecture. The number of hidden layers, the number of hidden neurons in each layer and the type of the transfer function applied on each hidden layer are key parameters of a typical neural network architecture. Finding the optimum neural network architecture could be challenging because of the existence of many combinations for a number of hidden neurons, number of hidden layers of each hidden layer and transfer functions. Therefore, determining the ANN architecture by manually changing these three parameters is not feasible most of the time. To address these issues, a parallel processing workflow can be employed to optimize the topology of the network models. The overall idea of the workflow will be randomly generating a large number of neural network architectures. With the help of the power of parallel processing, multiple trainings on different ANN architectures can be processed synchronously. This workflow not only tests big numbers of ANN architectures to find the optimum design, but also saves plenty of execution time decreasing the computational footprint.

ANN applications in reservoir engineering include two categories of problems: universal applications and specific reservoir applications. ANN models are developed to serve as universal surrogate models for production forecasting, well testing applications, EOR screening, etc. Training

universal ANN models utilizes synthetic data generated from high-fidelity simulation models. ANN models are trained to solve specific problems of a certain reservoir such as history matching and field development optimization. In this case, neural networks are trained using field data such as well logs, production history and seismic survey data. Under the two aforementioned categories, three classes of ANN models are developed, based on the objectives of the problems:

1. A forward-looking model utilizes reservoir properties and engineering design parameters as input to predict the production performance (response function). Forward-looking ANN models are employed as production forecasting tools.
2. An inverse history matching model utilizes production performance, such as production history (rate transient data), bottomhole pressure measurements (pressure transient data) and the corresponding project design parameters as inputs to predict the suitable reservoir rock and fluid properties. This type of ANN models are capable of solving reservoir engineering problems such as well testing applications and history matching problems.
3. An inverse engineering design model predicts the required project design parameters by knowing the reservoir characteristics and the desired production performance. The inverse engineering design ANN models are typically deployed for project optimization such as designing an enhanced oil recovery process and designing optimum well completion strategies.

2 Case Study

As a case study in this paper, a reservoir characterization example by integrating the available field data, which include seismic survey, well logs, well tests, and core data was carried out. By the help of such integration, infill well locations can be determined. Numerical reservoir simulation is broadly implemented to provide quantitative assessments of a field development plan. However, establishing a decent high-fidelity numerical model requires rigorous conversions from the raw field data to structural maps and petrophysical property distributions as its inputs. More importantly, numerical models need to be tuned iteratively to match the production history, which could be extremely time consuming. Therefore, it is attractive to explore and develop an alternative approach (expert systems) which could replace the conventional reservoir characterization and field development optimization workflow. This case study discusses an artificial-neural-network based expert system which functions as a powerful characterization and field development decision-making tool for an oil field in North America,

which utilizes seismic survey data, well log data and the field production histories. ANN technology is employed as a pattern recognition tool in an effort to comprehensively utilize the available field data and provide fast and accurate predictions for the purposes of reservoir characterization and field development strategies (infill drilling). To achieve the functionalities of the expert system, two sets of ANN tools can be developed. The first set of tools addresses the need for synthetic well logs. This tool set can generate various different types of synthetic well logs at any infill drilling location within the seismic boundaries. Moreover, synthetic logs for wells with complex architecture such as slanted wells and horizontal wells can be generated when a wellbore trajectory is specified. A second set of tools is devised to predict oil flow rates and cumulative oil production profiles at any desired location in the reservoir. ANN models developed in this work are validated by performing extensive blind tests. The testing results of the synthetic well log tool and the production performance tool show a good level of agreement with the field data. The expert systems devised in this study are capable to make fast evaluations on a field development plan or generate synthetic logs for the proposed infill drilling locations. Moreover, a forecasted productivity surface map can be generated by sweeping the entire field employing the developed expert systems. A process

streamlined as discussed here provides critical information for the decision-making processes of infill drilling location selection.

3 Summary and Concluding Remarks

In this study, it is obvious that expert systems can be effectively trained and can yield more than promising validation performances as they are able to capture the existing physical, chemical and thermo-dynamical mechanisms and processes effectively. It still needs to be highlighted that such good performances, however, do not yield full endorsements to fully replace the conventional engineering methodologies such as deterministic and stochastic models with ANN-based models. However, the integrated use of ANN-based modeling together with the conventional computational formalisms can provide a higher level of confidence to the reservoir engineer and geoscientists in making critical decisions. As the field performance data brings in the actual signatures of the specific on-going processes (physical, chemical and/or thermodynamical), the opportunity to generate higher resolution and more accurate representations and results will make this class of data analytics and its tools even further attractive in the years to come.

Part II

Advances in Petrophysical Characterization of Reservoir Rocks



Rock Typing: Reservoir Permeability Calculation Using Discrete Rock Typing Methods (DRT): Case Study from the Algerian B-H Oil Field Reservoir

Houssem Eddine Belhouchet and Mohamed Elsaïd Benzagouta

Abstract

Permeability is the ability of a saturated rock to let the fluid flow through its pores. Fluid flow circulation within the porous medium depends on the solid type and arrangement. It depends on diverse characteristics with a focus on mineralogical type and composition of the rock. Discrepancy on the petrophysical characteristics and essentially permeability and heterogeneity are associated to these listed factors. Accordingly, fluid flow is associated to solid–fluid and fluid–fluid contact by the involvement of properties such as wettability, contact angle and capillary pressure of fluid properties as well as the rock type, which together represent factors in charge, partially or totally, of the reservoir quality consideration. Thus, with the characterization of these property requirements and impact on fluid dynamics, a need of an intensive inquiry, aimed to enhance the possible physical phenomena and chemical contribution is vital. For the case study, our investigation is actually based on the determination of reservoir rock types using Discrete Rock Typing method. Application of the DRT method has been conducted towards the Ordovician in B-H Basin (Algeria). Outcomes have revealed the presence of six main reservoir rock types.

Keywords

Permeability • Reservoir • Rock typing
Pore throat • Hydraulic unite

H. E. Belhouchet (✉)

Faculty of Petroleum, University Kasdi Merbah, Ouargla, Algeria
e-mail: houssemeddine.belhouchet@gmail.com

M. E. Benzagouta

Department of Earth Sciences, University Larbi Ben Mhidi, OEB,
Algeria

1 Introduction

The reservoir rock can be composed of sandstones, limestone and dolomites. Knowledge of the physical properties of the reservoir rock and its interaction with the fluid is essential for understanding and evaluating the performance of the considered reservoir. Thus, understanding the multi-phase flows within the porous medium is very important for different elaboration and development strategies. Reservoir properties can be determined from laboratory analyses, log interpretations and seismic data, or by theoretical approaches where simulation and modelling are the leaders.

As known, the main properties characterizing the reservoir rock are; Porosity, Saturation, Permeability, Wettability, Surface and interfacial tension, Capillary pressure, and rock Compressibility—or compaction.

The reservoir petrophysical data are measured in different scales and manners. These scales and methods should be taken into consideration prior to any integration of parameters into reservoir assessment and modelling. Related to these statements, reservoir studies have become dependent on the existence of all information sources to provide a database which is as reliable as possible. Established records offer the possibility of ensuring consistent technical support in terms of reservoir characterization and field development.

For the case study, the aim is to apply the Discrete Rock typing (DRT) Method allowing classification of the reservoir rocks' porous medium, according to the Hydraulic Units (HU). On the basis of the output, the classification process, for defining Reservoir Rock Types (RRT) and to develop mathematical models for each type, concerning absolute permeability, becomes feasible.

Therefore, the presentation of various basic concepts of permeability determination can be reached. They are related to the combination of different sources of information provided to establish a reservoir model. This latter will make it possible to estimate the potential of the reservoir in question and also to establish accurate reservoir development strategy.

2 Permeability Determination

Four main processes in the reservoir engineering were followed to determine the permeability

- From corps data Analysis
- From well test interpretation
- From MDT interpretation
- From NMR interpretation.

2.1 From Corps Data Analysis

Darcy's experiment consists in measuring fluid flow and a pressure gradient which makes it possible to calculate a permeability using the following formula:

$$\frac{Q}{S} = V = \frac{k \Delta p}{\mu \Delta x}$$

This experiment was initially developed for homogeneous rocks. The permeability can be considered as a specific flow surface which closely depends on the geometry of the porous medium.

2.2 From Well Test Interpretation

A well test is essentially performed by creating a perturbation at the reservoir level and recording the pressure response at the bottom hole of the well during the time of the test. Well testing provides detailed information on reservoir characteristics reflecting static parameters such as: geometry, reservoir boundaries, permeability barriers location, drilling efficiency, and dynamic parameters such as reservoir pressure, permeability and productivity index.

The evolution pressure at the reservoir level is described by;

$$P_{wf} = P_i - \left[\frac{162.6 Q_o \mu B}{kh} \right] \left[\log \left(\frac{kt}{\bar{\phi} \mu C_t r_w^2} \right) - 3.23 + 0.87s \right]$$

After the well test interpretation, the reservoir permeability should be calculated by;

$$k(mD) = \frac{162.6 Q_o B_o \mu_o}{|m|h}$$

where m: is the slope of the curve of bottom hole pressure recorded as a function of time on semi-logarithmic plot for the transient zone.

2.3 From NMR Interpretation

The ability to estimate formation permeability is one of the earliest benefits of nuclear magnetic resonance (NMR) logging and remains the most important application. The NMR log interpretation provides a volumetric distribution of pore sizes. If it's assumed that the pores have a spherical shape, the permeability log can be calculated by the combination of pore size, pore volumes and fluid saturation.

NMR permeability is derived from empirical relationships that were developed from brine permeability measurements and NMR measurements concurrently made in the laboratory on hundreds of different core samples. The following formula is commonly used to determine the NMR permeability log:

$$K_{NMR}(mD) = C(\emptyset_{NMR})^4 (T_{2,\log})^2$$

with; K_{NMR} : NMR permeability (mD), \emptyset_{NMR} ; CMR total Porosity, $T_{2,\log}$; is the logarithmic mean of the T2 distribution (ms), and C is a constant depending upon the formulation, e.g. 4 for sandstones and 0.1 for carbonates.

2.4 From MDT Interpretation

The MDT is the tool by which we can test the formation, measure its pressure, its temperature and check its quality. It's also used for fluid bottom hole sampling.

The MDT interpretation starts by the control quality of the recorded data, which is done by controlling the corresponding mobility at the selected points (eliminating the weaker and the higher values of mobility). Then, it uses its data to determine the pressure gradient, calculate the permeability, identify the type of reservoir fluid and select the contacts.

Once mobility or hydraulic conductivity is defined, the permeability can be calculated from the following formula;

$$k(mD) = M * \mu(cP)$$

M: mobility (mD/cP), μ : Viscosity (cP).

3 Methodology

In this case study, the available core data were used to obtain mathematical correlations which presents the permeability evolution according to the porosity. Only core data and MDT data were presented. The permeability projection as a function of porosity has a low correlation coefficient, lower than 0.5 (Fig. 1a) which is reflected by the reservoir heterogeneity.

For a better understanding, it's important to explore mathematical models to illustrate the reservoir heterogeneity and to optimize the permeability calculation. Statistically, this work is based on maximizing the correlation coefficient of permeability–porosity correlation, applying the discrete rock typing (DRT). This method focused on the determination of hydraulic units. A classification process has been provided to present each reservoir rock type with its permeability model.

The workflow of this method is based on the calculation of FZI, then converting the continuous values into discrete values by the following formula:

$$DRT = Round[2 * \ln(FZI) + 10.6]$$

In the case where the permeability unit is in millidarcy (mD), Flow Zone Indicator, Rock Quality Index, and \emptyset_z are defined by:

$$FZI = \frac{RQI}{\emptyset_z}, RQI = 0.0314 \sqrt{\frac{k}{\emptyset_e}}, \emptyset_z = \frac{\emptyset_e}{1 - \emptyset_e}$$

RQI Rock quality index.

\emptyset_z Ratio between the pore volume and volume of solid.

FZI Flow zone indicator.

\emptyset_e Effective porosity
 k Permeability (mD).

4 Results

See Figs. 1 and 2, Table 1.

5 Discussion

In the case study, the exploitation of data sourced from cores and MDT tests has been used for rock typing classification. Geological and petrophysical results have been provided to determine the quality of the cores in terms of lithofacies, electrofacies, and petrofacies. The sedimentological analysis indicates the same lithofacies of all cores data consisting in sandstone. Thus, the rock classification should be applied to improve the permeability calculation. In order to reach these objectives, several processes have been proposed to select the appropriate method used for rock typing classification. Among these methods, there are; hydraulic unit, Flow zone indicator (FZI) method, Normal probability method, Winland method and DRT method.

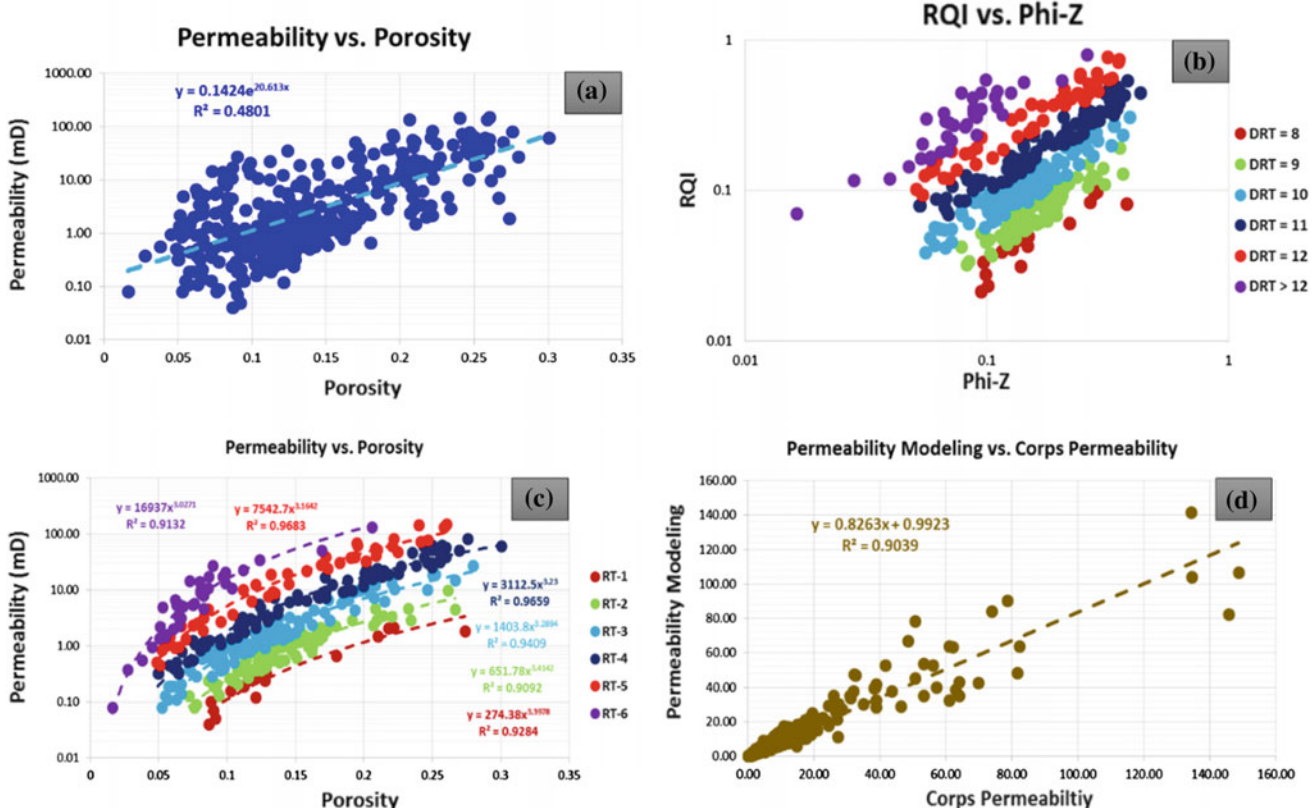


Fig. 1 Relation permeability versus porosity with the obtained different curves and coefficient of correlation: different clusters have come out with various hydraulic units leading to different rock typing (based on DRT method)

Fig. 2 Permeability calculation using DRT & permeability calculation by conventional method versus core permeability

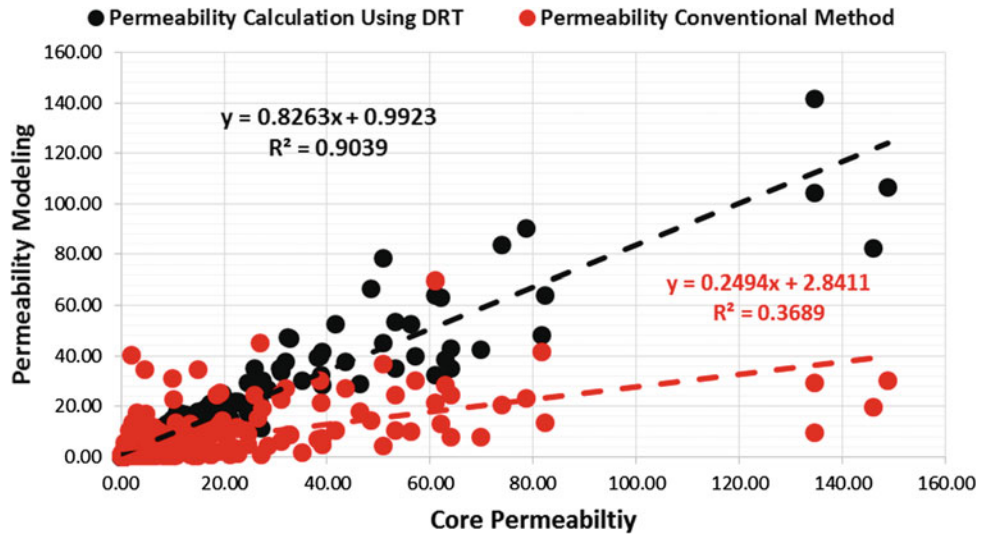


Table 1 Table summarizes the permeability model for each hydraulic unit

Rock types	DRT	Permeability	Correlation coefficient
1	8	$k = 274.38 * \phi^{3.3978}$	0.9284
2	9	$k = 651.78 * \phi^{3.4142}$	0.9092
3	10	$k = 1403.8 * \phi^{3.2894}$	0.9409
4	11	$k = 3112.5 * \phi^{3.23}$	0.9659
5	12	$k = 7542.7 * \phi^{3.1642}$	0.9683
6	>12	$k = 16937 * \phi^{3.0271}$	0.9132

In this study, the DRT method has been used to define the hydraulic units. The application of this method makes it possible to have six hydraulic units (Fig. 1b). Each of these units can be represented by a logarithmic, exponential, linear or power law. The choice of the mathematical model will be ensured by the correlation coefficient produced between porosity and permeability (Table 1). The classification is closely dependent on the value of DRT which means: each DRT value presents the same hydraulic unit.

All cores, having the same DRT value, should be grouped in the same cluster (Fig. 1b). This process allows us to classify rocks according to hydraulic units and improve the absolute permeability calculation especially for the petrophysical modelling. Six rock types have been defined.

Each cluster must have a large correlation coefficient, greater than 0.9, (Fig. 1c, Table 1) to have a consistent and representative petrophysical model. Finally, the application of this method (DRT method) allow improvement of the permeability calculation ($R^2 = 0.9039$) compared to the conventional method ($R^2 = 0.3689$). This latter method is

directly associated to the correlation of permeability versus porosity (Fig. 2).

To confirm that, all the hydraulic units have been selected, and using a statistical method, the cores' permeability are plotted as a function of calculated permeability provided by DRT method. Compatibility has been set between the considered two parameters, with a correlation coefficient greater than 0.9 and a trend of 0.8263 (Fig. 1d).

6 Conclusion

Identification of hydraulic units of any field is essential in order to develop more representative mathematical models.

The DRT method application in B-H field allows having six hydraulic units (six rock types). This method could also optimize the calculation of permeability in the non-cored zones and, therefore, illustrate the zones of high permeability able to set new producing wells.



A Fast and Less Expensive Test to Determine Permeability-Related Parameters on Well's Drilled Cuttings

Marco Ludovico-Marques

Abstract

This paper intends to contribute to a better understanding of the Statfjord Formation in the North Sea, based on the study of some lithotypes of the Lourinhã Formation analog. A mineralogical and physical characterization was performed. A Fast RILEM water absorption test is herein proposed to carry out on sandstone drilled cuttings and cores that were cut into specimens, to assess permeability-related parameters. Results in a faster way on rocks with porosity values higher than 15% are given by this test in comparison to traditional laboratory methods. A correlation factor of 4–5 was obtained between permeability (mD) and water absorption coefficient ($\text{lb}/\text{ft}^2\sqrt{\text{h}}$).

Keywords

Sandstones • Fast • Permeability • Karsten pipe

1 Introduction

Lourinhã Formation has fluvial successions similar to the Statfjord Formation in North Sea. Keogh et al. (2014) cited in [1] assigned these to Late Triassic and Lower Jurassic. In order to characterize the Statfjord Formation and contribute with data to the reservoir modelling of the Norwegian North Sea's Tampen fields, this Portuguese Formation in the western Region of Portugal was studied and field data were obtained [1].

Sandstone strata are the main rocks of Lourinhã Formation that has a thickness up to 900 m [1]. Stratigraphy and tectonics studies of the Lusitanian basin and Lourinhã Formation, assigned to Early Tithonian and Late Kimmeridgian

age, were given by Martinius and Gowland (2011) and Taylor et al. (2014) cited in [1].

In order to contribute to a deeper understanding of the North Sea's Statfjord Formation, an experimental work was carried out [1]. Mineralogical and physical properties data were obtained from samples collected from Lourinhã Formation analog. Also, a fast RILEM test was carried out on sandstone specimens and could also be performed on drilled cuttings and cores that were cut into specimens, to evaluate permeability-related parameters. Permeability and porosity of reservoir rocks are included in the most important physical properties used worldwide on reservoir characterization and modelling [1]. Fast methodologies for determining permeability-related parameters on drilled cuttings and cores from wells are very helpful tools which allow the correlation to other properties obtained from well logs, e.g. density, gamma ray, neutron, nuclear magnetic resonance, spontaneous potential, electrical resistivity and sonic [2].

Since samples were cleaned off oil using Soxhlet Extraction methodology [3] and were dried, this test gives results in a faster way on rocks with higher open porosity values in comparison to traditional laboratory methods. Moreover, a correlation between permeability and water permeability-related test data can be established in this experimental work herein presented.

2 Experimental Program

According to EN12407 recommendations [4], samples were collected from sandstone outcrops and thin section observations were performed under petrographic polarizing microscope. Following the point counting method, modal analysis was performed.

Sandstone blocks of M variety were cut in cubic and prismatic samples with circa 5 cm (2 in.)-long on cross section and a length of about 10 cm (4 in.) on the former samples.

M. Ludovico-Marques (✉)
Polytechnic Institute of Setúbal, ESTBarreiro Campus, 2839-001
Lavrado, Portugal
e-mail: marco.marques@estbarreiro.ips.pt

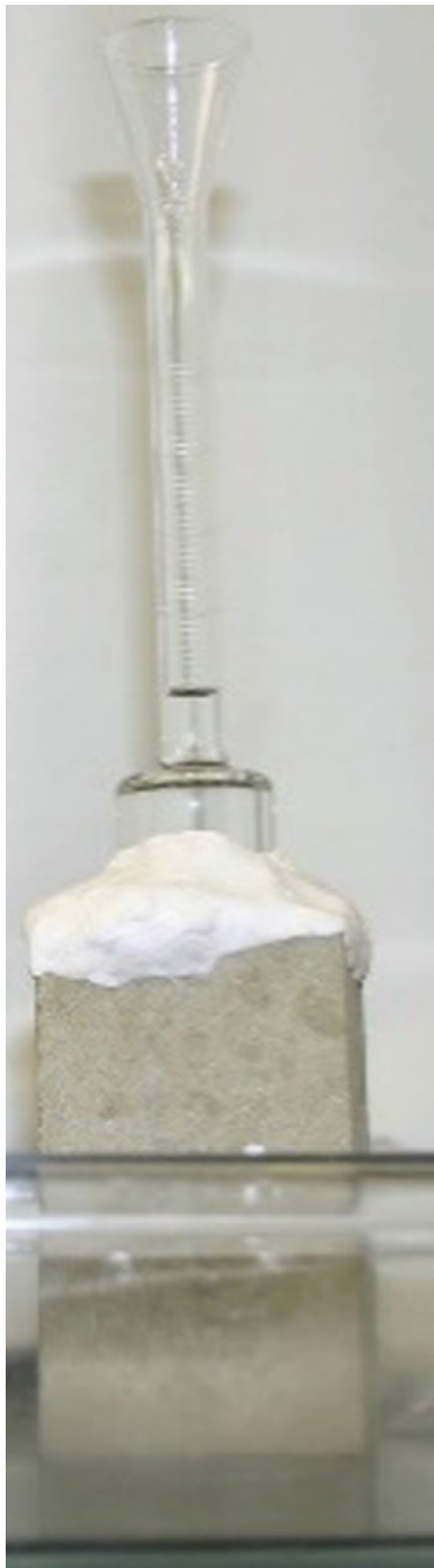


Fig. 1 Karsten pipe

According to RILEM [5] and EN1936 [6], porosity and density of sandstone samples were determined based on hydrostatic weighing and Archimedes principle, applied in these physical tests which were carried out.

AutoPore IV9500 of Micromeritics Instrument Corporation was used and pore size distribution for M variety sandstone was obtained. The pores radii's percentage lower than $7.5 \mu\text{m}$ was considered as microporosity [7]. The Katz and Thompson [8] method allowed to infer permeability from Mercury Intrusion Porosimetry.

The test of water absorption under low pressure (pipe method) was carried out on cubic and prismatic sandstone samples according to RILEM [5] procedure. Figure 1 shows the Karsten tube.

This device has a total measured height of water of 0.322 ft and a volume of $1.41 \times 10^{-4} \text{ ft}^3$. Water fills this vertical tube from the upper opening of the tube up to the graduation “0”. The Karsten tube is sealed on sample surface by a not deleterious and removable putty. The results are exhibited on graphs of water absorption, being:

$$\Delta m/S^2 \quad (1)$$

Δm is the variation of mass of water (lb) and S^2 is the area of absorption (ft^2). The graphs show these results in function of square root of time given in hours or seconds. The coefficient of water absorption of the test curve is given by the slope of the linear part.

3 Experimental Result

Four varieties of sandstones [1] were found on outcrops and were classified according to the classification of Folk [9] as lithic arkose containing carbonate cement. These four varieties were named A, B, C and M and are considered the lithotypes A + B and C + M. The lithotype A + B has around 34–40% carbonates and the lithotype C + M has circa 20–25% carbonates. The former lithotype has 30–32% quartz and the latter lithotype has 40–51% quartz. All these lithotypes contain circa 4–6% of minerals of mica.

Mean values of porosity of the samples of these two lithotypes range between 3.6% on A variety to 12.7% on C variety and 18.5% on M variety. The bulk density of M variety is about 446.5 lb/ft³. The percentage of microporosity of M variety is about 75% and the median pore radius is circa $3.6 \mu\text{m}$ (obtained at 50% of the total amount of volume of mercury injection). Katz and Thompson method [8] was applied and the inferred permeability values ranged from 20 to 30 mD.

Figure 2 and Table 1 show the results of the absorption of water under low pressure (Karsten tube) tests on M

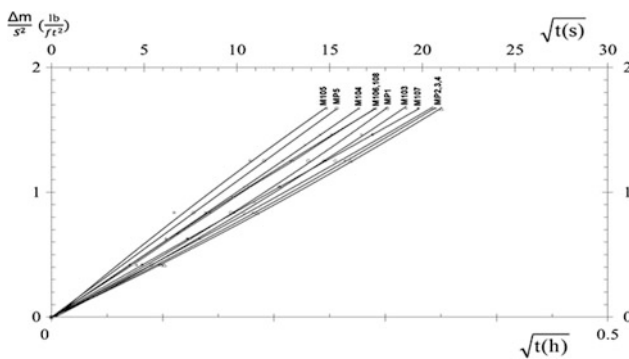


Fig. 2 Curves of absorption of water under low pressure (pipe method) obtained on M sandstone samples

Table 1 Values of the coefficient of water absorption k obtained on M sandstone samples

Samples	Coefficient of water absorption, k ($\text{lb}/\text{ft}^2\sqrt{\text{h}}$)	Coefficient of water absorption, k ($\text{lb}/\text{ft}^2\sqrt{\text{h}}$) Average \pm SD (CV%)
MP1	5.4	
MP2	4.8	
MP3	4.7	
MP4	4.8	
MP5	6.5 ^a	5.5 \pm 0.7 (12.7%)
M103	5.1	5.3 \pm 0.5 (9.4%) ^a
M104	6.0	
M105	6.9 ^a	
M106	5.8	
M107	5.1	
M108	5.8	

^aWithout higher values

sandstone variety. The average value obtained is about $5.3 \text{ lb}/\text{ft}^2\sqrt{\text{h}}$ with a coefficient of variation smaller than 10%.

4 Analysis of Experimental Results

These M variety samples collected in Lourinhã Formation, classified as lithic arkose with carbonate cement, with an average porosity \pm standard deviation of $18.5 \pm 0.4\%$ obtained on 140 specimens, revealed permeability inferred values of 20–30 mD. The average water absorption coefficient under low pressure is about $5.3 \text{ lb}/\text{ft}^2\sqrt{\text{h}}$.

Ehrenberg and Nadeau [10] reported that siliciclastic world reservoirs with median porosity statistical class of 17.5–22.5%, exhibited average values of permeability of

18 mD. Similar average values to those values mentioned are shown by samples of Sandstone M variety.

Further research should be carried out, but at a glimpse, a correlation between permeability and water absorption coefficient (pipe method) could be established: The permeability (mD) is about 4–5 times higher than the water absorption coefficient ($\text{lb}/\text{ft}^2\sqrt{\text{h}}$) on M variety sandstone.

This test procedure will require only several minutes or even seconds to give results on rocks with open porosity values higher than 15%. Permeability determinations from Mercury Intrusion Porosimetry inferred from Katz and Thompson [8] method was carried out and took at least half a day to be obtained. Air permeability obtained from steady state or transient pulse methods [11] needs much more expensive equipment, and even these tests require similar times in comparison to RILEM method.

5 Conclusions

An experimental study was carried out on M variety sandstone assigned to Lourinhã Formation, an analog of the Statfjord Formation in the North Sea. A mineralogical contribution study and a physical characterization was performed, including a fast RILEM permeability-related test. A correlation between permeability (mD) and water absorption coefficient ($\text{lb}/\text{ft}^2\sqrt{\text{h}}$) was obtained at a factor of about 4–5. However, further research should be carried out on other siliciclastic and carbonate Oil & Gas reservoirs.

References

1. Ludovico-Marques, M., Chastre, C.: Effect of artificial accelerated salt weathering on physical and mechanical behaviour of sandstone samples from surface reservoirs. In: Hamdy Makhoul, A.S., Aliofkazraei, M. (eds.) *Handbook of Materials Failure Analysis With Case Studies from the Oil and Gas Industry*, pp. 215–233. Elsevier, New York City (2016)
2. Nnaemeka, E.: *Petroleum Reservoir Engineering Practice*, p. 770. Prentice Hall, Upper Saddle River (2011)
3. Jobe, T.D.: Non-traditional techniques for microporosity evaluation in a low-permeability carbonate reservoir from a giant reservoir offshore Abu Dhabi, U.A.E. In: AAPG 2013 Annual Convention and Exhibition (2013)
4. EN 12407: Natural stone test methods—petrographic examination. Eur stand2000 (2000)
5. RILEM: Recommended tests to measure the deterioration of stone and to assess the effectiveness of treatment methods. Mater Constr., Bourdais-Dunoud **13**(75), 175–253 (1980)
6. EN 1936: Natural stone test method-determination of real density and apparent density, and of total and open porosity. Eur. Stand. (1999)

7. Pellerin, F.: La porosimétrie au mercure appliquée à l'étude géotechnique des sols et des roches. *Bull Liais Lab Ponts Chausse's* **106**:105–116 (1980)
8. Katz, A., Thompson, A.: Quantitative prediction of permeability in porous rock. *Phys. Rev. Online Arch.* **B34**, 8179–8181 (1986)
9. Folk, R.: Petrology of Sedimentary Rocks. Hemphill Publishing, Austin, TX (1974)
10. Ehrenberg, S., Nadeau, P.: Sandstone versus carbonate petroleum reservoirs: a global perspective on porosity-depth and porosity-permeability relationships. *AAPG Bull.* **89**(4), 435–445 (2005)
11. Filomena, C.M., Hornung, J., Stollhofen, H.: Assessing accuracy of gas-driven permeability measurements: a comparative study of diverse Hassler-cell and probe permeameter devices. *Solid Earth* **5**(1), 1–11 (2014)



The Method of Analytic Calculation of Initial and Ultimate Pressure Gradients to Flow for Low-Permeability Reservoirs

Oksana Shevchenko and Vladimir Astafev

Abstract

Recently, all over the world, hydrocarbon fuel reserves are deteriorating rapidly. The number of fields with hard-to-recover reserves is growing, the largest part of which are low-permeability reservoirs. In addition to problems with the development of this type of collectors, there is a difficulty in building hydrodynamic models of fields. All hydrodynamic simulators are based on the linear law of Darcy flow, so it is difficult to correctly adapt this model to the history of development, because this kind of objects has witnessed a nonlinear filtration. The construction of the hydrodynamic model is carried out in the simulator. Therefore, to adapt the model, it is necessary to select the parameters of the filtration medium, which are often far from the real studies of collectors. Tempest MORE of ROXAR, in which there is a possibility of modeling a nonlinear filtration for high-viscosity oil by “locking a gradient filter and a multiplier on the flow”. The former limits the well drainage area, and the latter reduces the fluid filtration rate multiple times. In the presented paper, the possibility of using this method to adapt the model for low-permeability reservoirs is described. Analytical methods for determining these critical pressure gradients are presented. Critical pressure gradients were analytically determined by using analytical methods following the example of the V. N. Vinogradova oil field with a low-permeability reservoir.

Keywords

Nonlinear filtering • Low-permeability reservoirs
Ultimate pressure gradients

O. Shevchenko (✉)
VolgogradNIPImorneft, LLC LUKOIL-Engineering,
Volgograd, 400078, Russia
e-mail: OShevchenko@lukoilvmn.ru

V. Astafev
Samara State Technical University, Samara, 443100, Russia

1 Introduction

An important feature of fields with low-permeability reservoirs, which requires a comprehensive study, is the presence of flow regimes that do not obey the linear law of filtration. Earlier, this fact was revealed by Churaev et al. [1] in filtering liquid in the clay deposits. In the recently published works by Baikov et al. [2–4], the results of their studies demonstrating the deviation from the Darcy law and the filtration of light oils in low-permeability reservoirs were presented, while the resulting deviation from the Darcy linear law in the filtration in low-permeability reservoirs is characterized by the presence of the effective initial and the limiting pressure gradients. The study and modeling of the effect of the flow velocity deviation from the linear law of filtration, in zones of low-pressure gradients, allow to reveal the peculiarities of filtration in low-permeability reservoirs and to find new solutions and approaches for the development of deposits confined to such collectors.

2 The Method of Analytic Calculation of Initial and Ultimate Pressure Gradients

It is known that the hydrodynamic simulator Tempest MORE of ROXAR has an option for modeling the effect of non-linear filtration OVPG (oil viscosity pressure gradient), which consists of three arguments—a multiplier on the oil flow (F_0) and two pressure gradients (GP_0 , GP_1) used to determine the variation of the flow (Fig. 1).

When the pressure gradient changes from GP_0 to GP_1 , the flow multiplier is distributed from F_0 to 1. But this option is intended for modeling the nonlinear filtration of high viscosity oil. However, due to the similarity of filtration mechanisms in low-permeability reservoirs and for fields with high viscosity oils, we will use this option to adopt the model in a low-permeability reservoir. The critical pressure gradients determine the method of selection;

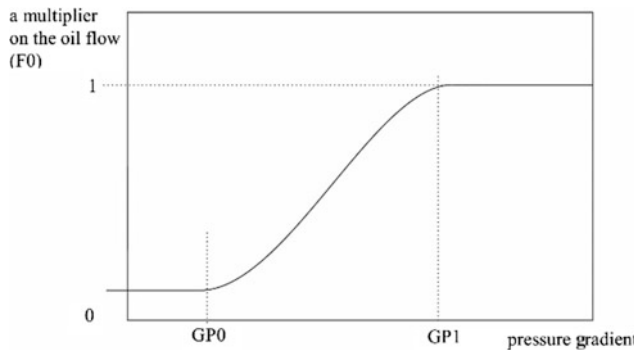


Fig. 1 An option for modeling the effect of non-linear filtration OVPG

however, this method assumes no scientific basis. Therefore, two analytical approaches to the determination of critical pressure gradients are proposed. The first one is based on some theoretical principles of slow flow fluid dynamics presented in the paper, which were used to determine the initial gradient of the oil reservoir (GP0) shear under conditions of a low-permeability reservoir by Chilingar et al. [5]. The second approach is based on works by Baikov et al., Li and Shevchenko [6–9], according to which, there is a certain critical filtration velocity at which the flow regime is changed. The critical pressure gradient (GP1) corresponding to this velocity was determined by the calculation method. Furthermore, by varying the permeability values, the values of the limiting pressure gradient at which the fluid flow changes from the permeability were obtained.

3 Results

3.1 The Objective of Study

The objective of this study is to determine the critical pressure gradients using the example of the reservoir of AC3 of the V. N. Vinogradova field. Commercial oil content of the Deposit set in clastic sediments of Frolovskaya suites of the Aptian lower Cretaceous layer K1A. The layer is composed of sandstones and siltstones. The type of collector is pore. The Deposit is confined to a lithologically-shielded trap, measuring 57×20 km, with a height of 120 m. At the moment, the accumulation of the layer of AC3 is at the stage of experimental-industrial works.

The AC3 reservoir is characterized by a complex geological structure, with numerous disjunctive disturbances and a high heterogeneity. It differs from traditional reservoirs by an ultra-low permeability (0.87×10^{-3} D), a low oil-saturated thickness and a low oil-saturation coefficient. The main problems that complicate the development of the field are the non-confirmation of initial oil flow rates and

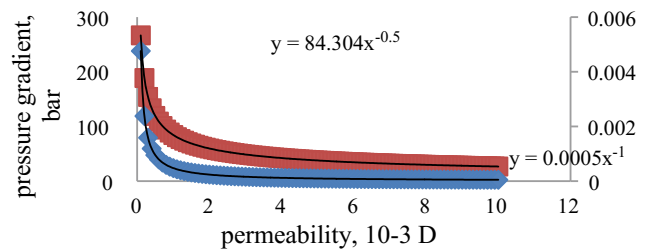


Fig. 2 The dependencies of the initial and ultimate pressure gradients from the reservoir permeability

high initial water content of wells, the high rates of well flow rates and bottom-hole pressures, and, as a consequence, the non-confirmation of the design levels of oil recovery. A trial study of the adaptation of the hydrodynamic model using nonlinear filtering was carried out on the sector. When calculating the initial pressure gradient, the permeability of the porous medium was varied. At the same time, based on the equation [5]:

$$\frac{\Delta P}{L} = \frac{0.0018As(1-m)^2}{apgk}, \quad (1)$$

where A is the constant of Hamaker J., a represents the intermolecular distances in the liquid m, p is the density of the filtered fluid in kg/m³, k is the permeability of medium m², s is the specific surface area of particles, and m is the porosity of the medium. To determine the limit pressure gradient, the critical filtration velocity was calculated, and then the calculation was carried out according to A. Krasnopol'sky formula [8, 9]. As a result of the calculations, the dependencies for determining the initial and ultimate pressure gradients from the reservoir permeability were obtained (Fig. 2).

4 Discussion

The above-mentioned dependencies were used to adapt the hydrodynamic model taking into account the nonlinear filtration. As a result of the calculations made, in sector 17, the difference in accumulated production between the linear and nonlinear model adaptation was 67%. At the same time, the analysis of the development history shows that oil production can be significantly overestimated when calculated under the conditions of linear filtration.

5 Conclusions

For the adaptation of the wells on the history of development with and without taking into account nonlinear filtering, it is revealed that the inclusion of nonlinear filtering

(option OVPG) improves the quality of adaptation of the performance of the wells (bottom-hole pressures). As for the assessment of the influence of nonlinear filtration on the accumulated oil production and field pressure in the vicinity of wells, it is established that forecast calculations under conditions of low-permeability reservoirs and under Darcy's law lead to an unjustifiably optimistic result—i.e. a significant overestimation of the accumulated oil production in wells (on average by 67%).

References

1. Churaev, N.V., Derjaguin, B.V., Muller, V.M.: Surface Forces. Springer, Heidelberg (2013)
2. Baikov, V.A., et al.: Nonlinear filtration in low-permeability reservoirs. Analysis and interpretation of laboratory core examination for Priobskoye oilfield. Sci. Tech. J. NK "Rosneft" **2**(31), 4–7 (2013) (in Russian)
3. Baikov, V.A., et al.: Nonlinear filtration in low-permeability reservoirs. Impact on the technological parameters of the field development. Sci. Tech. J. NK "Rosneft" **2**(31), 17–19 (2013) (in Russian)
4. Baikov, V.A., Davletbaev, A.Y., Ivashchenko, D.S.: Non-Darcy fluid inflow modeling in low-permeability reservoirs. Neftyanoe khozyaystvo **11**, 54–58 (2014) (in Russian)
5. Chilingar, G.V., Eremenko, N.A., Arye, A.G.: Abnormally high reservoir pressures in natural geofluidodynamic systems. Geol. Oil gas **5**, 19–27 (1997). (in Russian)
6. Baikov, V.A., et al.: Nonlinear filtration in low-permeable reservoirs. Laboratory core examination for Priobskoye oilfield. Sci. Tech. J. NK "Rosneft" **2**(31), 9–12 (2013) (in Russian)
7. Li, X.: Non-linear filtration of water in low-permeability reservoirs. In: Vesti Gazovoy nauki, vol. 3, issue 23, pp. 116–121. Gazprom VNIIGAZ, Moscow (2015) (in Russian)
8. Shevchenko, O.N.: Determination of values of critical pressure gradients and filtration rate of non-Newtonian fluid. Int. Res. J. Ekaterinburg **3**(45), part 2, 120–124 (2016) (in Russian)
9. Shevchenko, O.N.: Determination of critical values of filtration velocities under conditions of violation of the Darcy. Successes of modern science and education, vol. 2, pp. 140–145 (2016)

Development of an Empirical Model for Predicting the Cation Exchange Capacity of Shaly Sandstones Using Complex Dielectric Permittivity Measurements

Ali A. Garrouch

Abstract

Dimensional analysis is applied on measured complex dielectric permittivity data of shaly sandstone rock samples, for the purpose of modeling the cation exchange capacity (*CEC*). These measured variables consist of rock porosity, specific surface area, and five other parameters of the Cole-Cole function, which describe the frequency dependence of the complex permittivity of rock samples in the range of 10–1300 MHz. The Cole-Cole function parameters are the characteristic relaxation time, the spread parameter, the real dc conductivity of water saturated rocks, the static dielectric permittivity, and the high-frequency dielectric permittivity of the water-saturated shaly-sandstone rocks. The dimensional analysis revealed the existence of two dimensionless groups, denoted as the cationic dispersion number (π_1), and the conductivity number (π_2). The former group π_1 stands for the ratio of the cation exchange capacity to the electrical double layer dispersion. The latter group π_2 represents the ratio of the low-frequency ionic conductivity to the high-frequency electronic polarization. The dimensionless groups have been validated using measured complex permittivity data of 92 shaly sandstone rocks. The dimensional analysis resulted in the derivation of a model for the *CEC* as a function of fast and non-invasive dielectric properties measurements. In return, accurate and fast estimates of *CEC* are useful in many petroleum engineering applications. They can be used to identify clay types, and to quantify the volume of hydrocarbon in shaly sands using well log resistivity data. The results of this study represent a major advantage for formation evaluation and wellbore stability analysis, as well as for designing stimulation jobs.

Keywords

CEC • Shaly sand • Dielectric permittivity

1 Introduction

The *CEC* is a measure of the number of mobile counter-ions, or exchangeable cations associated with the negative charge deficiency of clay minerals in a reservoir rock. Although there are studies reporting the dependence between the experimentally measured permittivities of brine saturated rocks and the *CEC*, researchers have yet to establish a robust general empirical relation between the measured dielectric permittivity and petrophysical parameters like the cation exchange capacity. This study aims at analyzing an extensive set of measurements of the complex permittivity of brine saturated shaly sandstone rocks in the frequency range of 10–1300 MHz. The purpose of the analysis is to develop a generalized model that estimates the cation exchange capacity of shaly sandstone rocks as a function of the specific surface area (SA), the porosity (ϕ), and the Cole-Cole function parameters ($\sigma_s, \varepsilon_s, \varepsilon_\infty, \alpha, \tau$). In this notation, τ is an average characteristic relaxation time, α is the spread parameter, σ_s is the dc conductivity of the water-saturated rock and is a real number, and ε_o is the permittivity of free space. The symbols ε_s and ε_∞ are real numbers representing the static ($\omega = 0$) and the high-frequency dielectric permittivities of the water-saturated rock, respectively.

2 Methodology

The proposed *CEC* model uses non-destructive complex permittivity measurements, and is expressed generically as follows:

A. A. Garrouch (✉)
Kuwait University, 5969 Kuwait City, Kuwait
e-mail: ali.garrouch@ku.edu.kw

$$CEC = f(\phi SA, \frac{\sigma_s}{\varepsilon_\infty}, \varepsilon_s, \frac{\tau^2}{\alpha}, \bar{a}_p). \quad (1)$$

In the above notation, \bar{a}_p is an average pore radius. An *MLTQ* dimensional analysis for the dependence of *CEC* on the dielectric parameters and rock properties has been performed, in an attempt to identify dimensionless groups that can assist in revealing the dependence type that may exist between the variables shown in Eq. 1. *MLTQ* stands for the fundamental dimensions of mass (*M*), length (*L*), time (*T*), and charge (*Q*). Taking the *CEC* and $\sigma_s/\varepsilon_\infty$ as the non-repeating variables, and the parameters ϕSA , ε_s , (τ^2/α) , and \bar{a}_p as the repeating variables, allows to formulate the following two dimensionless groups:

$$\pi_1 = \frac{\tau^2 CEC}{\alpha \sqrt{\phi SA} \varepsilon_s \bar{a}_p} \quad (2)$$

$$\pi_2 = \frac{\tau^2 \sigma_s}{\alpha \varepsilon_\infty} \quad (3)$$

3 Results

The petrophysical as well as the complex permittivity parameters deduced from the complex impedance measurements for a set of 92 water-saturated sandstone samples, have been used to validate the derived dimensionless groups. A plot of π_1 versus π_2 in a log-log paper (Fig. 1) gives a straight line that suggests a power-law relation between the dimensionless groups, given by Eqs. (2) and (3). The fact that the experimental data for the 92 core samples complex permittivity measurements appear to yield the power-law relation between the two dimensionless groups validates the dimensional analysis.

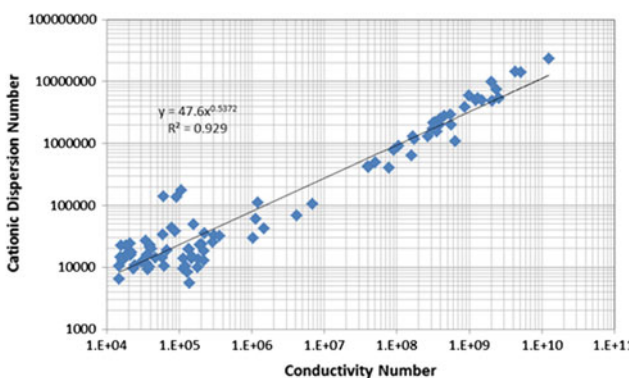


Fig. 1 Cationic dispersion number versus conductivity number for the sandstone data

4 Discussion

The dimensionless group, π_1 is designated as the *Cationic Dispersion Number*. It represents the ratio of the cation exchange capacity to the electric double layer dispersion. The second dimensionless group π_2 is designated as the *Conductivity Number*. It stands for the ratio of the low-frequency ionic conductivity to the high-frequency electronic polarizability. The ratio $\frac{\sigma_s}{\varepsilon_\infty}$ appears to be a rock property that reflects an average time to conduct ions from one end of a pore to the other end, for a given lithology characterized by an electronic storage capacity given by ε_∞ . This ratio should reflect important rock texture properties, for a given lithology type, like pore sphericity, pore sorting, and existence of authigenic crystals inside the pores.

The power-law relation between the dimensionless groups, shown in Fig. 1, is rearranged to relate the *CEC* explicitly to the other variables as:

$$CEC = \frac{B_1 \alpha^{1-B_2} \sqrt{\phi SA} \varepsilon_s \bar{a}_p}{\tau^{2-2B_2}} \left(\frac{\sigma_s}{\varepsilon_\infty} \right)^{B_2} \quad (4)$$

Equation 4 indicates that the *CEC* is proportional to the square roots of the specific surface area, the static dielectric permittivity, and the average pore diameter, respectively. The *CEC* appears to also be proportional to the static conductivity raised to a power B_2 . These results are confirmed by a number of experiments [1–3]. A plot of estimated *CEC* values using the empirical model given by Eq. 4 versus measured *CEC* values for the sandstone data set is shown in Fig. 2.

The estimated values of shaly sandstone *CEC* appear to be in a reasonable agreement with the measured *CEC* values. These results appear to be promising since they introduce an analytic model that can predict sandstone *CEC* values with a reasonable precision using non-destructive complex impedance measurements.

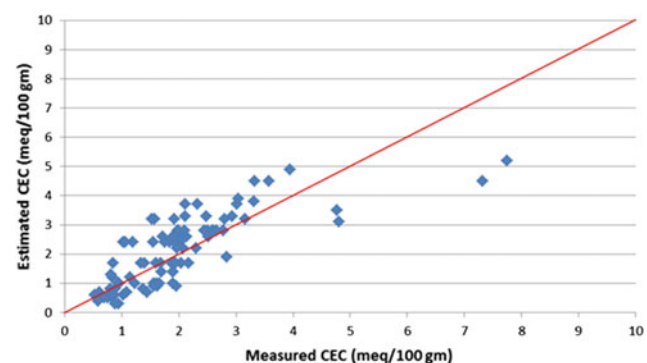


Fig. 2 Estimated *CEC* using dimensional analysis model versus measured *CEC* for the sandstone samples

5 Conclusions

Dimensional analysis has been used for deriving an empirical model for the *CEC* as a function of petrophysical rock properties, and complex permittivity parameters. In the frequency range investigated, the dielectric permittivity response of sandstone rocks is a complex function of the interfacial effects, the rock micro-geometry, and the pore fluid polarization characteristics. Measurements over this wide frequency range (10–1300 MHz) capture the entire distribution of relaxation times—and, therefore, allow to quantify the *CEC* when the rock specific surface area and porosity values are known.

With the *CEC* analytical model introduced in this study, it is possible to obtain reliable quantitative estimates of the

CEC of sandstone rocks using non-destructive frequency-dependent dielectric permittivity measurements.

References

1. Patchett, J.G.: An investigation of shaly sand conductivity. SPWLA paper U, presented at the 16th annual SPWLA symposium, New Orleans, Louisiana, 4–7 June 1975
2. Thomas, E.C.: The determination of Q_v from membrane potential measurements on shaly sands. *J. Petrol. Technol.* (September issue), 1087–1096 (1976)
3. Zhan, X., Schwartz, L., Smith, W., Toksoz, N., Morgan, D.: Pore scale modeling of rock properties and comparison to laboratory measurements. Presented at the 79th SEG international exposition and annual meeting, Houston, TX, 25–30 Oct (2009)



Back Propagation and Hidden Weight Optimization Algorithms Neural Network for Permeability Estimation from Well-Logs Data in Shaly Sandstone Petroleum Reservoirs: Application to Algerian Sahara

Leila Aliouane, Sid-Ali Ouadfeul, and Amar Boudella

Abstract

In this paper, we present an inexpensive approach based on a multilayer neural network, using two different algorithms to estimate permeability in petroleum reservoirs from well-logs data. In a supervised learning, the Back propagation (BP) and Hidden weight optimization (HWO) are tested in order to determine the best algorithm for better permeability predictions. The application to real data has been realized in the Algerian Sahara, exploiting data of several petrophysical parameters of Triassic reservoirs of two wells. The data of the first well are used to train the neural network machine as a pilot well, while the second well data were used for generalization to predict permeability. The obtained results are compared with permeability from core data.

Keywords

Shaly sandstone reservoir • Neural network
Permeability • Training algorithm

1 Introduction

Permeability estimation is a key parameter in reservoir engineering; it depends on its effective porosity and the type of clay or cementing material between sand grains [1].

Routinely, this parameter is obtained through core analysis, well testing, or by correlation to other more easily measured rock properties such as porosity from several

L. Aliouane (✉)
Laboratoire Physique de la Terre (LABOPHYT), Faculté des Hydrocarbures et de la Chimie, Université M'hamed Bougara de Boumerdes, Boumerdes, Algeria
e-mail: l.aliouane@univ-boumerdes.dz

S.-A. Ouadfeul
University of Khemis Miliana, Khemis Miliana, Algeria

A. Boudella
Geophysics Department, USTHB, Algiers, Algeria

empirical petrophysical models. The empirical models may not be applicable in regions with different depositional environments without making adjustments in the model, mainly, in shaly sandstone reservoirs [2].

Artificial Neural Network (ANN) is becoming very popular in geosciences and in petroleum reservoirs characterization from well-logs data [3].

The objective of this paper is to improve permeability predictions in shaly sandstones reservoirs through two kinds of neural networks techniques, which are the learning algorithms Back propagation (BP) and Hidden weight optimization (HWO). We have applied the proposed techniques to Triassic reservoirs of two wells located in the Algerian Sahara, where several petrophysical data are used. Data of the first well are used to train the neural network machine, and the second well data for permeability prediction. Results will be compared with permeability from core data.

2 Reservoir and Data Description

The presence of shale in sandy reservoirs can provide erroneous results of permeability, and Triassic reservoirs are generally shaly sandstone (Fig. 1a). The raw well-logs data of two wells located in the Algerian Sahara have been exploited. The raw well-logs data are: Natural gamma ray (GR), bulk density (RHOB), neutron porosity (NPHI), photoelectric absorption factor (PEF), and sonic transit time (DT). Core permeability data are also available for the two wells. Figure 1 shows the composite log of raw logs data of one borehole; Well-A.

3 Permeability Estimation Problem and Neural Network

The permeability estimation is a hard task; the presence of shale in sandy reservoirs is the main ambiguity, where all the relationships that provide permeability cannot be applied

Fig. 1 Petrophysical parameters recordings of Triassic reservoir; Well-A

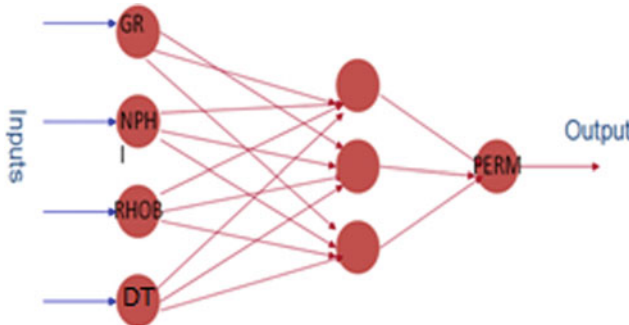
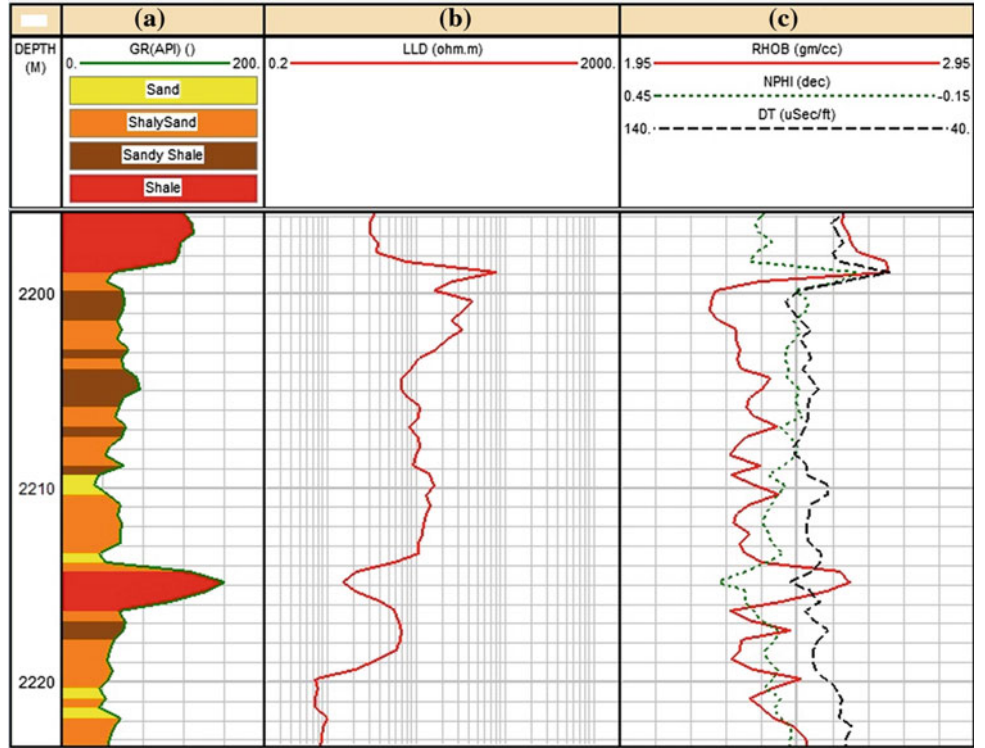


Fig. 2 MLP neural network architecture

[4, 5]. An artificial neural network can be applied in this case to resolve this ambiguity [6].

In this paper, a Multilayer Perceptron (MLP) has been implemented. It is constituted by three layers where the input layer has four neurons corresponding to gamma ray (GR), Transit travel time (DT), bulk density (RHOB) and neutron porosity (NPHI). The output layer has one neuron corresponding to permeability and one hidden layer (Fig. 2).

3.1 Back Propagation Algorithm

The first training algorithm is the back propagation, which is based on the minimization of the root mean square between the calculated and the desired output. More detailed explanation of the BP algorithm can be found by Aqil et al. [7]. Obtained results (Perm_BP) using this kind of learning algorithms are shown in Fig. 3.

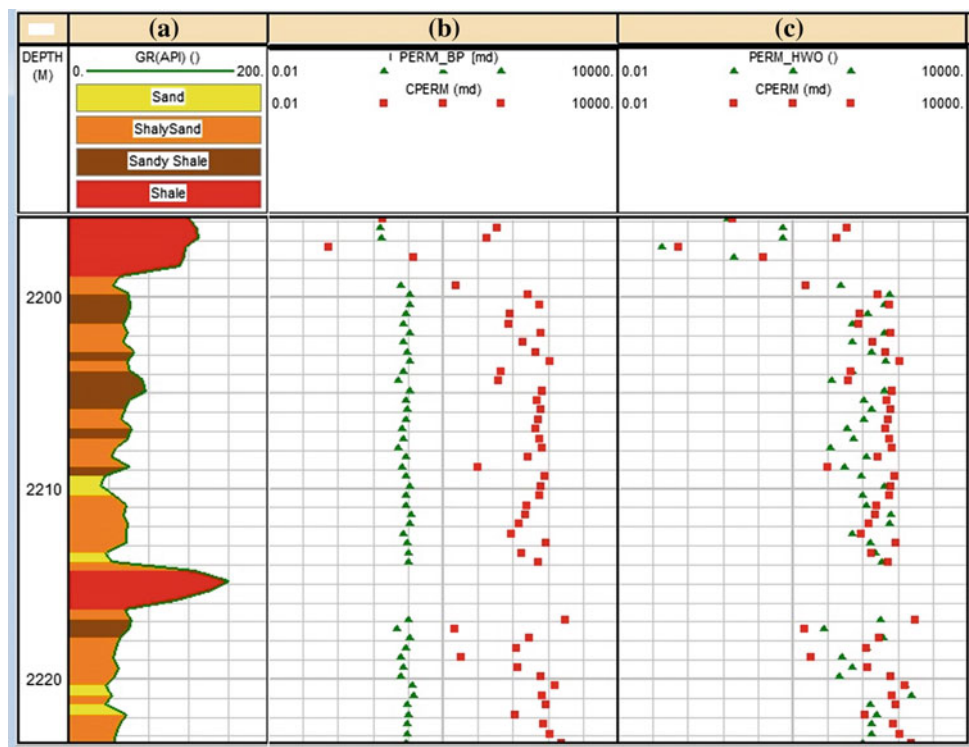
3.2 Hidden Weight Optimization Algorithm

The hidden weight optimization (HWO) training algorithm alternately solves linear equations for output weights and reduces a separate hidden layer error function with respect to hidden layer weights [8].

4 Results Interpretation

The obtained results (Fig. 3b, d) clearly show that the HWO algorithm predicts permeability in a better way, compared to the BP algorithm. Thus, the HWO results are very close to

Fig. 3 Permeability predicted from BP and HWO algorithm of Triassic reservoir, Well-B



core permeability (CPERM). Consequently, the HWO algorithm can be used to train the multi-layer neural network rather the BP algorithm for a better permeability estimation, to enhance the petroleum reservoir characterization.

5 Conclusions

Permeability is a key parameter in reservoir characterization, empirical models cannot be applied in shaly sandstone reservoirs, because they suppose that the reservoir is “clean”. The artificial neural network can be greatly used to predict permeability from well-logs data; the Hidden Weight Optimization training algorithm is highly recommended compared to the back propagation.

References

1. Tiab, D., Donaldson, E.C.: Petrophysics: Theory and Practice of Measuring Reservoir Rock and Fluid Transport Properties, 2nd edn. Elsevier (2004)
2. Ellis, D.V., Singer, J.M.: Well Logging for Earth Scientists, 2nd edn. Springer (2007)
3. Ouaadfeul, S., Aliouane, L.: Total organic carbon estimation in shale-gas reservoirs using seismic genetic inversion with an example from the Barnett Shale. *Lead. Edge.* **35**(9), 790–794 (2016)
4. Balan, B., Mohaghegh, S., Ameri, S.: State-of-the-art in permeability determination from well log data, part 1—a comparative study, model development. In: Eastern Regional Conference & Exhibition, West Virginia, U.S.A. SPE, vol. 30978 (1995)
5. Aliouane, L., Ouaadfeul, S., Djarfour, N., Boudella, A.: Permeability prediction using artificial neural networks. A comparative study between back propagation and Levenberg–Marquardt learning algorithms. In: LNESS. Springer (2013)
6. Aliouane, L., Ouaadfeul, S.-A., Djarfour, N., Boudella, A.: Petrophysical parameters estimation from well-logs data using multilayer perceptron and radial basis function neural networks. In: Huang, T., Zeng, Z., Li, C., Leung, C.S. (eds.) ICONIP 2012, Part V. LNCS, vol. 7667, pp. 730–736. Springer, Heidelberg (2012)
7. Aqil, M., Kita, I., Yano, A., Nishiyama, S.: Neural networks for real time catchment flow modeling and prediction. *Water Res. Manag.* **21**, 1781–1796 (2007)
8. Yu, C., Manry, M.T.: A modified hidden optimization algorithm for feedforward neural networks. In: Conference Record of the Thirty-Sixth Asilomar Conference on Signals, Systems and Computers, vol. 01, issue 2, pp. 1034–1038 (2002)
9. Nelson, P.H.: Permeability-porosity relationships in sedimentary rocks. *Log Anal.* **35**(3), 38–62 (1994)

Experimental Relationship Between Confining Pressure, Fluid Flowrates, Flow Time Period and Temperature on Effective Permeability to Water in High Porous Sandstone

Thomas Adebayo and Marie Lordinon

Abstract

This study uses a computerized formation evaluation system to investigate the permeability variation of high porous sandstone with reference to varying confining pressure, flowrate, time period of flow and temperature using brine as reservoir fluid. Permeability increases with increasing confining pressure, temperature and fluid flow period; however, it decreases with increasing fluid flowrates. The various permeabilities were determined at a confining pressure of 1060–3091 psi, a flow rate of 0.1–0.4 cc/min, an experiment duration of 10–40 min and a temperature of 26–42.3 °C. The results show that the time period of flow and fluid flowrates are two important parameters that are essential to obtaining an accurate permeability measurement but these cannot be operated at reservoir conditions during permeability determination, as these two parameters remain variables throughout the producing life of the reservoir.

Keywords

Permeability • Effective permeability • Confining pressure • Back pressure • Reservoir flow

1 Introduction

Permeability is an intrinsic property of porous materials and measures the easiness of a fluid flow within the reservoir rock. It is of great importance in determining the flow characteristics and production rate of hydrocarbons in oil and gas reservoirs. Permeability varies from tens to hundreds of milliDarcies, but when permeability is greater than 100 mD [1], the reservoir is producible naturally, i.e., without artificial stimulation. Many researchers have studied

T. Adebayo (✉) · M. Lordinon
Abu Dhabi Men's College, Higher Colleges of Technology,
Al Nahyan, Abu Dhabi, UAE
e-mail: tadebayo@hct.ac.ae

the effect of confining pressure, P_c , and pore pressure, P_p , on the permeability of rocks. Bruce et al. [2] measured the permeability of granite under high pressure (i.e. $25 < P_c < 444$ MPa and $15 < P_p < 40$ MPa) and concluded that the permeability of granite was decreasing when the effective confining pressure (defined as $P_c - P_p$) was also increasing. Similar conclusions were found by Patsouls and Gripps [3] on the permeability of Yorkshire chalk. Walch [4] researched the effects of pore pressure and confining pressure on fracture permeability. Experiments showed that the effective fluid permeability, K_{eff} , is proportional to $(P_c - sP_p)$ where s is a constant depending on the fracture characteristics. During the study of the effects of both pore and confining pressure on supercritical CO₂ permeability of sandstone, it was discovered that different permeabilities of the rock were obtained when water and gas were used as the flowing fluid, while varying the confining pressure and pore pressure [5].

A non-Darcy flow test with a high flow rate was conducted with the permeability estimated using the Forchheimer equation. An effective pressure coefficient χ , which is a function of P_c and P_p , was estimated to increase non-linearly as the difference between P_c and P_p decreased, with a maximum of 1.36 being observed. This helped to conclude that the power law model was appropriate to estimate the change in supercritical CO₂ permeability with varying confining and pore pressures. Caulk et al. [6] experimentally observed a fracture aperture change in an enhanced geothermal system. Specimens of granite were used in a column-like flow model to measure evolution of fracture permeability for 20 and 40 days using granite rock and in temperature conditions of 120 °C and 25–35 MPa pressure range. Effective permeability, fracture aperture, and mass of minerals dissolved were computed in relationship to the pore-pressure using X-ray computed tomography (CT) scan imaging. It was observed that increasing pore pressure correlates with declining permeability due to dissolution of minerals and formation of mechanical creeps. Arash [7] carried out an experimental study of fracture response in granite specimens subjected to wide ranges of temperatures

and pressures. Series of experiments were performed on artificially-fractured granite specimens at a pressure range of 5–36 MPa and rock temperatures of 25 and 130 °C. Fluids were injected and the effect on permeability and fractures closures were examined. It was discovered that increasing the temperature of the injected fluid resulted in increases in the recovery percentages of fracture openings and permeability after pressure was reduced. This paper presents the effect of confining pressure, flowrate, period of flow and temperature on the permeability of high porous sandstone, using brine as reservoir fluid. Tests were done using a computerized formation evaluation system.

2 Methods

The steps of investigation in this research are as follows;

- A computerized porosimeter-permeameter (Vinci) was used to measure the porosity and permeability of the sample.
- The sample was transferred to a computerized formation evaluation system and the permeability was measured for a confining pressure of 1060–3091 psi; a flowrate of 0.1–0.4 cc/min; within a flow period of 10–40 min experimental duration and at various temperatures.

3 Results

The permeability obtained, using a computerized formation evaluation system, when flowrates and temperature were varied is shown in Table 1. Permeability to water at different experimental durations and confining pressures is shown in Table 2. Permeability variation with flowrates and temperature is presented in Fig. 1, while permeability variation with length of experiment time and confining pressure is presented in Fig. 2.

4 Discussion

Permeability was observed to increase with increasing temperature at the flowrate of 0.1 cc/mins but the same permeability was observed to decrease with increasing flowrate, even when temperature increased slightly as shown in Fig. 1. This comes as a result of the fact that water mobility increases with increasing temperature, leading to a better and more effective permeability to water. Permeability was also observed to increase with increasing experimental time and

Table 1 High porous sandstone's permeability to water variation with flowrates and temperature using computerized formation evaluation system

Flowrate (cc.min ⁻¹)	Temp. (°C)	Effective permeability
		Keff (mD)
0.1	26.5	3.4149
0.1	38.2	4.4914
0.1	38.2	4.6391
0.1	42.6	5.6109
0.1	42.6	4.8739
0.1	42.6	4.4726
0.1	42.6	4.0786
0.2	38.2	7.3572
0.2	38.2	7.4046
0.2	38.2	7.9526
0.2	42.8	6.8049
0.2	42.8	5.4076
0.2	42.8	5.6722
0.2	42.8	5.8387
0.3	38.2	6.6404
0.3	38.2	7.1157
0.4	38.2	6.5298

Table 2 High porous sandstone's permeability to water variation with experiment duration and confining pressure using computerized formation evaluation system

Experiment duration (mins)	Effective permeability Keff (mD)	Confining pressure (psi)
10	5.4076	2508
10	5.6722	2508
10	5.8387	2508
20	7.4046	3091
20	7.9526	3091
20	7.3572	3091
20	6.6404	3091
20	7.4575	3091
20	7.1157	3091
20	6.5298	3091
30	4.4914	3091
30	4.6391	3091
40	3.4149	1060
40	5.6109	1279
40	4.8739	1279
40	4.4726	1279
40	4.0786	1279

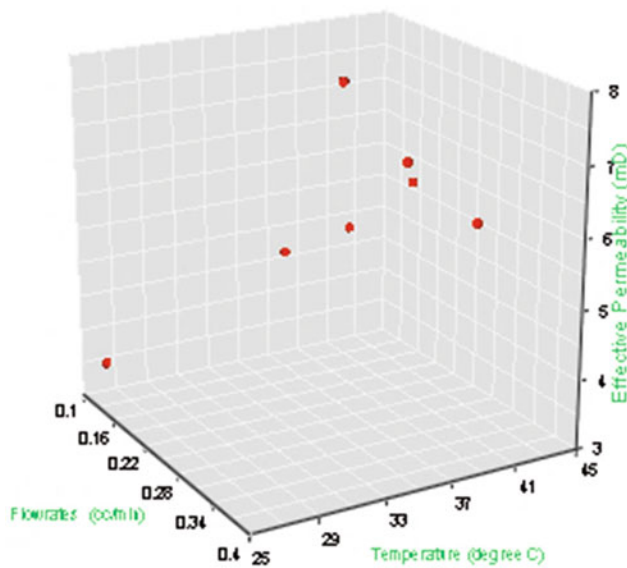


Fig. 1 Effective permeability variation with flowrates & temperature for sample 1

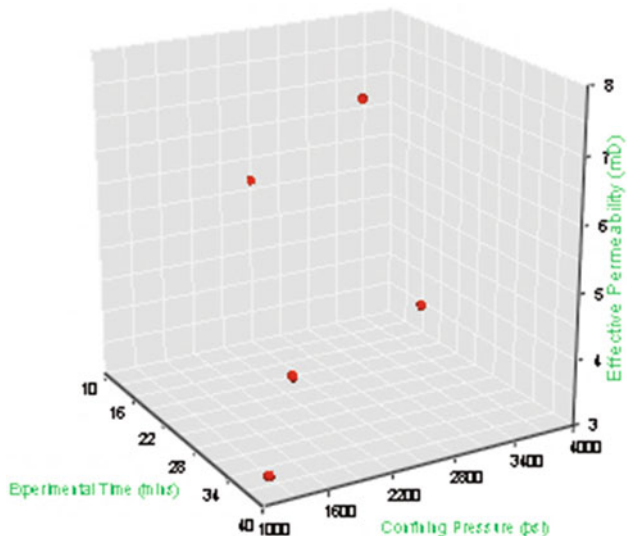


Fig. 2 Effective permeability variation with experiment time & confining pressure for sample 1

confining pressure, as shown in Fig. 2. The increase of permeability with increasing flow time period is probably due to a better flow stability with time, resulting in less frictional loss.

5 Conclusions

The influence of fluid flowrate, temperature, confining pressure and length of experiment on permeability was observed and measured. All these parameters should be considered at reservoir conditions, as much as possible, while determining the permeability of a reservoir rock. Unfortunately, it is not possible to run the experiment in reservoir conditions, especially for flowrate and the length of flow period. There is a need to run various permeability measurement experiments and find a mean value at various possible conditions.

References

- Bloomfield, P., Williams, A.T.: An empirical liquid permeability-gas permeability correlation for use in aquifer properties studies. *Q. J. Eng. Geol. Hydrogeol.* **28**(Supplement 2), S143–S150 (1995)
- Bruce, W.F., Walsh, J.B., Frangos, W.T.: Permeability of granite under high pressure. *J. Geophys. Res.* **73**(6), 2225–2236 (1978)
- Patsouls, G., Gripps, J.C.: An investigation of the permeability of Yorkshire chalk under differing pore water and confining pressure conditions. *Energy Sources* **6**(4), 321–334 (1982)
- Walsh, J.B.: Effect of pore pressure and confining pressure on fracture permeability. *Int J Rock Mech Min Sci Geomech* **18**(5), 429–435 (1981)
- Choi, C.S., Cheon, D.S., Song, J.J.: Effect of pore and confining pressure on the supercritical CO₂ permeability of sandstone: Implications for the effective pressure law. *J Geophys Res Solid Earth* **122**(8), 6231–6246 (2017)
- Caulk, R.A., Ghazanfari, E., Perdrial, J.N., Perdrial, N.: Experimental investigation of fracture aperture and permeability change within enhanced geothermal systems. *Geothermics* **62**, 12–21 (2016)
- Kamali-Asl, A., Ghazanfari, E., Perdrial, N., Bredice, N.: Experimental study of fracture response in granite specimens subjected to hydrothermal conditions relevant for enhanced geothermal systems. *Geothermics* **72**, 205–224 (2018)



Petrophysical Properties Modeling Using the Geostatistical Approach: Case Study of Barito Basin, Indonesia

Abdul Haris, Brianto Adhie Setya Wardhana,
Grace Stephani Titaley, and Agus Riyanto

Abstract

The Salemba Field is the largest productive oil field in Barito Basin. This field is located in the north-eastern area of Barito Basin. An improvement was required for the Field development, either from the geology, reservoir, or production aspect. The aim of this study is to build a reliable static reservoir model that can match the production history when it was simulated in the simulation reservoir. In this study, the targeted reservoirs were in the A and B zones, which have the biggest oil production. The A and B zones represent the most productive units in the synrift filling sequence in Tanjung Formation, which mainly comprises medium to coarse grained sandstone, well to moderately sorted volcanic litharenitic and feldspathic litharenitic sandstone, and volcanic pebble-dominated conglomerates. These reservoir zones are separated by a continuous shale break indicating differences in the depositional event. Modeling the distribution of A and B zones was guided by a detailed well-to-well correlation, tracer data and production history as a data constraint. The integrated interpretation of these data was then used to derive net sand maps which were used as trends to guide geomodel facies and properties modeling. After building the conceptual reservoir element distribution model, geostatistical analysis for facies parameter population was conducted. Probability distributions for net sand maps and vertical proportion curves for facies distribution variability were also constructed. The reservoir rock type is defined by Flow Zone Index (FZI) equation combined with geology facies

interpretation. The rock type will guide to generate permeability transform and J-function equation to distribute permeability (k) and water saturation (S_w) in the model. Our experiment shows that the model has a good agreement with the geological interpretation and production data. In addition, the base case model represents the best estimation. This model has been analyzed using a dynamic model and has shown a good simulation.

Keywords

Facies • Geostatistical • Dynamic model • Barito basin • Indonesia

1 Introduction

The Salemba Field is the largest productive oil field in the Barito Basin. This field is located in the north-eastern area of the Barito Basin [1]. The Salemba field has been producing since 1939 and has implemented a full-scale water flood project since 1995 in the A and B zones of the clastic reservoir. The field is defined by a thrust fault as a major fault and trapped in an asymmetrical anticline with a northeast-southwest direction. The driving mechanism which controls this area is the solution gas drive with weak water drive. An improvement was required for the Salemba Field development, either in geology, reservoir, or production. The best plan of development strategies can be achieved through a better understanding of the reservoir and making the reliable static model close enough to the real conditions.

The Barito basin is located along the southeastern edge of the Sundaland continent. The area is situated on the back-arc region, bounded by foredeep at the front zone of Meratus High in Sundaland. This basin is separated from other basins by Meratus High in the East, from Kutei basin by the Adang Flexure in the North, and it extends to the Java Sea in the South [2].

A. Haris (✉) · A. Riyanto
Geology and Geophysics Study Program, FMIPA Universitas
Indonesia, Depok, 16424, Indonesia
e-mail: abdharis@sci.ui.ac.id

B. A. S. Wardhana
Reservoir Geophysics Program, Department of Physics, FMIPA
Universitas Indonesia, Depok, 16424, Indonesia

G. S. Titaley
PT Pertamina EP, Jakarta, Indonesia

In the foredeep, the structural style is characterized by basement-involved tectonics, in which the folds are originated as faults-related folds. The structure is characterized by parallel trends of folds and faults that repeat in closely-spaced wavelike bands constituting the belt. The folds are bounded by high-angle westerly-hanging reverse faults. The structures increasingly imbricate towards the Meratus Range. Beyond the foredeep approaching Sunda-land, the basement is devoid of tectonics influence; otherwise the thin-skinned tectonics indicated by discontinuous decollements, ramps, and fault-propagation folds may have taken place [1].

The structural history of the East Barito Basin is marked by a great contrast in style between the Paleogene and Neogene. Rifting of the basement started structuring the basin in Plaeo-Eocene time [3]. The condition prevailed up to Oligo-Miocene time, during which localized and regional subsidence and lithospheric stretching impressed the basin. By mid Miocene time, the prevailing structural style changed to a more contracting nature. Regional uplift and compressional faults appeared in middle Miocene time up to Plio-Plistocene time, inverting and reactivating old extensional faults, resulting in the positive features typifying the area today.

2 Facies Determination

All of the available supporting data of this field have been used for this study. These data include static and dynamic data, from more than 100 well log data, with five wells being cored in each zone (RCAL and SCAL analysis of core data). Not only well data, the 3D seismic data analysis was also

included in building the static model. Furthermore, this study integrates dynamic data (daily production and productivity index of each well) to create a good static modeling. So, this static model can run synchronous with real data current and simulation.

Generally, A and B reservoirs represent the changes of depositional environment due to sea level change. The following paragraph provides detailed information about the facies and depositional environment of each reservoir in the Salemba Field.

The A sand represents the most productive unit in the Syn-rift fill sequence, and comprises mainly medium to coarse grained, well to moderately sorted volcanic litharenitic and feldspathic litharenitic sandstone, and volcanic pebble dominated conglomerated [3]. Only minor claystone and siltstone were recognized in the cores and wireline logs also indicate a marked scarty of finer grained argillaceous sediments. In the lower part of the A zone, massive conglomerates with fewer sands were deposited as longitudinal bars in a braided stream in a mid-alluvial fan setting/Massive coalesced laterally extensive gravel sheets enclose sandstone bodies over a limited lateral extent. Interconnectivity and reservoir properties largely depend on storage and flow capacities in the conglomerates. In the upper A zone, cross-bedded sands were deposited as transverse bars in lower (Fig. 1), distal alluvial fan setting/Massive coalesced sand sheets are separated by few laterally extensive conglomerates. Reservoir properties and good interconnectivity reflect storage and flow capacities of the sandstone. The sandstones demonstrate a similar, medium to poor reservoir quality, but the conglomerate shows a poor to fair quality. Fan deposits will pass distally into the braid plain and meandering fluvial sand sheets enclosed in fine clastic

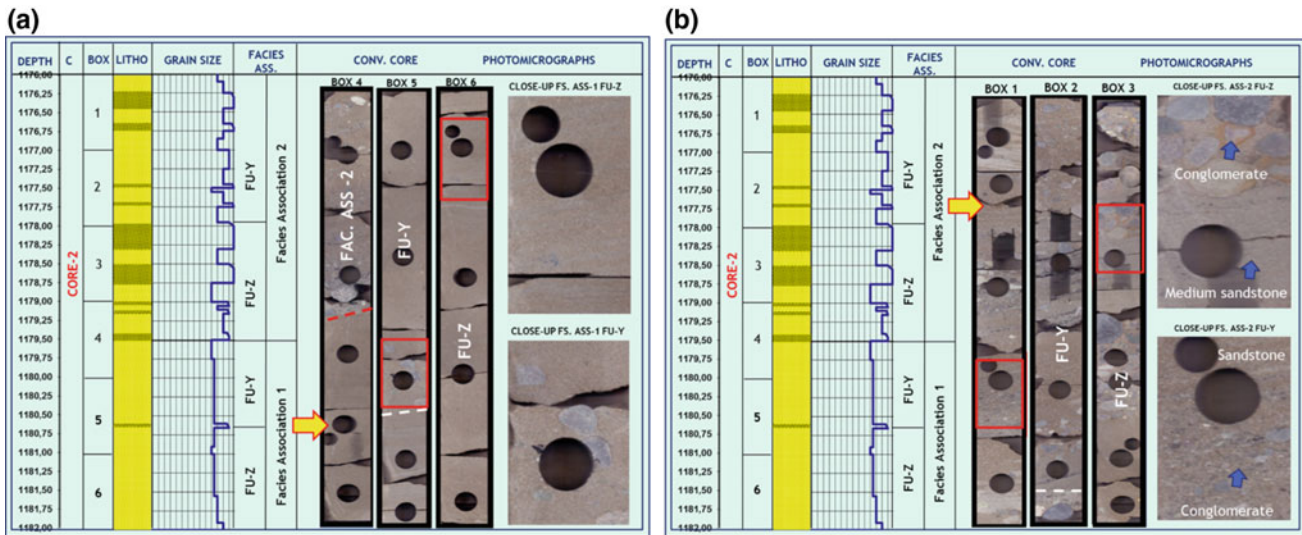


Fig. 1 Facies determination from cores data analysis

overbank sediments, and/or lacustrine deposits which may include small mouth-bar sand bodies.

The B sand occurs immediately above the A sand in the Syn-rift fill sequence. It is compositionally and texturally very similar to A sand, comprising mainly medium to coarse grained, well to moderately sorted volcanic litharenitic with lesser feldspathic litharenitic sandstone, and volcanic pebble dominated conglomerates. In the lower B zone, tabular cross-bedded stacked sands with fewer conglomerates were deposited as transverse bars in braided stream systems in a distal alluvial fan setting. In the upper B zone, pebble conglomerates with minor tabular cross-bedded sandstones were largely deposited as longitudinal gravel bars in a mid-fan setting. Sand body geometry, associated facies distribution, provenance, diagenesis and resultant reservoir properties are similar to those of the A Sand.

3 Static Modeling

The facies modeling is conducted based on the result of the geological analysis. The reservoirs are divided into four types of facies; shale, sandstone transverse bar, sandstone longitudinal bar, and conglomerate braided river. The division of facies was based on core data analysis, pattern of gamma ray log, resistivity log, density log and neutron porosity log.

The reservoirs zone is separated by a continuous shale break that marked the differences in the depositional event [4]. Modeling the distribution of A and B zones was guided by a detailed well to well correlation, a tracer data survey with production data constraints. The integrated interpretation of these data was then used to derive net sand maps

which were used as trends to guide the geomodel facies and properties modeling. After building the conceptual reservoir element distribution model, a geostatistical analysis for facies parameter population was conducted. Probability distributions for net sand maps and vertical proportion curves for facies distribution variability were also constructed. The facies modeling has been made by integrating all well data analysis with variogram analysis. The distribution in the reservoir zone used the sequential indicator simulation (SIS) method, and it was guided by a trend modeling analysis with sense of geology facies distribution. Figure 2 shows the result of facies modeling in zones A and B, and it shows a good correlation with depositional direction of geology regional.

Reservoir properties (volume of shale, porosity, rock type and permeability), as shown in Fig. 3, were built with the Sequential Gaussian Simulation (SGS) method. The SGS method is one of the statistical methods to create a petrophysical model in 3D, with normal distribution and variogram data analysis. The permeability was modeled using the transformation between permeability from core data and FZI. FZI is a unique and useful value to quantify the flow character of a reservoir and it is one that offers relationships between petrophysical properties. FZI provides the representation of the flow zones based on the surface area and tortuosity. We first examined the nature of relationships between permeability and porosity from core data, and we split these data according to two ways: the geological facies determination, and the hydraulic unit defined by the Flow Zone Indicator (FZI) [4]. Then, we extended the porosity-permeability relationship to production data using the Production Logging Tool (PLT) measurement and

Fig. 2 Facies model distribution results of zones A and B

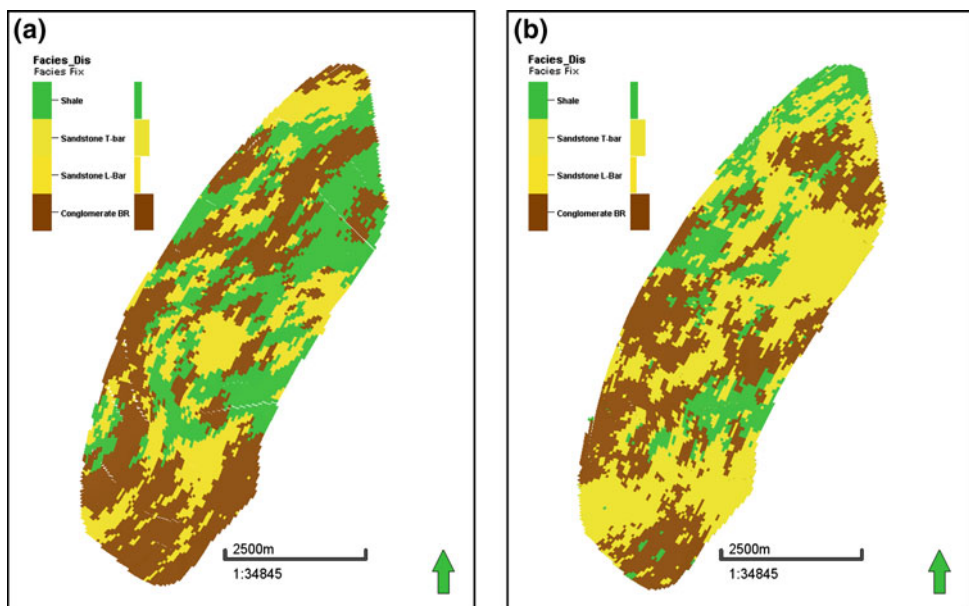
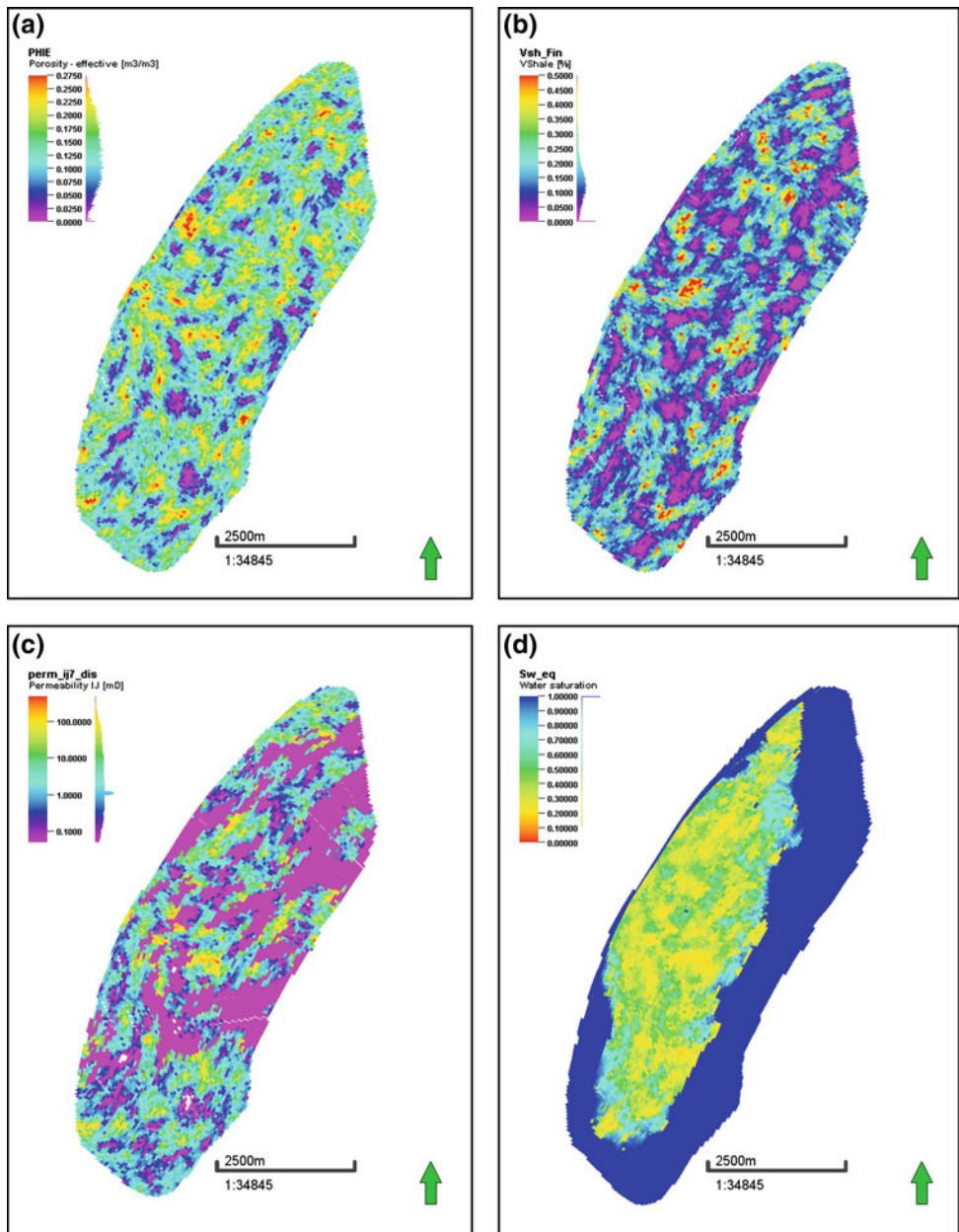


Fig. 3 Distribution results of vshale model, porosity model, rock type model, permeability model and water saturation model in zones A and B



applied it to well log data (petrophysical calculation). We found the relationship of geological facies and Hydraulic Flow Unit (HFU) with production data. The result is the permeability transform of each facies or rock type as a parameter to be an input to build permeability model.

Water Saturation was built from the trends of secondary data, from the calculation of J-function. In order to average capillary pressure curves obtained from laboratory measurements for several core samples, this study used Leverett's J-function. This is a dimensionless function that correlates capillary pressure with other reservoir parameters including permeability, porosity, interfacial tension and contact.

The history matching process was conducted by changing some parameters properties globally. Then, we will focus on some regional block and well basis. Because this model consists of four layers, with each one having two rock types and a high vertical heterogeneity, the parameter of rock types was used to classify the grid. The grid properties have been changed when history was globally matched or when the grid properties near the wells changed.

The sensitivity properties process has been done in global matching for compressibility and transmissibility, while at the regional level, the sensitivity properties are regional transmissibility, regional PV, Swc, and inter block Kr versus Sw curve for matching breakthrough time. The last matching

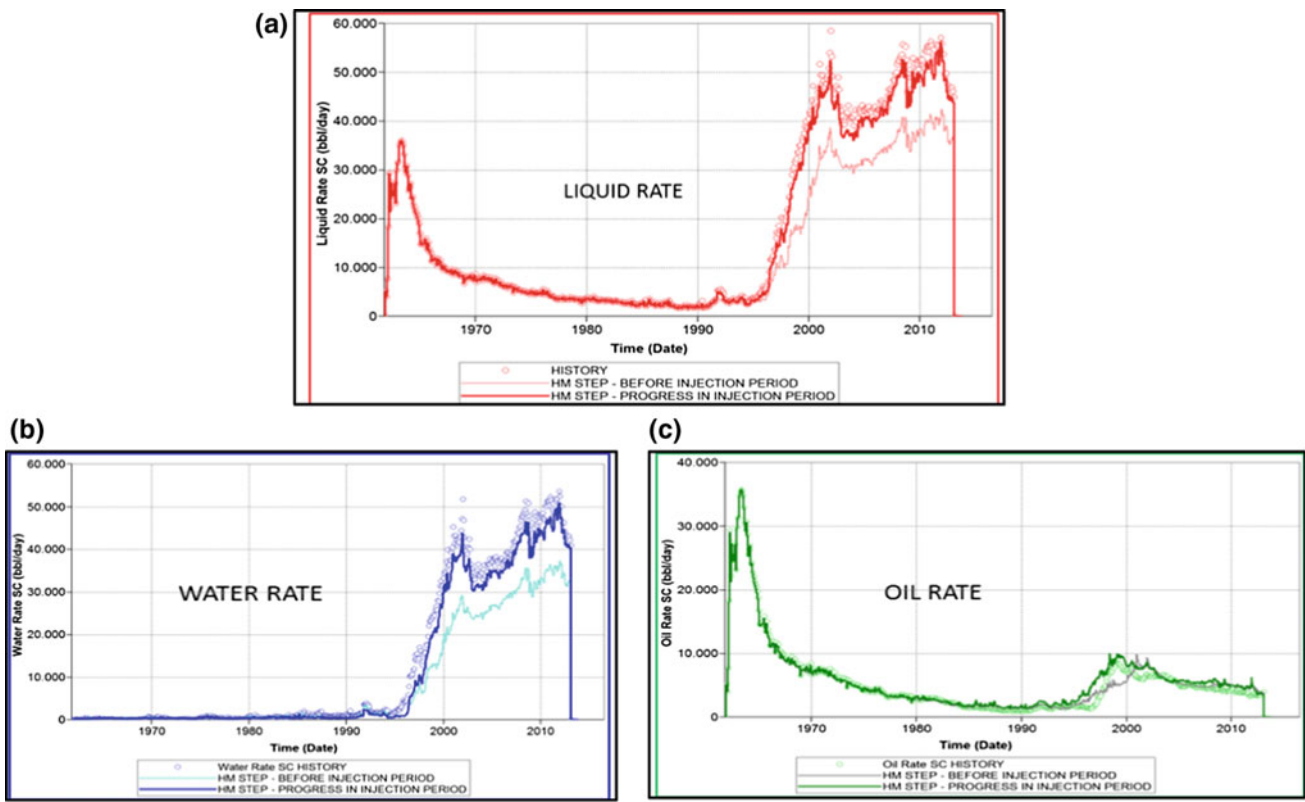


Fig. 4 Pre-primary simulation result from static model of Zones A and B

process is the sensitivity on the well basis. This sensitivity used the same concept as the regional matching, in addition to PI sensitivity, multiplied to meet the rate of production, when pumps were used, and the hydraulic fracturing, when the injection began in 1995. Figure 4 shows the result of the pre-primary run from static model. History matching results show a good history match with the production history, liquid rate, water rate and oil rate.

4 Conclusion

The A and B reservoirs are divided into 4 types of facies; shale, sandstone transverse bar, sandstone longitudinal bar, and conglomerate braided river. Detailed petrophysical modeling, along with an accurate method for distribution, was the key to creating this static modeling. To create a good 3D static model, the study must be included with static and dynamic data (current production). These reservoir characterization and simulation studies were performed to integrate geology, petrophysics, 3D seismic and engineering data into technically-sound 3D geologic and engineering models. This

model has been analyzed using a dynamic model (history matching and production forecasting) in accordance with the relative permeability end point and it has shown a good simulation.

References

1. Satyana, A.H., Silitonga, P.D.: Tectonic reversal in East Barito Basin, South Kalimantan: consideration of the types of inversion structures and petroleum system significance. In: Indonesian Petroleum Association, Proceedings 23rd Annual Convention, 1994
2. Sumotarto, T.A., Haris, A., Riyanto, A., Usman, A.: Shale Characterization on Barito field, Southeast Kalimantan for Shale Hydrocarbon Exploration
3. Kusuma, I., Darin dan, T.: The hydrocarbon potential of the lower Tanjung formation, Barito Basin, SE Kalimantan. In: Proceedings of the Indonesian Petroleum Association, 18th Annual Convention, 1989
4. Deghirmandjian, O.: Identification and Characterization of Hydraulic Flow Units in The San Juan Formation, Orocua Field, Venezuela. Thesis for Master Degree. (Texas A&M University, 2001)

Part III

Enhanced Oil Recovery Methods

Considerable Influence of Reservoir Properties on the Production Flow Rate During Low Salinity Water Flooding

Afshin Davarpanah

Abstract

Low salinity water flooding (LSW) is considered as the major proposed EOR technique in which the salinity percentage of the injected water is adjusted in order to improve oil displacement efficiency; that is to say LSWI is considerably influenced by the oil recovery factor regarding altering the wettability condition. The amount of Total Field Oil production (FOPT), Total Field Gas production (FGPT), Field Pressure Ratio (FPR) and Field Gas-Oil Ratio (FGOR) were simulated for 7400 days while taking into consideration four parameters including NTG, porosity, rock compressibility and permeability in Z direction. As a result, rock compressibility and permeability in Z direction have less impact on the amount of FOPT, FGPT, FPR and FGOR. Moreover, NTG and Porosity have significantly affected each of the aforementioned factors.

Keywords

LSWI • Porosity • Permeability Z • Rock compressibility • Oil production • Gas production

1 Introduction

Enhanced oil recovery techniques and their appropriate procedures exert a considerable influence on the volume of produced oil. During the drilling operation of an oilfield, natural drive mechanisms have played a substantial role in the first years of production. On the other hand, after the years of production, the energy of natural mechanisms drastically reduces due to the insufficient bottomhole pressure. Subsequently, there is a sense of urgency to utilize artificial recovery methodologies like secondary and tertiary

A. Davarpanah (✉)
Department of Petroleum Engineering, Science and Research Branch, Islamic Azad University, Tehran, Iran
e-mail: Afshin.Davarpanah@srbiau.ac.ir

processes to move the captured oil to the productive wells and improve the production rate. Enhanced oil recovery techniques involve the addition of extra materials such as chemical and non-chemical substances to stimulate the wells [1–7].

2 Methods

To develop a reservoir model, the required steps are being considered specifically to ease the enhancement processes properly. These steps consist in electing the proper simulator for modeling and estimating the processes analytically; a stunning range of data should be gathered to check the validity of the model; history matching and sensitivity analysis; efficient anticipation for operation of the projects and extensive literature studies to have considerable experiences of reservoir fundamentals. Based on field reports, which are taken from laboratory and experimental evaluations, the reservoir is a saturated fracture reservoir. In this reservoir three wells have been drilled; two wells were vertical and the other was horizontal. More details regarding the studied well are mentioned in Table 1.

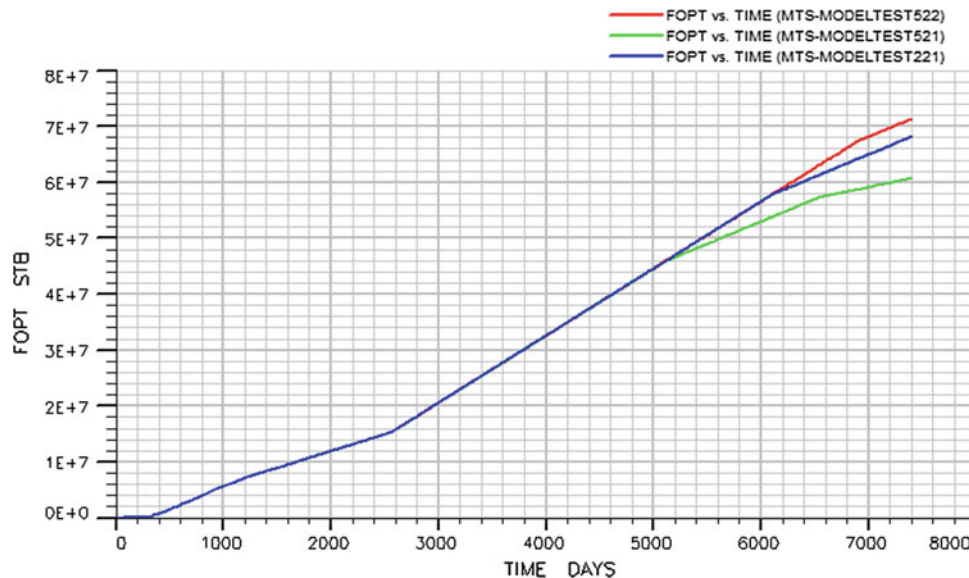
3 Results and Discussion

In this part of the study, different scenarios are being investigated in which each parameter has played a significant role in the optimum economical production of a reservoir. Four divergent scenarios including Net to Gross (NTG), Permeability, Rock Compressibility and porosity were studied in three color ranges that entailed max, min and default preface of Eclipse software. As can be seen in Fig. 1, the rate of FOPT has increased dramatically over time, rising to the amount of $NTG = 1.5$, so as to have the maximum amount of $FOPT = 7.1 \times 10^7$. Furthermore, the minimum amount of $NTG = 0.5$ is simulated to approximately 6.8×10^7 which is relatively considered the same. FGPT

Table 1 Reservoir fluid properties

Parameter	Differential liberation test value	Unit
Test temperature	180	°F
Bubble point pressure	3715	Psia
Oil formation volume factor at bubble point pressure	1.6822	Bbl./STB
Density of total gas evolved at standard condition	1.1761	Gal/L
Density of stock tank at standard condition	0.8575	Gr/cc
Density of reservoir fluid at bubble point pressure	0.6636	Gr/cc
Gas oil ratio at standard condition	1230.22	SCF/STB
Average compressibility factor	15.54	psi ⁻¹ * 10 ⁻⁶
Average thermal exponent factor	7.26	F ⁻¹ 10 ⁻⁴

Fig. 1 The rate of FOPT versus time for three testing models (NTG evaluation)



has the same trend in raising the amount versus time but it slightly varies in the prefaced NTG numbers (Fig. 1). Max and min amounts of NTG are reported as 5.6×10^7 and 5.2×10^7 , respectively.

4 Conclusions

- By increasing the amount of porosity, the amount of FOPT, FGPT, FGOR increases dramatically and it is evident that this parameter directly influences this type of reservoir.
- By increasing the amount of NTG, the amounts of FOPT, FGPT, FGOR increase dramatically in the NTG period of 1–1.5, and it is evident that this parameter directly influences this type of reservoir. On the contrary, the amounts of FOPT, FGPT, FGOR decreased in the NTG period of 0.5–1.

References

1. Alboudwarej, H., Sheffield, J.M.: Development and application of probabilistic fluid property (PVT) models for stochastic black oil reservoir simulation. In: SPE Western Regional Meeting. Society of Petroleum Engineers (2016)
2. Dai, Z., et al.: An integrated framework for optimizing CO₂ sequestration and enhanced oil recovery. Environ. Sci. Technol. Lett. **1**(1), 49–54 (2013)
3. Kothencz, R., et al.: Improvement of the selection method of surfactants and their mixtures for chemical enhanced oil recovery. Chem. Eng. Commun. **204**(4), 440–444 (2017)
4. Mohsenzadeh, A., et al.: Non-hydrocarbon gas injection followed by steam–gas co-injection for heavy oil recovery enhancement from fractured carbonate reservoirs. J. Petrol. Sci. Eng. **144**, 121–130 (2016)
5. Davarpanah, A.: A feasible visual investigation for associative foam-polymer injectivity performances in the oil recovery enhancement. Euro. Polym. J. (2018)

6. Davarpanah, A: The feasible visual laboratory investigation of formate fluids on the rheological properties of a shale formation. *Int. J. Environ. Sci. Technol.* 1–10 (2018).
7. Davarpanah, A., Akbari, E., Doudman-Kushki, M., Ketabi, H., Hemmati, M. Simultaneous feasible injectivity of foam and hydrolyzed polyacrylamide to optimize the oil recovery enhancement. *Energy Explor. Exploit.* 0(0), 0144598718786022. <https://doi.org/10.1177/0144598718786022>

Experimental Investigation of Low and High Salinity Water Injection Simulation and Their Comparison with Pure Water Injection to Determine Optimum Salinity

Afshin Davarpanah

Abstract

Analyzing the sensitivity of high and low salinity, according to the moderately low recovery factor of high and low salinity among injection scenarios, illustrates the low sensitivity of this parameter in a fractured carbonated reservoir. By reviewing different scenarios, it could be demonstrated that if water injection was being applied to the reservoir from the preliminary times of production, the recovery factor rate will increase. Pure water injection has a high recovery factor than salty water injection. By the way, these two methods have a little difference in their recovery calculating methods. Moreover, in water injection methods, if the injection rate of water increases, the recovery factor will increase and give rise to a higher efficiency. Besides, this parameter is significantly dependent on well-head equipment properties, safety factors and economic issues (water production). Analyzing the figures and the volumes of low salinity water injection after the injection of pure water in different injection scenarios showed that all these scenarios have the highest rate of recovery and the maximum production efficiency.

Keywords

Salinity water • Enhanced oil recovery
Recovery factor • LSWI

1 Introduction

Due to the growing population and increasing demand for energy in different areas of life, especially in major industries and in manufacturing, it seems that this God-given and non-renewable resource should be used optimally, and any improper use and application of this energy source is not

only causing problems at the present time but also jeopardizing the survival of future generations [1–5]. Fossil energy, such as oil, gas and coal, which at first glance looks great and endless, is generally not fully recoverable and huge amounts of wealth remain in situ. In general, it depends on the operation at harvest time, such as the speed and method of operation [6]. With the continuous drop in reservoir pressure, the production rate is gradually reduced until the normal production of the reservoir is no longer cost-effective. This point occurs when the oil recovery from the reservoir is relatively low. This recovery for Iranian reservoirs is about 15–20%; in other words, 80–85% of their oil remains in the Formation.

2 Methods

The economic output of the reservoir depends on water cut and wellhead pressure. If the wellhead pressure exceeds a specified level, injection scenarios have to be planned accordingly. Six different scenarios were defined based on the analysis of different degrees of salinity. Scenarios 1, 2, and 3 focus on the impact of salinity on the recovery factor, and scenarios 4, 5 and 6 compare previous scenarios. This study assumes a low salinity of 5 g/kg (density, 1005 kg/m³ and 1.15 cP at 15 °C) and a high salinity of 40 g/kg (density 1030 kg/m³ and viscosity 1.23 at 15 °C).

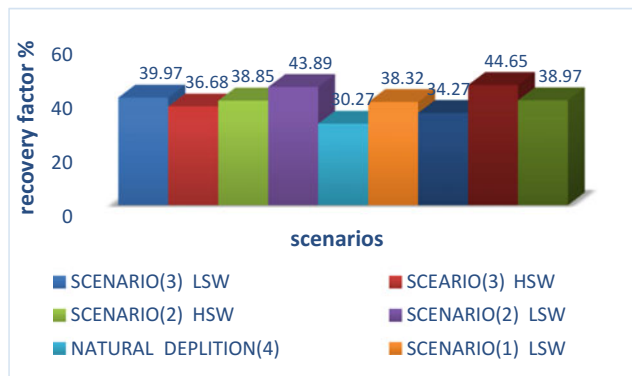
3 Results and Discussion

1. Among the different scenarios of water injection, scenario no. 5 with an injection rate of 2000 barrels per day is the best known injection plan (Fig. 1).
2. In case of a low salinity scenario, better support and performance efficiency results in marginal recovery.

A. Davarpanah (✉)

Department of Petroleum Engineering, Science and Research Branch, Islamic Azad University, Tehran, Iran
e-mail: Afshin.Davarpanah@srbiau.ac.ir

Fig. 1 Various scenarios of water injection and natural depletion mode



3. Water injection from the beginning of production supports better and higher efficiency performance.
4. Higher injection rate results in higher recovery.
5. Low salinity levels in all injection scenarios and maximum production efficiency result in the highest rate of recovery.

4 Conclusions

As time passes and production decreases significantly, the difference in salinity between the top and the bottom of a reservoir (before and after production) increases, which reflects the effects of high salinity water injection with time. Injection of pure water results in a higher recovery factor than low salinity water injection, although the difference in the recovery factors is less. This injection rate applies in both 1000 and 2000 barrels per day.

References

1. Zeinijahromi, A., Ahmetgareev, V., Ibatullin, R., Bedrikovetsky, P.: Sensitivity study of low salinity water injection in Zichebashkoe oilfield. *J. Petrol. Gas Eng.* **6**(1), 10–21 (2015)
2. Al-Shalabi, E.W., Sepehrnoori, K.: A comprehensive review of low salinity/engineered water injections and their applications in sandstone and carbonate rocks. *J. Petrol. Sci. Eng.* **139**, 137–161 (2016)
3. Teklu, T.W., Alameri, W., Graves, R.M., Kazemi, H., AlSumaiti, A. M.: Low-salinity water-alternating-CO₂ EOR. *J. Petrol. Sci. Eng.* **142**, 101–118 (2016)
4. Davarpanah, A., Zarei, M.: Analysis of enhanced oil recovery methods like gas injection in the fractured reservoirs and optimize its efficiency. *J. Mater. Sci. Eng.* **6** (2017)
5. Dang, C., Nghiem, L., Nguyen, N., Chen, Z., Nguyen, Q.: Mechanistic modeling of low salinity water flooding. *J. Petrol. Sci. Eng.* **146**, 191–209 (2016)
6. Davarpanah, A.: Evaluation of gas injection in the horizontal wells and optimizing oil recovery factor by Eclipse software. *J. Chromatogr. Sep. Tech.* **7** (2016)

Experimental Investigation of the Performance of Low Salinity Water Flooding at High Temperature

Hasan N. Al-Saedi and Ralph E. Flori

Abstract

The potential of divalent cation Mg^{2+} in formation water (FW) for low-salinity (LS) EOR effect was previously investigated [Al-Saedi et al. in Oil recovery analyses and formation water investigations for high salinity-low salinity water flooding in sandstone reservoirs. SPE, 190845, 2018 1], where the increase in divalent cations in FW lowered the effect of LS water. In this study, we studied the importance of the same divalent cation (Mg^{2+} only) in the injected water. Berea sandstone cores were successfully flooded with FW and LS water at 130 °C. While injecting both brines, samples of the effluent were analyzed for pH. Oil recovery experiments with a double Mg^{2+} concentration showed a lower LS water effect, meaning that the cores became more water-wet; however, the LS water effect was much greater when the amount of Mg^{2+} in the HS water was decreased by half.

Keywords

EOR • LSW • Petroleum geochemistry

1 Introduction

Experimental and field scale projects indicate that incremental oil recovery by Lo-Sal water injection varies significantly case-by-case in sandstone [2]. The experimental observations of Tang and Morrow [3] for LS water flooding set out conditions for how LS water works. The conditions were: (1) the crude oil must contain acid and base numbers and (2) sandstone should contain clay such as illite and

kaolinite. After several years, McGuire [4] and Lager and Webb [5] added another condition, which was that divalent cations must be present in the FW. The second condition of Tang and Morrow was no longer valid after the investigations of Al-Saedi and Brady [6] and Sohrabi [7]. The observations from chromatographic columns of quartz showed an increase in the acetate detachment from the quartz surface [6]. The oil recovery observations from the quartz column supported the proposed mechanism [8]. Lager and Webb [5] examined the effect of LS water during brine injection into a sandstone oil reservoir that had an identical amount of Mg^{2+} in the injected brine and formation water. Fluid–fluid interaction has been considered as one of the mechanisms for sand-stone [9]. The objective of this study is to investigate the role of the Mg^{2+} in both FW and LS water at a high temperature.

2 Materials and Methods

Reagent-grade salts were prepared with deionized water to make FW and LS water. The compositions of brines and core are listed in Table 1. Crude oil was delivered by Colt Energy from one of the Kansas oil fields (Bartlesville sandstone reservoir). The viscosity of the oil was 14 cp at 20 °C, and the density was 0.815 g/cc at 20 °C. The experimental setup is shown in Fig. 1. Berea sandstone was used in this study. The FW salinity in the reservoir is close to the synthetic brine we made at our laboratory, but there was no source of LS water in the field (Table 2).

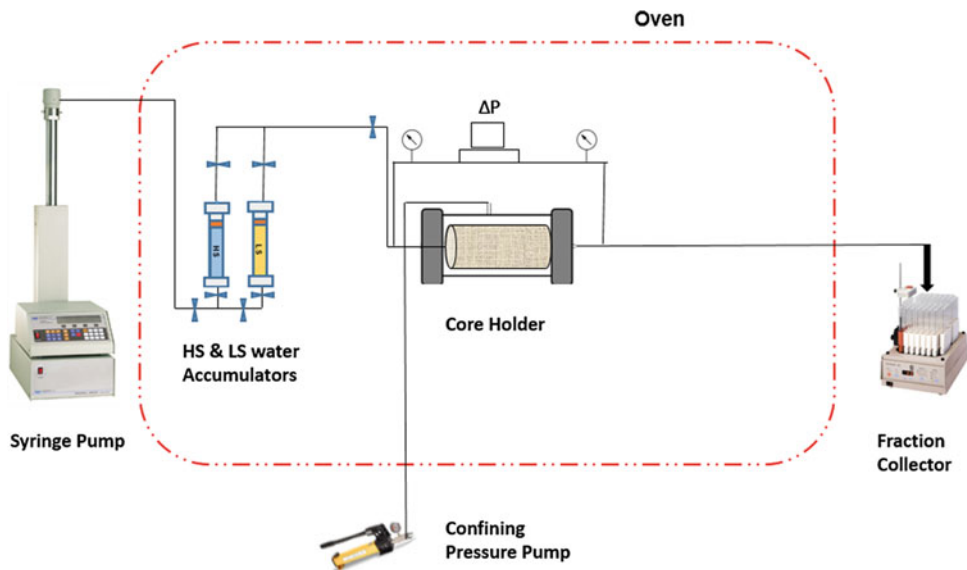
The cores were mounted in the core holder and left overnight for thermal equilibrium purpose. The Berean sandstone cores were flooded with 2 PV FW (96,100 ppm) as a secondary flooding, and then, 2 PV LS water (4000 ppm) was injected for the tertiary stage at a constant rate. While injecting brines, samples of the effluent were analyzed for pH. The injected FW and LS water pH were 7.36 and 7.66. The experiments were conducted as follows:

H. N. Al-Saedi (✉) · R. E. Flori
Department of Geosciences and Geological and Petroleum Engineering, Missouri University of Science and Technology, Rolla, MO 65401, USA
e-mail: hnav36@mst.edu

H. N. Al-Saedi · R. E. Flori
Missan Oil Company, Missan, 62001, Iraq

Table 1 Core properties and water description

Core	Quartz (%)	Kaolinite (%)	D (cm)	L (cm)	K (md)	ϕ (%)	Mg ²⁺ in FW (mM)	Mg ²⁺ in LSW (mM)	NaCl (mM)
Core A	95	5	2.54	14.77	~ 100	~ 21	90	30	3000
Core B				14.67			90	9	3000

**Fig. 1** Core flooding setup**Table 2** Oil recovery results for both FW and LS water flooding

Core	Ca ²⁺ in FW (mmole)	Mg ²⁺ in FW (mmole)	Mg ²⁺ in LSW (mmole)	Secondary oil recovery by FW (%)	Secondary residual oil saturation S _{or} (%)	Tertiary oil recovery by LSW (%)	ΔS _{or} (%)
Core A	0	90	30	52.5	47.5	0	47.5
Core B	0	90	9	52.2	47.8	1.5	46.3

- Core A was saturated with FW containing 90 mol Mg²⁺, and then flooded with the same FW followed by LS water containing 3 times diluted Mg²⁺ of the Mg²⁺ in FW at 130 °C.
- Core B was saturated with FW containing 90 mol Mg²⁺, and then flooded with the same FW followed by LS water containing 10 times diluted Mg²⁺ of the Mg²⁺ in FW, while keeping the salinity of the LS water the same as in core A by adding NaCl.

even at high concentrations. As the concentration of the divalent cations increases in the FW, the sandstone turned more water-wet and less LS EOR effect was observed. In the present study, the focus was on the divalent cations in the injected LS water. The oil recovery results have been discussed in relation to the concentrations of the injected divalent cations.

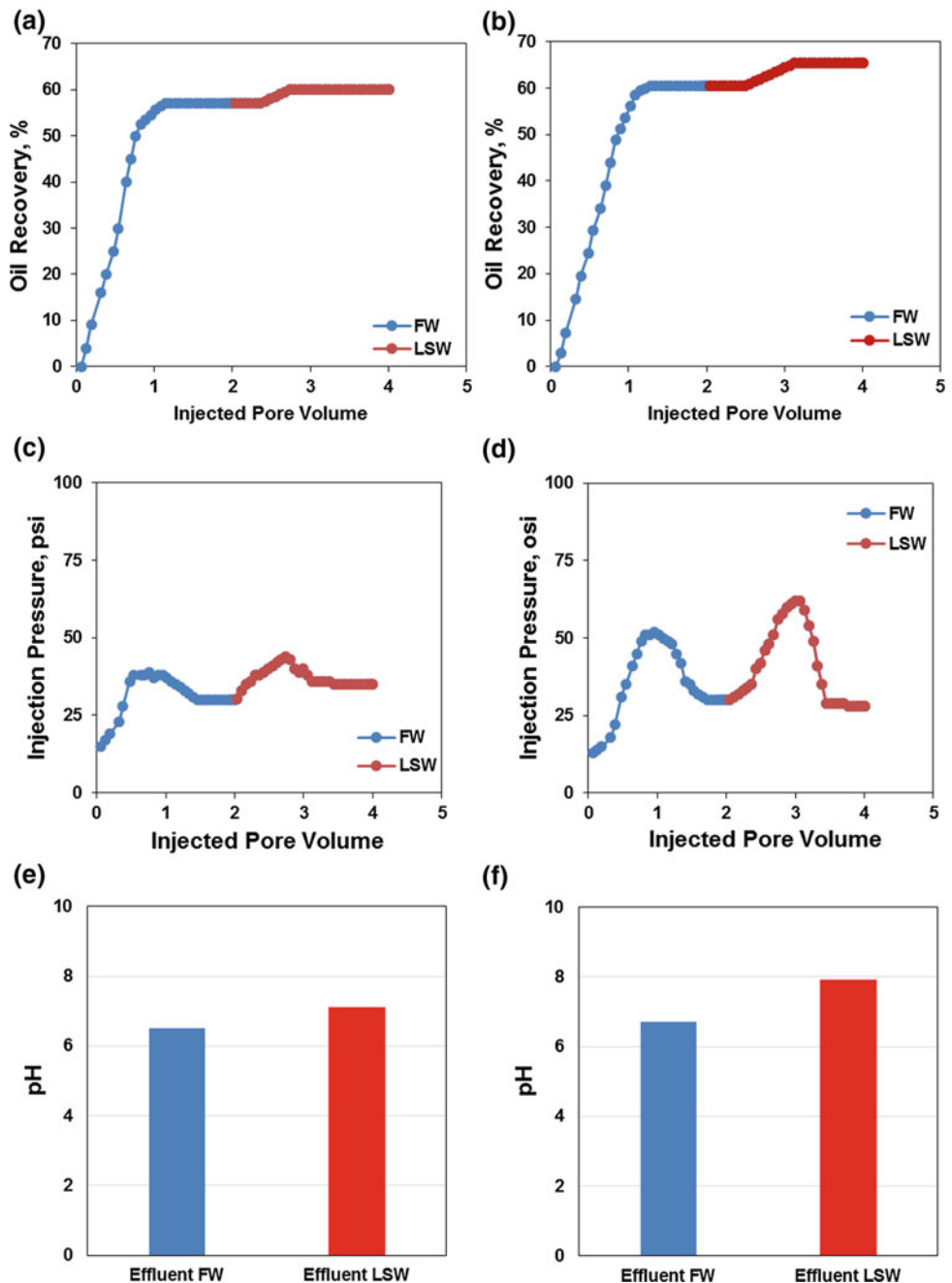
Oil Recovery Results

Core A. The outcrop core A was sequentially flooded with FW and LS water at 130 °C. The incremental oil recovery was 3% of OOIP during LS water flooding (d_{3Mg}^{2+}), after core A was flooded in secondary stage with FW. The ultimate oil recovery remained constant at 57% OOIP (Fig. 2). The measurements of the pH were logged for the FW and LS water. The pH reading for FW effluent was 6.5,

3 Results and Discussion

Previously [1], we examined the role of the divalent cations (Ca²⁺ and Mg²⁺) in the FW on the LS EOR and found that the role of the Mg²⁺ in FW is more effective than the Ca²⁺

Fig. 2 **a** Core A oil recovery, **b** core B oil recovery, **c** core A injection pressure, **d** core B injection pressure, **e** core A effluent pH, and **f** core B effluent pH. Core A and core B saturated in FW containing 90 mol Mg^{2+} and the rest NaCl. Core A and core B flooded with FW followed by LSW containing d_{3Mg}^{2+} and d_{10Mg}^{2+} . The FW salinity is 96,100 ppm and the LSW salinity is 4000 ppm



which must be sufficiently low to promote adsorption of polar components onto the sandstone surface. The injection pressure was 39 psi during the FW flood. The LS water injection pressure decreased to 44 psi (Fig. 2).

Upon switching to LS water, the pH of the LS water effluent increased to 7.1, which was a small pH increment due to the high concentration of Mg^{2+} in the injected LS brine, demonstrating very low wettability alteration. According to Lager and Webb [5] and Brady and Morrow [10], the difference in the upward shift in effluent pH between HS and LS water is traditionally ascribed to the

exchange of H^+ for divalent cations on clay surfaces. Our previous work showed a similar attitude on both free-clay sandstone and rich-clay sandstone [6]. More water-wet sandstone would be introduced due to that pH jump. It seems the core wettability has not been altered by the injected LS water because of the high concentration of the Mg^{2+} . Mg^{2+} was responsible for the low pH in the LS water effluent, and in turn, no additional oil recovery was obtained.

Core B. The core B was flooded the same way as in core A but with d_{10Mg}^{2+} LSW water. As pointed previously, core A and core B were saturated with FW containing 90 mol Mg^{2+} .

The oil recovery during FW forced imbibition reached a plateau at 60.5% OOIP. The oil recovery was similar to core A because they are both alike in their petrophysical properties and core preparations. Upon switching to LS water, the incremental oil recovery was 5% of OOIP (Fig. 2). The initial pH of the FW was 6.71, and the pH increased to 7.93 when switching to LS water, which was significantly higher than for core B. The pH during FW flooding provided a favorable environment for creating mixed-wet media. The pressure profile had similar behavior to that in core A. The same procedure was conducted at a lower temperature in a previous work [11] at a lower temperature and the trend was the same. The higher temperature prompts a higher recovery due to reducing oil viscosity. We believe that the abundance of the Mg²⁺ in the injected LS water could reduce the oil recovery from sandstone.

4 Conclusions

- When Mg²⁺ exists in the LS water, there is no oil recovery improvement during LS water flooding. There is no pH jump. It seems that Mg²⁺ disrupts LS water EOR effect.
- The experiments showed that Mg²⁺ is favorable for secondary oil recovery when the Mg²⁺ is presented in the FW and the injected FW during secondary flooding.
- An abundance of Mg²⁺ in the injected LS water could provide 0% in oil recovery improvement but diluting the Mg²⁺ to 10 times could improve the oil recovery.

References

- Al-Saedi, H.N., Flori, R.E., Brady, P.V., Al-Jaber, S.: Oil recovery analyses and formation water investigations for high salinity-low salinity water flooding in sandstone reservoirs. In: SPE, 190845 (2018)
- Lager, A., Webb, K.J., Collins, I.R., Richmond, D.M.: LoSal enhanced oil recovery: evidence of enhanced oil recovery at the reservoir scale. In: SPE, 113976 (2008)
- Tang, G.Q., Morrow, N.R.: Influence of brine composition and fines migration on crude oil brine rock interactions and oil recovery. *J. Pet. Sci. Technol.* **24**, 99–111 (1999)
- McGuire, P.L., Chatham, J.R., Paskvan, F.K., Sommer, D.M., Carini, F.H.: Low salinity oil recovery: an exciting new EOR opportunity for Alaska's North Slope. In: SPE, 93903 (2005)
- Lager, A., Webb, K.J., Black, C.J.J., Singleton, M., Sorbie, K.S.: Low salinity oil recovery—an experimental investigation. In: International Symposium of the Society of Core Analysts, Trondheim (2006)
- Al-Saedi, H.N., Brady, P.V., Flori, R.E., Heidari, P.: Novel insights into low salinity water flooding enhanced oil recovery in sandstone: study of the clay role. In: SPE, 190215 (2018)
- Sohrabi, M., Mahzari, P., Farzaneh, S.A., Mills, J.R., Tsolis, P., Ireland, S.: Novel insights into mechanisms of oil recovery by use of low-salinity-water injection. In: SPE, 172778-PA (2017)
- Al-Saedi, H.N., Almansour, A., Flori, R.E., Brady, P.V.: Evaluation of EOR LS water flooding in sandstone: eliminate the role of clay. In: Saudi Arabia Annual Technical Symposium and Exhibition held in Dammam, Saudi Arabia, pp. 23–26 (2018)
- Tetteh, J.T., Rankey, E., Barati, R.: Low salinity water-flooding effect: crude oil/brine interactions as a recovery mechanism in carbonate rocks. In: Offshore technology conference, 24 Oct 2017. <https://doi.org/10.4043/28023-ms>
- Brady, P.V., Morrow, N.R., Fogden, A., Deniz, V., Loahardjo, N. W.: Electrostatics and the low salinity effect in sandstone reservoirs. *Energy Fuels* **29**(2), 666–677 (2015)
- Al-Saedi, H.N., Flori, R.E.: Experimental investigation of the performance of low salinity water flooding as a novel enhanced oil recovery. *Eng. Technol. J.* (2018)



Effect of Rising Reservoir Temperature on Production of High-Viscosity Oil

Vladimir Astafev, Valeria Olkhovskaya, Sergey Gubanov, Kirill Ovchinnikov, and Victor Konovalov

Abstract

Production of high-viscosity oil and design of field development systems for such oil is one of the most promising directions in the development of world oil industry. As a rule, oil of this class has pronounced structural-mechanical properties. Nonlinear relationship between the pressure gradient and the rate of oil flow is due to the interaction of high-molecular substances, in particular, asphaltenes and tars that form a plastic structure in it. We have used the analytical model of stationary influx of nonlinear viscoplastic oil to the well bottom in order to provide rationale for the intensifying impact on a reservoir. We have also analyzed the method of periodic heating of a productive reservoir by means of dual-wells. The suggested method of systemic treatment of reservoirs with dual wells can be useful for fields of high-viscosity oil.

Keywords

High-viscosity oil • Thermal treatment • Non-Newtonian system • Dual-well system • Rheological characteristic

1 Introduction

Global prospects for development of the world fuel and energy complex are associated with extraction of high-viscosity oil today. Application of treatments in the near-well reservoir compartments allows to increase production well flow rates, while the features of high-viscosity oil as a rheologically complex system require special impact technologies [1]. The non-linear nature of the dependence of the rheological flow parameters on the pressure gradient

created in the near-wellbore zone (NWZ) shall be taken into account in mathematical models of inflow and in methods of predicting the technological effectiveness of impacts on the NWZ.

2 Theoretical Background

Various equations have been proposed for modeling the stress-strain state of viscoplastic fluids which is completely described in [2–7]. Experimental rheological studies have established a deviation from Newton's law of viscous friction, namely, violation of the linear relationship between the shear stress and shear deformation rate, in the particular case—presence of a critical shear stress. Such effects are accompanied by the capillary flow of viscoplastic fluid prone to formation of an internal solid structure which begins to break down with stress increase.

The authors [1] have experimentally established and theoretically justified the presence of two boundary shear stresses in high-viscosity oil: τ_r corresponding to the beginning of destruction of the internal structure, and τ_m corresponding to its final destruction. As a consequence, in the pore reservoir volume, the filtration rate in a certain combination of thermobaric factors does not obey Darcy's linear law. The basic characteristics of the nonlinear visco-plastic filtration model are two boundary pressure gradients, which are H_d and H_m , the parameters of the hydrodynamic process.

The main method of impact on high-viscosity oil and natural bitumen pool is thermal treatment. There are many technologies which are based on impact on the pool with coolant injected from the surface [8]. The authors of the article have considered the impact of increasing reservoir temperature on the well flow rates with the dual-well system. This technology is a draft version of the periodic thermobaric impact on the deposits of high-viscosity oil with placement of a heat source on the bottom hole of one of the two well bore-holes [9].

V. Astafev (✉) · V. Olkhovskaya (✉) · S. Gubanov ·
K. Ovchinnikov · V. Konovalov
Oil and Gas Development and Operation Department,
Samara State Technical University, 443100 Samara, Russia
e-mail: gubanov0393@gmail.com

3 Results

The data of the filtration experiment and generalized mathematical relationships connecting the boundary pressure gradients with the yield point $\theta \approx \tau_r$ and in-place permeability are used in hydrodynamic simulation of the well flow rate.

The oil of the proposed impact object is highly viscous, contains structure-forming components—asphaltenes and resins in concentrations from 3.68 up to 11.51% and from 9 to 13%, respectively, which is responsible for the manifestation of nonlinear viscoplastic properties. The reaction of rheological parameters to the temperature change in the range from 28 up to 80 °C is shown in Fig. 1.

Pair values “well flow rate–depression” were calculated to estimate the temperature influence on the production project targets. Determination of pair values of “well flow rate–depression” was performed using the equation of oil inflow to the well according to Darcy’s law, and also with the help of relationships [1] based on the flow model of nonlinearly viscoplastic oil. During the calculations, the effect of temperature on the viscosity and rheological characteristics of the reservoir system was taken into account.

The dependence of oil viscosity on the shear rate obtained for different temperatures on Modular Compact Rheometer MCR52 (Anton Paar GmbH, Austria) in the measuring cell “plate-plate” PP50 is shown in Fig. 2.

The calculation results of well flow rates and depressions in the form of indicator diagrams for different temperature conditions are shown in Fig. 3.

4 Discussion

While increasing temperature from 28 up to 80 °C, the values of the boundary pressure gradients decrease significantly, which is a consequence of the structural changes in nonlinear viscoplastic oil. The viscosity values corresponding to the scope of the strongest structure (maximum viscosity) and to the scope with extremely destroyed structure (minimum viscosity) are determined experimentally. It is noted that at a shear rate of up to 40 l/s, the viscosity of oil is variable, then the viscosity of the oil is constant.

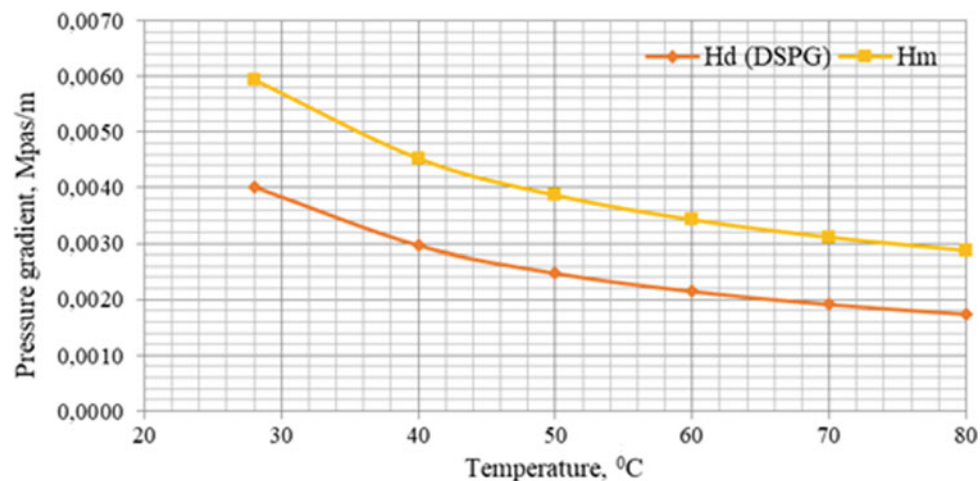
According to the indicator diagrams, the optimal heating temperature is determined to be 50 °C. Further increase in reservoir temperature does not lead to the significant increase in the expected oil flow rate at the same depression values.

5 Conclusions

Increase in the reservoir temperature to the optimum value, due to the rheological characteristics of the oil produced, can potentially help to increase the well flow rate with the dual-well system.

Selecting parameters of thermal effects, taking into account the nonlinearly viscous plastic flow of oil, makes it possible to optimize the location of the bottom hole and production branch hole and operating mode of the pumping equipment.

Fig. 1 Dependence of boundary pressure gradients on temperature of reservoir B₂



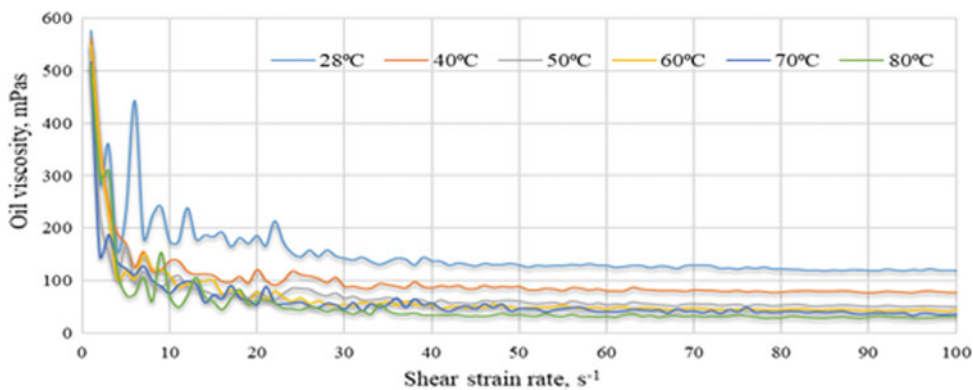


Fig. 2 Dependence of oil viscosity on the shear strain rate of reservoir B₂

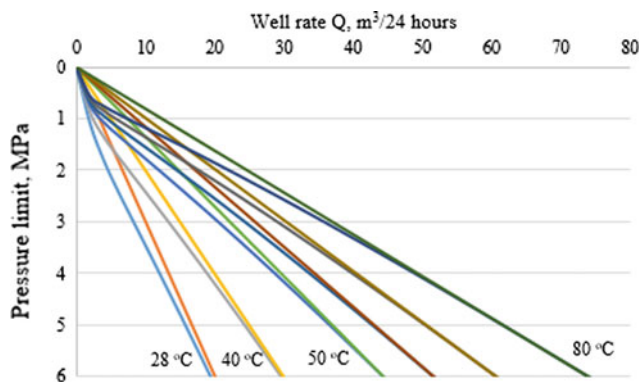


Fig. 3 Indicator diagram at drawdown up to 6 MPa

References

- Mishchenko, I.T., Bravicheva, T.B., Ermolaev, A.I.: Selection of the Oil Wells Operation with Hard-to-Recover Reserves. Gubkin Russian State University of Oil and Gas, Moscow (2005). (in Russian)
- Wilkinson, W.L.: Non-Newtonian Fluids: Fluid Mechanics, Mixing and Heat Transfer. Pergamon Press, London (1960)
- Bird, R.B., Armstrong, R.C., Hassager, O.: Dynamic of polymeric liquids, vol. 1: Fluid Mechanics. Wiley, New York (1987)
- Mirzadzhanzade, A.K., Khasanov, M.M., Bakhtizin, R.N.: Modeling of Oil and Gas Production Processes. Non-linearity, Non-equilibrium, Uncertainty. Institute of Computer Science, Moscow-Izhevsk (2005) (in Russian)
- Chhabra, R.P., Richardson, J.F.: Non-Newtonian flow and applied rheology: engineering applications. Butterworth-Heinemann, Oxford (2008)
- Basniev, K.S., Dmitriev, N.M., Chilingar, G.V.: Filtration of non-Newtonian liquid. In: Mechanics of Fluid Flow, pp. 489–512. Wiley, New York (2012)
- Mitsoulis, E.: Flow of viscoplastic materials: models and computations. *Rheol. Rev.* 135–178 (2007)
- Zhe, Y., Pengcheng, L., Shengfei, Z., et al.: Experimental study and numerical simulation of nitrogen-assisted SAGD in developing heavy oil reservoirs. *J. Pet. Sci. Eng.* 325–332 (2018)
- Astafev, V.I., Gubanov, S.I., Olkhovskaya, V.A., et al.: Analytical filtration model for nonlinear viscoplastic oil in the theory of oil production stimulation and heating of oil reservoir in a dual-well system. In: IOP Conference Series: Earth and Environmental Science, vol. 121, pp. 1–10, Sanya, China (2018)



Effect of CO₂-Oil Contact Time on the Swelling Factor and Viscosity of Paraffinic Oil at Reservoir Temperature

Muslim Abdurrahman, Asep Kurnia Permadi, Wisup Bae,
Shabrina Sri Riswati, Rochvi Agus Dewantoro, Ivan Efriza,
and Adi Novriansyah

Abstract

The objective of this experimental study is to investigate the effect of CO₂-oil contact time to oil swelling factor and viscosity. A sample from the central Sumatra basin was utilized in this study, which is categorized into paraffinic oil. The experiment condition follows the reservoir condition, which has a low fracture pressure. Thus, miscible injection scheme is impossible to apply. Therefore, the role of CO₂ in reducing oil viscosity and oil swelling is emphasized. The experiments were performed under reservoir temperature by using PVT cell, syringe pump, and HPHT Rheometer. The result from the experiments clearly indicates that oil swelling and viscosity reduction mechanisms are quite effective during 24 h of CO₂ injection. Optimum condition is obtained for the sample with 10 h of CO₂-oil contact-time, where the swelling factor and viscosity reduction still show significant values.

Keywords

CO₂ • Paraffinic oil • Swelling factor • Viscosity • Contact time

M. Abdurrahman · A. Novriansyah (✉)
Universitas Islam Riau, Pekanbaru, Indonesia
e-mail: adinovriansyah@eng.uir.ac.id; anba11181@gmail.com

A. K. Permadi · R. A. Dewantoro
Institut Teknologi Bandung, Bandung, Indonesia

W. Bae · S. S. Riswati · A. Novriansyah
Sejong University, Seoul, Republic of Korea

S. S. Riswati
Universitas Trisakti, Jakarta, Indonesia

I. Efriza
PT SPR Langgak, Pekanbaru, Indonesia

1 Introduction

One of the oil fields, located in the central Sumatra basin, has been producing paraffinic crude oil for more than a decade. This oil field is surrounded by an industrial site which has the potential to emit CO₂ gas into the atmosphere. Due to environmental reasons, the emission of CO₂ into the atmosphere could be minimized by injecting the gas (CO₂) into the oil field to enhance recovery. This project will be beneficial in both environmental and financial aspects, since CO₂ gas injection can increase oil recovery [1] and reduce Green House Gas (GHG) emission through subsurface storage [2].

The injection strategy will follow an immiscible injection scheme due to the shallow depth of the reservoir (1200 ft.) and to the low reservoir pressure (approximately 500 psi), which makes it impossible to use in its miscible condition. Oil swelling [3] and viscosity reduction [4] are two mechanisms which are dominant in this injection strategy. Although these two mechanisms yield an incremental level of oil recovery, an optimum time for CO₂ to dissolve inside the crude oil should be reconsidered. This is due to the longer time for crude oil contact with CO₂, the potential of more CO₂ solute inside the crude becomes higher, resulting in a high swelling factor and lower oil viscosity. Therefore, through this experimental study, we will investigate the effect of CO₂-oil contact time on the swelling factor and viscosity. Furthermore, an optimum contact time for oil and CO₂ will be determined based on a point above which an insignificant incremental of swelling factor and decremental of oil viscosity is given.

2 Methodology

The crude oil sample that is utilized in this study is categorized as paraffinic crude oil, which is reflected from higher cloud point. Moreover, the API gravity and viscosity of the

Table 1 Physical properties of crude oil

Parameter	Value	Unit
Oil gravity	30.8	API degree
Viscosity	17	Cp
Pour point	105–110	F
Bubble point pressure	113	Psi
Wax content	32.93	wt%
Asphaltene content	12.74	wt%

sample in reservoir temperature (136 °F) are 30.8 and 17 cp, respectively (Table 1). The hydrocarbon composition contains more than 95 wt% of hydrocarbon with a carbon number more than six. The swelling factor of the sample is obtained from the swelling test experiment using Stainless steel visual PVT cells. On the other hand, measurement of viscosity is performed by using high-pressure high-temperature (HPHT) rheometer. Each apparatus is equipped with a syringe pump from ISCO company and fully filled with liquid CO₂.

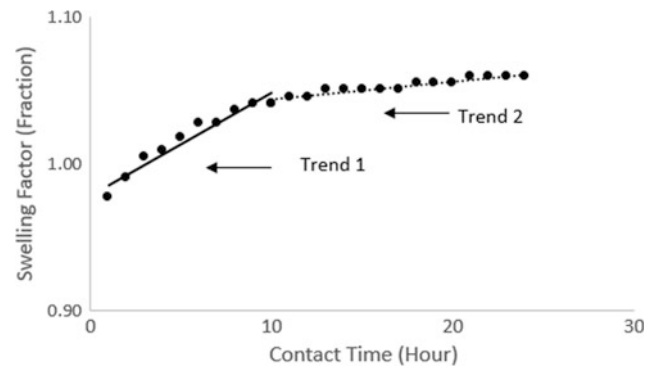
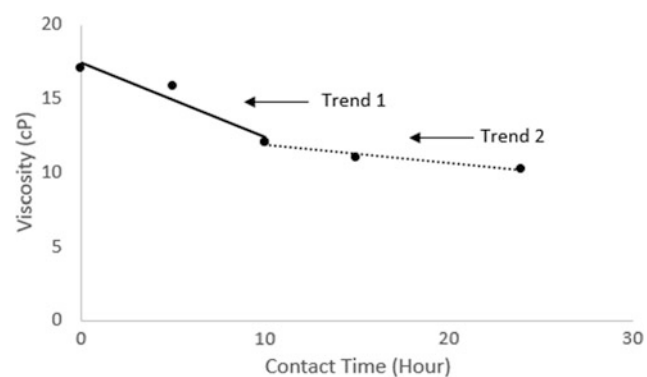
The procedure for determining the swelling factor was initiated with preparation of a 3 ml sample inside the PVT cell and initial height of the sample column was recorded. The PVT cell was then located inside the air bath, where its temperature was constantly maintained at reservoir condition. The tubing line end was connected to the PVT cell while the other was connected to a valve in the syringe pump. All connections were checked to detect the presence of any leakage. After the equilibrium temperature between cell and bath was achieved, the pump pressure was adjusted at a certain injection pressure [in this case, the observation pressure was 900 psi, which is below the fracture pressure (1000 psi)]. CO₂ was injected at constant injection pressure by opening the valve which connects the pump and the PVT cell. The column height of the sample was recorded and measured every hour during 24 h of injection time. The swelling factor was calculated by dividing height during injection with sample initial height.

In the measurement of oil viscosity experiment, the procedure was began by placing an 11 ml sample inside the rheometer cup, then, the cup was installed on the rheometer head in HPHT rheometer apparatus. A complete isolation of the annulus between rotor (cup) and stator (bob or spindle) must be confirmed. The rheometer head with the installed cup was lowered into the thermo-bath and the bath and sample temperature was increased up to reservoir condition, through temperature adjustment at the PC dashboard. The liquid CO₂ pressure was increased to 900 psi and set at constant pressure injection, while awaiting the equilibrium condition of the sample temperature. Liquid CO₂ was injected into the sample cup by opening the valve and the pressure inside became stable at 900 psi after 5 h. Oil

viscosity was obtain and recorded at 255 s⁻¹ sheer rates for every 5 h during 24 h of contact time.

3 Results

Results from the swelling factor and viscosity experiments are plotted against contact time (in hour unit) in Figs. 1 and 2, respectively. The sample volume swells up to 6% incremental when CO₂ is injected at 900 psi for 24 h. Viscosity plot versus contact time reveals a larger reduction of sample viscosity when the sample comes into contact with CO₂ for a longer period of time. During 24 h of CO₂-oil

**Fig. 1** Swelling factor versus contact time**Fig. 2** Viscosity versus contact time

contact time with 900 psi injection pressure, the oil viscosity was successfully reduced from 17 cp down to 10.2 cp, i.e. a nearly 40% reduction from its initial value.

4 Discussion

The plotted results in Figs. 1 and 2, clearly indicate that the oil swelling and viscosity reduction mechanisms, as reported by Al-abri and Amin [3] and Li et al. [4], occur during CO₂ injection into paraffinic oil. Compared to aromatic oil, the swelling factor value of paraffinic oil is relatively lower due to the more tightly bonded carbon chain or higher carbon number. Results from both experiments have shown two trends of data. The first trend ("Trend 1") shows a significant change of value compared to the second trend ("Trend 2"). Based on observation on Fig. 1, "Trend 2" has a lower incremental of swelling factor (0.12%), compared to "Trend 1" (0.7%). Moreover, the decline rate of oil viscosity for the second trend (Fig. 2) is lower (12.5%) than the first trend (50%). There is an insignificant change in the value of viscosity and swelling factor, after 10 h of elapsed time. This might have occurred because of CO₂ solubility in the oil at this particular pressure was nearly reached and, thus, the CO₂ dissolution process in the oil was almost completed, which was inspired from the works of Or et al. [5]. Therefore, 10 h is concluded to be the optimum time for CO₂ contact with paraffinic crude oil under 900 psi and 136 °F condition. Moreover, the effect of oil and viscosity reduction to oil recovery, will be investigated in the future. In addition, the collaboration with other experts such as geologists and mechanical engineers is required to understand the subsurface structure and the CO₂ separation process from the environment in order to launch a massive project in the future.

5 Conclusions

Two experimental studies have been performed to investigate the effect of CO₂-crude oil contact time to the oil swelling factor and viscosity. Paraffinic oil from central Sumatra Basin oil field was utilized in two different tests, for obtaining swelling factor and oil viscosity values. Results from the two tests reveal that the oil continuously swells and the viscosity tends to decrease when the CO₂-oil contact time is increased. Optimum condition of CO₂-oil contact time is attained after 10 h, beyond that the results become insignificant in oil swelling factor and low viscosity decline rate.

References

1. Bagci, S., Tuzunoglu, E.: 3D model studies of the immiscible CO₂ process using horizontal wells for heavy oil recovery. In: Annual Technical Meeting. Petroleum Society of Canada, Jan 1998
2. Hepple, R.P., Benson, S.M.: Geologic storage of carbon dioxide as a climate change mitigation strategy: performance requirements and the implications of surface seepage. Environ. Geol. **47**(4), 576–585 (2005)
3. Al-Abri, A., Amin, R.: Phase behaviour, fluid properties and recovery efficiency of immiscible and miscible condensate displacements by SCCO₂ injection: experimental investigation. Transp. Porous Media **85**(3), 743–756 (2010)
4. Li, H., Zheng, S., Yang, D.T.: Enhanced swelling effect and viscosity reduction of solvent (s)/CO₂/heavy-oil systems. SPE J. **18** (04), 695–707 (2013)
5. Or, C., Sasaki, K., Sugai, Y., Nakano, M., Imai, M.: Swelling and viscosity reduction of heavy oil by CO₂-gas foaming in immiscible condition. SPE Reservoir Eval. Eng. **19**(02), 294–304 (2016)



Mechanistic Simulation of Foam Injection in the Sandstone Oilfield to Optimize the Oil Recovery Enhancement

Afshin Davarpanah

Abstract

Foam flooding is considered as one of the beneficial chemical enhanced oil recovery techniques to increase the value of gas viscosity and, thereby, the recovery of the produced oil would be improved dramatically, more than other methodologies. The objective of this comprehensive study is to determine a suitable injection model for Iran's heterogeneous sandstone reservoir. Hydrolyzed polyacrylamide (HPAM) concentration in the foam solution has the most recovery factor in this case. Consequently, a concentration of 1200 ppm of HPAM in the foam solution produces a high volume of oil even after 10 years. Furthermore, by selecting three cores from the three wells in this field, it is clear that, owing to the increasing volume of foam in the injection fluid, the pressure dropped dramatically, leading to the production of a bigger volume of oil.

Keywords

Foam solution • Hydrolyzed polyacrylamide concentration • Enhanced oil recovery • Heterogeneous sandstone reservoir

1 Introduction

Chemical methods are divided into mobility-controlling materials (e.g., polymers and foams) and surfactant flooding. Foam is not thermodynamically stable, and the production of foam in the porous medium is always the same as the Foam Coalescence Process. There are two main mechanisms associated with the contiguity of foam; capillary adsorption and gas diffusion. The Capillary absorption leads to a direct lamellar failure, which is the first mechanism for foam

A. Davarpanah (✉)
Department of Petroleum Engineering, Science and Research Branch, Islamic Azad University, Tehran, Iran
e-mail: Afshin.Davarpanah@srbiau.ac.ir

interconnecting. Although both mechanisms are within the mechanism of capillary pressure, capillary adsorption utterly depends on the surfactant's formulation in comparison to the capillary snap-off. In the Foam Flooding techniques, diversion is the common performance of foam fluid and it is conceptually related to the blocking of higher permeability layers and subsequently channeling the foam flow through the low-permeability layer. In a gas injection process the foam injection solves the problems related to channeling and overcoming the gravity force [1–4].

2 Methods

2.1 Core Flooding Experiment

For a start, the core plug—which was collected from the studied field—was put in the core holder after vacuuming for one day before the brine injection. In the next stage, crude oil with the mentioned properties was injected into the core. One day later, water flooding and foam flooding were carried out sequentially so that to the core could produce the residual oil. In the final stage, water flooding was carried out to achieve ultimate oil recovery. The temperature and pressure were maintained according to reservoir conditions, i.e. 190 K and 4000 psi, respectively.

3 Results and Discussion

The studied reservoir is one of the heterogenous sandstone reservoirs in the Pazanan oilfield in the south-west of Iran. It has two sandstone layers divided by an impermeable shale layer. The porosity of the shale layer is estimated at approximately 21.6–24.4%. To investigate the profound impact of each injection scenario on the performance of oil displacement, separate experiments were conducted by injecting HPAM with and without polymer. To do this, three core floods were recovered from the studied field. For each

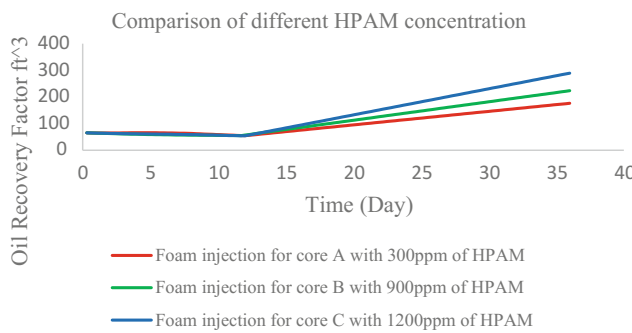


Fig. 1 Oil recovery factor versus time for different HPAM concentrations

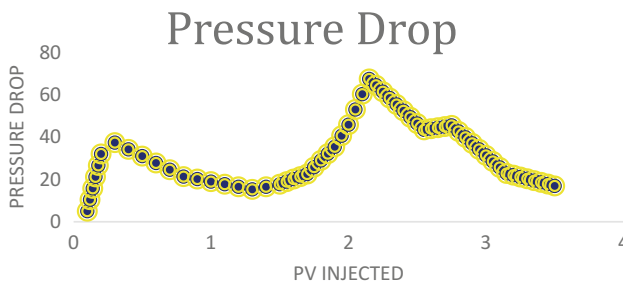


Fig. 2 Pressure drop versus PV injected for different HPAM concentrations

core, we have implemented two procedures to determine the validity of each scenario and subsequently obtain the matching results of the experimental core floods and simulation analysis by Eclipse software. Moreover, foam injection was carried out by varying the HPAM concentration in the laboratory conditions for a duration of 36 days. It is evident from Fig. 1 that with the increase in the HPAM concentration in the foam solution, the recovery factor increases gradually. The HPAM concentration of 1200 ppm oil recovery factor results in the highest value of recovery.

As can be seen in Fig. 2, the Pressure Drop increases gradually in the initial phase of water injection, but it decreased slightly before the injection of foam into the cores.

In the 1.5 pore volume injection, foam is added to the injection fluid causing an increase in the Pressure Drop dramatically in the pore volume injection of 1.5–2.2 pore volume. The Pressure Drop reached the maximum value of about 70 psi, after which the Pressure Drop decreased because of water injection.

4 Conclusions

Foam flooding is considered as one of the most preferable methodologies to increase the amounts of recovered oil which have started to decrease after several years of production. One of the chief aims of this study is to conduct an investigation into one of Iran's heterogeneous reservoirs by the simultaneous simulation procedures and experimental evaluation of HPAM concentration in the foam solution. Due to the increase of HPAM concentration in the foam solution, the oil recovery factor increased dramatically and subsequently resulted in a high cumulative oil production. Furthermore, after adding the specific volume of foam into the injection fluid, the Gas Pressure Drop increased drastically leading to production of more oil volume.

References

1. Davarpanah, A., Mirshekari, B., Behbahani, T.J., et al.: Integrated production logging tools approach for convenient experimental individual layer permeability measurements in a multi-layered fractured reservoir. *J. Pet. Explor. Prod. Technol.* **1**(1), 1–9 (2018)
2. Farajzadeh, R., Lotfollahi, M., Eftekhari, A., et al.: Effect of permeability on foam-model parameters and the limiting capillary pressure. In: IOR 2015-18th European Symposium on Improved Oil Recovery (2015). <https://doi.org/10.3997/2214-4609.201412134>
3. Fei-Peng, W., Jing, L., Xue-mei, W., et al.: A study on oxygen consumption mechanism of air-foam flooding in low-temperature oil reservoir. *J. Petrol. Sci. Eng.* **161**(1), 368–380 (2017)
4. Fisher, A., Foulser, R., Goodyear, S.: Mathematical modeling of foam flooding. In: *SPE/DOE Enhanced Oil Recovery Symposium*. Society of Petroleum Engineers. (1990). <https://doi.org/10.2118/20195-MS>



Nanoparticle-Stabilized CO₂ Foam Flooding

Feng Guo and Saman A. Aryana

Abstract

The efficacy of several nanoparticles [silica (Si), nanoclays, fly ash and iron oxide (IO)] in stabilizing CO₂ foam is studied via flow experiments in a microfluidic device. The resulting foam is characterized using modified bulk foam tests. Size and uniformity of nanoparticle (NP) dispersions are quantified using dynamic light scattering. Results indicate that the size distribution and surface charge of the particles are influential parameters on the stability and formability of the foam, which in turn have a direct relationship with oil recovery performance. Si, nanoclays and fly ash NPs assisted by surfactant mixtures generate stable foams and result in high ultimate oil recoveries (over 90%). Even though IO-surfactant mixtures generate foams with relatively inferior stability characteristics and ultimate recovery, approximately three quarters of the IO NPs are recovered once exposed to a magnetic field. Unlike nanoclays and fly ash, the use of Si and IO NPs as foam stabilizers results in significant improvements in recovery at much smaller pore-volumes injected (~ 10 PVIs).

Keywords

Nanoparticles • CO₂ foam • Microfluidic device • EOR

1 Introduction

Carbon dioxide (CO₂) Enhanced Oil Recovery (EOR) provides potential opportunities for CO₂ utilization and long-term storage [1, 2]. The relative low density and

viscosity of CO₂ may contribute to unfavorable volumetric sweep efficiencies resulting from severe channeling and gravity override [3]. CO₂ foam has been proposed as an alternative to mitigate these shortcomings [4] but has not been widely implemented in field applications due to concerns related to foam instability. NPs may serve as effective foam stabilizers with minimal losses in the subsurface due to their relatively high adsorption energy values under reservoir conditions [5, 6]. Foam stability and formability impact foam mobility and sweep efficiency in porous media and result in various oil recovery performances [7]. In this work, a microfluidic device featuring a porous medium, fabricated to represent a Berea sandstone [8], is used to visualize and characterize NP-stabilized CO₂ foam flow behavior, using silica (Si), nanoclays, by-product fly ash, and recyclable iron-oxide (IO) NPs. Foam properties are investigated using modified bulk foam tests, and their efficacy as an injectant is studied using displacement experiments in the microfluidic device.

2 Experiments

Four different types of nanoparticles are investigated: amorphous fumed silica T30 (unmodified, 100% SiOH coverage), nanoclays, fly-ash (two stage wet-grinded), and IO NPs (synthesized by a co-precipitation method). NPs are dispersed in deionized (DI) water and mixed with lauramidopropyl betaine (LAPB) and alpha-olefin sulfonate (AOS) surfactant mixtures. The NP/surfactant solution, CO₂ gas and a 30,000 ppm sodium chloride brine are used as injectants. A Gullfaks Blend crude oil with a viscosity of 45.9 cp serves as the resident fluid. A Brookhaven Zeta PALS instrument is used to characterize particle size distribution and zeta potential at 20 °C. The stability and formability of foams stabilized by various NPs are quantified via modified bulk foam tests, where foam generation as a function of time is measured using a transparent graduated cylinder [8, 9]. The microfluidic device features a pore

F. Guo · S. A. Aryana (✉)
University of Wyoming, Laramie, WY 82071, USA
e-mail: saryana@uwyo.edu

network with an area of 1.6 in. \times 1.4 in., and has a porosity of approximately 40%, and a permeability of approximately 0.35 Darcy. The relationship between oil recovery and foam stability is analyzed using high resolution images of the porous medium during experiments. The recovered IO NPs are quantified using a HACH DR/4000U spectrophotometer.

3 Results

Particle diameters and polydispersity indices are presented in Table 1 [8, 9]. All NP samples have net charges (zeta-potential) lower than -30 mV, which indicates a high stability [10]. Results from modified bulk foam experiments are presented in Table 2. The porous medium is initially saturated with brine, followed by the injection of 40 pore volumes (PVs) of the crude oil. Prior to foam flooding, 8 PVs of brine are injected at a rate of $4\ \mu\text{L}/\text{min}$, resulting in a recovery of approximately 40%.

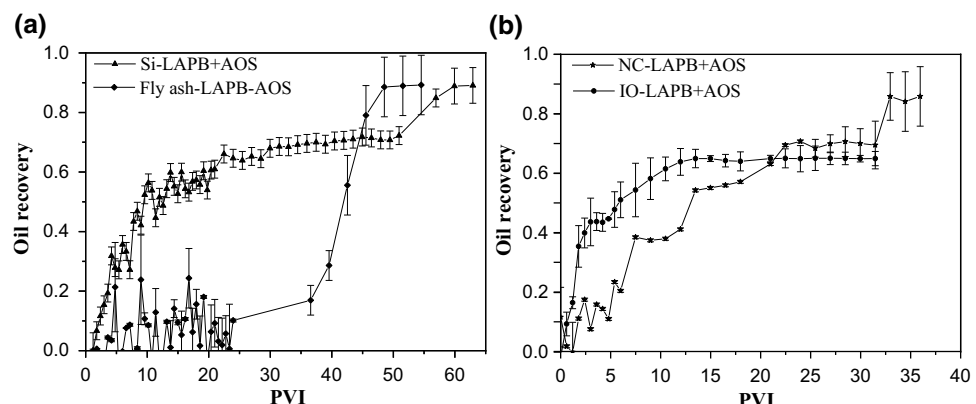
Table 1 Particle hydrodynamic diameters and zeta potential of different NPs dispersion

NP	Diameter \pm std. dev, nm	Polydispersity index	Zeta potential, mV
Nanoclay	424.8 ± 4.2	0.181	-52.12
Silica	179.3 ± 1.4	0.141	-57.23
Fly ash	232 ± 2.1	0.151	-53.64
Iron oxide	192 ± 27	0.136	-48.01

Table 2 CO_2 foam formability and stability

NP	Concentration, ppm	Concentration, ppm	Formability, min	Stability, min
Nanoclay	1000	1000	3.6	184
Silica	1000	1000	3.7	210
Fly ash	1000	1000	4.6	238
Iron Oxide	1000	1000	4.7	118
n/a	n/a	1000	4.5	83

Fig. 1 Oil recovery as a function of PVs injected. Each experiment is repeated three times



4 Discussion

All four NPs improve foam stability compared to the use of surfactants alone. Differences in stability of the four NP-assisted foams may be explained by differences in partial particle flocculation, contact angle and the resulting rearrangements at the foam lamella [11]. The absorption of the surfactant mixtures on Si and fly ash NP surfaces may result in contact angles between CO_2 , aqueous phase and NP surfaces (60° – 70°) that lead to an improved foam stability [12, 13]. In addition, arrangement of Si and fly ash NPs at the interfaces in the CO_2 -surfactant solution has a significant effect on maximum capillary pressure, which contributes to foam stability [14, 15]. In general, the improved stability of CO_2 foams due to the use of NPs results in higher oil recoveries compared to foams assisted by surfactants only [16]. The addition of Si, fly ash and nanoclay NPs in the surfactant mixtures results in stable foams and relatively high ultimate recoveries of over 90% (Fig. 1). Even though

the use of IO NPs in surfactant mixtures is not as effective in generating stable foams and recovering the resident fluid, approximately three quarters of the IO NPs are recovered at the outlet using a magnetic field. As seen in Fig. 1, the use of Si and IO NPs as foam stabilizers results in significant improvements in recovery after approximately ten pore-volumes injected (PVI), whereas significantly larger PVIs are needed to achieve similar recovery gains using fly ash and nanoclays.

5 Conclusions

This study focuses on the efficacy of four types of NPs in stabilizing CO₂ foams and on the resulting improvements in oil recovery due to foam injection in a microfluidic device. Fly ash NPs, a by-product from coal fired power plants, are a promising stabilizer of CO₂ foams. Their use in EOR processes may serve as a venue for their underground disposal and may improve the economics of CO₂ utilization and storage by replacing more expensive materials. IO NPs do not appear to be as effective as fly ash in stabilizing CO₂ foams; nevertheless, a significant portion of IO NPs may be recovered by subjecting the outflow stream to a magnetic field. The optimal choice of NPs as a foam stabilizer may depend not only on the stability of the resulting foam, but also on the PVI needed to recover the resident fluid and the associated material cost and operational expenditure.

References

1. Kalyanaraman, N., Arnold, C., Gupta, A., Tsau, J.S., Ghahfarokhi, R.B.: Stability improvement of CO₂ foam for enhanced oil-recovery applications using polyelectrolytes and polyelectrolyte complex nanoparticles. *J. Appl. Polym. Sci.* **134**(6) (2017)
2. Worthen, A.J., Bagaria, H.G., Chen, Y., Bryant, S.L., Huh, C., Johnston, K.P.: Nanoparticle-stabilized carbon dioxide-in-water foams with fine texture. *J. Colloid Interface Sci.* **391**, 142–151 (2013)
3. Kim, I., Worthen, A.J., Johnston, K.P., DiCarlo, D.A., Huh, C.: Size-dependent properties of silica nanoparticles for Pickering stabilization of emulsions and foams. *J. Nanopart. Res.* **18**(4) (2016)
4. Guo, H., Zitha, P.L.J., Faber, R., Buijse, M.: A novel alkaline/surfactant/foam enhanced oil recovery process. *SPE J.* **17**(04), 1186–1195 (2012)
5. Yekeen, N., Manan, M.A., Idris, A.K., Padmanabhan, E., Junin, R., Samin, A.M.: A comprehensive review of experimental studies of nanoparticles-stabilized foam for enhanced oil recovery. *J. Petrol. Sci. Eng.* **164**, 43–74 (2018)
6. Hua, X., Michael, A., Bevan, A.M., Frechette, J.: Competitive adsorption between nanoparticles and surface active ions for the oil-water interface. *Langmuir* **34**(16), 4830–4842 (2018)
7. Yousef, Z.A., Almobarky, M.A., Schechter, D.S.: The effect of nanoparticle aggregation on surfactant foam stability. *J. Colloid Interface Sci.* **511**, 365–373 (2018)
8. Guo, F., He, J., Johnson, P.A., Aryana, S.A.: Stabilization of CO₂ foam using by-product fly ash and recyclable iron oxide nanoparticles to improve carbon utilization in EOR processes. *Sustain. Energy Fuels* **1**, 814–822 (2017)
9. Guo, F., Aryana, S.A.: An experimental investigation of nanoparticle-stabilized CO₂ foam used in enhanced oil recovery. *Fuel* **186**, 430–442 (2016)
10. Hirasaki, G.J., Lawson, J.B.: Mechanisms of foam flow in porous media: apparent viscosity in smooth capillaries. *Soc. Petrol. Eng. J.* **25**(02), 176–190 (1985)
11. Hunter, T.N., Pugh, R.J., Franks, G.V., Jameson, G.J.: The role of particles in stabilizing foams and emulsions. *Adv. Coll. Interface Sci.* **137**, 57–81 (2008)
12. Shaw, D.: Introduction to Colloid and Surface Chemistry, 4th edn. Butterworth-Heinemann (1992)
13. Denkov, D.A., Livanov, B.I., Kralchevsky, A., Wasan, T.D.: A possible mechanism of stabilization of emulsions by solid particles. *J. Colloid Interface Sci.* **150**, 589–593 (1992)
14. Kapta, G.: Interfacial criteria for stabilization of liquid foams by solid particles. *Colloids Surf. A Physicochem. Eng. Asp.* **230**(1–3), 67–80 (2004)
15. Singh, R., Mohanty, K.K.: Synergy between nanoparticles and surfactants in stabilizing foams for oil recovery. *Energy Fuels* **29**(2), 467–479 (2015)
16. Worthen, A.J., Foster, L.M., Dong, J., Bollinger, J.A., Peterman, A.H., Pastora, L.E.: Synergistic formation and stabilization of oil-in-water emulsions by a weakly interacting mixture of zwitterionic surfactant and silica nanoparticles. *Langmuir* **30**(4), 984–994 (2014)

Foam Flooding in a Heterogeneous Porous Medium

Feng Guo and Saman A. Aryana

Abstract

The impact of heterogeneity on the flow behavior of CO₂ foam in the presence of crude oil is investigated in a complex, heterogeneous porous medium. A microfluidic device is fabricated featuring low and high permeability regions using a sequential photolithography technique. Two types of CO₂ foams are used as the injectant: (i) foam stabilized with surfactants and (ii) foam stabilized with a blend of silica nanoparticles (Si NPs) and surfactants. High-resolution images of the medium during displacement experiments reveal a phase separation between the high versus low permeability regions; foam sweeps the high permeability regions, whereas the surfactant solution, along with few gas bubbles, appears to invade the low permeability region. The gains in recovery from the low-permeability region are attributed to the resistance to flow due to a relatively high apparent viscosity of foam in the high-permeability region and the resulting diversion of flow into the low-permeability region. The enhanced stability of foams stabilized with Si NPs appears to reduce the phase separation between the two regions, which contributes to an additional recovery gain from the low-permeability region.

Keywords

Nanoparticles • CO₂ foam • Heterogeneity • Porous media • Microfluidic device

1 Introduction

Heterogeneities in porous media, along with unfavorable contrasts of viscosity and density between the resident and invading phases, contribute to flow instabilities and

relatively low sweep efficiencies in subsurface systems [1, 2]. Foam injection has the potential to improve the sweep efficiency due to its relatively high apparent viscosity, which contributes to an increase in resistance to flow in high-permeability regions [3, 4]. This phenomenon helps redirect the transport of the flowing phases into the otherwise under-swept regions in heterogeneous porous media [5, 6]. Foam injection experiments using microfluidic devices are often conducted using homogeneous porous media, which do not address the flow dynamics related to heterogeneities [7, 8]. A heterogeneous microfluidic device featuring a complex pore network with rigid walls would help elucidate the flow dynamics in subsurface systems [9]. Nanoparticle (NP)-surfactant mixtures synergistically generate foams with improved apparent viscosity and stability characteristics compared with those generated with surfactants alone [6]. This work examines the impact of heterogeneities on the flow behavior and the spatial distribution of foam within porous media. Two types of CO₂ foams are used as the injectant: (i) foam stabilized with surfactants and (ii) foam stabilized with a blend of silica nanoparticles (Si NPs) and surfactants. This work aims to demonstrate that foam stability is a significant contributing factor to sweep efficiency in heterogeneous systems. A glass heterogeneous porous medium is fabricated using a map of the channel network of a Berea sandstone. The porous medium has a centrally-located low-permeability region, bound on each side by a high-permeability region [10]. High-resolution images of the porous medium are captured during the flow experiments using a monochromatic 60 MP sensor. Pixel intensities are used to analyze the phase separation and displacement in high and low permeability regions.

2 Experiments

Dispersions of Si NPs (T30, 100% SiOH coverage) in deionized (DI) are mixed with lauramidopropyl betaine (LAPB) and alpha-olefin sulfonate (AOS) surfactant

F. Guo · S. A. Aryana (✉)
University of Wyoming, Laramie, WY 82071, USA
e-mail: saryana@uwyo.edu

mixtures (Table 1). CO₂ gas, a 30,000-ppm sodium chloride brine, and a Gullfaks Blend crude oil with a viscosity of 45.9 cp are used in the experiments. All measurements were carried out at 20 °C. The porous medium covers an area of approximately 1.6 in. × 1.4 in. Channels have a uniform depth of approximately 14 and 6 µm in the high-permeability and low-permeability regions, respectively. The two permeability regions have a permeability contrast of approximately two (0.28 Darcy vs. 0.13 Darcy).

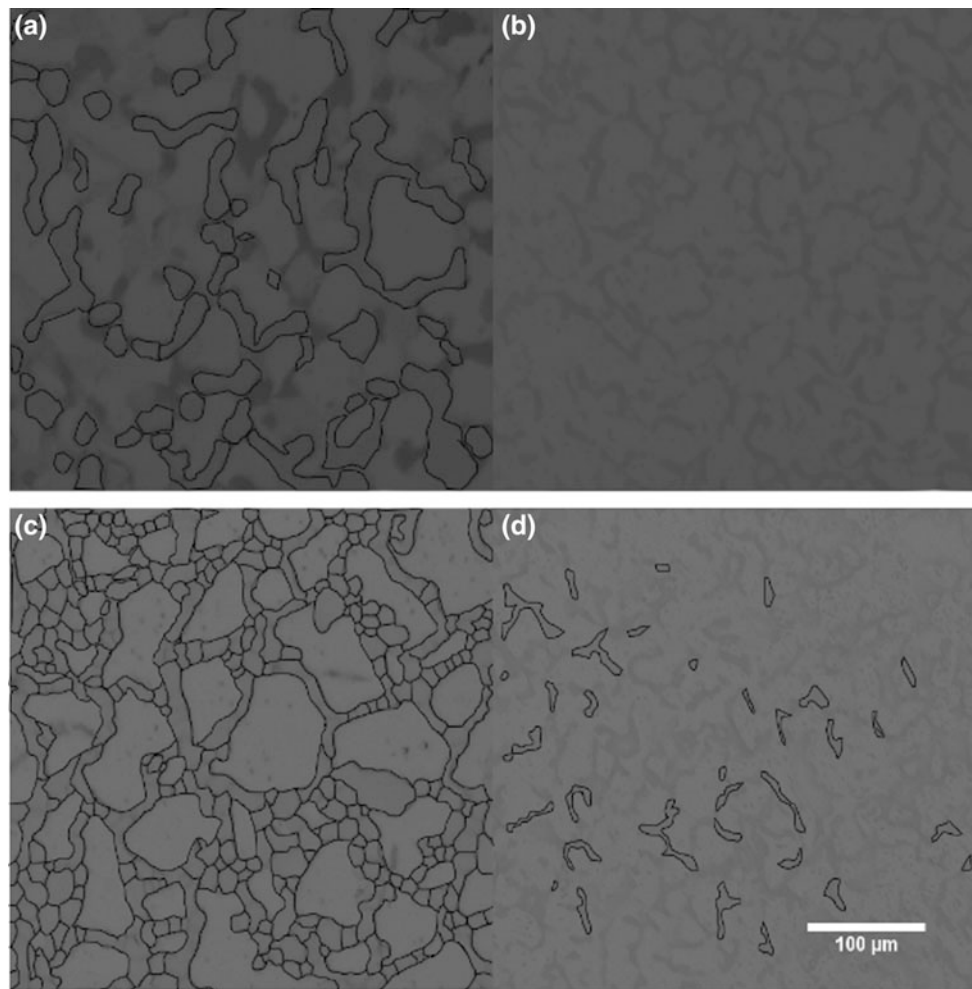
3 Results

An injection rate of 1 µL/min is used in all displacement experiments. Brine is injected in the oil saturated medium for 30 min, at which point the maximum water flooding oil recovery of approximately 50% is achieved. Subsequently, the surfactant, or the NP-surfactant mixture, and CO₂ gas are injected simultaneously. Figure 1 shows sample images of the medium after injection of two pore-volumes (PV) of

Table 1 Surfactants

Type	Family	Designation	Source
Anionic	Alpha-olefin sulfonate	AOS 14-18	Stepan Co.
Zwitterionic	Betaine	Lauramidopropyl betaine	Rhodia Co.

Fig. 1 The porous medium after two pore-volumes of foam injection. **a** and **c** are examples of the high-permeability region and **b** and **d** are examples of the low-permeability region. **a** and **b** are under flood by foam generated using surfactants only, whereas **c** and **d** are under flood by the NP-assisted foam. Gas bubbles in **d** are highlighted for clarity



foam. Approximately 40 and 49% incremental oil was recovered from the high and low permeability regions, respectively, as a result of the injection of the surfactant-stabilized foam. Compared to the foam generated using surfactants only [11], the more stable NP-assisted foam exhibits a higher lamella density in the high-permeability region. As a result, the mobility of the displacing fluid in this region is further reduced and the flow is redirected to the lower permeability region. A phase separation between the two regions is observed for both foams; however, the separation appears to be less severe in the case of NP-assisted foam. As a consequence, a higher incremental oil recovery from the low-permeability region is achieved using the more stable foam. The presence of gas bubbles in the low-permeability region of the NP-assisted foam flood indicates that a higher gas fraction is present in this region compared to the one with the less stable foam.

4 Discussion

Most of the oil remaining in the medium at the conclusion of the waterflood phase resides in the low-permeability region. Foam is able to mobilize and displace a portion of this trapped oil. Unlike the foam flood using surfactants only, a continuous foam phase is present in the high-permeability region of the NP-stabilized CO₂ foam flood, where almost all of the resident phase is displaced after two PVs of foam injection. The incremental recovery from the low-permeability region, during the foam-flooding phase, is superior in the case of the more stable foam. This is in part attributed to the invasion of the low-permeability region by gas bubbles, whereas in the case of the less stable foam, this region is mainly invaded by the surfactant solution with occasional gas bubbles in the periphery. The improved stability of the NP-assisted foam appears to enhance the recovery from heterogeneous porous media. Foam stability is a major contributing factor in its mobility control, which, in turn, has an appreciable impact of its ability to mobilize the resident fluid trapped in low-permeability regions of heterogeneous media.

5 Conclusions

Foam stability is demonstrated to have a significant impact on foam mobility control and sweep efficiency in a heterogeneous medium. Oil displacement experiments are conducted using CO₂ foams with different stability behaviors

and a glass heterogeneous microfluidic device. The NP-assisted foam exhibits higher stability and a higher lamella density in the medium, which leads to an improvement in the overall oil recovery from both high and low permeability regions. A ‘smart rheology’ (phase separation) is observed in both foam experiments—as the foam invades the low permeability region, it becomes more liquid-rich. Nevertheless, as demonstrated by the presence of gas bubbles, the more stable foam exhibits a less severe phase separation, caused by the heterogeneity and a relatively higher gas fraction in the low-permeability region compared to the less stable foam.

References

1. Aryana, S.A., Kovscek, A.R.: Experiments and analysis of drainage displacement processes relevant to carbon dioxide injection. *Phys. Rev. E* **86**(6), 66–78 (2012)
2. Furtado, F., Pereira, F.: Crossover from nonlinearity controlled to heterogeneity controlled mixing in two-phase porous media flows. *Comput. Geosci.* **7**(2), 115–135 (2003)
3. Guo, F., Aryana, S.: An experimental investigation of nanoparticle-stabilized CO₂ foam used in enhanced oil recovery. *Fuel* **186**, 430–442 (2016)
4. Fernø, M.A., Gautepllass, J., Pancharoen, M., Haugen, Å., Graue, A., Kovscek, A.R.: Experimental study of foam generation, sweep efficiency, and flow in a fracture network. *SPE J.* **21**(4), 1140–1150 (2016)
5. Xiao, S.Y., Zeng, Y.C., Vavra, D.E., He, P., Puerto, M., Hirasaki, J.G., Biswal, L.S.: Destabilization, propagation, and generation of surfactant-stabilized foam during crude oil displacement in heterogeneous model porous media. *Langmuir* **34**(3), 739–749 (2018)
6. Shi, S., Wang, Y., Li, Z., Ding, M., Chen, W.: Experimental study on stability and improving sweep efficiency with microfoam in heterogeneous porous media. *J. Dispersion Sci. Technol.* **37**(8), 1152–1159 (2015)
7. Muggeridge, A., Cockin, A., Webb, K., Frampton, H., Collins, I., Moulds, T.: Recovery rates, enhanced oil recovery and technological limits. *Philos. Trans. Ser. A Math. Phys. Eng. Sci.* **372** (2006), 1–25 (2014)
8. Riche, C.T., Zhang, C., Gupta, M., Malmstadt, N.: Fluoropolymer surface coatings to control droplets in microfluidic devices. *Lab Chip* **14**(11), 1834–1841 (2014)
9. Mijatovic, D., Eijkel, J.C.T., van den Berg, A.: Technologies for nanofluidic systems: top-down vs. bottom-up—a review. *Lab Chip* **5**(5), 492–500 (2005)
10. Guo, F., Aryana, S.A.: Improved sweep efficiency due to foam flooding in a heterogeneous microfluidic device. *J. Petrol. Sci. Eng.* **164**, 155–163 (2018)
11. Guo, F., He, J., Johnson, P.A., Aryana, S.A.: Stabilization of CO₂ foam using by-product fly ash and recyclable iron oxide nanoparticles to improve carbon utilization in EOR processes. *Sustain. Energy Fuels* **1**(4), 814–822 (2017)



Synergetic Effect of SLS Surfactant of Bagasse on Enhanced Oil Recovery

Rini Setiati, Septoratno Siregar, Taufan Marhaendrajana, and Deana Wahyuningrum

Abstract

The purpose of this research is to identify the synergistic effects of several parameters of an enhanced oil recovery mechanism by using sodium lignosulfonate (SLS) from bagasse. This is a laboratory research method conducted using SLS surfactant of bagasse injection process with that of light crude oil. The core injection was reinforced by the tested SLS surfactant characteristics such as IFT and contact angle. The core injection using SLS surfactant showed a high recovery factor at the two areas, at 5000 ppm salinity and at salinity of 80,000 ppm. At a higher salinity level, it produced a larger contact angle of 20°–50°. The interfacial tension value also increased from 2.73 to 4.11 mN/m. The value of oil recovery at these salinity variations ranged from 9.25 to 1.80%. The results of this research show that the mechanism of surfactant flooding depends on several parameters, like salinity, surfactant concentration, IFT and contact angle. The value of the formed contact angle also affects the performance of SLS surfactant in the oil purification process. Thus, it can be concluded that the parameters of the SLS surfactant in the injection process provide a synergistic effect on the oil recovery mechanism in terms of salinity, surfactant concentration, IFT, and contact angle.

Keywords

Contact angle • IFT • Salinity • Recovery oil • Surfactant SLS

R. Setiati (✉)
Petroleum Engineering Department, FTKE, Universitas Trisakti, Jakarta, Indonesia
e-mail: rini.setiati@gmail.com; rini.setiati@trisakti.ac.id

S. Siregar · T. Marhaendrajana
Petroleum Engineering Department, FTTM, Institut Teknologi Bandung, Bandung, Indonesia

D. Wahyuningrum
Chemistry Department, FMIPA, Institut Teknologi Bandung, Bandung, Indonesia

1 Introduction

Enhanced oil recovery is required to increase oil recovery from the reservoir. One of the methods is the chemical injection process by using Sodium Lignosulfonate (SLS) surfactant as an injection fluid. SLS surfactant as one type of surfactant anionic, can be synthesized from lignin contained in bagasse. Several previous studies have been conducted to obtain oil recovery by using organic sulfonate [1] or by using petroleum sulfonate [2]. Those previous research emphasize that lignin is the basic ingredient of lignosulfonate [3]. Further, other methods that have been carried out among others are in determining low levels of surfactants in produced oil field brines [4] and surfactant types that displayed good solubility in pure water and brines [5]. From the previous studies, there is an absence review of SLS surfactant from bagasse as an injection fluid for core flooding. It is, therefore, feasible to examine the use of SLS surfactant from bagasse as a surfactant injection in the Enhanced Oil Recovery (EOR).

2 Methodology

This is a laboratory research by using sodium lignosulfonate (SLS) surfactant synthesized from bagasse. The injection of surfactant is performed by using several concentrations of surfactant and salinity. The characteristic of SLS surfactant is also tested. The parameters used include the interfacial tension (IFT) of SLS surfactant and the contact angle between the injection fluid and the cores as well as the brine salinity and surfactant concentration factors.

The surfactant was injected into the core with a sample of light crude oil. The injection process was performed by inserting 1 inch-diameter synthesis core into the core holder. Followed by the injection of SLS surfactant into the core.

The injection process by using SLS surfactant solution of brine salinity was varied, i.e., 5000, 10,000, 20,000, 40,000 and 80,000 ppm with the concentration of SLS surfactant of 1.5, 3.0, 4.0 and 4.5%.

The injection product was stored in a scale tube so that the volume of oil could be obtained. The results of these core injections were reinforced by testing SLS surfactant characteristics such as IFT and contact angles in some variations of SLS surfactant concentration and salinity of brine. IFT measurements used the spinning drop whereas the angle of contact angle used the Sessile drop method which directly measured the angle of contact and determined the wettability tendency of solids by using oil and water.

3 Results

The results of injection of core using SLS surfactant from bagasse at concentration 1.5% can be seen in the following Table 1.

Figure 1 shows the results of the recovery factor from surfactant flooding at various salinities. This figure shows

the relationship of IFT and contact angle to surfactant flooding recovery factor. The concentration of used surfactant is 1.5%. The correlation between IFT, contact angle and oil recovery can be seen in Fig. 1. There are two different color areas, red-orange and green-blue. The red-orange areas show oil recovery in the range of 7–10%, occurring in areas with an IFT value of 2.73 and 3.61 mN/m, having a contact angle of about 40°–55°. High oil recovery areas also occur in other orange-red areas at 20°–25° contact angles. Table 1 emphasizes that this oil recovery occurs in salinity of 5000–10,000 ppm and salinity of 80,000 ppm. Green-blue color shows an area with low oil recovery that occurs at salinity above 10,000 ppm and below 80,000 ppm. This area has an IFT of 4.11–4.13 mN/m.

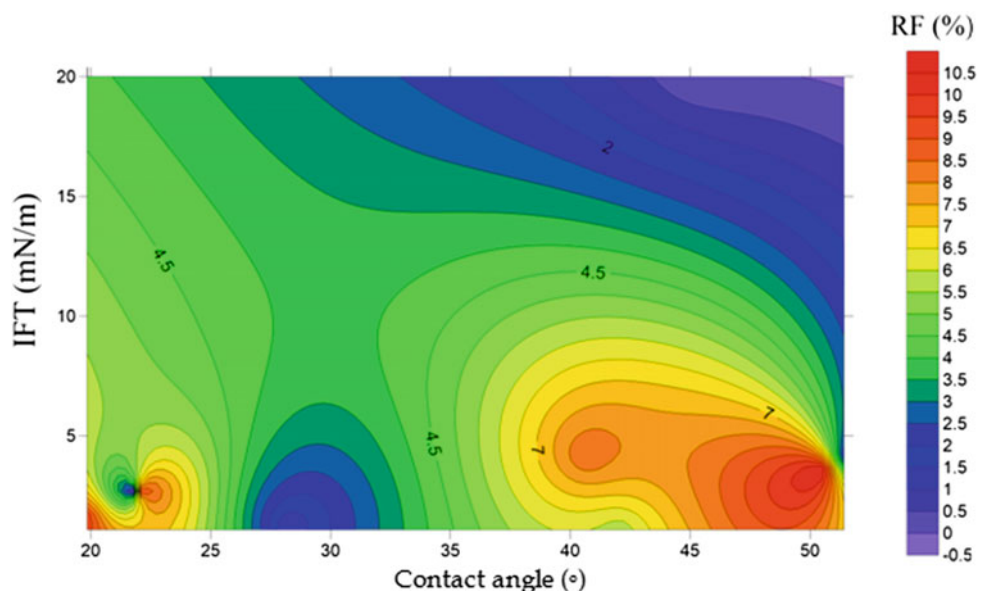
4 Discussion

The highest oil recovery occurs at the surfactant injection within the composition of 10,000 and 80,000 ppm with a surfactant concentration of 1.5%. This condition occurs because the composition produces a lower IFT than the other

Table 1 IFT and contact angle to recovery oil by surfactant SLS injection of bagasse (concentration of surfactant 1.5%)

No.	Salinity (ppm)	Concentration surfactant (%)	IFT (mN/m)	Contact angle (°)	Recovery factor from surfactant flooding (%)
1	5000	1.5	6.81	45.47	7.00
2	10,000	1.5	2.73	21.98	9.25
3	20,000	1.5	4.13	40.60	8.55
4	40,000	1.5	4.11	51.41	1.80
5	80,000	1.5	3.61	50.55	10.71

Fig. 1 FT—contact angle to recovery factor of SLS surfactant injection



compositions. In the condition of low salinity, there is a balance between oil and water in such a way that the hydrophil (head) component of SLS surfactant of bagasse goes through the surface and acts as a Surface Active Agent (surfactant). The lowest recovery occurs in the salinity composition of 40,000 ppm, 4.0% of surfactant concentration, which is only 1.80%. The results of this study highlight that IFT value increases when the salinity is above 10,000 ppm and below 80,000 ppm. Greater salinity means that SLS surfactants synthesized from bagasse cannot reduce the interfacial tension between oil and the surfactant solution. In this condition there is no balance between hydrophil and lipophil in which the hydrophil (head) component of the SLS surfactant bagasse cannot go through to the surface as a surfactant function. This condition is in line with the theory that has been put forward by Sandersen [6].

Interfacial tension test (IFT) between oil and microemulsion is one of the main parameters in the EOR process [7]. Interfacial tension (IFT) is a long unity force in the interface that is the phase margin between two phases with limited solubility, which is only a few molecules thick [8]. At the same concentration, the addition of salinity from 10,000 to 80,000 ppm turns the contact angle even larger.

For oil exploration and exploitation purposes, water-wet formation is easier for oil recovery. Wettability is defined as a fluid phase capability to wetting the solid surface in the presence of an immiscible fluid [9]. If θ is between 0° and 60° to 75° in such a system, it is defined as water-wet [10]. Thus, the measurement of the contact angle, in the injection mechanism of the SLS surfactant bagasse, shows that the wettability is wet water because the contact angle value is 21.98° – 51.41° . Hence, it is confirmed that SLS surfactant from bagasse can form the wet water system and can be used as a liquid injection to increase oil recovery.

5 Conclusions

Based on the results of this laboratory research and the above discussion, the following are the conclusions:

- Recovery oil from the result of surfactant flooding is influenced by some surfactant characters that are salinity, surfactant concentration, IFT and contact angle.
- SLS surfactant injection against light crude oil in core injection produces an oil recovery factor of 9.25–10.71% with an IFT value of 2.73–3.61 mN/m.

- The synthesis of SLS surfactants from bagasse can be used as surfactant flooding. In the SLS surfactant mechanism of bagasse, it can form a wet water system in essence with the formation of a contact angle of 40° – 55° with that value of IFT. This IFT can be low because of the balance between oil–water, in such a way that the hydrophil (head) component of SLS surfactant of bagasse goes through the surface and acts as a Surface Active Agent (surfactant).

It is, therefore, significant to conclude that salinity, SLS surfactant concentration, IFT and contact angle are synergistic effects that occur in SLS surfactant injection mechanism.

References

1. Johnson, J.J., Westmoreland, C.: Sacrificial adsorbate for surfactants utilized in chemical floods of enhanced oil recovery operations. Patent No. W-7405-ENG-26. US (1980)
2. Miller, C.A., Neogi, P.: Interfacial phenomena. Equilibrium and dynamic effects. *AiChe J.* (1986). <http://doi.org/10.1002/aic.690320.824>
3. Collepardi, M.: Mechanisms of action of superplasticizers. In: Proceedings of Second International Symposium on Concrete Technology for Sustainable Development with Emphasis on Infrastructure, pp. 527–541, Hyderabad, India, 27 Feb–3 Mar 2005
4. Hofman, Y.L., Angstad, H.P.: Analysis of Enhanced Oil Recovery Formulations, Chromatographia, Analysis of Enhanced Oil Recovery Formulations. Springer-Verlag (1987). ISSN 0009–5893. <https://doi.org/10.1007/BF02688564>
5. Karmada, W., Benzagouta, M.S., AlQuraishi, A., Amro, M.M.: Effect of temperature, pressure, salinity, and surfactant concentration on IFT for surfactant flooding optimization. *Arab. J. Geosci.* **6** (9), 3535–3544 (2013)
6. Sandersen, S.B.: Enhanced Oil Recovery with Surfactant Flooding. Center for Energy Resources Engineering—CERE, Denmark (2012)
7. Yanhua, J., Weihong, Q., Zongshi, L., Lubai, C.: A study on the modified lignosulfonate from lignin. *Energy Sources* **26**(4), 409–414 (2004). <https://doi.org/10.1080/00908310490281528>
8. Salager, J.L.: Physico-Chemical Properties of Surfactant-Water-Oil Mixture: Phase Behavior, Microemulsion Formation and Interfacial Tension. University of Texas, Austin (1977)
9. Andersen, W.G.: Wettability literature survey part 5: the effects of wettability on relative permeability. *J. Petrol. Technol.* **39**(11), 1453–1468 (1987). <https://doi.org/10.2118/16323-pa>
10. ElMofty, O.: Surfactant Enhanced Oil Recovery by Wettability Alteration in Sandstone Reservoirs. Missouri University of Science and Technology, Student Research & Creative Works at Scholars' Mine, Missouri (2012)



A Microfluidic Study of Immiscible Drainage Two-Phase Flow Regimes in Porous Media

Feng Guo and Saman A. Aryana

Abstract

The motivation for this work is an improved characterization of flow regimes for two immiscible phases in porous media. A microfluidic device featuring a water-wet porous medium that is based on a two-dimensional representation of a Berea sandstone is coupled with a high-resolution camera that allows the visualization of the entire domain, while being able to resolve features as small as 10 µm. Drainage flow experiments are conducted across a range of capillary numbers of 1E-4 to 9E-8. The viscosity ratios, defined as the viscosity of the resident fluid to that of the invading fluid, range from 1E-4 to 13.6E3. The findings are mapped on a two-dimensional parameter space (viscosity ratio and capillary number), and stability diagrams proposed in the literature are superimposed for comparison. Results suggest that the transition regime may occupy a much larger region of the flow regime diagram than is suggested in recent literature.

Keywords

Immiscible displacement • Porous media • Flow regime • Viscosity ratio • Capillary number

1 Introduction

Simultaneous flow of multiple phases in a porous medium is relevant to various practical areas of interest, such as enhanced oil recovery, geological carbon sequestration, and remediation of contaminated aquifers by the non-aqueous phase liquid (NAPL) [1, 2]. Complex fluid mixing occurs in displacement processes due to nonlinearities in flow equations and geologic heterogeneities [3]. Resulting instabilities

often appear in the form of fingers across the displacement front in porous media [4, 5]. An improved understanding of the emergence and evolution of flow instabilities due to nonlinearities enables the development of models that are more predictive [6]. Flow dynamics are determined by the interplay between capillary, viscous and gravitational forces, whose relative magnitudes are quantified via several dimensionless numbers, namely capillary number, mobility ratio and Bond number [7]. This work focuses on flow experiments in a homogeneous microfluidic device that is positioned horizontally. As a result, gravitational forces do not play a prominent role and the flow behavior is characterized using the capillary number (Ca) and the viscosity ratio (M), as

$$Ca = U\mu_1/\sigma \quad \text{and} \quad M = \mu_1/\mu_2 \quad (1)$$

where U is the invading phase Darcy velocity, σ is interfacial tension, μ is viscosity, and subscripts 1 and 2 refer to invading and resident phases, respectively. In this effort, a series of drainage displacement experiments is conducted over a relatively large range of capillary numbers (1E-4 to 9E-8) and viscosity ratios (1E-4 to 13.6E3), defined as the viscosity of the resident fluid to that of the invading fluid. Fluid migration and displacement behavior are investigated using a transparent glass microfluidic device.

2 Experiments

This work uses a representation of a natural geologic porous medium in multi-fluid displacement experiments. A microfluidic device is fabricated featuring a complex network of channels with rigid walls that are representative of a sample of Berea sandstone [8]. The medium is placed in the field of view of a high-resolution camera (monochromatic 60MP sensor) to capture data at prescribed time intervals [9]. The medium is imaged in its entirety, and the captured images have the resolution to discern features as small as

F. Guo · S. A. Aryana (✉)
University of Wyoming, Laramie, WY 82071, USA
e-mail: saryana@uwyo.edu

10 μm , which enables a quantitative analysis of the distribution of fluids. The etched pore network has a depth of approximately 10 μm , covers an area of 70 mm \times 21 mm and has a permeability of approximately 0.18 Darcy. Deionized water and glycerol mixtures are used as the wetting phase, and various mineral oils serve as the non-wetting phase. After saturating the microfluidic device with the resident fluid, the invading phase is injected at various flow rates (0.03–6 $\mu\text{L}/\text{min}$). All the displacement experiments are conducted at atmospheric pressure and room temperature.

3 Results

Sample images representing various observed flow patterns are shown in Fig. 1. Observed flow behavior is organized into four categories: stable displacement, capillary fingering, transition and viscous fingering. Displacements of the

wetting fluid by the non-wetting fluid are imaged at pre-scribed time intervals under continuous flow conditions. Figure 2 illustrates displacement fronts of several of the experiments, as plotted on a log Ca versus log M stability phase diagram.

4 Discussion

Experiments with $\log \text{Ca} < -6.3$ and $\log M < 2.48$ exhibit fingers that appear distributed in both lateral and longitudinal directions. The lateral extensions of the fingers appear especially magnified at low Ca values, where the capillary force dominates the displacement [4]. A different flow behavior exhibiting multiple narrow and disconnected, or loosely connected, fingers are observed at high values of M ($\log M > 2.48$). In this regime, displacements are controlled by viscous forces and viscous fingers which are prominent features of the displacement. At relatively high values of Ca

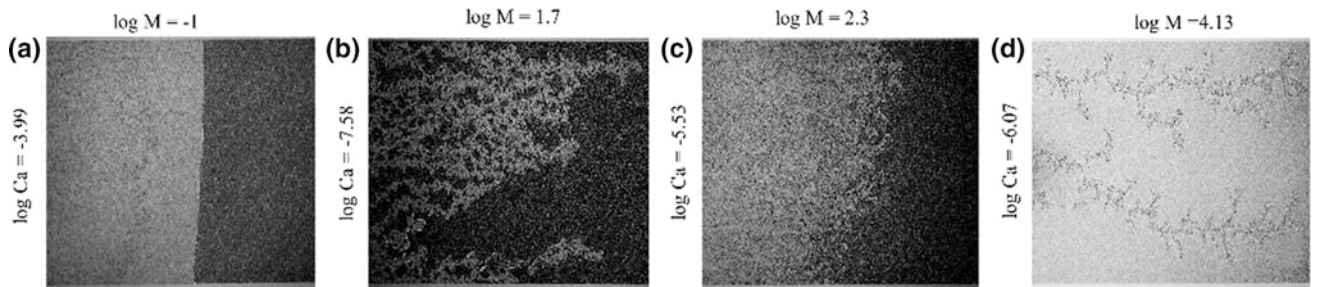
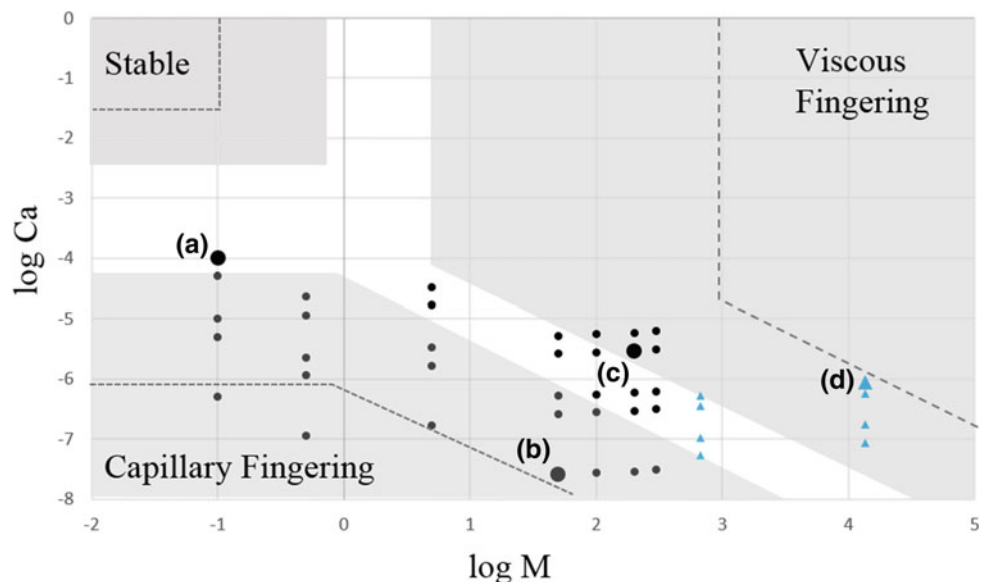


Fig. 1 Images of immiscible displacement fronts: **a** stable displacement, **b** capillary fingering, **c** transition and **d** viscous fingering. **(a), (b)** and **(c)**: the dark color represents a mixture of dyed water and

glycerol, and the bright color is a mineral oil. **(d)**: the dark color is gas and the bright color is a mixture of water and glycerol

Fig. 2 Drainage flow regime diagram; larger circles labeled **(a)**, **(b)**, **(c)** and **(d)** correspond to the images in Fig. 1. The blue triangles represent experiments where a gas phase is used as the injectant. The shaded areas are based on work by Zhang et al. [2] and the regimes delineated with dashed lines are based on work by Lenormand et al. [12]



($\log \text{Ca} > -5.20$), especially with a low value of M ($\log M < 0.7$), displacement features a uniform front distributed over the entire width of the porous medium. This regime results in efficient sweeps and is considered a stable or near stable displacement [10]. For moderate capillary numbers ($\log \text{Ca}$ between -5.53 and -6.20) at a relatively high M ($\log M = 1.7$, 2.3 and 2.48), both capillary and viscous fingers seem to play a role. In this zone, the dominant features and forces transition from capillary to viscous dominated [11]. The observations from the drainage experiments are mapped on a $\log \text{Ca}$ versus $\log M$ stability phase diagram, as shown in Fig. 2. Clear examples of stable displacement, capillary fingering, transition and viscous fingering are shown in Fig. 1. The areas in Fig. 2 corresponding to each flow regime have been delineated based on numerical and/or experimental observations of Lenormand et al. [12] (shown by dashed lines in Fig. 2) and Zhang et al. [2] (shown by shaded areas in Fig. 2). The experimental data in this work are more in line with the regime delineations prescribed by Lenormand et al. [12].

5 Conclusions

A series of two-phase displacement experiments is conducted in a glass microfluidic device, featuring a complex network of channels. The high-resolution images enable careful analysis of the displacement fronts, which may provide further insight regarding the interplay between viscous and capillary forces and the delineation of various flow regimes. Results from drainage displacement experiments are in agreement with flow regimes delineated by Lenormand et al. [6]. The transition regime in two-phase drainage experiments appears to occupy a much larger region of the flow regime diagram than surmised by recent experimental work using a medium that consists of uniformly spaced cylindrical pillars [2]. In future work, the boundaries of these regimes will be deduced from the experimental data by

careful characterization of the shape of the interfaces and associated displacement efficiencies.

References

- Carroll, K.C., McDonald, K., Marble, J., Russo, A.E., Brusseau, M.L.: The impact of transitions between two-fluid and three-fluid phases on fluid configuration and fluid-fluid interfacial area in porous media. *Water Resour. Res.* **51**(9), 7189–7201 (2015)
- Zhang, C., Oostrom, M., Wietsma, T.W., Grate, J.W., Warner, M. G.: Influence of viscous and capillary forces on immiscible fluid displacement: pore-scale experimental study in a water-wet micromodel demonstrating viscous and capillary fingering. *Energy Fuels* **25**(8), 3493–3505 (2011)
- Furtado, F., Pereira, F.: Crossover from nonlinearity controlled to heterogeneity controlled mixing in two-phase porous media flows. *Comput. Geosci.* **7**(2), 115–135 (2003)
- Cottin, C., Bodiguel, H., Colin, A.: Drainage in two-dimensional porous media: from capillary fingering to viscous flow. *Phys. Rev. E* **82**(4), 046315 (2010)
- Løvoll, G., Jankov, M., Måloøy, K.J., Toussaint, R., Schmittbuhl, J., Schäfer, G., Méheust, Y.: Influence of viscous fingering on dynamic saturation-pressure curves in porous media. *Transp. Porous Media* **86**(1), 305–324 (2011)
- Lenormand, R.: Liquids in porous media. *J. Phys.: Condens. Matter* **2**, 79–88 (1990)
- Aryana, S.A., Kovscek, A.R.: Experiments and analysis of drainage displacement processes relevant to carbon dioxide injection. *Phys. Rev. E* **86**(6), 066310 (2012)
- Guo, F., He, J., Johnson, P.A., Aryana, S.A.: Stabilization of CO_2 foam using by-product fly ash and recyclable iron oxide nanoparticles to improve carbon utilization in EOR processes. *Sustain. Energy Fuels* **1**(4), 814–822 (2017)
- Guo, F., Aryana, S.: An experimental investigation of nanoparticle-stabilized CO_2 foam used in enhanced oil recovery. *Fuel* **186**, 430–442 (2016)
- Savani, I., Bedeaux, D., Kjelstrup, S., Vassvik, M., Sinha, S., Hansen, A.: Ensemble distribution for immiscible two-phase flow in porous media. *Phys. Rev. E* **023116** (2017)
- Fernández, J.F., Rangel, R., Rivero, J.: Crossover length from invasion percolation to diffusion-limited aggregation in porous media. *Phys. Rev. Lett.* **67**(21), 2958 (1991)
- Lenormand, R., Touboul, E., Zarcone, C.: Numerical models and experiments on immiscible displacements in porous media. *J. Fluid Mech.* **189**, 165–187 (1988)



Creation of Saturation Maps from Two-Phase Flow Experiments in Microfluidic Devices

Yuhang Wang and Saman A. Aryana

Abstract

Microfluidic devices provide an experimental platform for direct observations of flow in complex channel networks. In this work, two-phase displacement experiments are conducted using a microfluidic device, featuring a complex network that is representative of a sample of Berea sandstone. The porous medium is placed in the field of view of a high-resolution camera with a monochromatic sensor—data captured in the form of images cover the entire medium while maintaining the resolution needed to discern features as small as 10 μm . This paper presents the series of steps required to convert these images into saturation maps that may be used for comparisons with predictions of numerical simulation models. The main steps include: exclusion of the grains; perspective transformation to correct minor misalignments of the device in each experiment; calculation of the Representative Elementary Volume; local thresholding strategy to account for non-uniform illumination across the medium; and finally, calculation of saturation maps.

Keywords

Porous media • Multiphase flow • Microfluidic device
Image segmentation • Nonparametric density estimation

1 Introduction

Microfluidic devices provide a platform for a direct visualization of flow in porous media [1]. Flow behavior is often captured via a microscope-mounted camera [2], which may, depending on the size of the medium and the chosen magnification, limit the area visible in each image. In such a case, multiple images must be taken, where each image covers a

portion of the medium. These images are then stitched together to provide an overall picture of the medium. The individual images are often not taken at the same point in time. This might be a cause for concern, especially in dynamic experiments where changes may occur in the medium during the elapsed time. In this work, a microfluidic device featuring a complex network that is representative of a sample of Berea sandstone is placed in the field of view of a high-resolution camera with a 60 MP monochromatic sensor [3]. Data captured in the form of images cover the entire medium while maintaining the resolution needed to discern features as small as 10 μm (pixel size $\sim 5 \mu\text{m}$). The channel network is 10 μm in depth and its smallest feature is approximately 15 μm . The porous medium has an overall dimension of approximately $21 \times 70 \text{ mm}^2$. This paper describes the elements required for the creation of accurate saturation maps from two-phase microfluidic flow experiments. Such maps may be used to benchmark and compare with results from numerical simulation experiments using macroscale descriptions of flow where saturation is a primary variable.

2 Methods

A projective transformation [4] is performed on the portion of each image corresponding to the medium. The transformation matrix is determined using coordinates of four points on both the original images and their target positions. Additionally, the constraint that any three of the four points cannot be collinear is imposed. The size of the Representative Elementary Volume (REV) is calculated; REV is defined as the smallest sample volume, or area in the case of microfluidic experiments, beyond which porosity is independent of the sample size [5, 6]. Continuum scale (macroscale) variables, such as porosity and saturation, are defined over this REV. Porosity values for a range of concentric window sizes are calculated at randomly selected locations in the medium.

An inspection of images reveals a slight non-uniformity in illumination across the porous medium. As a result,

Y. Wang · S. A. Aryana (✉)
University of Wyoming, Laramie, WY 82071, USA
e-mail: saryana@uwyo.edu

a global threshold value does not exist. Therefore, a local thresholding strategy is used to delineate phase saturations across the model [7]. Each image is partitioned into a set of sub-regions over which illumination is relatively uniform. The kernel density estimation method [8] is used to build the histogram for each sub-region. Three thresholding techniques are implemented: Histogram-based Detection (HD), Otsu's Method (OM), and Iterative Selection (IS). In HD, the minimum value between the modes of the bimodal distribution of pixel values serves as the threshold. In OM, threshold values are calculated based on local discriminant analyses [9]. In IS, the mean values for the two separate classes (the two immiscible phases in this case) are calculated and the threshold value is established based on their arithmetic average in an iterative manner [10].

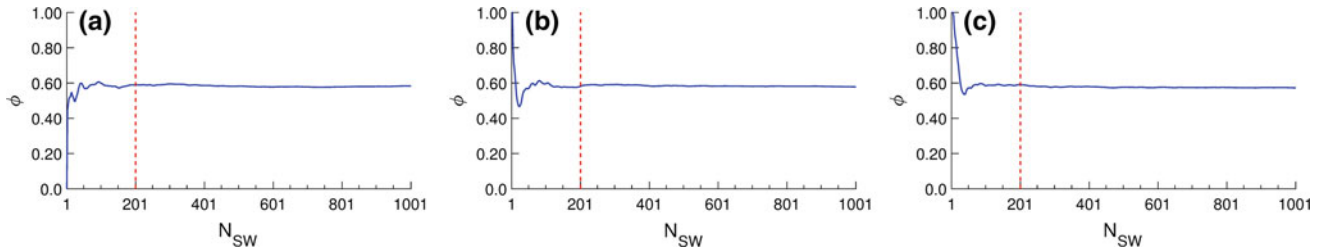


Fig. 1 Porosity versus window size at three random locations

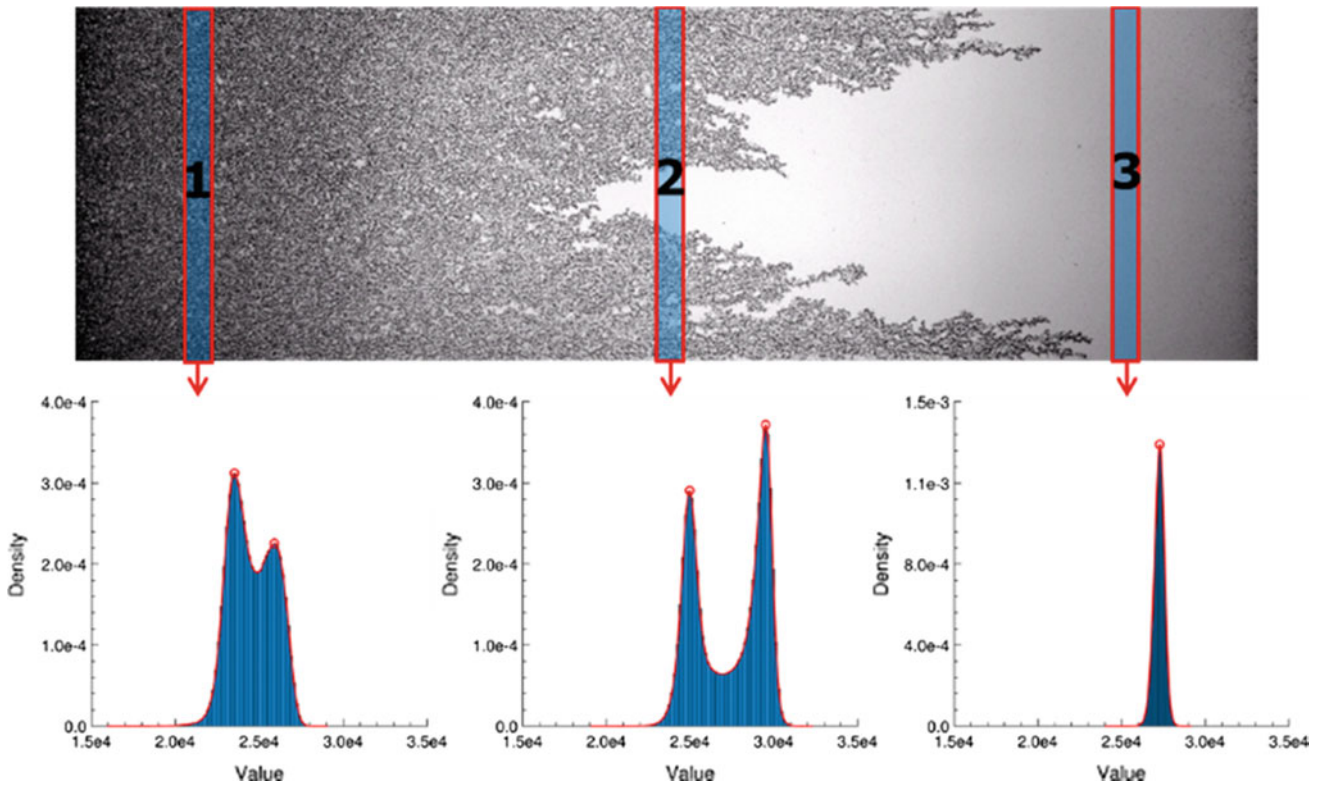


Fig. 2 An example of the image obtained from experiments and histograms of sub-regions at different locations

3 Results

REV sizes are calculated at 400 randomly selected locations. The porous medium is homogeneous and the sample size that minimizes the variations of local porosity of at least 90% of the selected locations is chosen as the medium's REV size. Figure 1 presents the results of porosity as a function of sampling size at three random locations.

An example image, along with three sub-regions, histograms of the pixel values for each sub-region and their Probability Density Functions obtained using kernel density estimation are shown in Fig. 2. The resulting saturation maps are presented in Fig. 3.

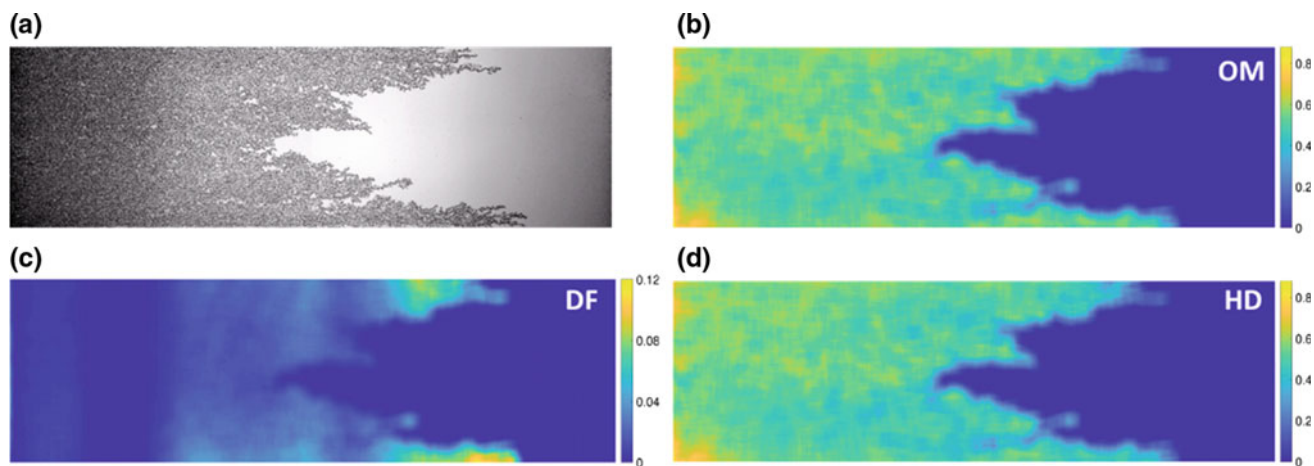


Fig. 3 **a** Experimental observation; **b** and **d** corresponding saturation maps using OM and HD methods; and **c** difference between the two saturation maps (DF)

4 Discussion

Figure 1 shows that pronounced fluctuations in porosity are observed at relatively small window sizes. These fluctuations become insignificant at a window size of 201 pixels in more than 90% of all sampled locations. As a result, a window size of 201 pixels is selected as the REV size for the medium. Given the rather large REV size (averaging window) compared to each pixel, errors associated with the resolution of the camera are negligible in the saturation maps. Pixel values in sub-regions where two phases are present exhibit bimodal distributions, whereas sub-regions fully saturated with one phase have only one mode (Fig. 2). The local threshold values calculated using OM and IS are nearly identical, whereas those obtained via the HD method differ significantly. As shown in Fig. 3c, the differences between HD and OM based saturation maps are more pronounced in the vicinity of the displacement front.

5 Conclusions

Practical issues that arise in the calculation of saturation maps from high-resolution images of porous media in microfluidic devices are addressed. A cohesive framework, comprising image alignment, determination of REV size, and image segmentation is discussed. Non-uniform illumination may make it unfeasible to select a global threshold value to discern various phases throughout the medium.

Therefore, it is crucial to find accurate local threshold values to calculate accurate saturation maps, especially in regions where more than one fluid phase is present. Three methods for local thresholding are implemented. Results from the IS method are consistent with those from OM, whereas saturation maps obtained using HD exhibit significant differences. These results are consistent with the comparative analysis reported in literature [11].

Acknowledgements The corresponding author gratefully acknowledges the Donors of the American Chemical Society Petroleum Research Fund (55795-DNI9) for the support of this research.

References

- Guo, F., Aryana, S.A.: An experimental investigation of nanoparticle-stabilized CO₂ foam used in enhanced oil recovery. *Fuel* **186**, 430–442 (2016)
- Buchgraber, M., Al-Dossary, M., Ross, C.M., Kovscek, A.R.: Creation of a dual-porosity micromodel for pore-level visualization of multiphase flow. *J. Petrol. Sci. Eng.* **86**, 27–38 (2012)
- Guo, F., He, J., Johnson, P.A., Aryana, S.A.: Stabilization of CO₂ foam using by-product fly ash and recyclable iron oxide nanoparticles to improve carbon utilization in EOR processes. *Sustain. Energy Fuels* **1**(4), 814–822 (2017)
- Szeliski, R.: Computer Vision: Algorithms and Applications. Springer Science & Business Media (2010)
- Bear, J.: Dynamics of Fluids in Porous Media. Courier Corporation (2013)
- Karadimitriou, N.K., Musterd, M., Kleingeld, P.J., Kreutzer, M.T., Hassanzadeh, S.M., Joekar-Niasar, V.: On the fabrication of PDMS micromodels by rapid prototyping, and their use in two-phase flow studies. *Water Resour. Res.* **49**(4), 2056–2067 (2013)

-
7. Pal, N.R., Pal, S.K.: A review on image segmentation techniques. *Pattern Recogn.* **26**(9), 1277–1294 (1993)
 8. Silverman, B.W.: Density Estimation for Statistics and Data Analysis, vol. 26. CRC Press (1986)
 9. Otsu, N.: A threshold selection method from gray-level histograms. *IEEE Trans. Syst. Man Cybern.* **9**(1), 62–66 (1979)
 10. Nagabhushana, S.: Computer Vision and Image Processing. New Age International (2005)
 11. Sehairi, K., Chouireb, F., Meunier, J.: Comparison study between different automatic threshold algorithms for motion detection. In: 4th International Conference on IEEE Transactions, pp. 1–8. IEEE, Algeria (2015)



Nonequilibrium Effects in Immiscible Two-Phase Flow

Yuhang Wang and Saman A. Aryana

Abstract

Two-dimensional, high-resolution, numerical solutions for the classical formulation and two widely accepted nonequilibrium models of multiphase flow through porous media are generated and compared. Flow equations for simultaneous flow of two immiscible phases through porous media are written in a vorticity stream-function form. In the resulting system of equations, the vorticity stream-function equation is solved using a spectral method and the transport equation is discretized in space using a central-upwind scheme. A semi-implicit time-stepper is used to solve the coupled system of equations. The solutions reveal that inclusion of dynamic capillary pressure sharpens the front and lengthens the viscous fingers. The inclusion of nonequilibrium effects in constitutive relations introduces diffusion and smears the otherwise highly resolved viscous fingers in the saturation front.

Keywords

Multiphase flow • Nonequilibrium effects
High-resolution methods • Flow instability

1 Introduction

An accurate mathematical description of multiphase flow in porous media is essential in many practical applications. Classical macroscale models rely on the assumption of instantaneous equilibrium [1] (referred to as the CLA model). To date, a number of nonequilibrium models have been proposed to address this deficiency, including the dynamic capillary pressure-saturation relation proposed by Hassanzadeh and Gray [2] (herein referred to as the H&G

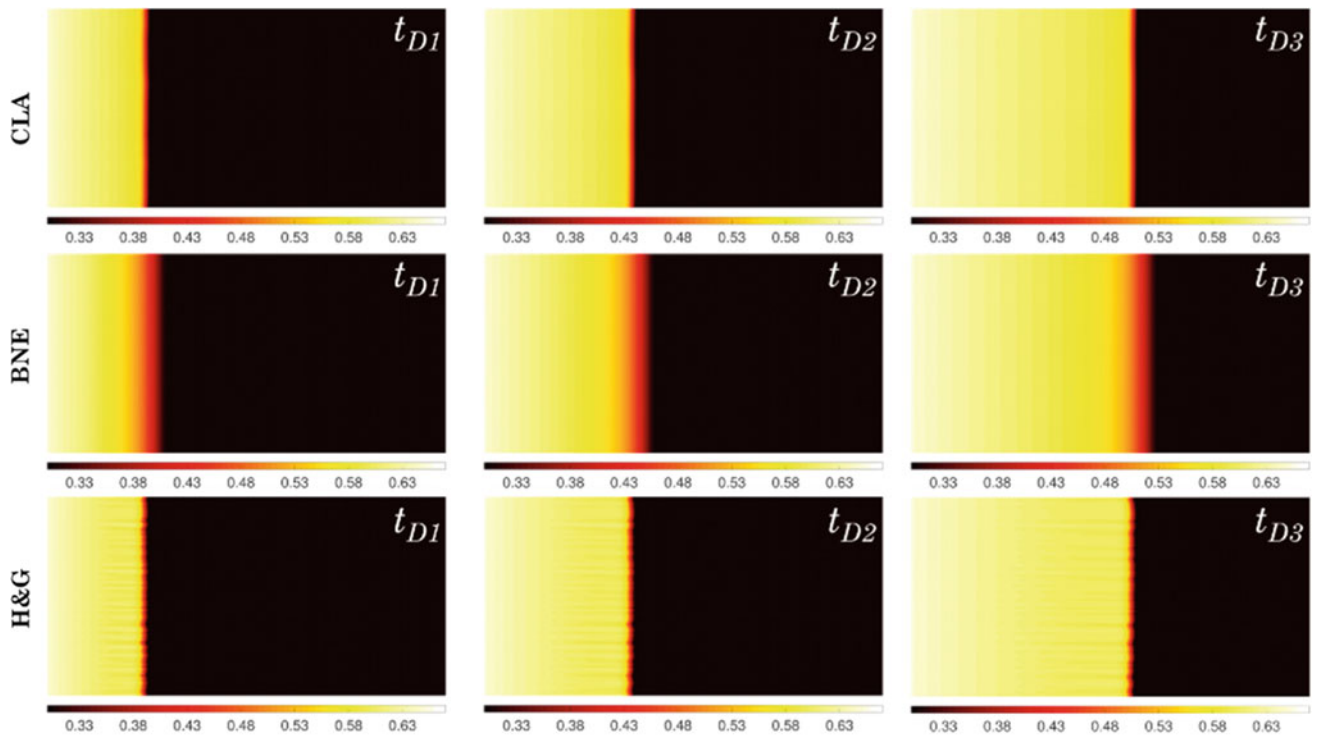
model), the nonequilibrium model proposed by Barenblatt [1] (referred to as the BNE model), and the general nonequilibrium formulation developed by Aryana and Kovscek [3] (referred to as the A&K model). Despite the development of alternate constitutive relations, competing models (i.e., BNE and H&G models) exhibit limited improvements in terms of predictive capacity [4] and lead to prohibitive computational costs and stability concerns in numerical simulation. All the aforementioned numerical experiments are in one-dimension, and fail to capture the impact of the development of fingers. Moreover, these numerical experiments rely on low-order numerical methods for spatial discretization of the flux terms, resulting in artificial (numerical) diffusion in the solutions.

In this work, a high-resolution, two-dimensional mathematical framework is proposed. A spectral method [5] is used to solve the vorticity stream-function equation, and a central-upwind scheme [6, 7] is used for the spatial discretization of convection flux in the transport equation. The coupled system is solved using a semi-implicit time stepper. Results from the numerical simulation of the CLA, BNE, and H&G models are compared and analyzed.

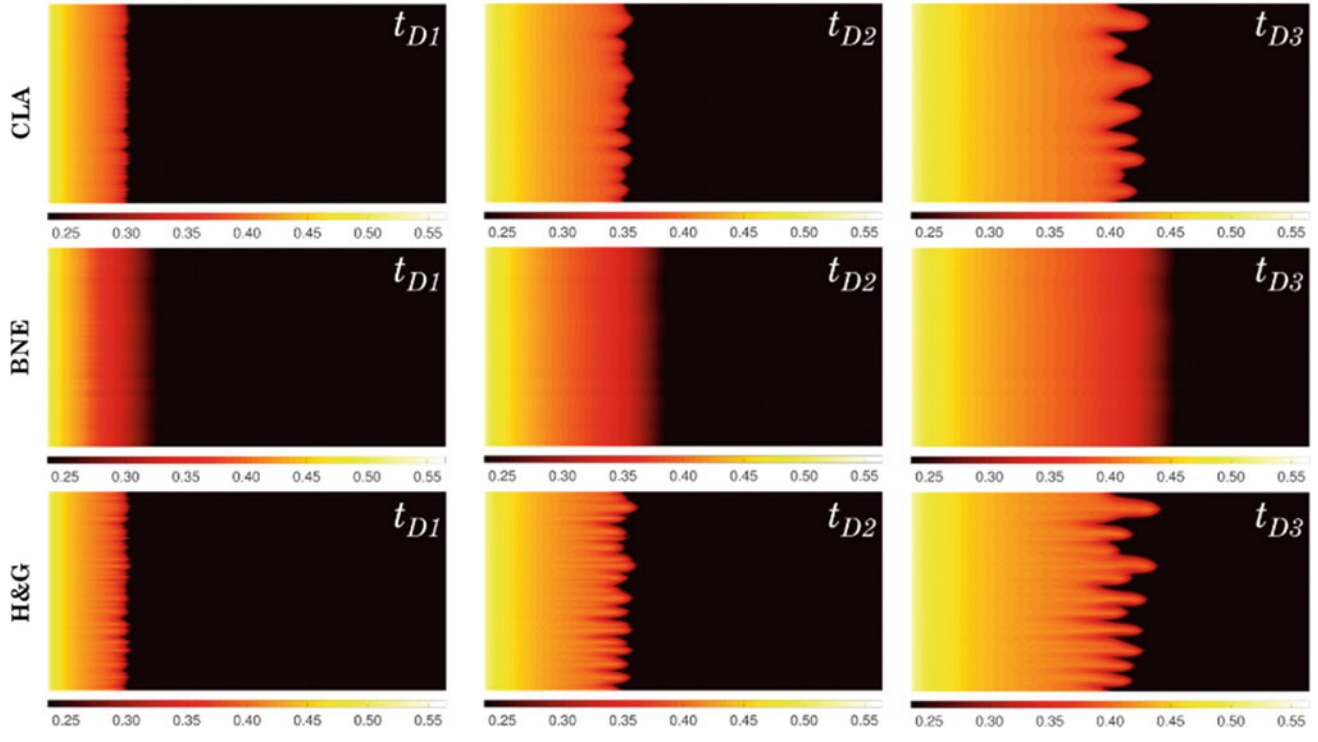
2 Methods

Numerical simulation is performed in a two-dimensional domain, i.e., a rectangle with width, W , and length, L . The invading phase with a viscosity of μ_2 is injected into the porous medium at the left boundary ($x = 0$) with a constant velocity, U , and displaces the resident phase with a viscosity of μ_1 . A constant pressure condition is used at the outlet (right) boundary ($x = L$). A no-flux boundary condition is imposed at the bottom and top boundaries ($y = 0$ and $y = L$). Multiphase flow in porous media is governed by expressions of conservation of mass and momentum (multiphase extension of Darcy's law). The formulation is simplified by assuming incompressible and isothermal conditions. The medium is assumed to be homogeneous with a constant

Y. Wang · S. A. Aryana (✉)
University of Wyoming, Laramie, WY 82071, USA
e-mail: saryana@uwyo.edu



(a) Shock mobility ratio = 0.82 (case I)



(b) Shock mobility ratio = 2.29 (case II)

Fig. 1 Saturation maps obtained using CLA, BNE and H&G models

permeability, k , and porosity, φ . The governing system of equations is given by

$$\begin{cases} \mathbf{u} = -k\lambda_T(S_w)\nabla P_n + k\lambda_w(S_w)\nabla(P_c(S_w)), \\ \nabla \cdot \mathbf{u} = q, \\ \phi \partial_t S_w + \nabla \cdot (\mathbf{u} f_w(S_w)) = -\nabla \cdot (k f_w(S_w) \lambda_n(S_w) \nabla P_c(S_w)) + q_w, \end{cases} \quad (1)$$

where S , q , and λ represent saturation, volumetric flow rate and mobility, \mathbf{u} is the total velocity, P is phase pressure, and P_c is capillary pressure. Subscripts n and w refer to the nonwetting and wetting phases, respectively, and λ_T is total mobility. The closed system given by Eq. (1) is referred to as the classical model (CLA). The H&G model defines a dynamic capillary pressure given by

$$P_c(S_w)^{\text{dyn}} = P_c(S_w) - \tau_H(S_w) \partial_t S_w, \quad (2)$$

where $\tau_H(S_w)$ is a phenomenological coefficient [2]. Governing equations for the H&G model are obtained by replacing the static capillary pressure with the dynamic capillary pressure in Eq. (1). The BNE model incorporates nonequilibrium effects in constitutive relations. The dynamic constitutive relations are evaluated using the effective saturation given by

$$\eta_w = S_w + \tau_B(S_w) \partial_t S_w, \quad (3)$$

where $\tau_B(S_w)$ is redistribution time [1]. Governing equations for the BNE model are obtained by replacing the actual saturation with the effective saturation when evaluating the constitutive relations in Eq. (1). To solve the governing system of Eq. (1), flow equations are written in a vorticity stream-function form. The Fourier Transform [8] is used to solve the vorticity stream-function equation, and the convection flux in the transport equation is solved using a central-upwind scheme. The coupled system of equations is solved using a semi-implicit time-stepper. Governing equations that incorporate nonequilibrium models use the same discretization scheme.

3 Results

Two systems of fluids with shock mobility ratios [9] of 0.82 (case I) and 2.29 (case II) are simulated (Fig. 1). The initial condition is created by stacking one-dimensional solutions of Buckley-Leverett equation with the front position located at $0.1L$ along the y -axis, followed by random perturbations

of the one-dimensional solutions to initiate instabilities. The value of τ_H is $1.0e6$ Pa.s, and the value of τ_B is 150.0 s for both cases. Results from numerical simulation using the classical model (CLA), and two nonequilibrium models (BNE and H&G) are presented in Fig. 1.

4 Discussion

Based on results from the CLA model, case I appears to be stable, whereas case II exhibits instabilities. These results suggest that the shock mobility ratio is a valid indicator of flow instability for the numerical results. The BNE model smears the saturation front, which helps capture the spreading fronts observed in unstable flow experiments [10]. In the unstable case, the fingers that are present in solutions to the CLA model are not visible in the BNE solutions. Additionally, the H&G model lengthens the mixing zone and causes the instabilities to become more prominent compared to the CLA model.

5 Conclusions

This paper presents a high-resolution, two-dimensional numerical simulator that incorporates H&G and BNE nonequilibrium models. A semi-implicit time-stepping scheme is used to solve the coupled vorticity stream-function equation and transport equation. Numerical results indicate that the H&G model has a sharpening effect, and the BNE model has a smearing effect on the saturation map.

References

1. Barenblatt, G.I., Patzek, T.W., Silin, D.B.: The mathematical model of nonequilibrium effects in water-oil displacement. *SPE J.* **8**(4), 409–416 (2003)
2. Hassanzadeh, S.M., Gray, W.G.: Thermodynamic basis of capillary pressure in porous media. *Water Resour. Res.* **29**(10), 3389–3405 (1993)
3. Aryana, S.A., Kovscek, A.R.: Nonequilibrium effects and multiphase flow in porous media. *Transp. Porous Media* **97**(3), 373–394 (2013)
4. Ren, G., Rafiee, J., Aryana, S.A., Younis, R.M.: A Bayesian model selection analysis of equilibrium and nonequilibrium models for multiphase flow in porous media. *Int. J. Multiph. Flow* **89**, 313–320 (2017)

-
- 5. Canuto, C., Hussaini, M.Y., Quarteroni, A., Thomas Jr., A.: Spectral Methods in Fluid Dynamics. Springer Science & Business Media (2012)
 - 6. Kurganov, A., Tadmor, E.: New high-resolution central schemes for nonlinear conservation laws and convection–diffusion equations. *J. Comput. Phys.* **160**(1), 241–282 (2000)
 - 7. Kurganov, A., Noelle, S., Petrova, G.: Semidiscrete central-upwind schemes for hyperbolic conservation laws and Hamilton-Jacobi equations. *SIAM J. Sci. Comput.* **23**(3), 707–740 (2001)
 - 8. Kutz, J.N.: Data-Driven Modeling & Scientific Computation: Methods for Complex Systems & Big Data. Oxford University Press (2013)
 - 9. Berg, S., Ott, H.: Stability of CO₂–brine immiscible displacement. *Int. J. Greenhouse Gas Control* **11**, 188–203 (2012)
 - 10. Riaz, A., Tang, G.Q., Tchelepi, H.A., Kovscek, A.R.: Forced imbibition in natural porous media: comparison between experiments and continuum models. *Phys. Rev. E* **75**, 036305 (2007)

Part IV

**Advances in Petroleum Exploration
and Management**

Gravity Changes, Earthquakes and Oil Field (Italy)

Valentino Straser and Mario Campion

Abstract

The gravitational variations are a recurring registered event from the possibly experimental station of Rovigo (Italy). The intervals of variations have a duration from 9' to 21' 23' and these continue to happen for temporary intervals from some hours to some weeks. The important variations of local microgravity, roughly 27 milligal, is registered as an equivalent of a strong earthquake. The gravitational variations should rarely happen in the absence of seismicity. The authors interpret the complex phenomena of gravitational local variations as the results of undulatory interferences generated from the Oil reservoir in areas of definite hydrocarbon occurrence. The study, which started in 1999, should add new geophysical concept suggesting a new non-invasive research preliminary method in order to locate oilfield hydrocarbon deposits.

Keywords

Oil field • Earthquake • Microgravity • Gravimeter
Gravitational pulsations

1 Introduction

The hypothesis that we can measure local “gravitational variations” to be related to oil fields represents a new concept in the study of geophysics. The gravitational monitoring is carried out with a specific gravity meter eight decimal places, located in Rovigo (Italy) 24/7, and active since 1999 [1]. The data were deduced from the daily variations in local

gravity and the gravitational anomalies generated by strong earthquakes, even very distant, such as the case of Japan or south-east Asia. During the monitoring, gravitational variations were also identified with recurrent periods and with defined intervals, at the moment still without explanation. In this study, it is hypothesized that local micro-gravitational variations, periodically induced by seismic waves, can be related to local hydrocarbon reservoirs. It is excluded that gravitational anomalies can be generated by an electromagnetic nature, as the “pulsations” are also present in the recordings with the totally diamagnetic oscillator and therefore not influenced by the Earth’s electromagnetic field. Instead, we believe that the phenomenon can be generated by “gravitational pulsations” as they are often detected by the gravimeter and not always by the seismograph, probably due to mass movements in the subsoil or to changes in a hydrocarbon reservoir.

2 Instruments and Methods of Measurement

The gravimeter is located in the town of Rovigo, Italy—coordinates: Latitude 45.07 N. and Longitude 11.778 E. The instrument created by Dr. Mario Campion differs significantly from these three types: gravimeter with constant length, with free-fall gravimeter and gravimeter with sensing element electromagnetic balance. The tool measures the average value of gravity in a defined time interval.

The precision of the oscillator performs 1000 or 100 or 10 oscillations, dividing the value by the number of oscillations itself.

The variations of the average period are inversely proportional to the variations of gravity g , in the range within which the instrument carried out the measurement, as resulting from the formula of the simple pendulum. To complete the description of the device, consider that it is controlled by a computer possibly “27*7” which manages the operating cycle automatically.

V. Straser (✉)
Italian Ministry of Education, Parma, Italy
e-mail: valentino.straser@gmail.com

M. Campion
Rovigo, Italy

3 Results

The monitoring lasted five months, from 28 August, 2017, to 28 January, 2018. During this period the gravitational variations of 10 earthquakes of magnitude higher than M5 were recorded, compared to 78 earthquakes occurring on a global scale, with only three earthquakes of a magnitude less than 4.5. The monitoring took place during a period of relative seismic quiescence in Italy (Table 1).

4 Discussion

The instrument detects variations in the milligal order and a standard deviation of 1.47×10^{-7} . With these measurements, if we exclude the error due to the instrument, we can analyze both the nature of the subsoil and the presence of water or hydrocarbons. The data collected since 1999 indicated that the earthquake's hypocenter and the high-quake energy are nearer, the gravitational variations are more intense [2]. The earthquakes, perceived at the instrumental level, produce variations and gravitational levels of about 20 milligal, as indicated by the graphs with characteristic peaks [3]. The time elapsed between the increase, the peak and the return to the initial state is variable and generally from 5' to 20'. The event, therefore, is not of an impulsive nature, as would be expected from the passage of a seismic wave. The velocity of the wave is attenuated and able to move volumes, inducing micro-variations in the acceleration of gravity. Among the hypotheses taken into consideration, it is included that of the migration of fluids (hydrocarbons?) induced

by energies in the order of 60 kJ, corresponding to an earthquake of magnitude 2 on Richter scale. From the analysis of the data, we can deduce that the velocity of arrival of the seismic waves and the corresponding change in the gravitational level is variable. The recent earthquakes in New Caledonia on November 19, 2017 (Table 1), provide an opportunity for discussion. The distance calculated by the monitoring station is 16.641 km. The first earthquake, of magnitude 6.6, occurred at 16:09:04 15:09:04 and the shock was not recorded by the seismograph, while the gravimeter drew an evident wave. The second shock occurred at 23:43:31 and was recorded by both the seismograph and the gravimeter. In the second shock, the delay of the seismic waves, recorded by the seismograph and the gravimeter, is about the same, that is about 21 min (Fig. 1). If we consider the distance of 16,641 km, we can presume that the P waves should have taken about 30 min, while the graphs indicate that the two earthquakes are approximately 21 min apart. The waves, almost certainly, have made a different path from the superficial one, and they in turn may have moved at different speeds. These two shocks are very interesting because they happened in the same place, in very short times and at the same depth. They are therefore comparable in some parameters that constitute fixed points of reference. Then, there is a further consideration, namely that the two peaks on the graph are turned upside down. This makes the interpretation very problematic and uncertain and tends to bring down the theory of seismic waves that, by discharging their energy end up creating a compression of the ground. Therefore, a subsequent and spontaneous rarefaction of the soil. It could be hypothesized that the inversion of the signal

Table 1 List of earthquakes with magnitude greater than M3.7. recorded in Rovigo from 1 September 2017 to 25 January 2018

N.	Day	M	Zone	Latitude	Longitude	Distance epicenter (km)	Time lapse
1	2018-01-23	7.6	United States	55.91	149.05	8096	13 min
2	2018-01-14	7.1	Peru	-15.72	-74.58	9248	18 min
3	2018-01-10	7.4	Honduras	17.32	-83.62	7240	14 min
4	2018-01-04	5.2	Montenegro	42.62	19.89	631	6 min
5	2017-11-19	4.4	Italy	44.75	10.08	142	30 s
6	2017-11-19	6.9	N. Caledonia	-21.35	168.73	16,641	21 min
7	2017-11-19	6.6	N. Caledonia	-21.47	168.64	16,641	23 min
8	2017-11-12	7.2	Iran	34.80	45.87	3095	6 min
9	2017-11-04	6.2	Tonga Is.	-15.10	173.04	16,606	20 min
10	2017-11-03	4.1	Bosnia	43.18	17.87	519	3 min
11	2017-11-01	3.7	Italy (Sea)	40.28	13.53	676	2 min
12	2017-09-20	6.3	Vanuatu Is.	-18.76	169.03	16,413	20 min
13	2017-09-10	3.7	Italy	44.82	9.69	166	3 min

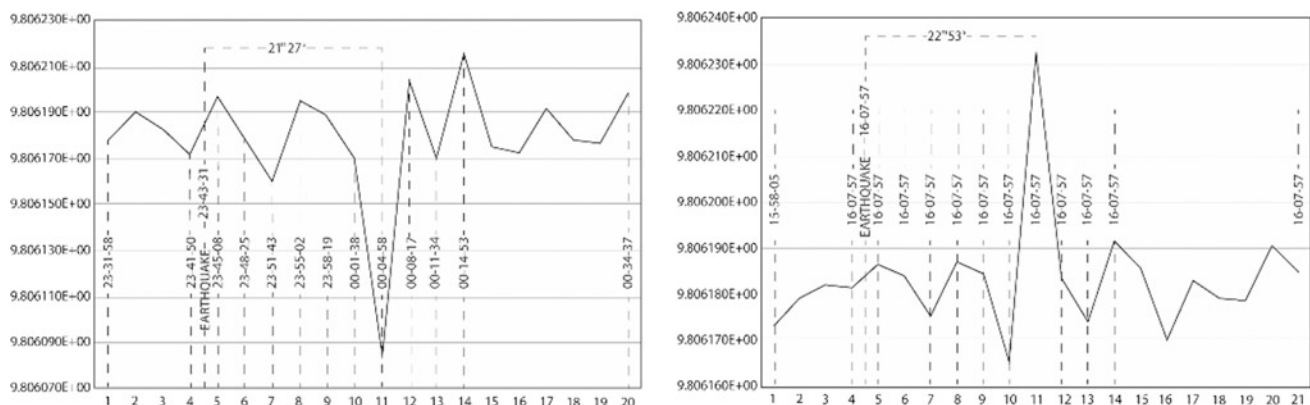


Fig. 1 Increase and decrease of the microgravity measured in Rovigo (Italy) during two strong New Caledonia earthquakes occurred on November 19, 2017

depends on the sign of the disturbance of the incoming seismic waves, which could favor the oscillation, or slow it down. This hypothesis, however, is to be discarded, because the vibration of the earth following earthquakes so far are almost nil, as evident by the fact that the seismograph, with great sensitivity, does not signal them. This means that they are of irrelevant amplitude, especially for a moving pendulum and then spread the variation on one hundred oscillations. Another element supporting this hypothesis is the fact that the gravimeter detects the seismic phenomenon on more extensive times even two or three times, compared to those of the seismograph, that is when it has totally stopped. Among the mechanisms that determine the micro-variations of "g", the following causes are hypothesized: (a) the filling and emptying of chambers and tanks; (b) mixing of immiscible liquids of different densities, for example water and hydrocarbons; (c) the change in liquid-gas-liquid state and the consequent spatial relocation of the liquid parts and the gaseous parts. All these phenomena could derive from changes in pressure, temperature and mechanical shaking due to the passage of the seismic wave.

5 Conclusions

The repetitiveness of gravitational vibrations, detected in the last 20 years by the monitoring station in Rovigo (Italy), especially in correspondence with global seismic events,

usually of magnitude higher than 6 on Richter scale, indicate the persistence of the physical phenomenon. The micro gravitational variation of local character leads to the hypothesis of mass displacements in the subsoil, probably of hydrocarbons, according to a mechanism comparable to that of geyser filling, to the immiscibility of fluids or to changes in physical state. This diagnostic and experimental method of investigation can be used both for hydrocarbon research and a new tool for the study of crustal diagnosis.

References

1. Straser, V.: Variations in gravitational field, tidal force, electromagnetic waves and earthquakes. *New Concepts Glob. Tecton. Newslet.* **57**, 98–108 (2010)
2. Straser, V.: Variations in the geomagnetic and gravitational background associated with two strong earthquakes of the May 2012 sequence in the Po Valley Plain (Italy). In: *Geophysical Research Abstracts*, vol. 15, EGU2013-1949. EGU General Assembly (2013)
3. Straser, V., Campion, M.: A possible relationship between gravitational variations and earthquakes in Central Italy. *Int. J. Eng. Sci. Invent. (IJESI)* **6**(3), 71–76 (2017)



Significance of Microbial Anomalies in Identifying the Hydrocarbon Prospects in Parts of a Petroliferous Region [Tunisia]

Mohamed Seddik Mahmoud Bougi, Jawhar Gharbi, Syrine Baklouti, Mohamed Abdul Rasheed, P. L. Srinivasa Rao, Syed Zaheer Hasan, and Mohamed Ksibi

Abstract

Microbial prospecting for oil and gas (MPOG) method for bacterial detection is widely applied in surface geochemical exploration for oil and gas deposits. The modified MPOG method was applied in the Guebiba-Sfax basin of the Tunisian Republic which showed signs of hydrocarbon generation and proved oil production. This technique is based on seepage of light hydrocarbon gases such as C1–C5 from the oil and gas reservoir to the shallow surface, providing a good environment for the development of highly specialized microbial populations. These bacteria utilize hydrocarbon gases as the only food source and are found enriched in the near-surface soils above the hydrocarbon bearing structures. The present research work employs methodologies of high significance with the potential to reduce risk in petroleum exploration. For this purpose, we collected a total of 51 soil samples from the Eastern central region of Tunisia and we used the propane oxidizing bacteria as an indicator in the present study.

Keywords

Exploration • Geochemical • Microbial prospecting hydrocarbon • Microseepage • Propane oxidizing bacteria

M. S. M. Bougi (✉) · J. Gharbi
UR17ES30 “Genomics, Biotechnology and Antiviral Strategies”
Research Unit, Higher Institute of Biotechnology, University of
Monastir, BP74, Tahar Haddad Street, 5000 Monastir, Tunisia
e-mail: mmedsed@gmail.com

M. S. M. Bougi · S. Baklouti · M. Ksibi
Laboratory of Environmental Engineering and Ecotechnology,
National School of Engineers of Sfax, University of Sfax,
Route de Soukra Km 4, Po. Box 1173 Sfax, 3038, Tunisia

M. A. Rasheed · P. L. Srinivasa Rao · S. Z. Hasan
Gujarat Energy Research and Management Institute, PDPU,
Gandhinagar, India

1 Introduction

The microbial prospecting for oil and gas (MPOG) method is an indirect approach based on the detection of anomalous population of light hydrocarbon oxidizing bacteria in the near-surface soils that indicate the presence of hydrocarbon accumulations. The surface geochemical technologies are established based on the seepage of light hydrocarbon gases from the petroleum reservoirs to the shallow surface. This seepage can raise light gas to oxidation-reduction zones leading to the development of diverse pathways of chemical and mineralogical changes. Bacteria utilizing hydrocarbon gases as the only food source can be found in high densities in the near-surface soils above the hydrocarbon bearing structures. This is a good indicator for active oil and gas reservoirs. To the best of our knowledge, this is the first time that such a technique has been tested in Tunisia for oil and gas exploration.

Locating subsurface reservoirs and prospecting for the occurrence of hydrocarbons on the surface consist in investigating near soil/sediments. The hydrocarbons seep to the surface from the subsurface accumulations through faults or capillary rise and leave their signatures on the surface (this is a basic assumption of all near-surface prospecting techniques.) [1–3] identified various migration mechanisms of hydrocarbon such as diffusion, effusion, advection with moving waters and permeation. Anomalous concentrations of the gases such as methane, ethane, propane and butane are detected in the surface soils, which serves as the direct evidence addressing the accumulation of petroleum system in an area [2, 4]. C1–C4 in the surface soils are used to assess the hydrocarbon generation potential which has anomalous concentration.

A rapid and cost-effective technique of adsorbed soil-gas helps in evaluating a frontier basin for hydrocarbon exploration oxidation-reduction zones lying above the reservoirs, which are responsible for altering the behavior of soils and sediments and also the activities of hydrocarbon-oxidizing bacteria causing the development. The energy source for

specialized bacteria largely depends on light-hydrocarbon gases. C1–C4, rising from the oil and gas pools to the shallow surface, provide the suitable conditions for the development of highly specialized bacterial populations, hence, it is a current study “topic”. Integrating this method with the new technologies gives a comprehensive picture which reduces financial commitments towards the exploration and subsequently the development and management of hydrocarbon resources.

Microbial anomalies were also observed in the northern and central regions of the study area. Incidentally, all the anomalous zones are near the major oil-producing fields. This demonstrates the usefulness of microbial prospecting techniques in hydrocarbon exploration as a tool to locate the new prospects. To reduce the risk in oil exploration, this research work has the potential to employ high-significance methodologies. For the identification of potential hydrocarbon areas, this method could be well applied when integrated with other technological tools.

2 Geological Setting

The studied oilfield is called Guebiba. This area is located in eastern Tunisia at about 12 km southwest of Sfax city (Fig. 1).

The study region (Fig. 1) comprises the area between the Cap Bon to the North and the Gulf of Gabes to the South. The Eastern part of Tunisia (both offshore and onshore) constitutes the foreland of the Atlas system. It corresponds to a transition zone located between the folded Atlas domain in northern and west-central Tunisia towards the Pelagian Sea [6]. It corresponds to a young continental margin, formed mainly during the Mesozoic and Cenozoic times.

The Pelagian domain is an active subsident area controlled by a NW-SE major fault set. This basin is characterized by the presence of major tectonic trenches parallel to the Sicily Channel [7]. In Sfax region, Guebiba geological structure is one of such asymmetric low amplitude fold. This folded trap structure is oriented NW-SE and affected by longitudinal normal faults.

3 Materials and Methods

3.1 Sampling Techniques

The grid 1×1 km pattern was adapted to collect the soil samples to optimize the number of sampling points spread

over the study area in Sfax. We collected 51 samples for microbial analysis in pre-sterilized whirl pack bags under aseptic conditions from a depth of about 1 m and we stored them at 2–4 °C till analysis.

3.2 Isolation of Propane Oxidizing Bacteria

Isolation and enumeration of propane oxidizing bacteria were carried out using the enrichment culture method followed by serial dilution and the Standard Plate Count (SPC) method. We suspended one gram of sediment sample in 9 mL of pre-sterilized water for the preparation of decimal dilutions (10^{-1} to 10^{-7}). We plated 0.1 mL aliquot of each dilution onto Mineral Salts Medium (MSM) containing petri plates. After incubation, we manually counted the developed bacterial colonies of n-propane utilizing bacteria using a colony counter and we reported the bacterial colonies in a colony forming unit (cfu/gm of soil sample) [8, 9].

4 Results and Discussion

The population of Propane Oxidizing Bacteria (POB) was counted using a colony counter and reported in colony forming units per gram (cfu/g) of sample and the POB population was found to be ranging between nil and 2.44×10^5 cfu/g. The anomaly distribution map of POB population shows distinct microbial anomalies in the North Eastern and Central Western parts of the study area. The possibility of locating hydrocarbon reservoirs through a microbiological method has been emphasized by the fact that the population of hydrocarbon oxidizing bacteria which ranges between 10^3 and 10^6 cfu/g in soil/sediment confirms that the hydrocarbon micro-seepages depend on the ecological conditions [10, 11].

Figure 2 shows that the population of hydrocarbon oxidizing bacteria in the studied area varies between nil and 2.44×10^5 cfu/g of soil which significantly substantiates the seepage of lighter hydrocarbon from the reservoirs [9, 11, 12]. Figure 2 also exhibits the existence of high densities of bacteria in black-circled locations in the sampling area, which confirms the high probability of detecting hydrocarbon reservoirs in the SW part of the sampling area. Thus, the anomalies observed can be used as indicators and as reliable indirect methods for detecting light hydrocarbon seepages.

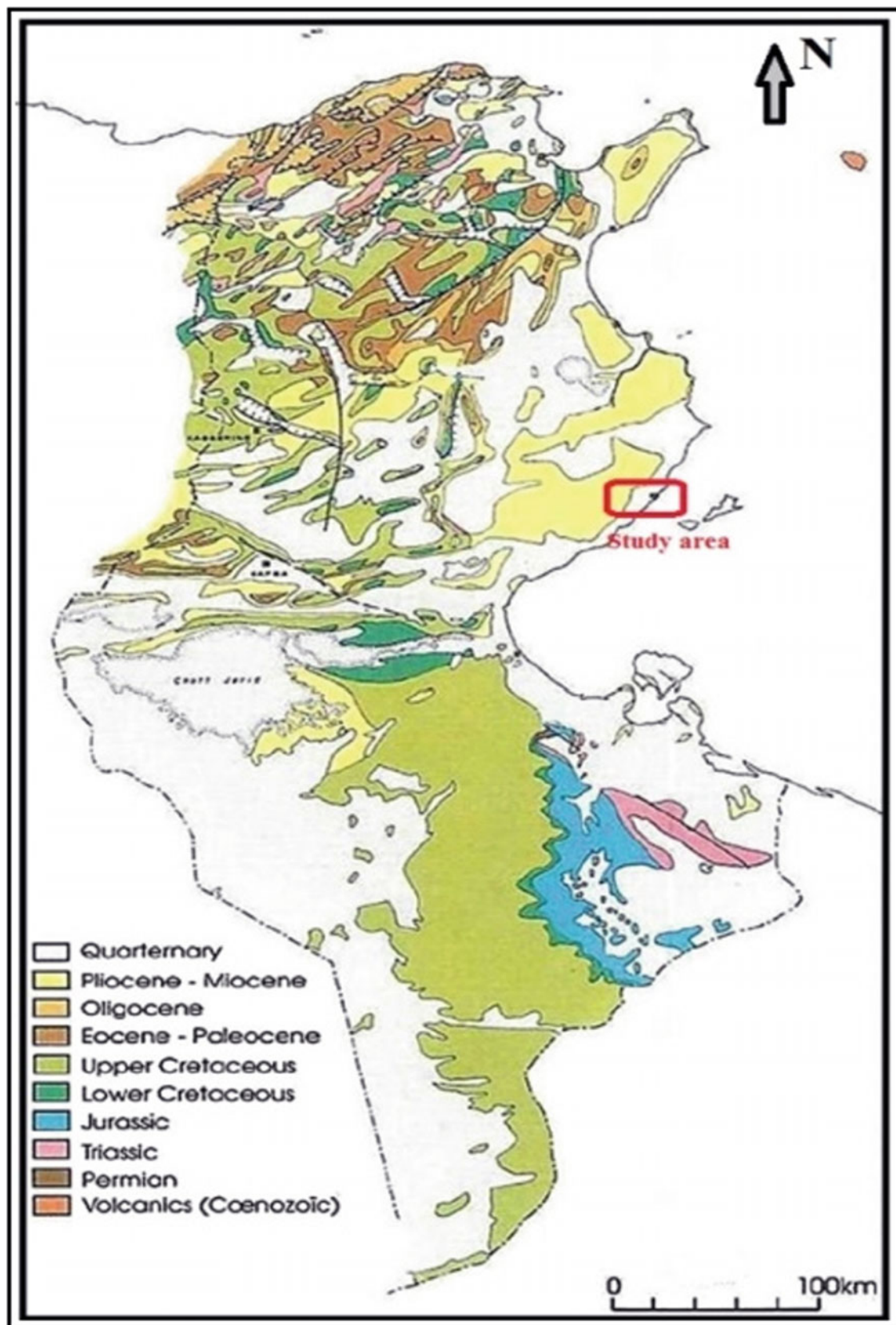
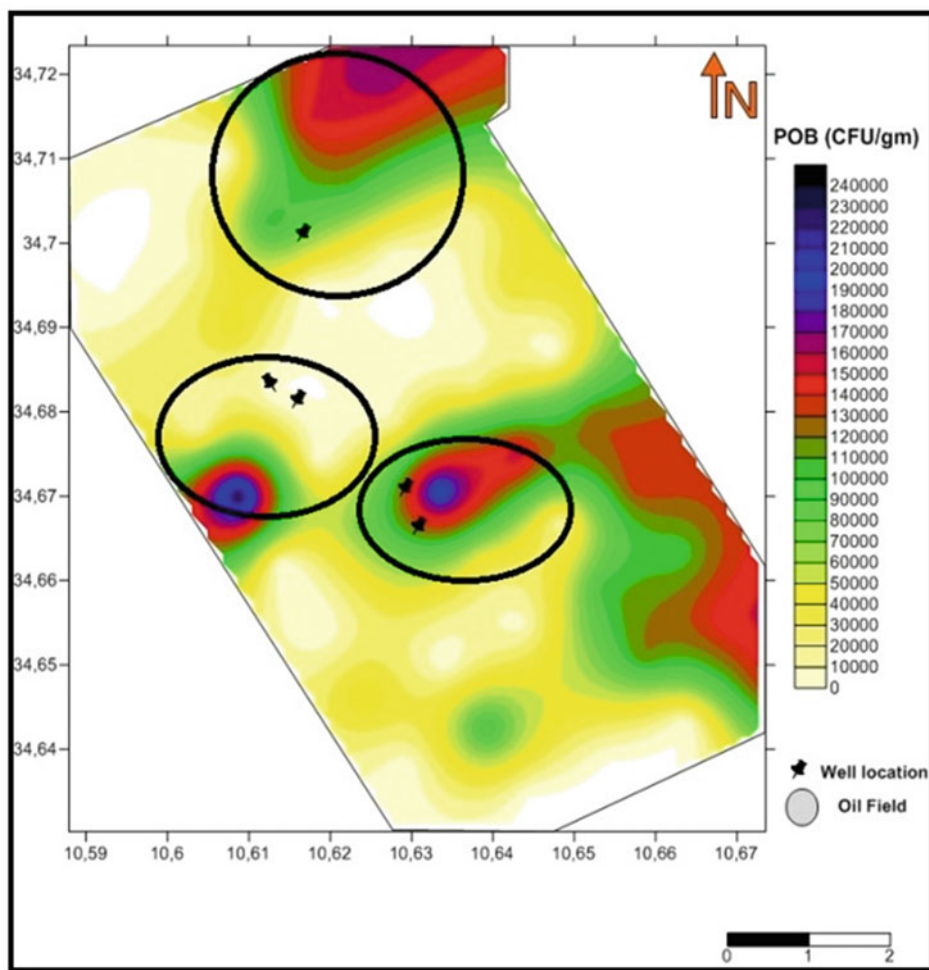


Fig. 1 Location map of study area. *Source* Gaiad et al. [5]

Fig. 2 Microbial distribution map (Propane Oxidizing Bacteria) of sampling area in Guebiba oilfield. The POB anomalies correlated with wells' location



5 Conclusions

Microbial anomalies are observed with a higher probability in the SW than in the NE regions of the sampling area. These anomalies are found close to the oil-producing fields. The hydrocarbon oxidizing bacterial populations used as proxy indicators have shown a good understandable correlation with the existing wells. The study shows that the adapted methodology can work as an efficient and cost-effective indicator to identify hydrocarbon seepage. This will be of great significance when applied in conjugation with other geoscientific techniques to confirm the zones of hydrocarbon accumulation through seepage.

References

- Rice, G.K.: Near-surface hydrocarbon gas measurement of vertical migration. In: Davidson, M.J. (eds.) Unconventional Methods in Exploration for Petroleum and Natural Gas IV. Southern Methodist University Press, Dallas (1986). [Online]. Available: <https://scholar.googleusercontent.com/scholar.bib?q=info:y6YodQH7r3UJ:scholar.google.com/&output=citation&scisig=AAGBfm0AAAAAWrNOtKhAoZYWWXS2BB6nx7pDfTz9zJ4P&scif=4&ct=citation&cd=-1&hl=fr>. Accessed 22 Mar 2018
- Tedesco, S.A.: Radiometrics. In: Surface Geochemistry in Petroleum Exploration, pp. 73–97. Springer US, Boston, MA (1995)
- Klusman, R.W., Saaed, M.A.: Comparison of Light Hydrocarbon Microseepage Mechanisms, pp. 157–168 (1996)
- Klusman, R.W.: Soil Gas and Related Methods for Natural Resource Exploration. Wiley, New York (1993)
- Gaiad, M.E., Ben Haj Ali, M., Chabani, F., Zaghrani, M.F., & Tamallah, M.N.: Les pierres marbrées de Tunisie. Tunis: ONM (2000)
- Rouvier, H.: Géologie de l'extrême Nord-tunisien. Thesis, Université Pierre et Marie Curie, Paris, France, 1000 p (1977)
- Rekhiss, F.: Modèle d'évolution structurale et géodynamique à l'extrême orientale de la chaîne Alpine d'Afrique du Nord. Unpublished Ph.D. thesis. El-Manar University, Tunis (2007). [Online]. Available: <https://scholar.googleusercontent.com/scholar.bib?q=info:J2gZpkwmCcJ:scholar.google.com/&output=citation&scisig=AAGBfm0AAAAAWrNQ-C5m1ExjNLtK5fh16K1roy7V6FTB&scif=4&ct=citation&cd=-1&hl=fr>. Accessed 22 Mar 2018
- Wilkinson, J.F.: Enrichment, Isolation and Some Properties of Methane-Utilizing Bacteria, pp. 205–218 (1970)

9. Rasheed, M.A., Lakshmi, M., Kalpana, M.S., Dayal, A.M.: Significance of trace metal anomalies in finding hydrocarbon micro-seepage in petroliferous areas of Krishna Godavari Basin, India. 9th Biennial International Conference & Exploration on Petroleum Geophysics (2012)
10. Rasheed, M.A., Lakshmi, M., Rao, P.L.S., Patil, D.J., Dayal, A.M., Sudarshan, V.: Relevance of pentane-and hexane-utilizing bacterial indicators for finding hydrocarbon microseepage: a study from Jamnagar Sub-basin, Saurashtra, Gujarat, India. Natural Resour. Res. **21**(4), 427–441 (2012)
11. Wagner, M., Wagner, M.: Case histories of microbial prospection for oil and gas, onshore and offshore in Northwest Europe. AAPG Stud Geol. (1), 453–480 (2002)
12. Singh, N., Kapoor, S., Jain, A.K., Kumar, A., Kumar, M., Manisha, A.J.: Evaluation of hydrocarbon microseepage pattern through geomicrobial survey. In: Proceedings of Petrotech, New Delhi (2003). [Online]. Available: https://scholar.googleusercontent.com/scholar.bib?q=info:D2kMoO_1nZsJ:scholar.google.com/&output=citation&scisig=AAGBfm0AAAAAWwGAhgBw7JQY-rgaK_etHd2sKgcue-_T&scisf=4&ct=citation&cd=-1&hl=fr. Accessed 20 May 2018



Conductivity and Temperature Corrections in the Djelfara Basin (Tunisia): Impact of the Basin Heat Flow Reconstructions

Insaf Mraidi, Amina Mabrouk El Asmi, and Ahmed Skanji

Abstract

The heat flow (Q) of a sedimentary level depends on two basic parameters which are: temperature and thermal conductivity. However, so far in Tunisia, heat flow estimations are usually carried out based on temperature corrections only. This study tries to emphasize the effect of thermal conductivity variations on the thermal history of the Djelfara Basin, through the evaluation of its conductivity change following a high-resolution appraisal (5 m margin). The thermal flow, determined by the Fourier and the Bullard Plot methods, was estimated using the temperature corrections equation combined with the conductivity corrections based on porosity data. Consequently, we believe that a better reconstruction of the regional distribution of the thermal flow of the region in relation to its geodynamic evolution was achieved. The most realistic scenario compared to the geologic model shows an average heat flow equal to 82 mW/m^2 , which is higher than the global average of about 64 mW/m^2 .

Keywords

Heat flow • Thermal conductivity • Temperature • Djelfara basin • Geodynamic evolution

1 Introduction

Heat flow (Q) depends on two basic parameters which are temperature (BHT and DST) and thermal conductivity. However, so far in Tunisia, heat flow estimations have usually been carried out based on temperature corrections only. In fact, the determination of the thermal conductivity,

I. Mraidi (✉) · A. Mabrouk El Asmi
El Manar University, 1068 Tunis, Tunisia
e-mail: InsafmraidiGBS@gmail.com

A. Skanji
Tunisian Company of Petroleum Activities (ETAP), Tunis,
Tunisia

which represents a basic parameter, has been general and imprecise. This has led to an underestimation of basin reconstructions. As accurate estimations of heat flow require a better evaluation and correction of both temperature and thermal conductivity, this work aims to calculate the heat flow using both temperature and conductivity corrections. It will aid to assess the effect of thermal conductivity variations on the thermal history of a studied region.

The area of interest is located in the region of Ben Guerdane–Tataouine and is commonly known as the ‘Djelfara Basin’. This area can be subdivided into two distinct morpho-structural sub-domains, which are the paleo-basin of Djelfara and the Dahar Plateau formed after a reactivation of Pan-African faults [3]. The structural history of the Djelfara Basin is complex and multiphase following the succession of several tectonic phases since the Paleozoic.

2 Materials, Methods and Data Set

For our study, 13 wells located in the Ben Guerdane and Tataouine regions were chosen to be studied (W1–W13). Data were provided by the Tunisian Company of Petroleum Activities (ETAP). A total of 25 values of Bottom Hole Temperature (BHT) were collected from 6 boreholes among 13 studied wells. Cores, cuttings and composite logs allow the lithological subdivision of the different crossed columns ensuring, thereafter, the determination of the thermal conductivity.

To estimate the real formation temperature, corrections must be applied. The most common mean of correction is the Horner Plot. As this approach is only functional at specific conditions mostly not suitable for the Tunisian basins, the corrected geothermal gradient was estimated using temperature corrections as proposed by Bouaziz et al. [2]:

$$\text{BHT}_c = 1.036 * \text{BHT}_{uc} + 5.9; \quad (1)$$

where BHTc: corrected BHT, BHTuc: uncorrected BHT.

Temperature at the ground surface is the other element needed for computing the average vertical thermal gradient for each studied well. For its determination, the local temperature of ground surface that characterizes each well was determined using the following equation [1]:

$$T_{gs} = 27.6 - 0.0414 * L - 0.00599 * L^2 \quad (2)$$

where T_{gs} : temperature at the ground surface ($^{\circ}\text{C}$), L : latitude (in degree).

Estimating the mean conductivity of a rock or a formation requires the choice of a mixing model that best describes its geometry. Indeed, a rock, or formation, composed of layers stacked perpendicular to the direction of heat flow is best modeled using the harmonic mean ($\lambda_m = \Delta Z / \sum_i \left(\frac{Z_i}{\lambda_i} \right)$).

A rock composed of a mixture of different minerals can be modeled with either a geometric mean ($\lambda_m = \prod_i^n \lambda_i^{\phi_i}$) or square-root mean ($\sqrt{\lambda_m} = \sum_i^n \phi_i \sqrt{\lambda_m}$) model.

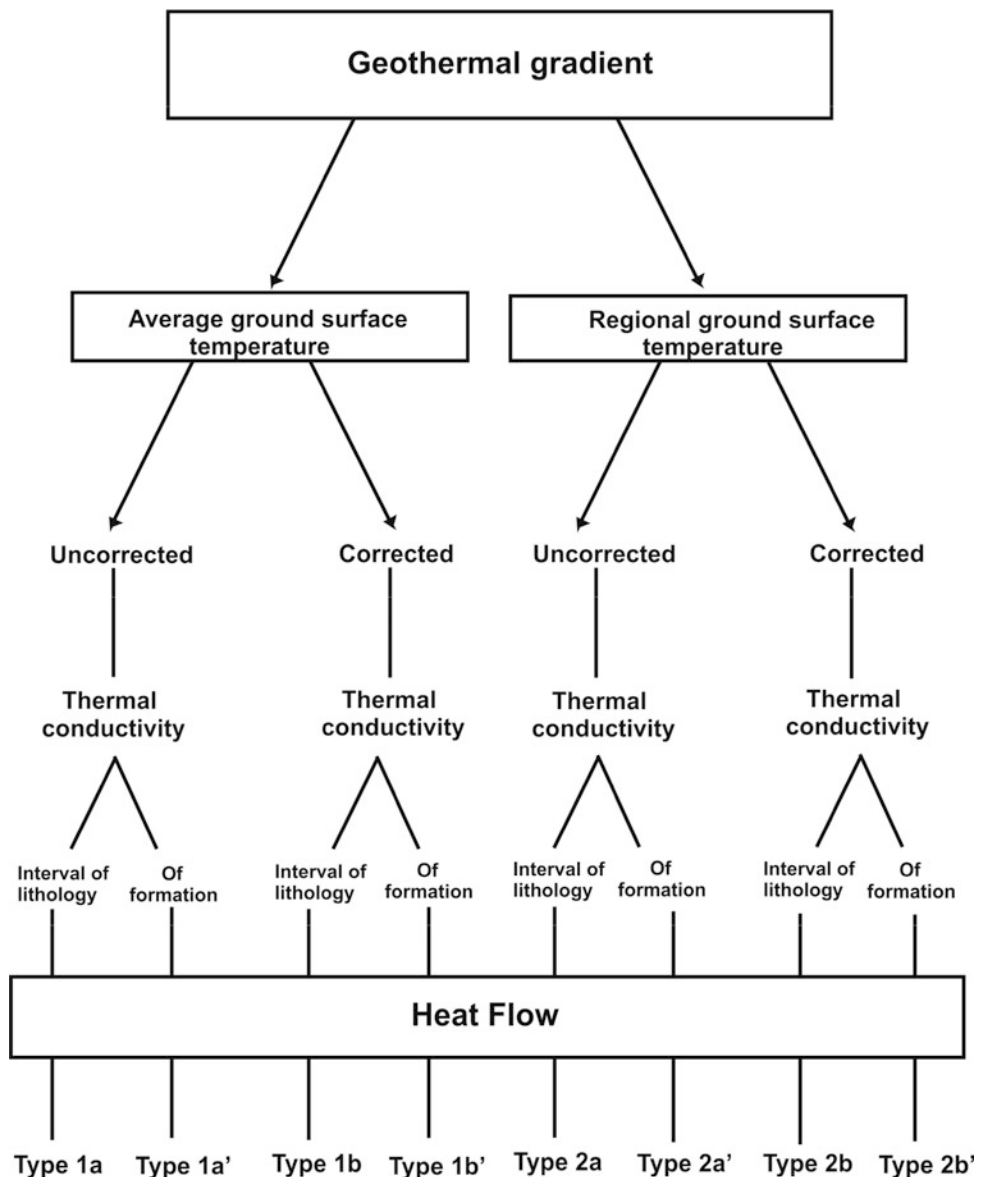
Porosity is the major variable controlling the conductivity of sedimentary rocks. For that, we need to carefully assess the porosity of a formation before we could accurately model its conductivity. This modeling was done using the following equation:

$$\lambda(D) = \left[(1 - \phi) \cdot \lambda_{ma}^{1/2} + \phi(Z) \cdot \lambda_f^{1/2} \right] \quad (3)$$

where λ_{ma} = matrix conductivity; ϕ : porosity, D : depth; λ_f = fluid conductivity

Depending on the types of these two parameters used each time, eight types of heat flow, shown in Fig. 1, were

Fig. 1 Flowchart of the different studied types of heat flow



finally determined using two different methods; the Fourier law ($Q = -\lambda \Delta T / \Delta Z$) and the Bullard Plot which is a graph of temperature against thermal resistance.

3 Results

3.1 Temperature Correction

Temperature values range between a minimum value equal to 15 °C and a maximum of 19 °C with an average of 17.9 °C that was used thereafter, along with the regional mean temperature of ground surface, to calculate the geothermal gradient. Two types of gradients were then calculated, the first one using the average temperature (17.9 °C, type 1) and the second one with the regional mean (20.56 °C, type 2).

The uncorrected geothermal gradient values for individual wells (type 1) tend to increase towards the northeast from 22 °C/km at W11 to 30 °C/km at W13 with a high local anomaly at W3 (32 °C/Km). The regional mean is about 27.7 °C/km. For the second type, the geothermal gradient shows the same direction of values elevation. It ranges between 20 °C/km at W11 and 29 °C/km at W13 and W3 with a regional mean equal to 26.3 °C/km.

3.2 Conductivity Correction

Drilling cuttings are only available for W1, so, first of all, the square root mean was applied to determine the thermal conductivity for each layer. The evaluation of the thermal conductivity was done following a high-resolution appraisal (5 m margin). Then, the average thermal conductivity of each formation is generally the harmonic mean of the

conductivities of all horizontally bedded layers (5 m margin) within the depth interval.

The variation of the effective thermal conductivity, shown in Fig. 2, ranges from 1.59 W/m/K for well 1 (W1) to 3.3 W/m/K for well 6 (W6). The highest values are located in the southwestern part of the basin, in proximity of the Tataouine area. The lowest ones are in the northeastern Djelfara basin, in proximity of the Ben Guerdane area.

3.3 Heat Flow Correction

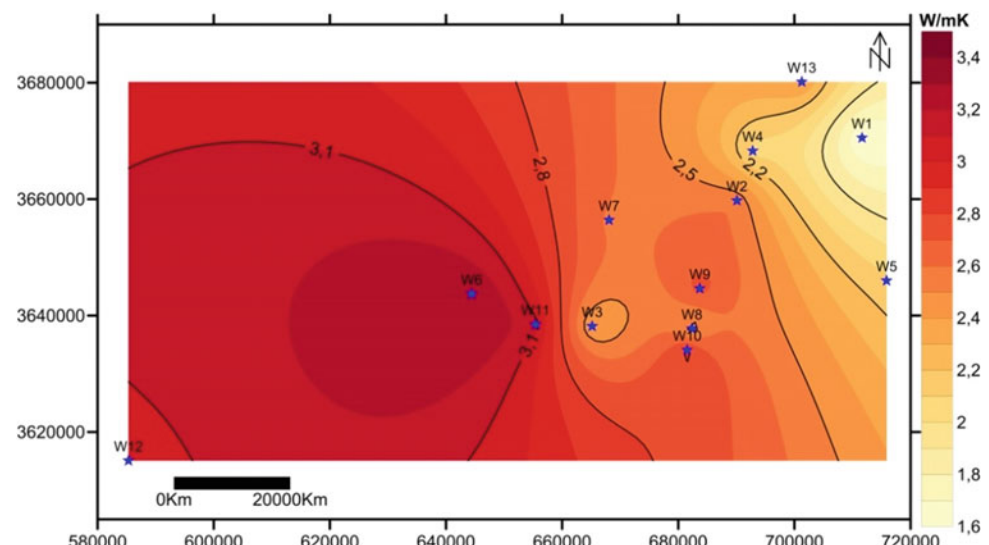
Corrected heat flow values tend to increase towards the Southwestern Djelfara from 58 to 90 mW/m² with a high local anomaly at W3 (132 mW/m²). The trend of the spatial distribution of uncorrected heat flow between wells is slightly different from that after corrections. The common point is that the South western Djelfara is always the hottest area.

4 Discussion

After temperature correction, the geothermal gradient rises for both types and becomes higher. The highest values are for wells located in the eastern basin, and the lowest values are for wells in the western basin. The geothermal gradients (corrected/uncorrected) tend to increase towards the northeast.

However, the thermal conductivity values show a general tendency of increase from low conductivities in the northeastern basin towards higher values in the southwestern basin (Fig. 1), which is closely related to the difference of lithologies between the formations crossed by eastern wells and those crossed by the western wells.

Fig. 2 Spatial distribution map of the average thermal conductivity



These large regional variations of the geothermal gradient and thermal conductivity may explain the regional variation of the heat flow in the study area. Indeed, the highest estimated heat flow values are recorded for wells of the southwestern basin, i.e., in the high zones (plateau of Dahar, Arch of Bounemcha).

5 Conclusions

A large and rich database of thermal conductivity was collected, after an evaluation following a high-resolution appraisal (5 m margin). These data were investigated to determine their impact on calculated heat flow of the Djefara Basin. The study aims to achieve a better reconstruction of the regional distribution of the thermal flow of the region in relation to its geodynamic evolution. After comparing the results, the most realistic scenario, compared to the geologic model, is found to be the one calculated with the corrected thermal conductivity (lithologic interval) and the corrected

geothermal gradient. It shows an average heat flow equal to 82 mW/m² which is higher than the global average of about 64 mW/m² [4].

References

1. Barker, C.E.: A paleolatitude approach to assessing surface temperature history for use in burial heating models. *Int. J. Coal Geol.* **43**(1–4), 121–135 (2000)
2. Bouaziz, A., Mabrouk, A., Skanji, A., El Asmi, K.: A new borehole temperature adjustment in the Jeffara basin (Southeast Tunisia): inferred source rock maturation and hydrocarbon generation via one dimensional modeling. *AAPG Bull.* **99**(9), 1649–1669 (1969, Sept 2015)
3. Rabia, M.C.: Système d'Informations Géo-scientifique et Télédétection multicapteurs: Application à une étude mult-thèmes de la Jeffara orientale. Thèse de Doctorat, Université de Tunis II, 320 p (1998)
4. Takherist, D., Lesquer, A.: Mise en évidence d'importantes variations régionales du flux de chaleur en Algérie. *Can. J. Earth Sci.* **26**, 615–626 (1989)

Fault-Controlled on Hydrocarbon Migration and Accumulation of Baodao Northern Slope in the Qiongdongnan Basin, South China Sea

Xinshun Zhang, Hongju Zheng, and Congsheng Bian

Abstract

Based on the oil-gas exploration data of Baodao Northern Slope in Qiongdongnan basin, the abundance of the adsorbed hydrocarbon and the abundance of brine inclusions with hydrocarbon were evaluated by quantitative grain fluorescence experiment. Combined with stages of fault activities, fault sealing capacity and the oil-gas charging time, the fault control on hydrocarbon migration and accumulation characteristics of Baodao Northern Slope was analyzed. The results show that the oil and gas reservoirs of the N1m–N1s Formation (21–10 Ma) of Baodao Northern Slope were formed very late, so, the particle surface adsorbed hydrocarbon abundance of shallow N1m–N1s Formation is prevalent and high with a low abundance of intragranular hydrocarbon. However, the oil and gas reservoirs of E31 Formation (30–21 Ma), close to the Baodao Sag, were formed earlier but most of them were destroyed later, and therefore the hydrocarbon abundance characteristics are different. Because of the limited migration ability, the oil and gas generated from the Baodao Sag mainly contributed to the south of Baodao Northern Slope, and they have little contribution to the northern part. The hydrocarbon generated from Oligocene source rock migrated vertically through the widely developed faults rather than along the lateral delta front sands.

Keywords

Quantitative grain fluorescence • Hydrocarbon abundance • Fault sealing capacity • Accumulation • Qiongdongnan basin

X. Zhang (✉) · H. Zheng · C. Bian
Research Institute of Petroleum Exploration and Development,
PetroChina, Beijing, 100083, China
e-mail: vvzxs@126.com

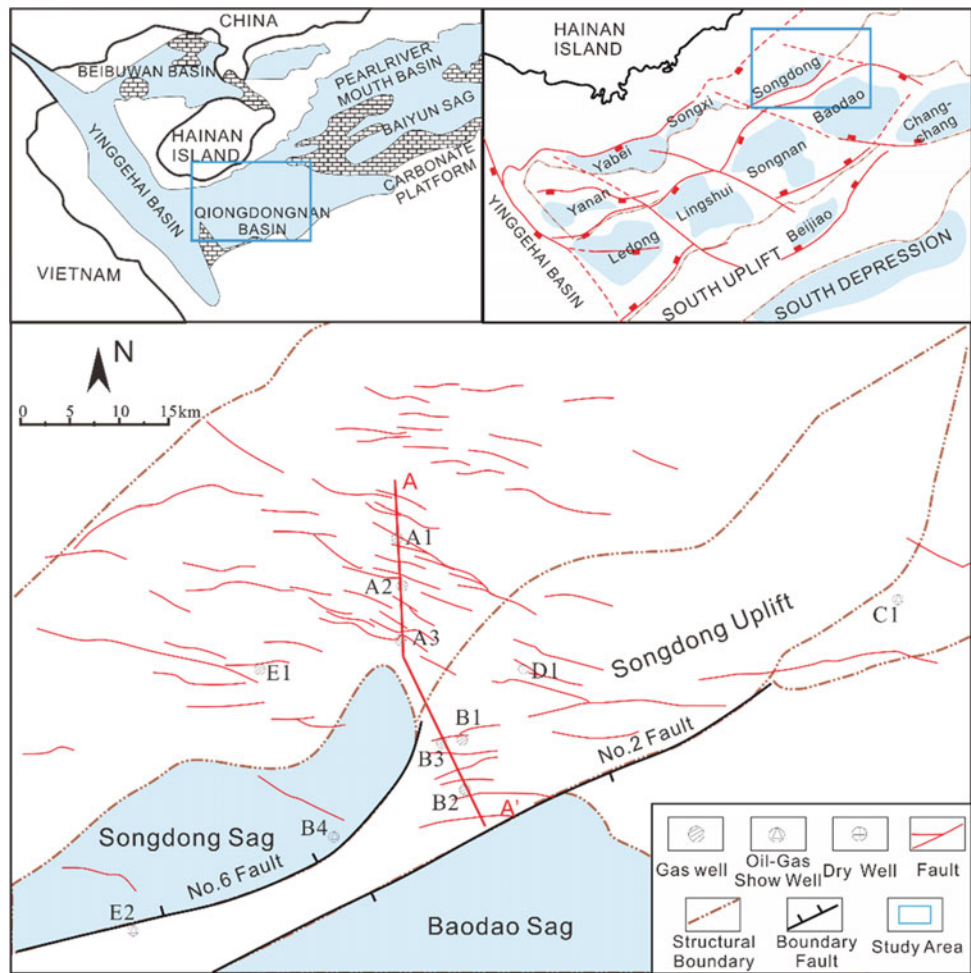
1 Introduction

Qiongdongnan Basin is petroliferous passive margin basin, which is developed on the Cenozoic basement (Fig. 1). Several oil and gas fields have already been found in the basin, such as Lingshui Gas Field in the southwest of the basin [1]. Due to the breakthrough in the west of the basin, we believe that Baodao Sag has high-quality source rock in the depocenter similar to the west of the basin [2]. However, the oil and gas exploration of Baodao Northern Slope has had no breakthrough for a long time. However, the reservoir rock, seal rock, and fault-related traps are developed on the slope. This paper focuses on the analysis of the fault sealing capacity which has great influence on the trap availability and the oil and gas migration characteristics. To determine the fault sealing capacity, we analyze the grain fluorescence features of different reservoir layers. Combined with the features and active periods of the faults and the hydrocarbon characteristics in different wells, we can determine the sealing capacity of faults in the study area, which help us to get the oil and gas accumulation model in the study area.

2 Methodology

Quantitative Grain Fluorescence (QGF) is a method of fluorescence detection and analysis. Compared with other means, it has higher sensitivity, better selectivity, faster analysis speed, less sampling requirement and many other significant advantages [3, 4]. In this paper, quantitative grain fluorescence (QGF) and quantitative grain fluorescence on extract (QGF-E) techniques are used to study hydrocarbon inclusions with the main instrument which is the high sensitivity fluorescence spectrophotometer (Cary Eclipse, American-Australian modification). The parameters used in this paper are mainly QGF index, QGF-E index, $\Delta\lambda$, λ_{max} and the corresponding spectra.

Fig. 1 Structural units of Baodao Northern Slope in the Qiongdongnan Basin (Baodao Sag is one of the four main sags in the basin, and the sediments' thickness is over ten thousand meters. Compared with other sags, Baodao Northern Slope is also a favorable play)



Quantitative Grain Fluorescence experiments have good results on detecting present oil reservoirs and ancient oil reservoirs [4]. The gas reservoirs of Baodao Northern Slope generally contain condensate, which also has the fluorescence feature. This quantitative grain fluorescence experiment is based on 66 samples of Baodao Northern Slope and the samples are mainly cuttings.

3 Results

The QGF-E intensity data of Baodao Northern Slope indicates that most of N1m–N1s formation reservoirs have high QGF-E strength, which are generally greater than 40. This indicates that the region's oil and gas is rather active, and the possible reason is the widely distributed faults. However, the regional characteristics of dominant gas and associated condensate result in QGF-E intensity values of less than 60. In addition, from the QGF index distribution of Baodao

Northern Slope, the difference between the north and the south is relatively great (Fig. 2).

4 Discussion

Through the method of Knipe triangle map and fault opening index [5], the main faults' sealing capacity is poor in the E3l formation and relatively good in N1m formation. Faulting pattern, formation temperature and pressure suggest that the deeper part of the faults acted as a good path for oil and gas migration. The fault growth index suggests that faulting dominated during Early Neogene. The poor sealing capacity of the deeper part of the faults in area B is the main reason that the deep reservoirs of B area have a low QGF-E intensity. While the high QGF Index of area B is due to the paleo-oil/gas reservoirs destroyed later. In addition, we also got some supportive evidence from carbon isotope of the gas and biomarkers of the oil [5]. Because the faults have partial

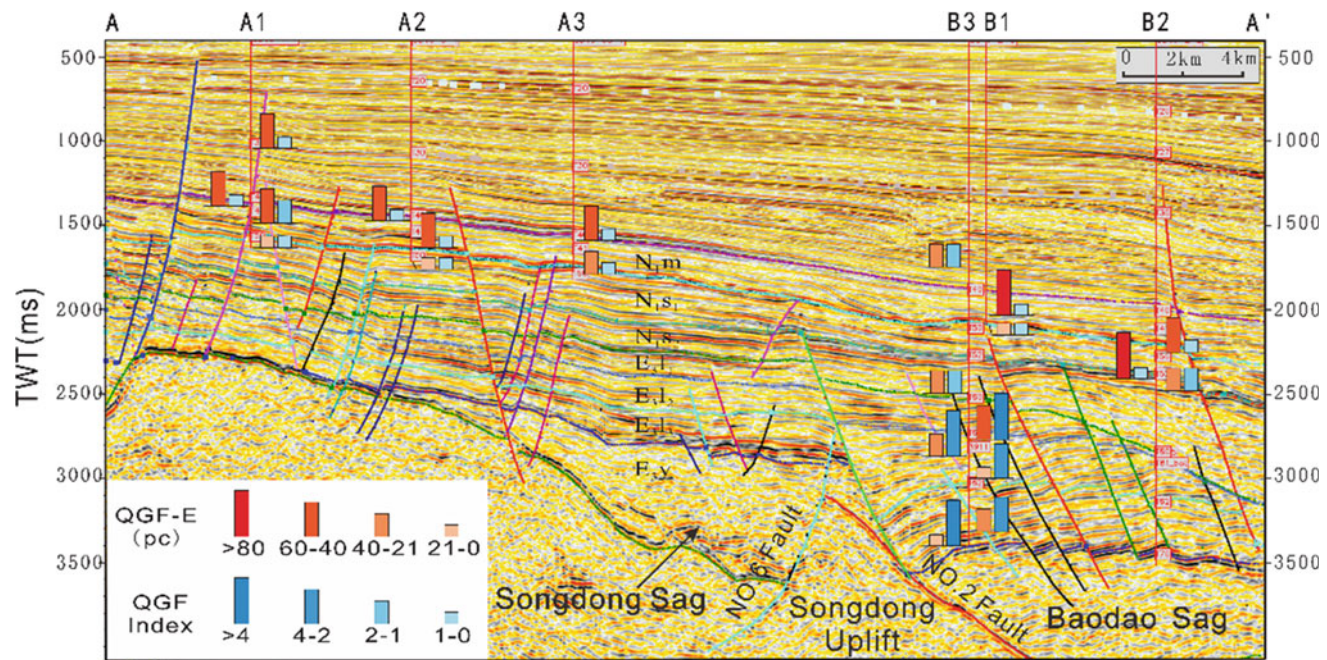


Fig. 2 Distribution map of QGF-E index and QGF index at Baodao Northern Slope. The red histogram represents QGF-E intensity, while the blue histogram represents the QGF index. From the section, it is

clear that paleo-oil/gas reservoirs were formed in the deep formations of B area, and the current oil/gas reservoirs are mainly in the shallow formations of the whole study area (for section location see Fig. 1)

sealing capacity, they lead to relatively good trap availability in the upper N₁s formation and N₁m formation, but poor trap availability in the E₁l formation. So, it is very hard to form an oil/gas reservoir in the E₁l formation, even though oil/gas has been seen during drilling in E₁l formation.

5 Conclusions

QGF experimental results have good correlation relationship with the oil/gas reservoirs in the study area. The results show that paleo-oil/gas reservoirs were formed in deep formation (Paleogene) of area B, but now the oil/gas reservoir is mainly distributed in the shallow formation (Neogene).

The fault sealing capacity was poor in the deep formation, and the main active period of the faults are the early Neogene. The faults' activities and/or the poor sealing capacity are the main reasons for the distribution of the current oil/gas reservoirs, which are mainly distributed in the shallow formation.

References

- Zhu, W., Huang, B., Mi, L., Wilkins, R.W., Fu, N., Xiao, X.: Geochemistry, origin, and deep-water exploration potential of natural gases in the Pearl River Mouth and Qiongdongnan basins, South China Sea. *AAPG Bull.* **93**(6), 741–761 (2009)
- Baojia, H., Heting, H., Li, L., Lifeng, W.: Characteristics of marine source rocks and effect of high temperature and overpressure to organic matter maturation in Yinggehai-Qiongdongnan basins. *Mar. Orig. Pet. Geol.* **15**(3), 11–18 (2010)
- Chen, D.X., Pang, X.Q., Zhang, J., Li, M.G.: Application of quantitative grain fluorescence techniques to study of subtle oil migration pathway of lithological pool. *Acta. Geol. Sin.* **81**, 250–254 (2007)
- Liu, K., Eadington, P.: Quantitative fluorescence techniques for detecting residual oils and reconstructing hydrocarbon charge history. *Org. Geochem.* **36**(7), 1023–1036 (2005)
- Zhang, X.S., Huang, Z.L., Fan, C.W., Wu, H.Z., Xu, X.D., Li, M. N.: Fault sealing capacity and relationship with oil-gas accumulation at Baodao Northern Slope. *Nat. Gas. Geosci.* **24**(2), 356–364 (2013)

A Visual Investigation of Different Pollutants on the Rheological Properties of Sodium/Potassium Formate Fluids

Afshin Davarpanah

Abstract

Nowadays, the adverse effect of drilling operations on the ecological system pushed the oil industry specialists to achieve optimum drilling performances. Volume and toxicity of discharged materials evaluate surface discharge severity. The ubiquitous utilization of formate fluids has revolutionized the way petroleum industries have conquered the lower drilling inefficiencies. As an objective of this extensive study, the profound impact of different pollutants on the potassium/sodium formate fluids was investigated by experimental tests. The particular sample for mud pollution test was formate fluid with starch biopolymers. To do this, five samples of formate fluids were made, and each one of them was polluted by several contaminants such as cement, lime, acid, alkali and stucco. Consequently, the rheological properties and the pH changes, as well as their effects on the formate fluids were evaluated.

Keywords

Formate fluids • Rheological properties • Pollutants • Core samples

1 Introduction

The ubiquitous utilization of numerous types of drilling fluids in petroleum industries is considered as one of the significant principal issues that should revolutionize the way petroleum engineers drill hydrocarbon formations. Due to the fact that the accurate selectivity of a proper drilling fluid is always a significant concern for petroleum industries, the latter have tried to choose the drilling fluids which are the most adapted to the reservoir characteristics. An essential

A. Davarpanah (✉)
Department of Petroleum Engineering, Science and Research
Branch, Islamic Azad University, Tehran, Iran
e-mail: Afshin.Davarpanah@srbiau.ac.ir

drilling fluid is contained in two main phases, a continuous phase and a discontinuous phase, which are utterly dependent on the types of the selected formation. To achieve the best and optimum results in the drilling operations and completion performances of a well, the proper estimation of the formation properties to provide the sufficient requirement before commencing the drilling procedures should be taken into consideration [1–4].

2 Methods

The studied field is one of the Persian Gulf fields in the south of Iran that is vertically drilled to provide the necessary information for the experimental investigation. The objective was to drill an 8 1/2 in. hole section from 10,900 ft. to the casing point at a measured depth (MD) of 12,500 ft. A 7 in. casing string was then to be run and cemented. The appropriate measurements of rheological properties were one of the major issues to be adequately addressed to obtain the best results. The rheological properties of the drilling fluid which were investigated in this experiment are apparent viscosity, yield point, plastic viscosity and gel strength.

3 Results and Discussion

Figure 1 demonstrates the fluid rheological properties such as apparent viscosity, plastic viscosity and yield point for polluted fluid and formate base fluids. As it can be seen in Fig. 1, mud rheology properties' changes after being polluted by several contaminants were not significant, and when formate fluid is opposed to several pollutants, it almost maintains its properties, and it does not have a steep rise or remarkable decrease in its rheological properties. Furthermore, those drilling fluids which are polluted with Hydrochloric acid, cement, and stucco have more impact on the amount of apparent viscosity, plastic viscosity, and yield point than the other fluids; similarly, rheological properties

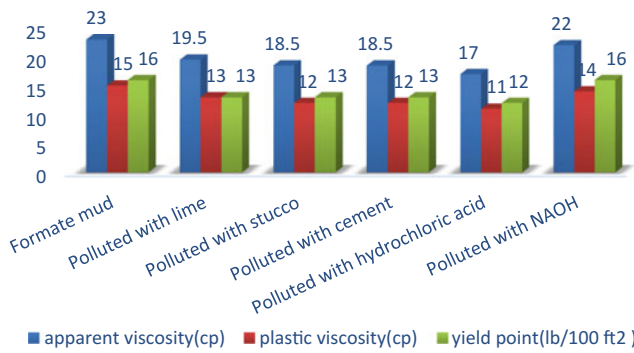


Fig. 1 Mud rheological properties' changes in the presence of several pollutants

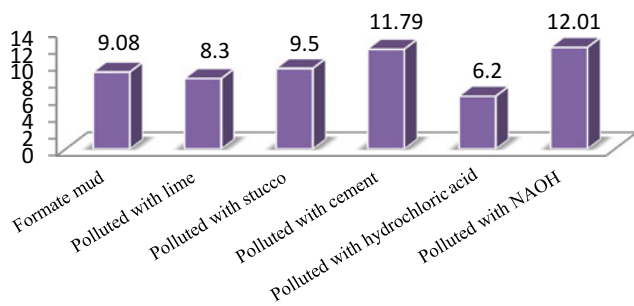


Fig. 2 pH changes in the presence of several pollutants

of this material which was added to the drilling fluid, had lower amounts than the other fluids.

Figure 2 illustrates the amount of pH for formate fluids in comparison to several pollutants. The amount of pH for formate fluid is approximately 9. However, as it can be seen in Fig. 2, the amount of pH after being polluted with lime decreased a little (nearly 8.3), the amount of pH after pollution with stucco increased slightly (about 9.5). The highest increase of pH in formate fluid is the one caused by NaOH pollution (nearly 12) and the second highest increase is the one related to cement (nearly 11.8). Adding a significant amount of hydrochloric acid (35 cc hydrochloric acid 37%) caused the amount of pH to suddenly decrease to 6.

4 Conclusions

In this comprehensive paper, experimental laboratory tests indicate the comparison of influential effects of several pollutants on formate drilling fluids; however, pollutants like lime, stucco, cement, and acids change mud's rheological properties. In some cases, the effect of these parameters on the formate drilling fluid diminishes. Furthermore, sodium/potassium formate fluids maintain their properties properly, and they do not cause any significant increase or decrease in the mud's rheological properties. The amount of pH for sodium/potassium formate fluids in the presence of several pollutants does not cause a noticeable change. In comparison to hydrochloric acid, it can be observed that formate fluids have a considerable resistivity. Moreover, by adding a large amount of hydrochloric acid (35 cc hydrochloric acid 37%), the amount of pH decreased suddenly to 6.2. The buffering properties of these fluids are the cause of this reduction when carbonate and bicarbonates are added. Consequently, it can be considered that formate fluids have a small reduction in the amount of pH.

References

1. Khodja, M., Khodja-Saber, M., Canselier, J.P., Cohaut, N., Bergaya, F.: Drilling fluid technology: performances and environmental considerations. InTech (2010). ISBN 978-953-307-211-1
2. Patil, R.C., Deshpande, A.: Use of nanomaterials in cementing applications. In: SPE International Oilfield Nanotechnology Conference and Exhibition, SPE-155607, Noordwijk, Netherlands, 12–14 June 2012
3. Moake, G.L.: Format mud effects on density logs. In: SPWLA 53rd Annual Logging Symposium, Cartagena, Colombia, 16–20 June 2012
4. Gao, P., Yin, D.: Simulation study on the conditions of converting injection wells to production wells in low permeability reservoirs. *J. Daqing. Pet. Inst.* **6**, 12–22 (2006)



The Integration of the Two Key Levers for the Success of a Company

Rima Derradji and Rachida Hamzi

Abstract

Most managers know that process-risk mapping is essential in enterprise design so as to obtain better understanding and management practices. Organizations need an effective and robust process of management that is less sensitive to changes in the business environment. The main purpose of this paper is the integration of process mapping and risk mapping, with a case study applied in an Algerian company in the oil and gas industry.

Keywords

Process mapping • Risk mapping • Risk analysis • Modeling • Integration

1 Introduction

Nowadays, most companies spend a great deal of time each year developing strategic objectives and goals. They are needed to understand how the process works, where they are being executed and how they interconnect.

zur Muehlen and Rosemann [1] indicate that a “business process is subject to errors in each of the components discussed by Hwang and Hang [2], a successful completion of business process it necessary to understand and manage the risks associated with each process activity and the process overall. Unmanaged risks can be difficult to estimate and accommodate, especially when those risks occur during the business process execution. A much more sophisticated approach is necessary for achieve the objectives by “integrating process-risk mapping”, previous researches have given due importance to process and risk mapping such as [3–7] in different domains. The basic idea of our work is

how “Risk and process mapping is used within an enterprise to better manage default risks and existing processes, in order to understand the risks inherent in each process that may affect the continuity of the business, it is possible to detect all the risks in all the processes that the company and its divisions can undergo, thus, making it possible to achieve the objectives of the company”. We integrate risk mapping in the process mapping in order to improve the target process and increase performance to achieve an ideal and perfect company. The aim is to provide an overall and standardized view of the different types of risks facing the company, which should facilitate the overall management of the organization and the integration of new employees. This paper is organized as follows: section one is the proposed framework: “integration of process-risk mapping”, the second is a case study to illustrate and propose a model in the oil industry.

2 Integrating of Process Mapping and Risk Analysis

Process mapping is one of the most powerful weapons in the process management of a company, as discussed by Cowell James Forge Insurance Group [8], given the complete simplification of the process map: “Process mapping helps represent work processes visually and identify problem areas and opportunities for process improvement; it provides a common understanding of the entire process and specific roles and contributions of process participants”. Risk mapping is a tool used by life insurers in the identification, control, and management of risk, it is an iterative process that refines managements’ understanding of the exposures that it is managing, and measures the effectiveness of the mitigation strategies employed in controlling risk [5]. It is an excellent visual tool for companies to utilize in their risk management programs [9]. According to Le blog IENA [3], “The development of this mapping allows an effective management of the performance, based on risk management,

R. Derradji (✉) · R. Hamzi
LRPI Laboratory, University of Batna 2, Batna, Algeria
e-mail: rimmixx@yahoo.fr

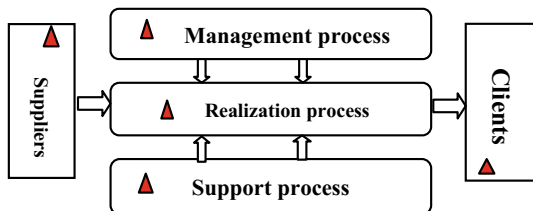


Fig. 1 The principal of integrated risk in processes. Adopted from Sienou [10]

compliance and control and operational steering. This combination of process and risk analysis approaches ensures the integrity and security of operations by working on the significant risks of the most critical processes". Risk mapping and process mapping have been acknowledged as distinct disciplines and independent of each other. Form two complementary worlds, they seem to be getting more comfortable with one another. Our approach is a management and decision-making tool based on risk and process integration principal as presented in the next Fig. 1.

- (1) **Describe the company:** Set the perimeter of a joint study; to work on critical processes, it is useful to have an overall view of the organization, and to get more clarity to define the objectives and a common plan of process and risk.
- (2) **Definition of processes of the company:** In this phase, we need a macroscopic representation of the company in order to limit its processes and its interaction between them, differentiate between the different risks inherent in the process, in the input and in the output, as well as those related to the process itself, i.e. management and control, and support.
- (3) **Identification of the risks inherent in each process:** After the global mapping of the enterprise, it is time to identify all the risks that can affect the company in each process and determine a set of propositions as handling options by using the FMECA method (failure modes effects and criticality analysis) to facilitate the analysis later because the company must draw up a list containing all the potential risks.
- (4) **Evaluation criterion:** Other dimensions of risk take into account in the risk assessment: *Risk timing or timing of risk: Risk timing can change the impact of risk by aggravating it. *The duration of the consequences: the longer the risk, the greater the consequences for the company.

Thus, gravity was measured by the product of these two quantities:

$$G = \text{Timing} \times \text{Duration of consequences}$$

Subsequently, the criticality was measured by the product of

$$C = \text{Timing} \times \text{Duration of consequences} \\ \times \text{Probability of occurrence}$$

- (5) **Risks rating:** From the identification of risks in each process modelling by the macroscopic mapping of the company and the evaluation of those inherent risks, we must rate those risks by considering the timing of risk and duration of the consequences, we get a quote that will help us work on the annual corrective action plan
- (6) **Control and monitoring:** After the identification and analysis of risk, the manager must monitor the risk residual, and execute risk response plans while evaluating their effectiveness through a variety of techniques. The foundation of this approach lies in the understanding of the effectiveness, [11, 12] as the effective management of risks requires an effective consideration of risks during the whole business process management.

3 Case Study

The management of Haoud Berkaoui is part of the Production Upstream Division of Sonatrach in Ourgla, Algeria. The region of Haoud Berkaoui includes the sites of Haoud Berkaoui, Guellala, Benkahla, Guellala Northeast and Drâa-Tamra.

- (1) **Description of the company:** Firstly, we must give a description of the company in the Table 1.

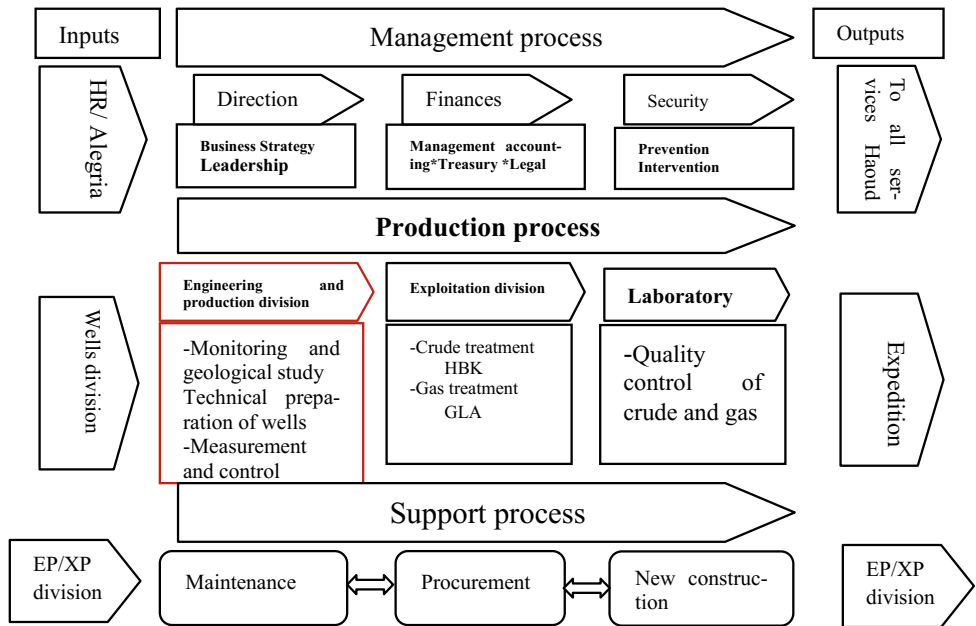
In this mapping, we limit our work to only the processes that have a direct impact on production; we use the principle of multi-level analysis to build our mapping as shown in the following figure. We chose some sub-process divisions to apply our approach, namely the engineering and production divisions (Fig. 2):

- (2) **Engineering and production division modelling:**
 - Monitoring and geological study
 - Technical preparation of wells
 - Measurement and control
 - Wells intervention.

Table 1 Description of “Sonatrach of HBK Ourgla, Algeria”

	Analysis objects “The system”	Outside “environment”	Inside “sub-processes”
Level: 1 Enterprise analysis	The enterprise: “Sonatrach of HBK Ourgla, Algeria”	<ul style="list-style-type: none"> • The market • Competition • Customers 	<ul style="list-style-type: none"> • Divisions (finance, maintenance, drilling ...)

Fig. 2 Macroscopic mapping of processes related to HS/DP Haoud Berkaoui Ourgla



(2.1) Monitoring and geological study service: “process sheets”

Upstream process	Downstream process		
Inputs element	Actor	Activity	Outputs elements
ENAGO/ENAFOR	Geological engineer	Geological field study	The layers (sieving)
Deposit		Petro physical study of the reservoir	Laboratory
Geological study		Logging interpretation	
		Introduction of data	
		Establishing log correlations	
		Track drilling progress	
Drilling wells		Coring	

(2.2) Technical well service

Upstream process		Downstream process		
Wells in production		Wells in oil producers		
Input elements		Actor	Activity	Outputs element
Wells in production	SERVICE REPORT	Technician	Monitoring of production	Daily report
	Reports of malfunctions and / or anomalies		Monitoring of wells and deposits, inspection and control	Implementation of the study
	Information Modeling	Geological engineer	Choice of operation necessary + established the program: (Wire line, Snubbing, work over, fracturing, acidification ...) Results interpretation Use of reservoir fluid calculation software	The bearing parameters

(2.3) Service measurement and control

Upstream process		Downstream process		
Producer wells		Wells Operation		
Input element		Actor	Activity	Output element
Wells in production	Control instruments	Technician	Daily well control	Daily report
	Anomalies (modification corrosion, leakage etc ...)		Maintenance of Pipe collection network Repair of leaks	Good operation
	Control instruments	Technician	Parameter reading (pressure ...)	Reporting
	- Change of the Duse - Well stimulated - Anomalies in the wellhead		Gauging	exploitation
		Technician (operator)		
		Engineer (exploitation of results)		

(2.4) Service intervention well

Upstream process			Downstream process		
Measurement/technical service at the well			Wells exploitation		
Inputs	Actor	Section	Activity	Outputs	
Wells	ENAFOR	Work over		Change of completion. Securing the well. Realization of the Sides Truck (deviation).	
	EP/SH			The return of the well in production	
	ENTP EP/SH	Completion		Prepare well for re-production	
	ENSP EP/SH	Snubbing		Increase well production	
	EP/SH BJSP Halliburton Schlumberger	Stimula tion	Hydraulic billing		
			Acidification		
			Cleaning and start-up		
	EP/SH	Wire line		The delivery of wells in production	
	ENSP	Interview		Keeping the well in production	

(3) Risks identification, evaluation:

In this step, we will identify the risks presented in the risks related to the activities of the EP division by applying the FMECA method. The following tables show the application of the method to the EP division processes. In this table, we chose some risks which can affect the process.

4 Results and Discussion

(Because of the limited number of pages, we choose one process, and sub-process to analyze the risks around it and apply the proposed approach).

In this paper, we propose an integration of process mapping and risk mapping, at the macroscopic level, to

process	Activity	Risk	Effect	P	G		C	Correctives measures	
					Ti m	D.c			
Monitoring and geological study	Geological field study	Study error Poor soil analysis	<ul style="list-style-type: none"> -Fall of block, • Landslide, • Flood, • Seismicity, • Phase of shrinkage of clays, • Rise of groundwater, • Compressing of compressible soil 	P1	T3	D3	ALARP	Use multiple analysis parameters Maintenance Interview	
	Petro physical study of the reservoir			P1	T3	D3			
	Logging Interpretation	Error of interpretation		P1	T3	D3			
	Introduction of data			P1	T2	D2			
	Track drilling progress	Explosion, Fire, H2S gas release	Human material damage and Death, Loss of Time	P2	T4	D3			

improve the performance of the company and to get better efficiency and value from the analyzed process. Generally, to obtain a successful organization, it is necessary to use an approach that allows managing the processes as well as their risks at the same time. To this end, we used both the bibliographical research and our estimation to identify and evaluate the risks associated with each activity. Thereafter, the existing and/or proposed corrective measures were approved at the level of these processes. Finally, we mapped this whole process to show the relationship between the processes and their risks.

5 Conclusion

This paper presents an approach that combines two main domains: process mapping and risk-management mapping.

The main contribution of this work is a robust method to improve the quality of management, reduce the complexity of events, and increase organizational maturity.

Therefore, the results presented in this paper are very promising and show that great potential of improvement exists in terms of process-risk integration. In addition, it could lead to a more comprehensive understanding of the actual situation of the current process which can be very helpful in analyzing the shortcomings and in identifying the best practices to be implemented.

Our current and future work involves more exploratory case studies in different service organizations in the context of integration of process-risk management to ensure the benefits given by this approach in different industrial, health and commercial domains.

An evolution in terms of methodology and a growing need to secure processes made proposing this solution an urgent necessity.

Acknowledgements We would like to thank the anonymous referees for their useful suggestions.

References

1. zur Muehlen, M., Rosemann, M.: Integrating risks in business process models. In: Australasian Conference on Information Systems, p. 10, 2005
2. Yu, F.-J., Hwang, S.-J., Huang, Y.-H.: Task analysis for industrial work process from aspects of human reliability and system safety. *Risk Analysis* **19**(3), 401–415 (1999)
3. Le blog IENA: Cartographie des processus et cartographie des risques : comment les mettre en cohérence? Le blog IENA [Online]. Available: <http://blog.iena.com/cartographie-des-processus-et-cartographie-des-risques-comment-les-mettre-en-coherence/>. Accessed: 15 Aug 2017
4. Cecima, “Modéliser les Processus Métier Cartographier les SI,” 2010
5. Ingram, B.D., Headey, P.: For The Risk Mapping Process
6. Halseth, K.: Process Modelling and Mapping: The Basics. David Thompson Heal. Reg
7. Biazzo, S.: Process mapping techniques and organisational analysis Lessons from sociotechnical system theory. *Bus. Process Manag. J.* **81**(1), 42–52 (2002)
8. Processes, P., Map, O.P., Charts D.: A Guide to Process Mapping. pp. 1–4
9. Cowell James Forge Insurance Group: What Is Risk Mapping And Why Should You Care?—Cowell James Forge Insurance Group [Online]. Available: <https://www.cjfig.com/news/what-is-risk-mapping-and-why-should-you-care/>. Accessed: 15 Aug 2017
10. Sienou, A.: Proposition d'un cadre méthodologique pour le management intégré des risques et des processus d'entreprise (2009)
11. Committee of Sponsoring Organizations of the Treadway Commission (COSO): Enterprise risk management—integrated framework. COSO **3**, 1–16 (2004)
12. Grüner, D., Brucker-Kley, E., Keller, T.: Business process management workshops. In: Lecture Notes in Business Information Processing, vol. 202, Sept 2005, pp. 463–474 (2015)



Quantitative and Qualitative Characterization of Oil Field Produced Water of Upper Assam Basin (India)

Debasish Konwar, Subrata Borgohain Gogoi, Joyshree Barman, and Monem Kallel

Abstract

Produced water is the largest volume of wastewater generated during oil and gas production. It comprises of organic and inorganic compounds. The amount of produced water from various oil fields of Upper Assam Basin are increasing with the ageing maturity of the oil field. Produced water adversely affect the environment as it contains different toxic compounds such as petroleum contaminants and impurities include oil, naturally occurring radioactive minerals, oil & grease, hydrocarbons, production chemicals and various materials. This paper determines the quantitative and qualitative characterization of physical and chemical properties of produced water generated from different depths and horizons of Upper Assam oil fields. As produced water is re-injected into the reservoir for pressure maintenance and is discharged into the environment, so its characterization is highly significant for environment and reservoir management. The characterized physical and chemical properties of produced water have higher values which will adversely affect the environment. The characterized results are validated in Lenntech software to determine the corrosion and scaling forming tendency of produced water on the basis of Ryznar stability index and Langelier saturation index. The produced water samples are found to be highly corrosive and it has tendency to form scale. The samples are also highly corrosive.

Keywords

Produced water • Characterisation • Contaminants • Scaling • Corrosion

1 Introduction

The major waste stream of oil and gas production facilities is produced water. Oil reservoirs frequently contain large volumes of water, while gas reservoirs tend to have smaller quantities [1]. The North–East India oil field PWs are the by-products generated during various operations in the hydrocarbon exploration industries are major sources of pollution in the area [2]. This waste needs to be treated in order to restrict the bioaccumulation in marine organisms. This wastewater also transfers harmful chemicals to food chain thus affecting the components of the food chain [3–5]. Varying concentration of inorganic and organic compounds are present in produced water. Produced water comprises of formation water, injected water and condensed water [6, 7]. Low and high molecular weight petroleum hydrocarbons, dissolved compounds, naturally occurring radioactive materials, heavy metals, salts, dispersed and dissolved oil, suspended solids and dissolved gases are present in produced water [6, 8]. Various options have been adopted by the hydrocarbon exploration industries, but the most adopted method is the re-injection into the reservoir for pressure maintenance which enhances the recovery of the field [9, 10]. The Langelier Saturation index an indicator of the degree of saturation of water with respect to calcium carbonate. It approaches the concept of saturation using pH as a main variable. It can be interpreted as the pH change required to bring water to equilibrium. It can be mathematically represented as:

$$LSI = \text{pH} - \text{pHs}$$

D. Konwar · S. B. Gogoi (✉) · J. Barman
Department of Petroleum Technology, Dibrugarh University,
Dibrugarh, Assam, India
e-mail: subrata@dbru.ac.in

D. Konwar
e-mail: jrf_debasish@dbru.ac.in

J. Barman
e-mail: rs_joyshreebarman@dbru.ac.in

M. Kallel
ENIS, Sfax University, Sfax, Tunisia
e-mail: monemkallel@gmail.com

The Ryznar stability index correlate an empirical database of scale thickness observed in wastewater. The Ryznar stability index has its basis in the concept of saturation level. The Ryznar stability index can be mathematically represented as:

$$RSI = 2(pH_s) - pH$$

where,

pH measured water pH

pH_s pH at saturation in calcite or calcium carbonate

$$pH_s = (9.3 + A + B) - (C + D)$$

where:

$$A = (\text{Log}10 [\text{TDS}] - 1) / 10$$

$$B = -13.12 \times \text{Log}10 (oC + 273) + 34.55$$

$$C = \text{Log}10 [\text{Ca}_2 + \text{as CaCO}_3] - 0.4$$

$$D = \text{Log}10 [\text{alkalinity as CaCO}_3].$$

2 Materials

Ten (10) samples of PWs were collected from Oil Fields of Upper Assam Basin. The chemicals that were used are ethylene di-amine tetra acetic acid, erichrome black indicator, sodium chloride, hydrochloric acid, phenolphthalein, pH buffer, potassium chloride, calcium carbonate, lithium carbonate, petroleum ether and methyl orange.

3 Methodology

3.1 Characterization of Produced Water

pH, salinity, Total dissolved solids, Conductivity, Dissolved Oxygen, turbidity were determined in Water Analyser (Make: Systronics, Model: Water Analyser 371) Sodium, Potassium, Calcium, Lithium were determined in Flame Photometer (Make: Systronics, Model: Flame photometer 128, Compressor 126) and Iron, Copper, Chromium, Manganese were determined in Atomic Absorption Spectrometer. (Make: Perkin Elmer, Model: AAnalyst 200).

3.2 Validation of Results

The results were validated in Lenntech software to determine the corrosion forming tendency of produced water on the basis of Ryznar stability index and Langelier saturation index (Table 1).

Table 1 Characterization of produced water

Parameters	1	2	3	4	5	6	7	8	9	10	Permissible limit of WHO for disposal
pH	7.7	7.5	7.62	7.77	7.65	7.54	7.68	7.99	7.89	7.56	6.0-9.0
Conductivity (mS)	3.73	4.45	2.5	2.5	2.02	6.5	1.43	2.04	4.05	3.2	0.25-0.75
Total dissolved solids (ppm)	1.55	2.3	1.5	1.32	1.24	3.89	1.4	1.25	2.3	2.2	24.59
Dissolved oxygen (ppm)	4.4	4.2	4.1	4.4	4.7	4.3	4	4.2	4.2	4.4	7
Salinity (ppt)	1.89	2.68	1.5	1.8	1.78	4.5	1.9	1.23	2.03	1.89	0.2-0.4
Turbidity (NTU)	4.5	4.2	1.7	2.99	5.3	3.5	3.2	2.4	1.5	4.5	5-10
Hardness (mg/L)	68	70	50	48	40	53	42	58	62	33	300
Oil and gas (mg/L)	2000	3500	1333.3	1000	2000	1100	1778.9	2360	2778.6	1356.8	10
Iron (ppm)	2.47	1.011	0.024	0.337	0	0.312	1.236	2.13	0.216	0.056	3.0
Copper (ppm)	0	0	0	0	0	0	0	0	0	0	3.0
Chromium (ppm)	0	0	0	0	0	0	0	0	0	0	2.0
Manganese (ppm)	0.057	0.057	0.046	0.031	0.075	0.072	0.052	0.048	0.047	0.039	0.050
Sodium (ppm)	437.8	613.2	400.1	323	396.6	422.3	515.3	368.9	392.4	435.6	200
Potassium (ppm)	26.3	44.2	19.46	8.74	14	32.5	10.2	7.1	22	9.2	20
Calcium (ppm)	982	379	56.6	446.9	513.4	522	98	21	141.9	135.6	75
Lithium (ppt)	4.4	5.3	3.2	2.99	2.4	2.2	4.8	4.6	4.7	4.2	2

4 Results

4.1 Characterization of Produced Water

The physical and chemical properties of produced water samples were characterized as shown (Table 1).

It shows that the most of the parameters of produced water showed values higher than the maximum permissible limits for safe disposal. Copper and Chromium are absent in all the samples. Due to high salinity, all the samples showed high values of sodium. The concentration of Calcium is also very high resulting in increasing hardness of the produced water samples. Manganese, Potassium and Lithium are also present in produced water sample to some extent.

4.2 Validation of Results

See Tables 2 and 3.

Table 2 Table of Ryznar stability index

Sample	Ryznar stability index (RSI)	Indication	
		Ryznar [11]	Carrier [12]
1	8.9	Water is very aggressive	Heavy corrosion
2	12		Corrosion intolerable
3	13		
4	10		
5	11		
6	11		
7	11		
8	12		
9	12		
10	11		

Table 3 Table of Langelier saturation index

Sample	Langelier saturation index (LSI)	Indication	
		Langelier [13]	Improved Langelier by Carrier [12]
1	0.30	Water is supersaturated with respect to calcium carbonate and there will be occurrence of scale Water is falling short of being saturated with calcium carbonate Undersaturated water removes existing calcium carbonate protective coatings in pipelines and equipment	Slightly scale forming and corrosive
2	-1.4		Serious corrosion
3	-1.9		
4	-0.75		
5	-0.75		
6	-0.17		Slightly corrosive but no scale formation
7	-0.80		Serious corrosion
8	-1.2		
9	-0.39		
10	-0.71		Slightly corrosive but no scale formation

5 Discussion

The pH values of ten samples are almost neutral. Produced water has high conductivity values as compared with WHO guidelines (Table 1). Due to the presence of ions, produced water has high conductivity which is above pure water of 0.55 mS. Produced water has dissolved and suspended solids which lead to increase in total dissolved solids. Dissolved Oxygen signifies the presence of gaseous oxygen present in water. Marine organisms need dissolved oxygen for respiration. It is necessary for the survival of fish, invertebrates, bacteria and underwater plants. DO is also needed for the decomposition of organic matter as low oxygen concentration leads to warm, humid termite colonies which favors incomplete reduction of organic molecules to methane and other trace gases. DO values showed lower values than the discharge regulation values which is harmful for the aquatic animals. The high values of turbidity are due to the presence of suspended and dissolved solids in PW as there are particles present in water which lead to haziness or cloudiness of produced water. High turbidity leads to the presence of high values of viruses, parasites and some bacteria as they can be attached to the dirt present in water. The amount of dissolved calcium and magnesium in water is hardness of water. All the produced water samples showed high values of hardness (Table 1) which is detrimental for human health. The produced water samples also have a high value of oil and grease (Table 1) which includes fats, oils, waxes and other related constituents. These can interfere with biological life in surface waters and create unsightly films.

The results were validated in the Lenntech software. The Ryznar stability index (Table 2) and Langelier saturation index (Table 3) were calculated. Both the indexes show that the PW samples are highly corrosive and there is a tendency for scale formation. According to Langelier saturation index,

sample 1 and 2 the presence of calcium carbonate is above the saturation point and so there is a tendency for scale formation whereas in sample 3–10, the presence of calcium carbonate is below the saturation point. Undersaturated water removes the protective coatings in pipelines and equipment. According to Ryznar stability index all the produced water samples are highly aggressive (Table 2). These produced water samples gains minerals and metals, which corrodes iron and copper surfaces of the pipelines.

6 Conclusions

The PWs collected from the oil fields of Upper Assam Basin were characterized for physico-chemical and inorganic parameters and their values were compared with the WHO specification for safe disposal of water into the environment. It is inferred that some of its parameters have higher values than the safe limits which can be adversely affect the environment. EC, turbidity, hardness, Na and Ca showed values much higher than the safer limits for its disposal whereas pH, salinity, and gives satisfactory results. This experiment proves that sample 1 & 8 shows high salinity, EC and due to the presence of Na ion. From Ryznar stability index and Langelier saturation index it can be inferred that PW samples are highly corrosive and it has a tendency to form scale. All the water samples are also highly aggressive.

References

- Gogoi, S.B., Tamuli, A.S.: Recent advances in treating oil field produced water: a review. *J. Pet. Eng. Technol.* **4**(2), 366–370 (2014)
- Konwar, D., Gogoi, S.B., Barman, J., Gogoi, M.P.: Correlation analysis of formation water of upper Assam basin for a greener ecosystem. *Int. J. Eng. Technol. Sci. Res. (IJEITSR)* **4**(8) (2017). ISSN 2394–3386
- Fakhru'l-Razi, A., Pendashteh, A., Abdullah, L.C., Biak, D.R.A., Madaeni, S.S., Abidin, Z.Z.: Review of technologies for oil and gas produced water treatment. *J. Hazard Mater.* **170**(2–3), 530–551 (2009).
- Kpeglo, D.O., Mantero, J., Darko, E.O., Emi-Reynolds, G., Faanu, A., Manjon, G., Vioque, I., Akaho, E.H., Garcia-Tenorio, R.: Radiochemical characterization of produced water from two production offshore oilfields in Ghana. *J. Environ. Radioact.* **152**, 35–45 (2016).
- Jain, P., Sharma, M., Dureja, P., Sarma, P.M., Lal, B.: Bioelectrochemical approaches for removal of sulphate, hydrocarbon and salinity from produced water. *Chemosphere* **166**, 96–108 (2017).
- Ozygun, H., Ersahin, M.E., Erdem, S., Atay, B., Sayili, S., Eren, E., Hoshan, P., Atay, D., Altinbas, M., Kinaci, C., Koyuncu, I.: Comparative evaluation for characterization of produced water generated from oil, gas, and oil-gas production fields. *Clean-soil Air Water* **41**(12), 1175–1182 (2013).
- Coday, B.D., Hoppe-Jones, C., Wandera, D., Shethji, J., Herron, J., Lampi, K., Synder, S.A., Cath, T.Y.: Evaluation of the transport parameters and physiochemical properties of forward osmosis membranes after treatment of produced water. *J. Membr. Sci.* **499**, 491–502 (2016).
- Weschenfelder, S.E., Borges, C.P., Campos, J.C.: Oilfield produced water treatment by ceramic membranes: bench and pilot scale evaluation. *J. Membr. Sci.* **495**, 242–251 (2015).
- Patel, H., Borgohain, D., Jena, S.: Hydro geochemistry of Upper Assam oil field. *J. Pet. Technol.* **2**, 11–14 (2003)
- Stone, B.: Management of Produced Water. Oxford publications, Washington, pp. 37–41 (2003)
- Ryznar, J.W.: A new index for determining amount of calcium carbonate scale formed by a water. *J. Am. Water Works Assoc.* **36**(4), 472–486 (1944)
- Carrier Air Conditioning Company: Handbook of Air Conditioning System Design. McGraw-Hill Books. New York (1965)
- Langelier, W.F.: The analytical control of anti-corrosion water treatment. *J. Am. Water Works Assoc.* **28**(10), 1500–1521 (1936)



Analyses and Treatment of Oil Field Formation Water of Upper Assam Basin (India)

Tapan Jyoti Gogoi and Subrata Borgohain Gogoi

Abstract

Formation water constitutes the biggest oil by-product of oil exploration and production industries, which disturbs the ecological balance. In view of the above, this study is an attempt to examine the physical and chemical parameters of formation water and to determine the scaling potential of untreated and treated formation water by Ryznar stability index and Langelier saturation index calculators. Ten samples of crude oil containing more than 70% formation water are collected from the wellheads of ten production wells of the Upper Assam Basin. Analyses of the parameters of the separated formation water from crude oil are found to be outside the permissible range set by the Central Pollution Control Board of India which gives us a clear view that the untreated water cannot be discharged to the environment until proper treatment is done. The formation water samples are treated in a parallel flow hollow fiber membrane module by micro-filtration, ultra-filtration and nano-filtration membranes in sequence. The parameters of the treated samples by nano-filtration are found to be within the range set by the Central Pollution Control Board of India, therefore, it can be disposed of without affecting the environment. The scaling potentials are evaluated by Ryznar stability index and Langelier saturation index calculators of the untreated and treated formation water. The untreated water sample forms heavy scales than the treated ones.

Keywords

Formation water • Parameters • Membranes
Scaling

T. J. Gogoi · S. B. Gogoi (✉)
Dibrugarh University, Dibrugarh, Assam, India
e-mail: subrata@dbru.ac.in

T. J. Gogoi
e-mail: pf_tapanjyoti@dbru.ac.in

1 Introduction

The focus in the oil industry is to carry out exploration and exploitation and to develop hydrocarbon prospects and commercially produce oil and natural gas in an environmentally harmonious manner. It produces around 77 billion barrels of water per annum globally which contains inorganic salts, organic compounds, total dissolved solids, suspended solid—with a presence of bacteria and microbes, oil and grease and heavy metals [6]. Oil wells in some oil fields of the Upper Assam Basin are producing 98% formation water (FW) and 2% crude oil [5]. The most efficient way of handling this large quantity of formation water is to use it in a water injection plant for reservoir pressure maintenance or re-inject it in disposal wells after treatment. The water quality parameters set by the Pollution Control Board of India can be achieved efficiently through membrane processes which is an economically viable physical process. The primary objective of this paper is to treat the contaminated formation water by membrane filtration to remove the major pollutants, so as to dispose of the treated water without affecting the environment along with determining the scaling potential using Ryznar stability index and Langelier saturation index calculators.

2 Materials and Methods

Materials: Ten samples of FW were taken for analysis along with potassium hydroxide, ethanol, petroleum ether, ethylene di-amine tetra acetic acid (EDTA) disodium salt di hydrate, erichrome black T, potassium chloride, sodium chloride, calcium carbonate, lithium carbonate, hydrochloric acid, phenolphthalein, toluene and filter paper were used.

Methods: The pH, conductivity, salinity, TDS, turbidity and DO were analyzed in a water analyzer (Systronics 371). The BOD was tested in a BOD incubator (Velp scientifica). The Na, Li, Ca were determined in a flame photometer

(Systronics 128), while Al, B, P, Be, Bi, Ca, Cd, Co, Cr, Cu, Fe, Mn, Mg, Ni, Pb, Sr, Te, Zn, Ti were determined in an atomic adsorption spectrometer (AAnalyst 200) and induced coupled plasma optical emission spectrometer (Optima 2100DV). The membrane treatment was done in a hollow fiber membrane module set up with microfiltration (MF), ultrafiltration (UF) and nano-filtration (NF) membranes. While the scaling effect on the membranes were evaluated in RI and LSI calculators.

3 Results

3.1 Results of Water Cut Analysis

See Table 1.

3.2 Results of Physic-Chemical Analysis

See Figs. 1, 2, 3, 4, 5, 6, 7 and 8.

4 Discussion

Table 1 shows the water cut analysis of the FW which gives us an apparent view of the presence of a high quantity of water along with crude oil due to ageing of the oil fields of the Upper Assam Basin. Figures 1, 2, 3, 4, 5, 6, 7 and 8 show the results of the physicochemical analysis. This provides a comparison between untreated FW and stages of filtration in MF, UF and NF membranes. It gives us a clear view that the pore size is inversely proportional to the removal of contaminants. NF membrane provides maximum removal of contaminants and its water is considered for

disposal as all the parameters are within the range set by the Central Pollution Control Board of India.

The untreated FW has a high value of pH which affects its chemical properties. The conductivity of pure water is 0.35 mS/cm which is well below the conductivity of FW due to the presence of ions in it [3]. The removal of total dissolved solids is a challenge given the sheer number of ion particles that are smaller than 2 μm and range from <2000 to >150,000 ppm [1]. The complete removal of all total dissolved solids from water can only be achieved through MF, UF and NF membranes together in a sequence. The conductive ions basically come from inorganic materials such as alkalis, chlorides, sulphides and carbonate compounds. The presence of suspended solid may damage the formation by plugging the pores while injecting FW through the injection wells. The FW was found to be highly saline and rich in dissolved minerals. The main contributing ions are Na, Mg, Ca, K, chloride, sulphate, bicarbonate and bromine. The hardness was predominantly caused by divalent cation such as Ca, Mg, Al, Ba, Fe, Mn, Sr and Zn. Alkalinity was primarily due to hydroxide, carbonate and bicarbonate contents. The oil and grease was present in FW in the form of free oil, dispersed oil and emulsified oil. These have to be completely removed from FW as it contains harmful constituents which are not suitable for disposal into the environment. The principle behind the separation of oil and grease from FW is Stokes law [7]. BOD measures, the quantity of oxygen used by microorganisms in the oxidation of organic matter which is must be as low as possible so that the aquatic animals are provided with adequate oxygen. The hydrocarbons are directly related with environmental pollution and biological toxicity problems where the metallic elements are human carcinogens which may induce multiple organ damage even at lower levels of exposure [2, 8]. By calculating the scaling effect, it was found that all the RI values remained around 6 and the LSI values remained

Table 1 Table of water cut analysis

Sl. No.	Sample ID	Geologic formation/depth (m)	Reservoir pressure (kg/cm^2)	Reservoir temperature ($^\circ\text{C}$)	Water cut i.e. water in crude oil (%)
1	1	Barail (2950)	190	82	86
2	2	Barail (3100)	200	88	91
3	3	Barail (2800)	240	85	73
4	4	Barail (3100)	180	89	82
5	5	Barail (3350)	240	89	89
6	6	Barail (2900)	250	83	76
7	7	Barail (2850)	230	81	77
8	8	Barail (3100)	220	86	95
9	9	Barail (3300)	180	90	90
10	10	Barail (3200)	210	87	83

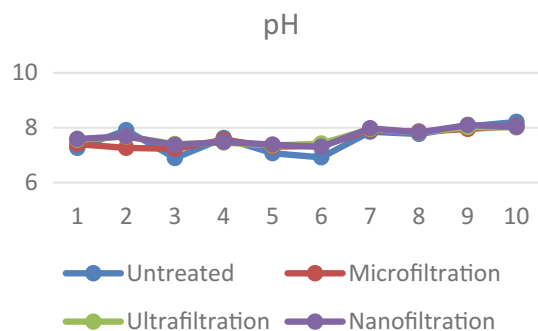
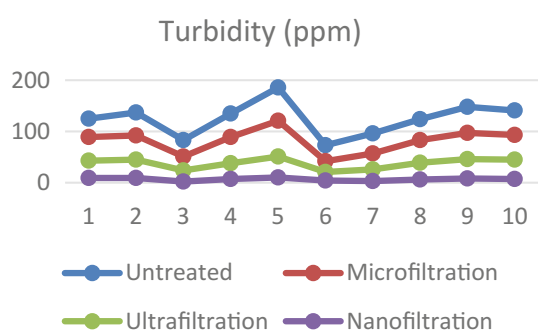
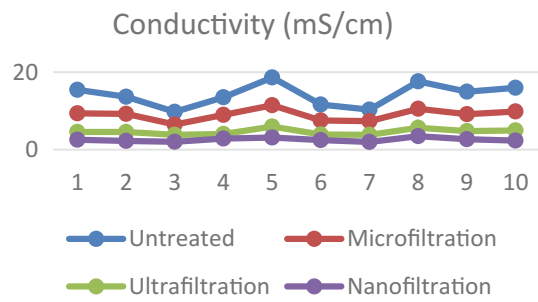
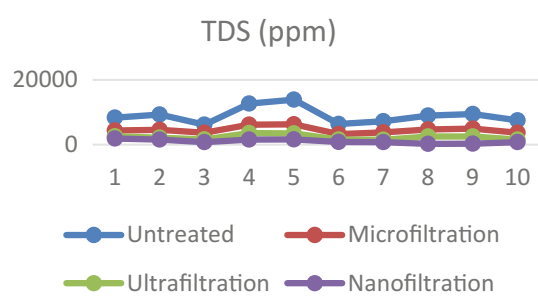
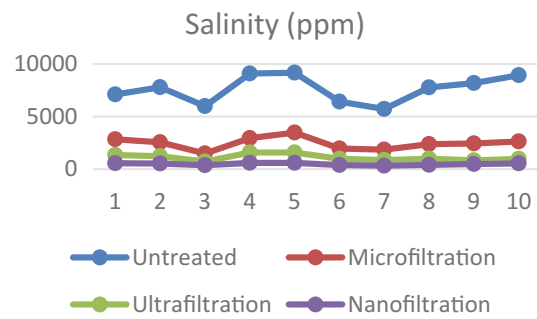
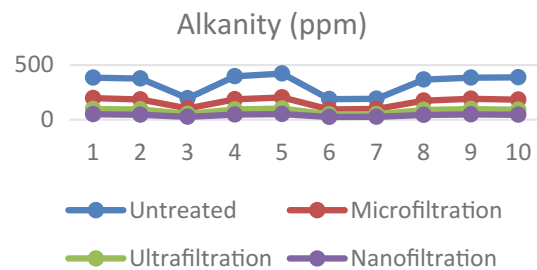
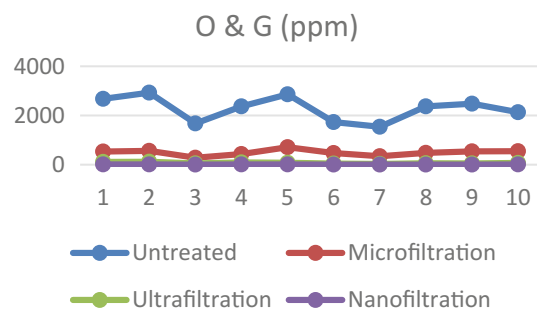
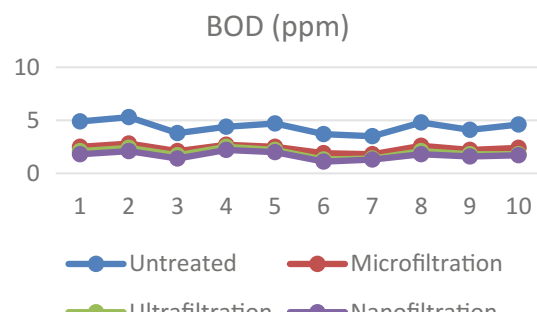
**Fig. 1** Comparison of pH after stages of membrane treatment**Fig. 2** Comparison of turbidity after stages of membrane treatment**Fig. 3** Comparison of conductivity after stages of membrane treatment**Fig. 4** Comparison of TDS after stages of membrane treatment**Fig. 5** Comparison of salinity after stages of membrane treatment**Fig. 6** Comparison of alkalinity after stages of membrane treatment**Fig. 7** Comparison of O&G after stages of membrane treatment**Fig. 8** Comparison of BOD after stages of membrane treatment

Table 2 Membranes with average pore diameters

Sl. No.	Membrane	Molecular weight cut-off (MWCO) (kDa)	Average pore diameter (μm)
1	MF	–	0.2
2	UF	44	12.9
3	NF	400	1.04

around 0.5, which shows that the untreated FW forms a heavy scale whereas the treated water shows a light scale, while scaling indicates the presence of CaSO_4 , BaSO_4 and SrSO_4 [4].

5 Conclusions

This paper reveals the effect of untreated FW on the ecosystem. It affects the soil and water bodies if requisite treatment is not done by oil and gas industries. The FW reduces dissolved oxygen concentration and leads to the formation of sludge in the environment which damages the aquatic biota.

Table 2 gives us an idea about the average pore diameter and molecular weight cut-off of the MF, UF and NF membranes with which the FW is being treated. The average pore diameter which remains uniform throughout the whole membrane. After consecutively treating with all the membranes, it was found that all the parameters were within

range set by Central pollution control board of India. The presence of CaSO_4 , BaSO_4 and SrSO_4 in FW lead to the occurrence of scales on filter membranes. The scaling effect of on the membranes were evaluated in RI and LSI calculators. Heavy scales formation was observed during untreated FW filtration process, while light scale formation was observed during untreated FW filtration process.

References

- Arthur, J.D., Langhus, B.G., Patel, C.: Technical summary of oil & gas produced water treatment technologies (Mar 2005)
- Gakwir, C., Raut, N., Al-Saadi, A., Al-Aisri, S., Al-Ajmi, A.: A critical review of removal of zinc from wastewater. In: Proceedings of the World Congress on Engineering 2012, vol. I, July 2012
- Gogoi, S.B., Sen, R.K., Rajbongshi, A., Hazarika K.: Characterization of oil field produced waters of Upper Assam Basin, India. Int. J. New Technol. Sci. Eng. 2(1) (2015). ISSN 2349-0780
- McCartney, R.A.: Conditions under which anhydrite precipitation can occur in oil reservoirs as a result of seawater injection (2008)
- Neff, M.J., Lee, K., DeBlois, M.E.: Produced water: overview of composition, fates and effects (Jan 2011)
- Rangarajan, T.D., Ali, H., Amr, H.: State of the art treatment of produced water (2016)
- Rudolfs, W., Babbitt, H.E., Bloodgood, D.E., Edwards, C.P., Faber, H.A., Genter, A.L., Heukelekian, H., Miles, H.J., Mohlman, F.W., Ruchhoft, C.C., Sawyer, C.N., Setter, L.R., Van Kleech, L.W.: A critical review of the literature of 1945 on sewage and waste treatment and stream pollution (1946)
- Tchounwou, B.P., Yedjou, C.G., Patlolla, A.K., Sutton, D.J.: Heavy metals toxicity and the environment (Aug 2012)



Experimental Analysis and Cement Slurries Properties Evaluation Using Novel Additives

Masoud Rashidi, Biltayib Misbah Biltayib, and Adel Asadi

Abstract

This project focuses on the changes in the characteristics and properties of cement slurry while adding different environmentally friendly additives. To properly implement the cementing job, cement should have the desired properties and characteristics. It should have very low permeability, high strength, sufficient thickening time and pump-ability to reach the target depth and the desired density, depending on the conditions of the well. To control the cement properties and obtain the desired characteristics, additives are usually used and mixed with plain cement. In this project, new and novel additives, including cactus powder, hay bran, hay bran ash, rice husk, and rice husk ash were used and mixed separately with the plain cement. The plain and blended cement samples were exposed to various API cement tests, including the compressive strength test, gas-permeability test, fineness test, and density test. This paper focuses mainly on the results of the compressive strength test conducted on the plain cement and rice husk ash, hay bran ash blended with cement. Results showed that the rice husk ash blended cement at a 10% replacement level exhibited the highest value of compressive strength, whereas the other non-ash additives adversely affected the strength of the cement.

Keywords

Cement slurry properties • Rice husk ash
Rice husk • Hay bran ash

M. Rashidi (✉) · B. M. Biltayib
Petroleum Engineering Department, School of Engineering,
Australian College of Kuwait, West Mishref, Kuwait
e-mail: m.rashidi@ack.edu.kw

A. Asadi
Department of Petroleum Engineering, Science and Research
Branch, Islamic Azad University, Tehran, Iran

1 Introduction

Cement plays a vital role in the drilling industry where it holds the casing in place and is essential to stabilize the wellbore. It also helps isolate the unwanted zones to prevent the migration of fluids between the subsurface formations [6]. Cement in drilling industries should be designed in a way to enhance the operations of drilling and ensure the safety and protection of shallow water aquifers, it should be cost-saving and environment-friendly in order to protect the environment. The cementing job is known to be a very expensive operation in drilling industries, and failure of primary cementing can cause extra costs on the process of cementing.

1.1 Portland Cement

Cements that are used in the drilling industries are mostly Portland cement type and API classes, used based on conditions of wells [8]. Portland cement is manufactured by calcining limestone, slag, shale, and clay together at 2000–6000 °F in a rotary kiln. After the calcining process, a material is formed and is called clinker. Clinker is then cooled and grounded with a small amount of gypsum to form Portland cement [1]. The main components of the Portland cement are iron, alumina, silica, and lime. When these components are heated, they form complex compounds that make up the cement. These compounds are Tricalcium aluminate (C_3A), Tetracalcium aluminoferrite (C_4AF), Tricalcium silicate (C_3S) and Dicalcium silicate (C_2S) [1].

When water is mixed with the Portland cement, hardening and setting reactions begin to occur. The four compounds of the Portland cement begin to react chemically with the water. This chemical reaction is what we call as “hydration”. The compounds undergo hydration, and recrystallization, which results in a set and hardened product. Once the Portland cement is set, high strength and low

permeability are exhibited in the cement. When mixed with water, as a result of Hydration reactions, Tricalcium silicate (C_3S) and Dicalcium silicate (C_2S) which make up to 80% of Portland cement, produce “hydration products”. The hydration products formed when the cement is hydrated and hardened are Calcium silicate hydrate ($C_3S_2H_3$) and Calcium hydroxide $Ca(OH)_2$ [CH].

1.2 Novel Additives

- i. Hay Bran: Hay is a grass or green fodder that has been stored and dried to an extent where its properties do not change. Several cereal plants can be made into hay, such as wheat, oat, barley, etc. Bran is the integral part of any cereal grain. Hay bran is the by-product of the bran milling process. Hay bran's chemical composition consists of cellulose, hemicellulose, lignin, chloride, and sodium [4].
- ii. Hay Bran Ash: Hay bran ash is the product formed from the combustion of the hay bran. Hay bran's ash chemical composition consists of oxides of silicon, magnesium, potassium, sodium, and carbonates.
- iii. Rice Husk: Rice husk is the hard covering or the outer layer of the rice grains. The rice grains are removed from their hard coverings during the milling process to obtain the rice husk or what is called as rice hulls. The chemical composition of the rice husk consists of cellulose, lignin, hemicellulose, extractives, and water [3].
- iv. Rice Husk Ash: Rice husk ash is formed following the combustion of the rice husk. Its chemical composition consists of silica, alumina, iron oxide, calcium oxide, magnesium oxide, sodium oxide, potassium oxide, and sulfur oxide [7].
- v. Cactus: The chemical composition of the cactus consists of water, potassium, calcium, magnesium, fat, and phosphoric acid [2]. In this project, dry cactus (free of water) was used and grinded to obtain a cactus powder.

2 Tests and Procedures

2.1 Fineness Test

The fineness test is done to identify the degree of the cement particles fineness. Sieve analysis, using the sieve analysis machine, was conducted to determine the fineness of cement. The sieve analysis machine is an electric sieve shaker that vibrates for 60 min continuously, on a certain speed, to obtain the separation of fine particles from coarse particles based on a sample inserted from the top tray and received at the bottom tray. This machine consists of eleven

sieves trays, each comes with a different mesh size, and placed in an order from a mesh sieve tray 4 (4750 μm) to a mesh sieve tray 200 (75 μm). The mesh sieve tray 200 was used to determine the cement fineness. It was then used to sieve all the additives and obtain a particle size as fine as the cement.

2.2 Compressive Strength Test

The compressive strength test is conducted to measure the ability of the set cement to resist compression. The device applies a compressive load on the set cement sample until the fractures in the sample are induced. To prepare the strength test samples, 250 g of cement was used for preparing each sample. As per the water requirement for API Class G cement, 44% water by weight of cement, 110 mL of water was mixed with each 250 g of cement, which resulted in a water-cement ratio of 0.44.

Additives were added with different replacement levels. After mixing the cement slurries, they were then placed and compacted in cube-shaped molds. After 24 h, the set cement samples were removed from the molds and kept in water for 20 days for curing. After the period of curing, the samples were removed from the water and tested.

2.3 Permeability Test

The permeability test is conducted to measure the ability of a fluid to flow in the interconnected pore spaces existing in the set cement under different pressure conditions. For preparing the permeability test core samples, 50 g of cement was used for preparing each sample. As per the water requirement for API Class G cement, 44% water by weight of cement, 22 mL of water was mixed with each 50 g of cement.

Additives were added with different replacement levels. After mixing the cement slurries, they were placed and compacted in custom-made cylindrical molds. After 24 h, the core samples were removed from the molds and tested. To measure the permeability of the cement, a Gas Permeameter device was used, where nitrogen gas was forced through the set cement core sample at different flow rates and pressures. Pressures and flow rates were then recorded to obtain the permeability using Darcy law.

2.4 Density Test

The density of the slurry cement was determined by using the mud balance. To conduct the density test, 250 g of cement was used for preparing each sample. As per the water requirement for API Class G cement, 44% water by weight

of cement, 110 mL of water was mixed with each 250 g of cement. The cement slurries were poured in the cup of the mud balance, and density readings were recorded. The density test was conducted on plain cement, hay bran ash blended cement, and rice husk ash blended cement.

3 Results

The investigation of the properties of rice husk ash blended cement in terms of compressive strength were studied. The effect of the rice husk ash particle size and the different replacement levels on the compressive strength is investigated and discussed.

3.1 Compressive Strength Test Results

As shown in Table 1, only hay bran ash and rice husk ash blended cements showed good results. However, compared with the plain cement which withstands a compressive load of 89.9 kN, the rice husk ash blended cement, with a 10% replacement level has a higher compressive strength as it withstands a compressive load of 95.1 kN.

3.2 Permeability Test Results

As shown in Table 2, the results showed a very high permeability for the blended cements compared to the plain cement (3.6 md). The only satisfactory results that showed a

permeability less than 10 md were of hay bran at 4 wt% replacement level and rice husk ash at 8 wt% replacement level, where they exhibited a permeability of 7.8, and 5 md respectively. Rice husk ash at 10 wt% replacement level has strengthened the cement. High strength means low porosity and low permeability, so that might explain the low permeability of the rice husk ash at 8 wt% replacement level.

3.3 Density Test Results

As shown in Table 3, hay bran ash blended cement at 5 and 15 wt% replacement levels showed less density than the plain cement. Rice husk ash at all replacement levels showed less density than the plain cement. This is due to the presence of high concentrations of silica in the rice husk ash. Silica is considered one of the most common extenders. Extenders are additives added to the cement to reduce its density.

4 Discussions

Rice husk ash blended cement was previously experimented and tested for its compressive strength; however, using coarser grains, results showed a very weak cement, mostly due to the influence of rice husk ash particle size. A finer rice husk ash cement showed a comparatively higher strength, because when the coarse particles of additives are blended with the fine particles of the cement, pores will be created,

Table 1 Compressive strength test results (Max compressive load applied in kN)

Replacement level (wt%)	Hay bran ash	Rice husk ash	Hay bran	Rice husk	Cactus	Plain cement
5	68.2	60.4	0.7	3.4	—	89.9
10	59.3	95.1	1.4	0.7	—	89.9
15	23.6	45.2	6.3	4.7	—	89.9

Table 2 Permeability test results (Units are in md)

Replacement level (wt%)	Hay bran ash	Rice husk ash	Hay bran	Rice husk	Cactus	Plain cement
4	14.7	41.7	7.8	17.7	59.7	3.6
8	12.0	5.0	34.8	28.6	132.5	3.6
12	27.9	15.3	40.6	27.8	—	3.6

Table 3 Density test results (g/cc)

Replacement level (wt%)	Hay bran ash	Rice husk ash	Plain cement
5	1.8	1.8	1.9
10	1.9	1.8	1.9
15	1.9	1.9	1.9

and compressive strength will decrease; but, when the fine particles of additives are blended with the fine cement, a well compacted material is formed with a very low porosity.

The higher compressive strength of rice husk ash is due to the presence of reactive silica and finer particles of rice husk ash. Due to the large amount of reactive silica in the rice husk ash, it is considered a Pozzolan, which is a siliceous material mainly consisting of silica (SiO_2), and does not have any cementitious properties solely, but when water and cement are mixed, they undergo a pozzolanic reaction where the silica reacts chemically with Calcium Hydroxide ($\text{Ca}(\text{OH})_2$) to produce Calcium Silicate Hydrate (C-S-H gel) which gives strength to the cement. This pozzolanic reaction and the calcium hydroxide released from the hydration process produce more calcium silicate hydrate C-S-H gel, which results in a higher compressive strength [5].

The rice husk ash blended cement with a 10 wt% replacement level of rice husk ash exhibited the highest compressive strength as indicated by the highest compressive load applied (95.1 kN). A replacement level of 5 wt% of the rice husk ash showed lower compressive strength than the 10 wt% level, which can be explained by the fact that with the 5 wt% replacement level, there is less amount of silica, and this amount is not enough to react with all calcium hydroxide (CH) released from the hydration of cement. Thus, the pozzolanic reaction produced less amount of C-S-H gel, and less strength is reached. A 15 wt% replacement level of the rice husk ash showed a lower compressive strength compared to the 10 and 5% replacement levels, due to the increased amount of silica that is not consumed by the pozzolanic reaction. The amount of CH released from the hydration process is not enough to react with all the silica added to the cement, and a portion of the silica will remain non-reactive, and will not add strength to cement.

Thus, rice husk ash can be considered as a good additive for the cement in terms of compressive strength. A 10 wt% replacement level of rice husk ash is recommended to be used as an additive for the cement. Further investigations and other concentrations must be tested to conclude if this additive is a good one or not.

As a result of permeability tests observations, a microstructure investigation is needed to observe the pores structure of the blended cements in order to investigate the reason for their high permeability. The use of X-ray

diffraction (XRD) technique is therefore recommended to study the structure of the blended cements molecules.

As a result of density tests observations, we concluded that rice husk ash is considered to be an extender, and it can be used for a low fracture gradient and narrow mud weight window sections of the wells.

5 Conclusions

The rice husk ash blended cement with 10 wt% of rice husk ash exhibited a higher compressive strength when compared with the other blended cements and plain cement. This is explained by the composition of the rice husk ash. Rice husk ash is considered as a pozzolan due to the presence of reactive silica. When added to water, it undergoes a pozzolanic reaction where it reacts chemically with $\text{Ca}(\text{OH})_2$ to form additional C-S-H, which gives the cement more strength. Increasing the fineness of rice husk ash is an important factor in developing the strength of the blended cement. Rice husk ash is also considered as an extender which reduces the density of the cement. The rice husk ash blended cement with 8 wt% of rice husk ash exhibited a low permeability of 5 mD. Implementing the use of the rice husk ash in well-cementing jobs will help protect the environment by reducing pollution and contamination, reduce the cost of cementing, and enhance the properties of the cement.

References

1. Adams, N.: *Drilling Engineering: A Complete Well Planning Handbook*. Pennwell Corp., Tulsa, Oklahoma (1985)
2. FAO: Cactus (*Opuntia Spp.*): As Forage. FAO Plant Production and Protection Papers (2002)
3. Kumar, P.S., Ramakrishnan, K., Kirupha, S.D., et al.: Thermodynamic and kinetic studies of cadmium adsorption from aqueous solution onto rice husk. *Braz. J. Chem. Eng.* **27**(02), 347–355 (2010)
4. Meneses, R., Varela, G., Flores, H.: Evaluating the use of *Atriplex nummularia* Hay on feed intake, growth, and carcass characteristics of Creole kids. *Chil. J. Agric. Res.* **72**(01), 74–79 (2012)
5. Michaux, M., Nelson, E., Vidick, B.: Cement chemistry and additives. *Oilfield Rev.* **1**(01), 18–25 (1989)
6. Rabia, H.: *Well Engineering and Construction*. Entrac Consulting (2001)
7. Ramezanianpour, A.A.: *Cement Replacement Materials: Properties, Durability, Sustainability*. Springer, Berlin (2013)
8. Smith, D.K.: *Cementing*. Society of Petroleum (1979)

Part V

Evaluation of Hydrocarbon Source Potential and Petroleum System Modeling



Petrographical Features of Organic Matter from Upper Jurassic Naokelekan Formation, Kurdistan-Iraq: A Study on Regional Thermal Maturity Trends

Rzger A. Abdula, Kamal Kolo, Victoria Raftopoulou, Polla Khanaqa, and Stavros Kalaitzidis

Abstract

Upper Jurassic Naokelekan organic-rich strata are ubiquitous across the Kurdistan Region of Iraq. Laterally, continuous layers, of substantial thickness, outcrop in the highly folded and imbricated zones and in subsurface sections in the Low Folded Zone. In this study, 15 samples from 5 outcrops, viz., Barzinja, Sargelu, Barsarin, Karak, and Bnavya, were examined, which represent the entire lithological alternations of limestones and shales encountered in the Whole Naokelekan Formation. This study assesses the type, the thermal maturity and the petroleum generation potential of the organic matter contained in the upper Jurassic Naokelekan formation throughout the area. The qualitative petrographical evaluation of the studied samples revealed that the main organic constituents are solid hydrocarbons, in the form of microgranular migrabitumens, with minor amounts of pyrobitumens. Equivalent vitrinite reflectance estimations ($0.59\text{--}1.12\% R_o$) indicate that the upper Jurassic sequence in the western part of the area is at a mature stage, while the same sequence in the eastern part is at late mature stage.

Keywords

Naokelekan Formation • Solid bitumens
Maceral • Vitrinite reflectance

1 Introduction

The Naokelekan Formation is one of many Jurassic formations of significant hydrocarbon source rock characteristics all over Iraq. The type of organic matter and its maturity level in potential rocks are important qualities in oil exploration. Hence, this study aims to: (1) define the type of organic matter; (2) determine the thermal maturity of the organic matter; and (3) assess the hydrocarbon potentiality of the Naokelekan Formation in Iraqi Kurdistan in five surface stratigraphic sections (Fig. 1).

2 Materials and Methods

All the outcrop sections are located in the High Folded and the Northern Thrust zones of the mountainous area that stretches 600 km along an east-southeast to north-northwest axis in the eastern parts of Iraq. The studied outcrops are: (1) Barzinja section that runs along a road cut and is located at 2 km to the northeast of Chinara Village and 10 km to the east of Barzinja Town; (2) Sargelu Village is located 5 km from Surdash Town, on the Surdash anticline, Sulaimani District; (3) Barsarin Village, the exposure of Naokelekan Formation is located about 55 m downstream from the old footbridge in Barsarin Village, about 10 km away from Soran Town; (4) Karak section lies in the core of the Korak anticline, east-southeast of Karak Village and about 7 km south of Rawanduz Town; and (5) Bnavya section runs along a road cut between Bnavya and Hidena villages and is located at 5 km to the northwest of Kani Masi Town.

Fieldwork on Naokelekan outcrops was performed during the summer of 2015, and 15 samples were collected along a

R. A. Abdula (✉) · K. Kolo
Department of Petroleum Geoscience, Soran University, Soran,
Iraq
e-mail: rzger.abdula@soran.edu.iq

R. A. Abdula · K. Kolo
Scientific Research Center, Soran University, Soran, Iraq

V. Raftopoulou · S. Kalaitzidis
Department of Geology, University of Patras, Patras, Greece

P. Khanaqa
Kurdistan Institution for Strategic Studies and Scientific Research,
Sulaimani, Iraq

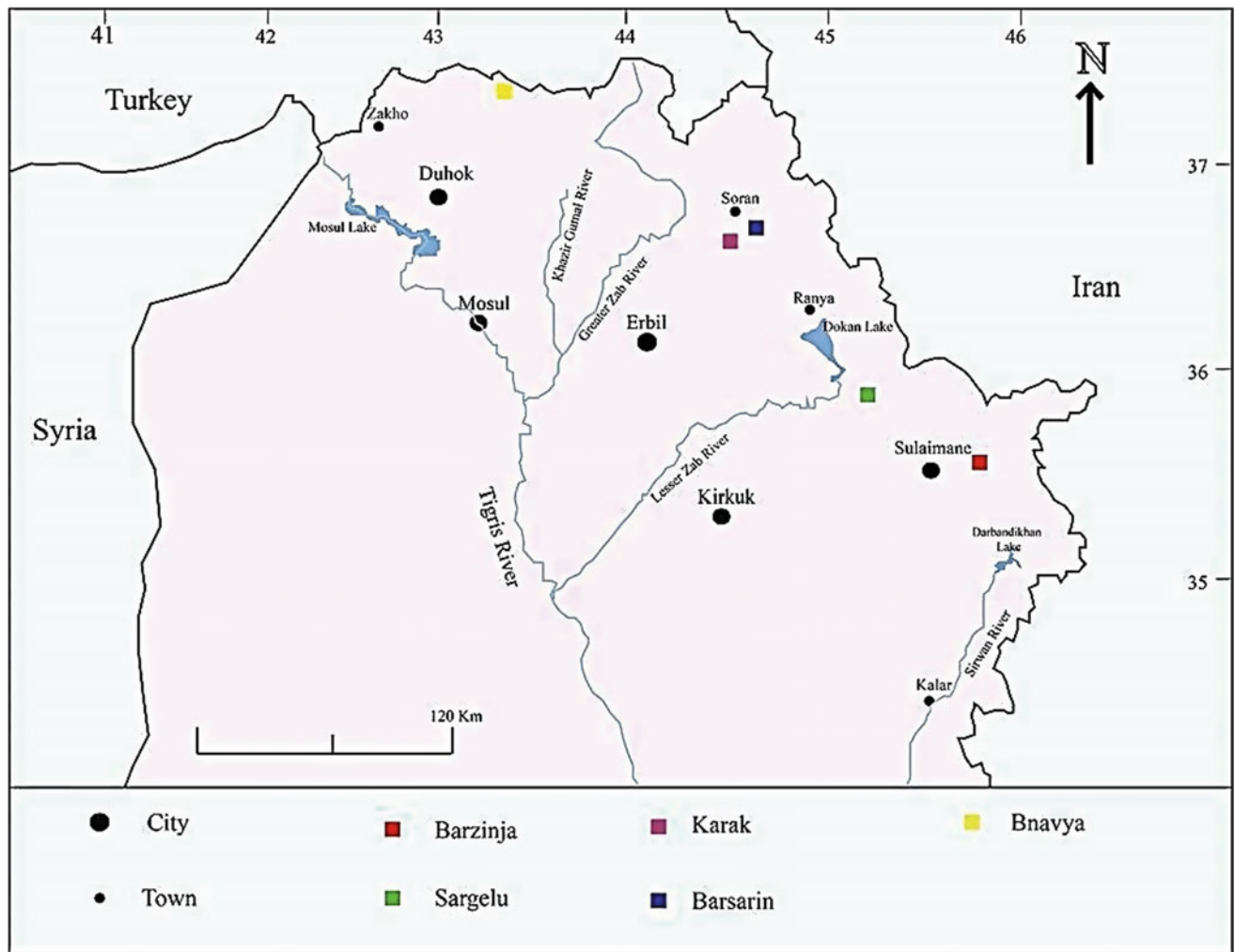


Fig. 1 Map of Iraqi Kurdistan showing the sampling locations

traverse perpendicular to the bedding plane based on vertical lithological and facies changes. Polished blocks were prepared from slightly crushed samples ($\phi < 3$ mm) according to the International Standards [1] in the laboratories of the University of Patras, Greece. Maceral identification and reflectance measurements were performed in oil immersion, using a LEICA DMRX coal-petrography microscope equipped with an MPV system, according to ISO [1] and ASTM [2], following the nomenclature of the Stoops-Heerlen System as modified by ICCP [3–6], as well as of Jacob [7] regarding the solid bitumens.

3 Results and Discussion

The qualitative petrographical evaluation of the studied samples revealed that solid hydrocarbons are the main organic constituents. The prevailing organic particles represent microgranular migrabitumens, whereas homogenous ones are rare. Pyrobitumens were also observed as fractures-filling bodies in few samples. Very fine (<5 μm) non-fluorescing organic matter is also disseminated throughout some samples, and in some cases bituminite was also observed.

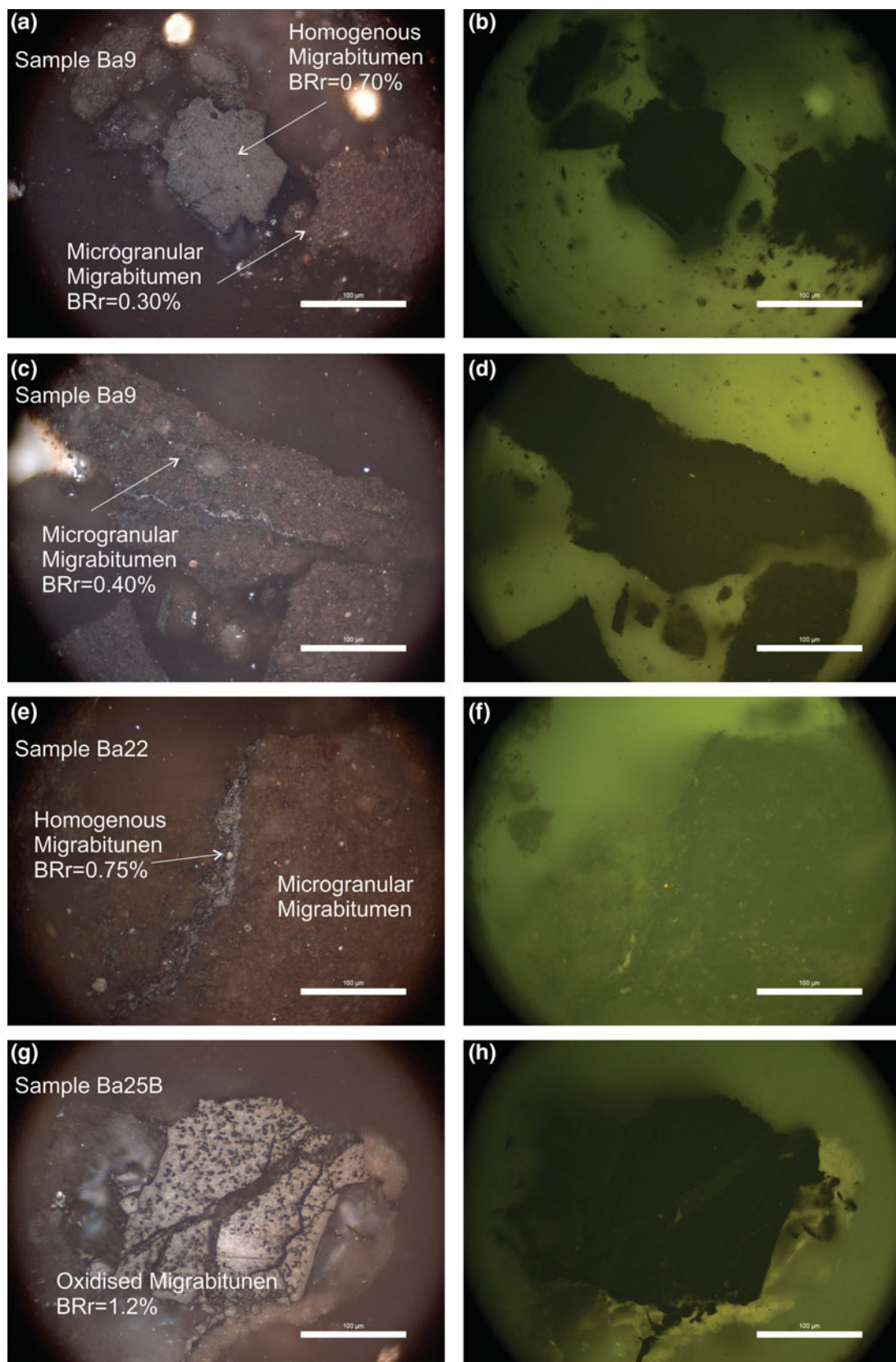


Fig. 2 Photomicrographs of Naokelekan samples viewed under white (**a, c, e, g**) and blue (**b, d, f, h**) reflected light. Oil objective magnification 500×

Equivalent vitrinite reflectance estimations (0.59–1.12% Ro) indicate that the upper Jurassic sequence in the western part of the area is at a mature stage, while the same sequence in the eastern part is at late mature stage (Fig. 2).

4 Conclusions

- a. Certain layers of the upper Jurassic Naokelekan Formation contain significant amounts of organic matter;
- b. The main solid organic phase in the bulk samples is in the form of migrabitumens and secondary pyrobitumens, with a very rare occurrence of bituminite and/or vitrinite particles; and
- c. The thermal maturity level of the contained organic matter, estimated mostly in solid bitumens, shows an increasing trend from west to east, with the western part being in the early maturity phase and eastern part within the pick oil window.

References

1. International Organization for Standardization (ISO) 7404-5: Methods for the petrographic analysis of bituminous coal and anthracite—Part 5: Method of determining microscopically the reflectance of vitrinite. International Organization for Standardization, 11 p. Geneva, Switzerland (2014)
2. American standard for testing and materials (ASTM) D7708: Standard test method for microscopical determination of the reflectance of vitrinite dispersed in sedimentary rocks. 10 p. (2014)
3. International Committee for Coal and Organic Petrology (ICCP): The new vitrinite classification (ICCP system 1994). *Fuel* **77**, 349–358 (1998)
4. International Committee for Coal and Organic Petrology (ICCP): The new inertinite classification (ICCP system 1994). *Fuel* **80**, 459–471 (2001)
5. Sýkorová, I., Pickel, W., Christianis, K., Wolf, M., Taylor, G.H., Flores, D.: Classification of huminite—ICCP system 1994. *Int. J. Coal Geol.* **62**, 85–106 (2005)
6. Pickel, W., Kus, J., Flores, D., Kalaitzidis, S., Christianis, K., Cardott, B.J., Misz-Kennan, M., Rodrigues, S., Hentschel, A., Hamor-Vido, M., Crosdale, P., Wagner, N.: Classification of liptinite—ICCP system 1994. *Int. J. Coal Geol.* **169**, 40–61 (2017)
7. Jacob, H.: Classification, structure, genesis and practical importance of natural solid oil bitumen (“migrabitumen”). *Int. J. Coal Geol.* **11**, 65–79 (1989)

Visual Kerogen Typing: A Case Study of the Northern Song Hong Basin (Vietnam)

Quan Vo Thi Hai and Giao Pham Huy

Abstract

Microscopic observations were conducted on cutting samples of well A, in the northern Song Hong basin. This is to estimate the hydrocarbon source potential by classifying different types of kerogen based on composition. In the section of 1646–2350 m, the organic matters comprise vitrinite particles of more than 50% mixed with secondary assemblages of algae, amorphous, resin and liptodetrinite. This is classified as mainly type III with minor type II/I kerogens, indicating that it is mainly associated to gas-prone and minor oil-prone source rock. In the section of 2445–2850 m, the organic matters contain more amorphous matters than the former section (35–50%), while vitrinite particles range between 35 and 40%. This represents major type I and III kerogen mixed with minor type II kerogen, indicative of both oil- and gas-prone source rocks.

Keywords

Kerogen • Vitrinite • Organic matter • Microscope
Song Hong basin

1 Introduction

Kerogen, as the precursor of defining and classifying organic matter, provides information on the type and source of organic matter in sediments, paleoenvironments, paleoclimates and ancient biological activities. The optical microscopic method for kerogen typing has been widely used, and it can provide some relevant information that effectively supports the interpretation of Rock-Eval data, where kerogen mixtures can be generated by kerogen during the maturation

Q. V. T. Hai (✉) · G. P. Huy

Geosystem Exploration and Petroleum Geoengineering (GEPG)
Program, School of Engineering and Technology, Asian Institute
of Technology, Bangkok, Thailand
e-mail: st114217@ait.ac.th

process [1, 2, 4, 6]. By applying this to assess the kerogen quality of drilling cuttings of well A in the Song Hong basin, this study aims to define the type of kerogen depending on the presence of different structured and amorphous assemblages and their hydrocarbon generation potential.

2 Data and Method

Kerogen is the complex, high molecular weight fraction of the organic matter in rocks that is insoluble in all organic solvents [3]. All samples in this study were washed, dried and picked by geologists. Then, selected samples were treated by organic solvent. Finally, finely dispersed kerogen was taken and glued to a glass slide with epoxy. Kerogen assemblages were looked under transmitted and fluorescent lights of CRAIC 308 PV™ microscope spectrometer. All samples were performed and analyzed at the Geochemical lab of Vietnam Petroleum Institute by my colleagues and me.

Kerogen assemblages are classified based on each kerogen particle type, having a special hydrocarbon-generating capacity [7] and counted to determine the relative percentages of four groups: Amorphinite (non fluorescene and fluorescene amorphous), Alginite (algae), Exinite (pollen, spores, cuticles), woody (materials from land-plant), and Inertinite (recycled and plant materials) [5]. Figure 1 shows the main particles that are grouped as types I, II, and III kerogens.

3 Results

The results obtained from the analysis are presented in Table 1 and Fig. 2. Based on change the amount of amorphous assemblages and vitrinite particles in the whole section, the interpretation is divided into 2 sections. Kerogen in Sect. 1 (1646–2350 m) contains predominantly vitrinite particles (more than 50%) and minor amorphous

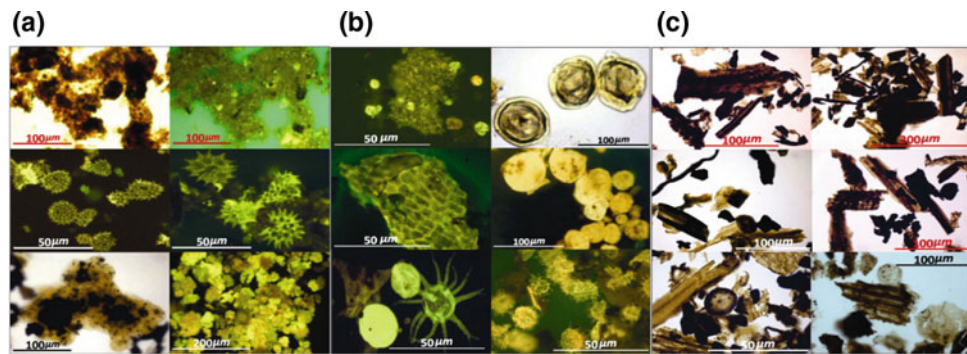


Fig. 1 Photomicrographs of immature particles in transmitted white light and in fluorescence mode. **a** Kerogen type I: amorphous organic matter, *Pediastrum* and *Botryococcus* Algae; **b** kerogen type II:

amorphous organic matter, Cuticle, Prasinophyte Algae, Acritharch and Dinocysts; and **c** kerogen type III: wood tissues

Table 1 Summary of kerogen data

Depth (m)	Amorphinite (%)		Exitinite (%)				Vitrinite (%)	Inertinite (%)
	NF	F	A	C	S&P	R&L		
1646–1650	5	10	5	—	—	5	75	—
1745–1750	10	5	13	—	2	10	60	Tr
1845–1850	Tr	10	8	—	Tr	15	67	Tr
1945–1950	—	5	15	—	—	17	63	—
2045–2050	—	5	8	—	Tr	17	70	Tr
2145–2150	—	Tr	15	—	—	15	70	—
2245–2250	—	10	10	Tr	—	18	62	—
2345–2350	5	10	20	Tr	2	12	51	—
2445–2450	—	45	5	Tr	Tr	10	40	—
2545–2550	—	40	10	Tr	Tr	10	40	—
2645–2650	—	35	15	Tr	—	10	40	—
2745–2750	10	40	10	Tr	Tr	10	30	—
2845–2850	—	45	5	—	—	15	35	—

NF Non fluorescene, F fluorescene, A algal, C cuticle, S&P spores and pollen, R&L resin and liptodetrinite; Tr trace

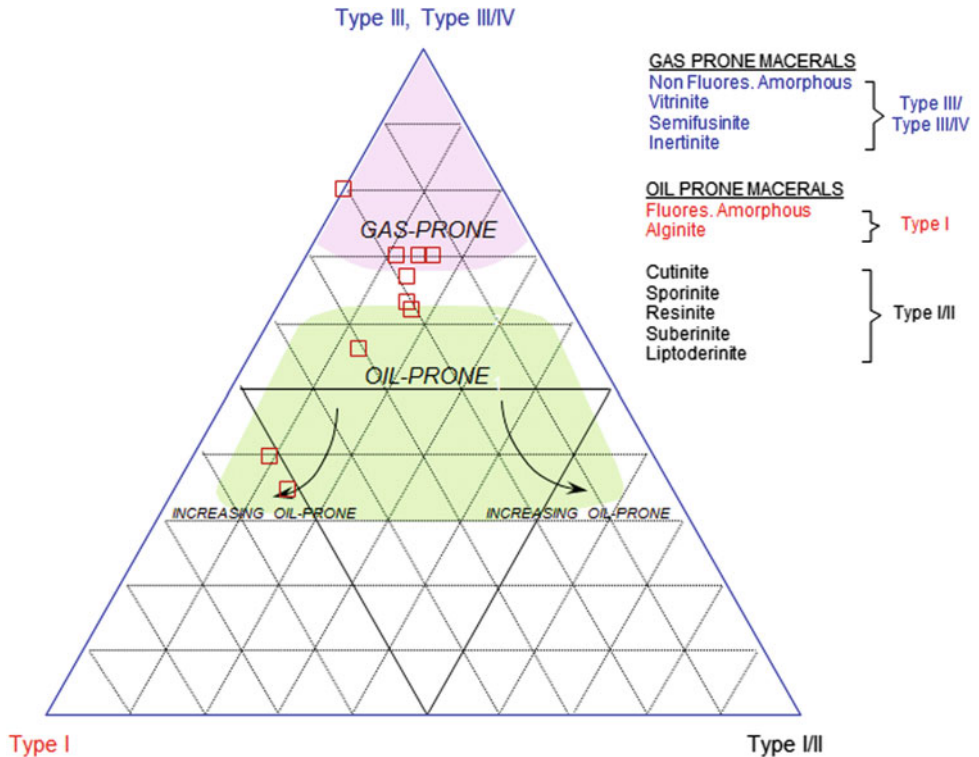
components. In Sect. 2 (2445–2850 m), kerogen assemblages show differences in relative proportions of vitrinite and amorphous, having a bias towards fluorescene amorphous components. The other structured categories (algae, resin, liptodetrinite) are found to be present in the entire well with low quantities. Therefore, type III kerogen was defined dominant in Sect. 1 and mixed with subordinate type II/I kerogens. However, type I kerogen was observed to be more dominant in Sect. 2, compared to that in the former section and also mixed with dominant type III and minor type II kerogens (Fig. 2).

Depending on the above results, two zones of hydrocarbon-generating potential were defined: kerogens in Sect. 1 was identified as a major gas-prone and minor

oil-prone source. In the deeper section, kerogen was composed of more fluorescene amorphous assemblages, indicative of an oil- and gas-prone source.

4 Discussion

The dominance of oil and/or gas in the product (as kerogen cracks over time under the influence of heat in the subsurface) is determined by the type of organic matter and level of thermal maturity. Differences of fluorescence color of spore/pollen or other assemblages indicate a different origin of organic matter and/or a different maturity.

Fig. 2 Maceral composition plot

This study shows favorable evidences for the investigation of shale gas potential in the northern Song Hong basin.

5 Conclusions

Visual kerogen typing is not widely applied in the interpretation of data of the sedimentary basins in Vietnam. This study focuses on the method that gives further evidences, which added to the insights of previous reports on the kerogen type in the Song Hong basin. It confirms that most of the potential source rocks in basin contain type III kerogen, but type III mixed with type II and type I kerogens are also present in some parts of the basin. This study also reveals that most of the samples, especially those at the deeper sections of the basin, display high quantities of fluorescene amorphous assemblages, which suggests a dominant contribution of a more oil-prone nature of the organic matter to the potential source rocks. And this case study deals with the changes of vitrinite and fluorescene amorphous from the upper part to the lower part.

References

1. Dembicki, Jr. H.: Three common source rock evaluation errors made by geologists during prospect or play appraisals. *Am. Assoc. Pet. Geol. Bull.* **93**, 341–356 (2009)
2. Dembicki, Jr. H., Horsfield, B., Ho, T.T.Y.: Source rock evaluation by pyrolysis-gas chromatography. *Am. Assoc. Pet. Geol. Bull.* **67**, 1094–1103 (1983)
3. Durand, B., Niçaise, G.: Procedures for kerogen isolation. In: Durand, B. (ed.) *Kerogen. Insoluble Organic Matter from Sedimentary Rocks*, pp. 35–53. Paris (Éditions Technip) (1980)
4. Giraud, A.: Application of pyrolysis and gas chromatography to geochemical characterization of kerogen in sedimentary rocks. *Am. Asso. Pet. Geol. Bull.* **54**, 439–451 (1970)
5. Hunt, J.M.: *Petroleum Geochemistry and Geology*, 2nd edn, pp. 273–283. W. H. Freeman, New York (1996)
6. Larter, S.R., Douglas, A.G.: A pyrolysis-gas chromatographic method for kerogen typing. *Phys. Chem. Earth* **12**, 579–583 (1980)
7. Staplin, F.L.: Sedimentary organic matter, organic metamorphism and oil and gas occurrence. *Bull. Can. Pet. Geol.* **17**, 47–66 (1969)

Characterization of Potential Source Rock Intervals of Late Mesozoic to Cenozoic Age in the On- and Offshore Area of Cyprus and Their Impact on Petroleum Systems in the Eastern Mediterranean Sea

Sebastian Grohmann, Maria Fernanda Romero-Sarmiento,
Fadi Henri Nader, Francois Baudin, and Ralf Littke

Abstract

Potential organic-rich rocks have been sampled onshore Cyprus and offshore, along the Eratosthenes Sea Mount. Offshore, potential source rock intervals are mainly present in the Upper Eocene and in the Lower Upper Cretaceous. In the onshore area, good source rock properties are reached in Upper Miocene intervals. These samples contain marine oil-prone type II kerogen. TS/TOC as well as several biomarker ratios indicate anoxic depositional conditions for the onshore samples and dysoxic conditions for the offshore ones. T_{max} values around 420 °C and VR_r values lower or equal 0.5 indicate an immature state of the organic matter. However, in terms of biogenic gas, these immature rocks might contribute to natural gas generation in the area. Furthermore, the Upper Miocene as well as the Upper Eocene sections might continue in the deeper offshore parts, where burial depths are sufficient for thermal maturation. The presence of thermogenic hydrocarbon generation is indicated by the presence of solid bitumen staining in Lower Eocene offshore intervals.

Keywords

Source rocks • Petroleum systems • Cyprus
Eastern Mediterranean Sea • Organic geochemistry

1 Introduction

During the last decade, significant biogenic gas discoveries (Fig. 1) have rendered the Eastern Mediterranean Sea and especially the Levant Basin to one of the world's most promising exploration frontier areas.

For the assessment of petroleum systems, detailed knowledge about potential source rocks is required and can help to reduce the risks in exploration. In this contribution, we present new geochemical and petrographical data of organic-rich rocks of Late Mesozoic to Cenozoic age from the on-and offshore area of Cyprus and discuss their implication for petroleum systems in the area.

2 Materials and Methods

Potential organic matter (OM)-bearing rock samples have been investigated in the on-and offshore area of Cyprus. Onshore, 147 samples were collected during two field campaigns and comprise mainly calcareous claystones and shales of Mesozoic and Miocene age. Offshore, 161 samples were collected from the ODP Leg 160 wells, which were drilled along the Eratosthenes Sea Mount (ESM) south of Cyprus and comprise argillaceous carbonates to almost pure limestones of Late Cretaceous to Late Miocene (Messinian) age.

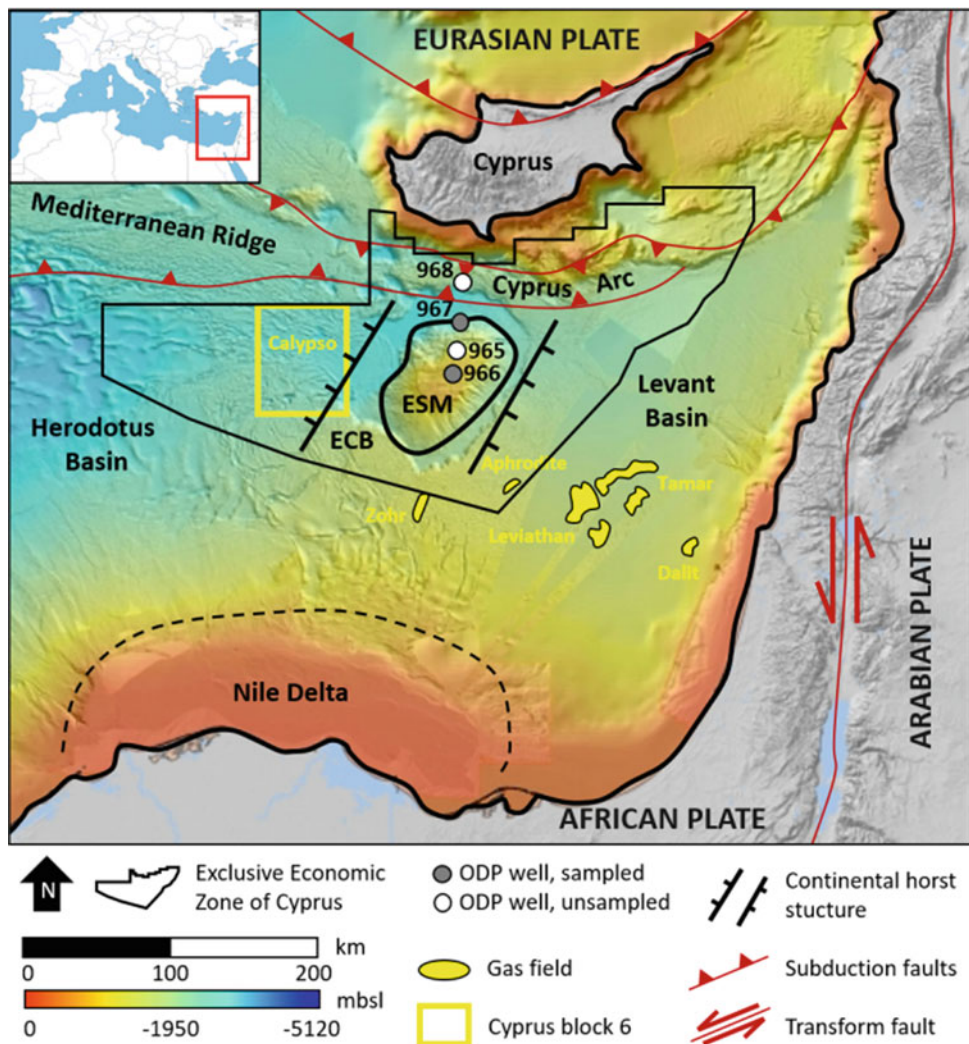
For analysis, a variety of organic geochemical methods [combustion, Rock-Eval pyrolysis, elemental analysis, gas chromatography-mass spectrometry (GC-MS)] and optical investigations [palynofacies, organic petrography, vitrinite reflectance (VR_r)] were performed.

S. Grohmann (✉) · M. F. Romero-Sarmiento · F. H. Nader
IFP Énergies Nouvelles (IFPEN), Direction Géosciences, 1 et 4
Avenue de Bois-Préau, 92852 Rueil-Malmaison Cedex, France
e-mail: sebastian.grohmann@emr.rwth-aachen.de

F. Baudin
Institut Des Sciences de La Terre de Paris, Sorbonne Université—
UPMC, 4 Place Jussieu, 75005 Paris, France

R. Little
Energy and Mineral Resources Group (EMR), Institute of Geology
and Geochemistry of Petroleum and Coal, RWTH Aachen
University, Lochnerstrasse 4-20, 52056 Aachen, Germany

Fig. 1 Overview of the Eastern Mediterranean Sea, showing the main tectonic features and recent biogenic gas field discoveries



3 Results and Discussion

The geochemical and petrographic results prove the existence of OM-rich intervals in the onshore (Upper Miocene) as well as in the offshore (Upper Eocene and Lower Upper Cretaceous) area of Cyprus. The OM in the analyzed samples comprises marine oil-prone type II kerogen with HI values between 100 and 600 mg HC/g TOC. With TOC contents up to 10 wt% many of these samples show fair to excellent source rock properties (Fig. 2). However, all samples are of immature state indicated by T_{max} values around 420 °C and VR_f values lower or equal 0.5% and no petroleum generation has yet occurred by these rocks. Nevertheless, the recent hydrocarbon discoveries in the Eastern Mediterranean Sea such as the giant field Zohr comprise mainly natural gas of biogenic origin [2]. Biogenic gas production occurs at shallow burial depths and low temperatures, thus even these immature source rocks might contribute to HC production.

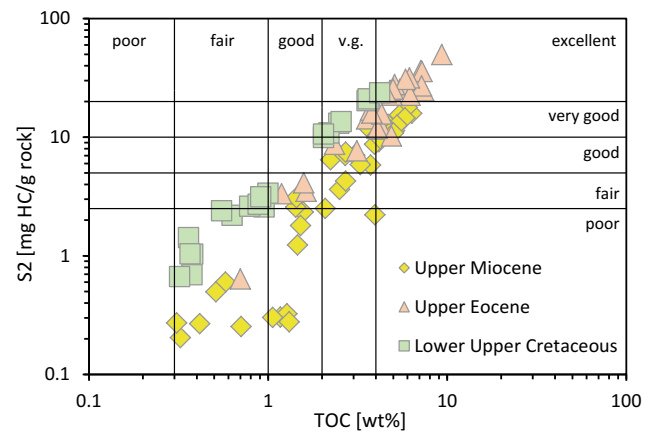


Fig. 2 Source rock quality classification based on the total organic carbon (TOC) content and the hydrocarbon generation potential (S2). Upper Miocene samples originate from onshore Cyprus while the Upper Eocene and Lower Upper Cretaceous originate from the Eratosthenes Seamount

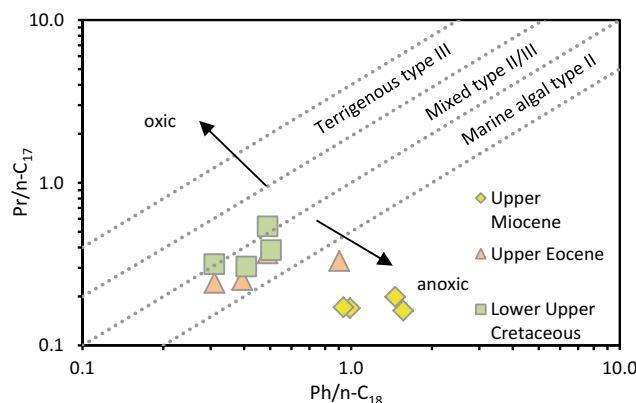


Fig. 3 Pristane (Pr)/n-C₁₇ versus phytane (Ph)/n-C₁₈ ratios indicating mainly dysoxic depositional conditions for the offshore samples (Upper Eocene and Lower Upper Cretaceous) and anoxic conditions for the onshore samples (Upper Miocene)

TS/TOC ratios > 0.36 [1] as well as Pr/n-C₁₇ versus Ph/n-C₁₈ ratios (Fig. 3) in the onshore Upper Miocene samples indicates a deposition under anoxic conditions, which is in accordance with the idea of several anoxic silled sub-basins around the island of Cyprus during the Miocene [3]. These basins continue in the southeastern offshore part where sufficient burial depths might be reached for thermal maturation.

For the offshore intervals, TS/TOC [1] as well as Pr/n-C₁₇ versus Ph/n-C₁₈ (Fig. 3) ratios indicate dysoxic conditions during deposition, which might be the result of temporarily active upwelling systems, implying that deposition and preservation of OM was likely restricted to the closer surrounding of the ESM. However, since the Mid Eocene the Eastern Mediterranean Basin was successively cut off from the Indian Ocean to the east, due to the subduction of Afro-Arabia below Eurasia [4], which might have favored the evolution of anoxic bottom waters in the Levant Basin. Thus, OM might have been redeposited by mass flow transport (e.g. turbidites) towards the deeper parts of the basin, where it was preserved under anoxic conditions and buried deep enough to reach thermal maturity.

The presence of such deep buried source rock intervals is indicated by the microscopically observation of solid bitumen in Lower Eocene sections.

4 Conclusions

- (a) Type II kerogen source rocks are present in the Lower Upper Cretaceous and Upper Eocene (offshore) and in the Upper Miocene (onshore).
- (b) T_{max} and VR_r values and several biomarker ratios indicate immature OM.
- (c) TS/TOC as well as biomarker ratios indicate dysoxic conditions for the offshore samples and anoxic conditions for the onshore samples.
- (d) Upper Miocene and Upper Eocene source rocks might continue in the deeper offshore parts.
- (e) The analyzed sections might contribute in biogenic gas production.
- (f) The presence of thermogenic HC generation is indicated by solid bitumen staining in offshore Lower Eocene sections.

References

1. Berner, R.A.: Sedimentary pyrite formation: an update. *Geochim. Cosmochim. Acta*. **48**(4), 605–615 (1984)
2. Cozzi, A., Cascone, A., Bertelli, L., Bertello, F., Brandolesi, S., Minervini, M., Rochni, P., Ruspi, R., Harby, H.: Zohr giant gas discovery—a paradigm shift in Nile delta and Eastern Mediterranean exploration. In: AAPG/SEG 2017 International Conference and Exhibition, London, England (2017)
3. Eaton, S., Robertson, A.: The Miocene Pakhna formation, Southern Cyprus and its relationship to the Neogene tectonic evolution of the Eastern Mediterranean. *Sed. Geol.* **86**(3–4), 273–296 (1993)
4. Robertson, A., Parlak, O., Ustaömer, T.: Overview of the Palaeozoic-Neogene evolution of Neotethys in the Eastern Mediterranean region (southern Turkey, Cyprus, Syria). *Pet. Geosci.* **18**(4), 381–404 (2012)



Source Rocks and Hydrocarbon Accumulation Characteristics of Upper Cretaceous to Paleogene in the Northern Kaikang Trough, Muglad Basin, Sudan

Congsheng Bian, Youliang Feng, Jun Li,
Xuexian Zhou, Yongxin Li, and Xinshun Zhang

Abstract

This paper investigates the sedimentary characteristics, geochemical indicators of source rock, and the hydrocarbon potential in detail within the Paleogene and Upper Cretaceous in the northern Kaikang trough, Muglad Basin. Analysis shows that the thickness of good source rocks in Paleogene ranges from 50 to 200 m, and the TOC value can reach 0.5–1.3%, but it is immature and has no hydrocarbon generation potential. Nevertheless, the Upper Cretaceous source rocks had mostly entered the maturity threshold, with a TOC value of only 0.5–0.8%, and a thickness of only 10 m, so the hydrocarbon generation is limited. The main effective source rock is the AG Group in the Lower Cretaceous, which is distributed throughout the area. The evolutionary history shows that most of the structures in the central troughs lack hydrocarbon potential, because they were formed since the Paleogene, which is later than the main accumulation period of the AG source rock. Petroleum discovery was made in the fault terrace zones on both sides of the Kaikang Trough, but the distribution of oil layers is very complicated. Hydrocarbon accumulation is controlled by formation dips, fault activity intensity and fault lateral docking characteristics. The weaker active fault block in late time and the more effective trap are the key to hydrocarbon enrichment at the fault terrace-zones.

Keywords

Source rocks • Hydrocarbon accumulation
Upper cretaceous • Paleogene • Kaikang
trough • Muglad basin

1 Introduction

The Kaikang Trough is located in the middle of the Muglad Basin and can be divided into the north and the south sub-depressions. The area of the north sub-depression is approximately 7000 km². After intensive hydrocarbon exploration, only a few reservoirs have been discovered within the Upper Cretaceous and Paleogene. It is unclear whether the Upper Cretaceous and Paleogene in the Kaikang Trough are capable of hydrocarbon generation, or secondary reservoirs can be formed.

2 Methods

In view of above geological problems, the authors have investigated the stratigraphic characteristics of sediments, hydrocarbon generation potential of source rocks, and the main controlling factors of hydrocarbon accumulation, in detail, within the Paleogene and Upper Cretaceous of the area.

The log data and core data of 8 wells in the area were analyzed, and the characteristics of the sedimentary facies were studied. Well logging method was utilized to calculate the TOC value of the source rock in every well, due to the lack of core geochemistry analysis in this area. By restoring the history of regional tectonic evolution, the formation period of the tectonic structure in the trough, and its relationship with the hydrocarbon generation history of the source rocks are inferred. The reservoir types and their structural features as well as failed wells are analyzed, to study the main controlling factors of reservoirs and the next exploration direction. Key issues that need attention are proposed.

C. Bian (✉) · Y. Feng · J. Li · X. Zhou · Y. Li · X. Zhang
PetroChina Research Institute of Petroleum Exploration &
Development, Beijing, 100083, China
e-mail: bcs_1981@petrochina.com.cn

3 Results

3.1 Sedimentary Facies Characteristics

Based on logging curves and sedimentary combination analysis, the Upper Cretaceous and the Paleogene of the Kaikang Trough were dominantly developed in river-flooding plain, delta and shore-shallow lacustrine facies. The river-flooding plain facies were mainly developed in the Paleogene Amal-Nayil Formation. They are mainly composed of sandstone, red and green mudstones, with upward-finishing intervals in lithology, and an erosional base. These sedimentary features show meandering river deposits. The Upper Cretaceous strata of Zarqa, Gazal and Baraka Formations are mainly composed of deltaic sediments, and the deltaic plains contain sandstone, green and red mudstones. The delta fronts are composed of sandstone and gray mudstone, with upward-coarsening intervals. Aradeiba Formation in the lower part of the Upper Cretaceous comprises delta-front and shallow lake deposits, consisting of grey muddy sandstone and siltstone.

3.2 Characteristics of Source Rocks

The main proven source rock in the Muglad Basin is the AG Group in the Lower Cretaceous, which is distributed throughout the area, where a large number of oil reservoirs have been discovered. The existence of source rocks in Upper Cretaceous and Paleogene, in this area, has not yet been confirmed. In this study, the most widely used TOC evaluation methods for well log curves are used to calculate the TOC values for eight representative wells in the study area. The results show that the effective source rocks of Paleogene are mainly distributed in the central and northern regions, which are close to the distribution of the

sedimentary center of the Kaikang Trough. The thickness of the Paleogene source rock ranges from 50 to 200 m, and the TOC content can reach 1–4%, which indicates a high quality source rock.

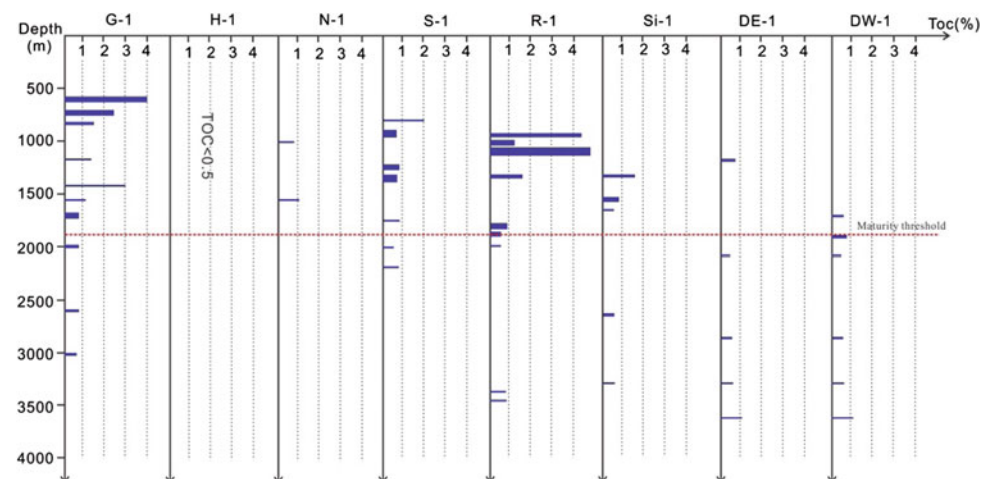
The distribution of source rocks in the Upper Cretaceous is similar to the Paleogene, but the thickness is relatively thin, about 10–25 m. In addition, the TOC content of the Upper Cretaceous source rocks is only 0.5–0.8%, which is a moderate-quality source rock, with a limited hydrocarbon generation potential. The history of thermal evolution in this area indicates that the burial depth of 1800 m corresponds to 0.6% of Ro, so this depth is the threshold of effective source rock in this area. However, the burial depth of the Paleogene source rock with a TOC of 1–4% is mostly 1500 m or less, and it is immature. Nevertheless, the Upper Cretaceous source rock mostly entered the maturity threshold, its TOC value is only 0.5–0.8%, and its thickness is about 10 m, so the hydrocarbon generation potential is limited (see Fig. 1).

The thermal evolution simulations of AG group indicate that it entered the peak of oil production during the deposition time of Aradeiba-Baraka Formations, and entered the gasification window in the period of Amal sedimentary time, which has now reached a high state of maturation.

3.3 Hydrocarbon Accumulation Characteristics

Since the wells in the central Kaikang Trough were drilled before the 1990s, the data and information were incomplete. The reinterpretation of the reservoirs and hydrocarbons for 5 wells showed that the reservoir of Paleogene and Upper Cretaceous is well developed, with an average porosity of 10–18%, and a thickness of up to 50–200 m. However, there is no hydrocarbon display during drilling and logging, so all these wells are interpreted as dry wells. The analysis of the evolutionary history of the central Kaikang Trough shows

Fig. 1 Distribution of TOC values of source rocks in 8 wells with depth. Those source rocks with high TOC values (1–4%) did not enter the hydrocarbon generation threshold



that most of the structures in the central troughs were formed since the Paleogene, which is later than the main accumulation period of the AG hydrocarbon source. These structures lacked oil filling, so the hydrocarbon potential is limited.

The reinterpretation of the four wells in the stepped zone, on both sides of the Kaikang Trough, shows that the Cretaceous and Paleogene reservoirs were well developed, with an average porosity of 7–12%, and a thickness up to 10–30 m. Several oil layers were discovered in two wells, and heavy oil was obtained from one of the tested wells, which indicates that the hydrocarbon potential of the fault terrace zones is better than that in the center of the trough. However, due to the complicated structures of the fault terrace zones and the fault contact relationship, the distribution of petroleum layers is very complicated.

4 Discussion

Based on the analysis of the reservoirs, and of the oil and gas wells found in the Kaikang Trough, the main controls of hydrocarbon accumulation are formation dips, fault distance and fault lateral docking characteristics. Firstly, the reservoirs with good hydrocarbon accumulations often have a lower structural dip, mostly less than 3°. Secondly, most of the oil reservoirs have a fault distance less than 200 m, and there are hardly any hydrocarbon accumulations in

reservoirs which have a fault distance greater than 200 m, especially greater than 500 m. The third factor is the formation lithology on both sides of the fault. Sandstone and mudstone connection can seal the reservoir, but sandstone and sandstone docking can invalidate the trap. Therefore, the weaker active fault block in late time and the more effective trap are the key to hydrocarbon enrichment at the fault terrace zones in the faulted depression.

5 Conclusions

This paper shows us that the source rocks in the Upper Cretaceous and the Paleogene have limited hydrocarbon generation potential, and the main effective source rock is the AG Group in the Lower Cretaceous. The hydrocarbon potential of the Paleogene in the northern Kaikang Trough is poor, because the structures in the central troughs were formed since the Paleogene, which is later than the main accumulation period of the AG hydrocarbon source. The main controls of hydrocarbon accumulation in the Kaikang Trough are formation dips, fault distance and fault lateral docking characteristics. The eastern stepped zone developed many fault blocks with a small dip angle, which is beneficial to the large-scale lateral migration of hydrocarbon from the AG source rock. So, those are the favorable areas for oil exploration.



Ech Cheid Salt Structure and Its Influence on the Maturity of the Bahloul Fr Source Rock

Mohamed Malek Khenissi, Mohamed Montassar Ben Slama, Amina Mabrouk El Asmi, Anis Mohamed Belhadj, and Moncef Saidi

Abstract

The geological landscape in Northern Tunisia is dominated by its diapiric structures that started its ascending movements since the late Triassic to Early Cretaceous. This movement is driven by a mechanism known as Halokinesis. The main objective of this study is to establish the relationship between the salt structure setting and the maturity of the surrounding source rocks especially the Cenomanian-Turonian Bahloul Fr. In order to assess the maturity history of the source rock, we analyzed several black shale samples from around Jebel Ech cheid by means of Rock Eval pyrolysis and GC/MS. Our results demonstrate a total organic Carbon (TOC) percentage of 1–9% and a Tmax maturity between 424 and 445 °C. In addition, the distributions of the source rock biomarkers saturated as well as aromatic, change in a specific trend of increasing maturity from the SW to the NE of the structure. This change is also proven when using GC/MS technique to analyze the saturated and aromatic biomarkers such as Ts/Ts+Tm ratios, 22S/22S +22r values for C31 homohopanes, and 20S/(20S+20R) ratios for C29. The results from Rock Eval and GC/MS analyses demonstrate that the salt structure played a role in modifying the geothermal gradient of the basin and in the maturity of the source rock in Bahloul Fr., the individualization of subsidence and deep-seated faults are the main reasons behind the maturity contrast between the studied zones. The organic matter has reached different stages of thermal maturity with a general increasing maturity trend (SW to NE).

Keywords

Halokinesis • Salt body • Jebel Ech Cheid
Source rock maturity • Bahloul Fr

1 Introduction

The geological setting of northern Tunisia is well known by its diapirism. During the late Triassic and early Cretaceous, an extension phase induced the development of multiple salt structures and complex systems in northern Tunisia, these complex systems contributed to several geochemical modifications on source rocks [1].

Salt bodies can have a major effect on the temperature distribution in sedimentary basins [2]. This can create thermal anomalies that modify the source rock maturity [3, 4]. The objective of our research is to study thermal anomalies in Jebel Ech Cheid and, how it has affected the maturity of the Cenomanian-Turonian source rock of the Bahloul Fr.

2 Methods

The lab analysis was carried by means of (1) Rock Eval pyrolysis to measure the maturity of the source rock, (2) Chromatography techniques to analyze biomarkers.

3 Results

3.1 Rock-Eval Results

The source rock samples analyzed were from four main locations around our target structure (Oued El Merir, Jebel Lakhouet, Oued Siliana, Oued Lahmar) (Fig. 1). These Bahloul Fr samples have shown differences on the maturity. Through the pyrolysis analysis, we have obtained Tmax

M. M. Khenissi (✉) · M. M. B. Slama · A. Mabrouk El Asmi
Earth Science Department, Faculty of Science of Tunis, Tunis,
Tunisia
e-mail: medmalek.khenissi@etudiant-fst.utm.tn

A. M. Belhadj · M. Saidi
Tunisian Enterprise of Petroleum Activity (ETAP), Tunis, Tunisia

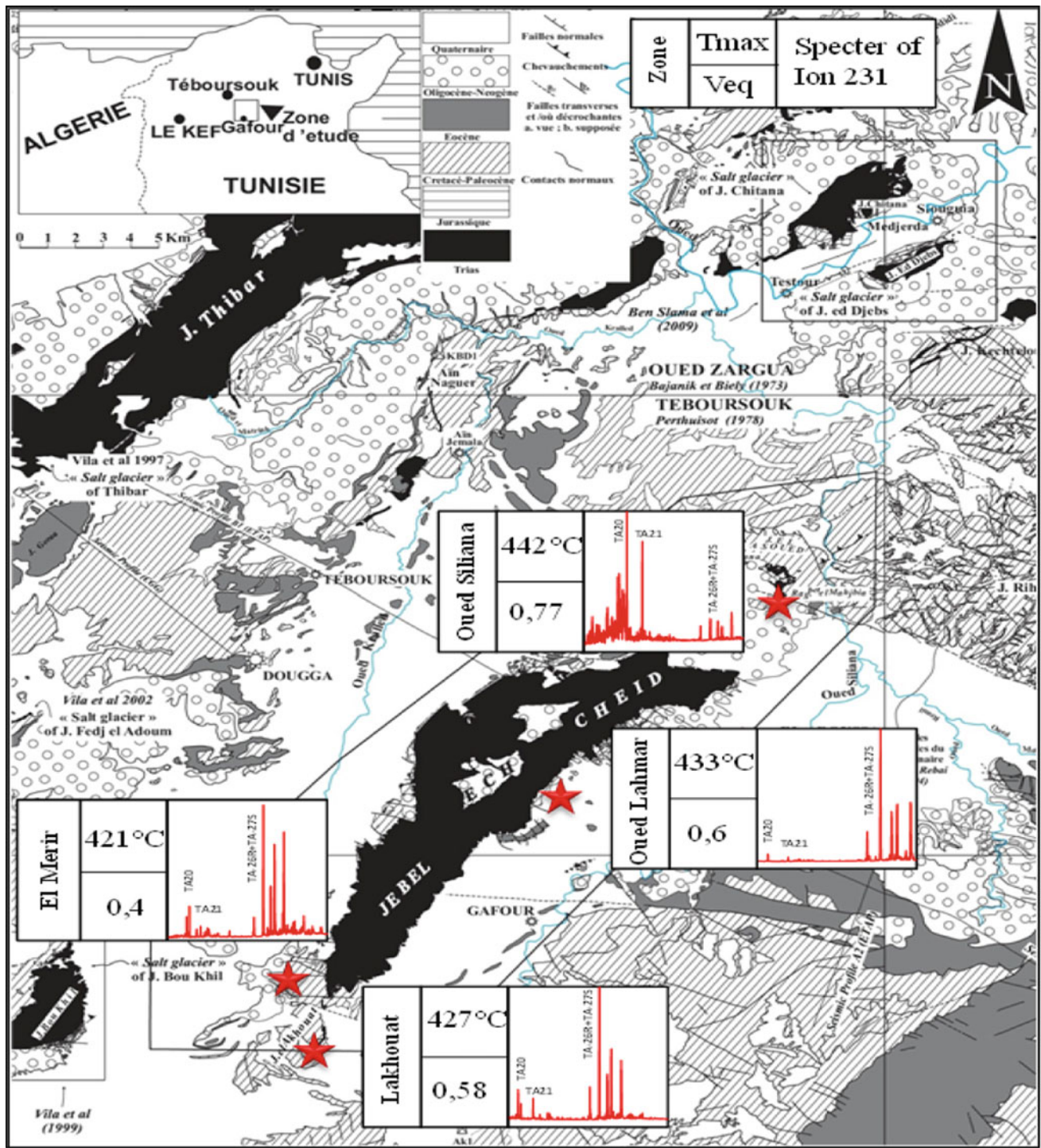


Fig. 1 Summary figure showing the maturity distribution of the studied zone with their Tmax, Veq, and their Ion 231 specters

responses that gave us different values depending on the samples localization with regard to Ech Cheid structure (Fig. 1).

The Tmax and Veq (calculated) responses show us a different stage of maturation around the salt structures with a specific maturity tendency (Fig. 1).

3.2 GC/MS Results

The distribution of the studied biomarkers showed a variability in their maturity status and a specific tendency of the maturity progress, aromatic biomarkers maturity including 4-MDBT/1-MDBT, 2MN/1MN, MPI1, MPI2 and

Fig. 2 Cross plot MPI-1 versus MPI-2 shows maturity

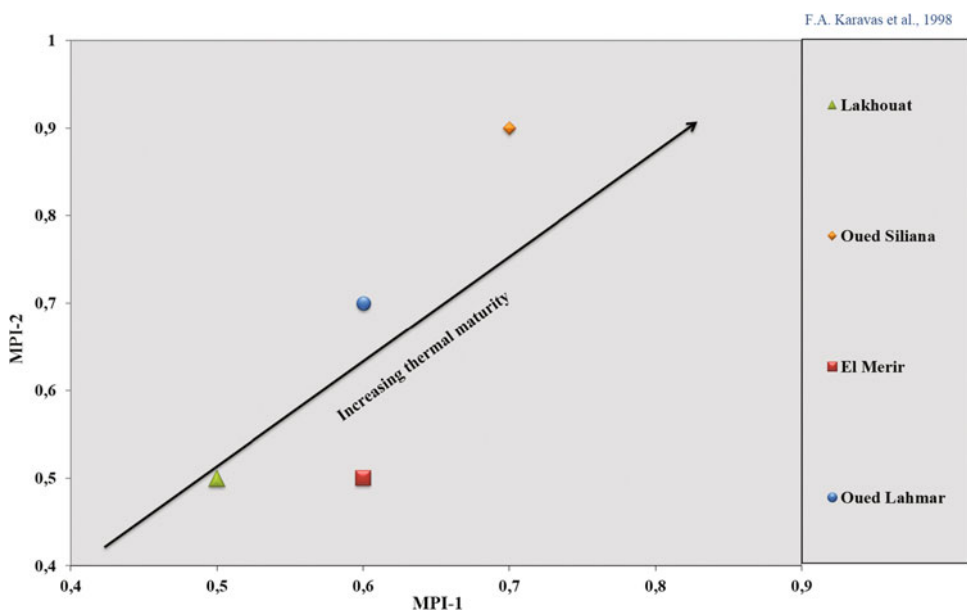
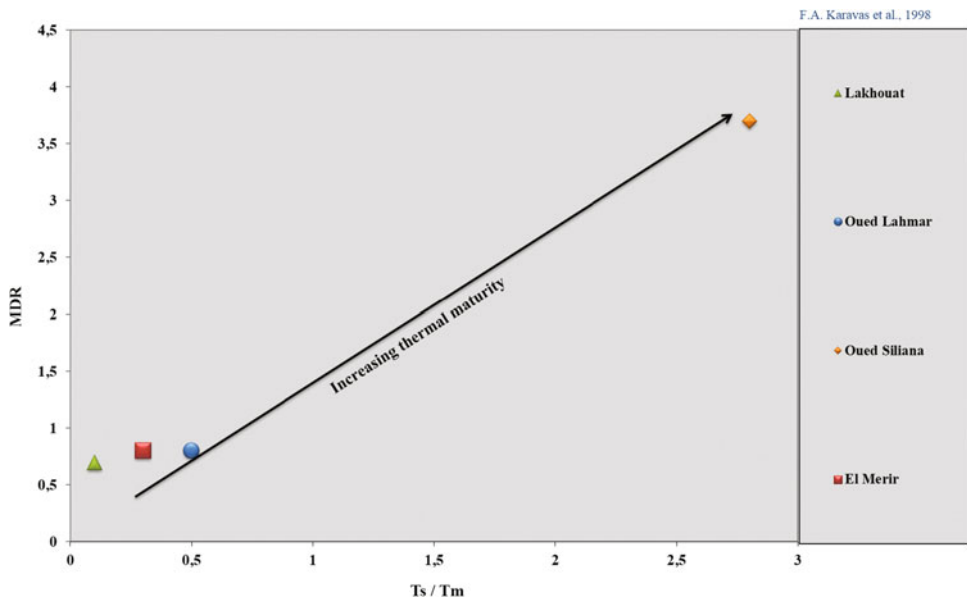


Fig. 3 Maturity assessment using the Cross MDR versus Ts/Tm cross plot



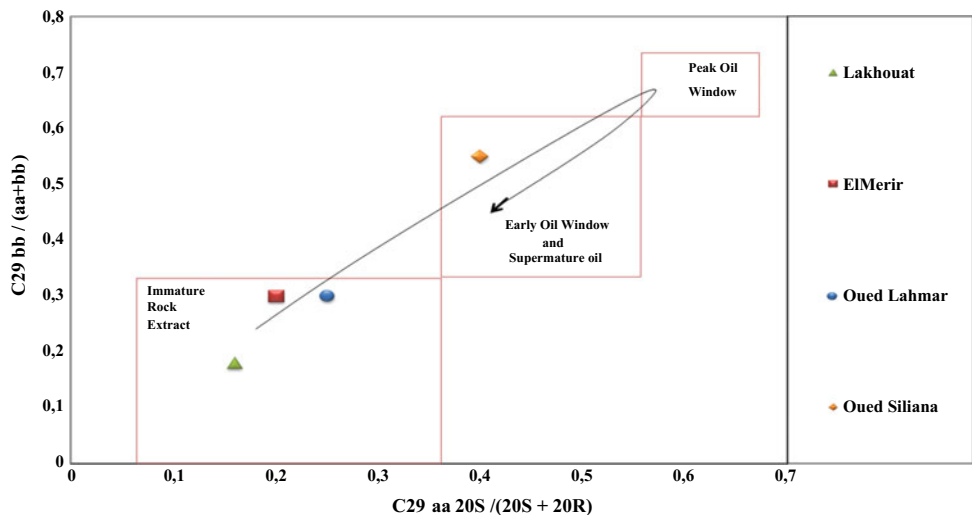
C₂₀/(C₂₀+C₂₈) were the most efficient on assessing the maturity of the analyzed samples.

Maturity parameters derived from both the chromatograms ion m/z 191 and ion m/z 217 such as 20S/(20S+20R) C₂₇, C₂₀, C₂₁ (Fig. 4) and Tm/Ts (Fig. 3) are good indicators of the source rock maturity. The cross plot of MDR versus Ts/Tm and the cross plot of MPI-1 versus MPI-2 (Fig. 2) show that the maturity differences between the different studied zones are compatible with the Tmax and Vitrinite equivalent previously studied.

4 Discussion

Differences of Geochemical values and maturity levels can be explained by a certain tectonic evolution that was the main factor of the subsiding zones individualization that allowed the burial of the organic matter but it was also a factor of individualization of heights (Haud fond) that might be caused by the salt movement.

Fig. 4 Maturity level based on $20S/20S+20R$ versus $\beta\beta/\beta\beta+\alpha\alpha$



In fact, different factors can be involved in the structuration of the diapirs zone in Tunisia, one of them is the tectonic and the Triassic extrusion that took place from the Upper Aptian to the lower Albian. The current study has shown a general thermal maturity evolution following a SW to NE direction. In the NE, the remarkable maturity of the source rock in the zone of Oued Siliana can be related mainly to the deep-seated faults. One of the possible explanations of the lack of maturity in the southern part of Jebel Ech Cheid (Jebel Lakhouet and Oued El Merir) is that the setting of Ech Cheid structure during the Aptian played an important role for a high zone to take place and, therefore, prevented the burial of the organic rich sediments of the Cenomanian-Turonian series. Therefore, we can say that this Triassic extrusion prevented the normal thermal evolution of the source rock in order to reach maturity. Moreover, the peri-diaperic sediments represent an immature organic matter, due to the Uplifting of the sedimentary floor by the Triassic extrusion.

5 Conclusions

Thus, from the Rock-Eval pyrolysis and GC/MS results we can conclude that the salt structure of Jebel Ech Cheid played a significant role in the thermal maturity of the surrounding source rocks. The magnitude and nature of the impact depend on many factors related to the size of the diaper and also to the regional geological and geodynamic history.

Our research also confirms that (1) Jebel Ech cheid has a significant effect on the local distribution of anoxic depocenter (Cenomanian-Turonian) and (2) the thermal anomaly surrounding Jebel Ech Cheid salt structure had an influence on the maturity of the Cenomanian-Turonian source rock. This influence induced a maturity contrast between the different analyzed zones. The individualization of heights in the southern-west of the structure prevented the burial of source rock and, therefore, their maturity. On the other hand, the deep-seated faults in the northern-east part of the structure were the main cause of the geothermal gradient increase and the source rock maturity.

References

1. Khenissi, M.: The influence of salt structure on the maturation and thermal history of Bahloul source rock (Jebel Ech.cheid) and neighboring structures. Master thesis, University Tunis Carthage, Faculty of Science of Bizerte (2016)
2. Down, N.M.: The effect of Salt diapirson the thermal maturity of surrounding sediments in the Western Pyrenees, Spain. Thesis, University of Nevada, Las Vegas (2009)
3. Mello, U.T., Karner, G.D., Anderson, R.N.: Role of salt in restraining the maturation of subsalt source rocks. Mar. Pet. Geol. **12**, 697–716 (1995)
4. Jensen, P.K.: Calculations on the thermal conditions around a salt diapir. Geophys. Prospect. **31** (1983)



Geochemical Characterization of the Permian Series and Associated Oil Indices in the Jeffara Area: Origin of Hydrocarbon and 1D Thermal Maturity Modeling

Khawla Ouerghi, Amina Mabrouk El Asmi, Anis Bel Haj Mohamed, and Moncef Saidi

Abstract

Permian rock samples from two wells (W-1 and W-2) drilled in the Jeffara basin (Southern Tunisia) were analyzed using the Rock Eval pyrolysis (RE) and Gas chromatography coupled to Mass Spectrometry (GC/MS). Oil indices from the same series were also examined. The two objectives pursued through this study were: (1) First, to geochemically characterize the Permian series in order to determine their source rock potential; (2) Second, to identify the origin of hydrocarbons occurring in the Permian layers through oil-oil correlations and oil correlations to source rocks candidates (Permian, Azzel, Fegaguira, and Zoumit). The attained results show that the lower part of the Permian series is rich in organic matter and may constitute a good source rock of an “Oil and Gas-prone” quality. The oil indices found in the top part of the Permian series were generated simultaneously by the Permian source rock and the Paleozoic source rock (Azzel and Fegaguira). The 1D basin modeling results indicate that, overall, the hydrocarbon generation started since the Permian (240 Ma) while oil expulsion took place during the Upper Triassic (230 Ma).

Keywords

Jeffara area • Permian • Source rock • Biomarkers
CPL • GC/MS • Rock Eval • 1D modeling

1 Introduction

The Tunisian Jeffara basin (Southern Tunisia) is considered among the most promising areas for hydrocarbon exploration in Tunisia [1]. This explains, to some extent, the high number of exploration permits, issued by the Tunisian National Oil Company (ETAP, Tunisia), within this province (Fig. 1).

In addition, in this area, Paleozoic series are being held as major targets for oil exploration, either as reservoir rocks or source rocks. Previous geological and geochemical studies have identified the existence of at least three stratigraphic levels that are rich in organic matter and are considered as potential hydrocarbon source rocks in the region, corresponding to: The Tannezuit Formation, the Fegaguira Formation and the Aouinet Ouenine Formation. Nevertheless, the Permian series were the least addressed from a geochemical point of view. Although the Permian series outcrop in the Jebel Tebaga (Mednine), they are frequently encountered in boreholes that have been drilled in the Ghadames basin and the Chotts basin. Based on final well reports, this series encountered frequent oil appearances and dark black shales, which may indicate the presence of a high amount of organic matter. Hence, this study was proposed, aiming to geochemically characterize the organic matter contained in these Permian horizons (richness, nature, thermal maturity, depositional environment ...), and to determine the origin of the oil appearances (oil/source rock correlation). The study also focused on the reconstruction of the thermal history, the chronology of the generation and the expulsion of hydrocarbons through 1D modeling.

2 Methods

Several samples of cuttings taken from the Permian series, crossed by the wells W-1 and W-2 in the Jeffara region, were analyzed using Rock Eval pyrolysis, Gas Chromatography (GC), and Gas Chromatography coupled to Mass

K. Ouerghi (✉) · A. Mabrouk El Asmi
Geology Department, Faculty of Sciences of Tunis, University Campus, 2060 Tunis, Tunisia
e-mail: ouerghi.khawla@gmail.com

A. Bel Haj Mohamed · M. Saidi
Entreprise Tunisienne des Activités Pétrolières, 4 rue des Entrepreneurs, Charguia II, 2035 Tunis, Tunisia

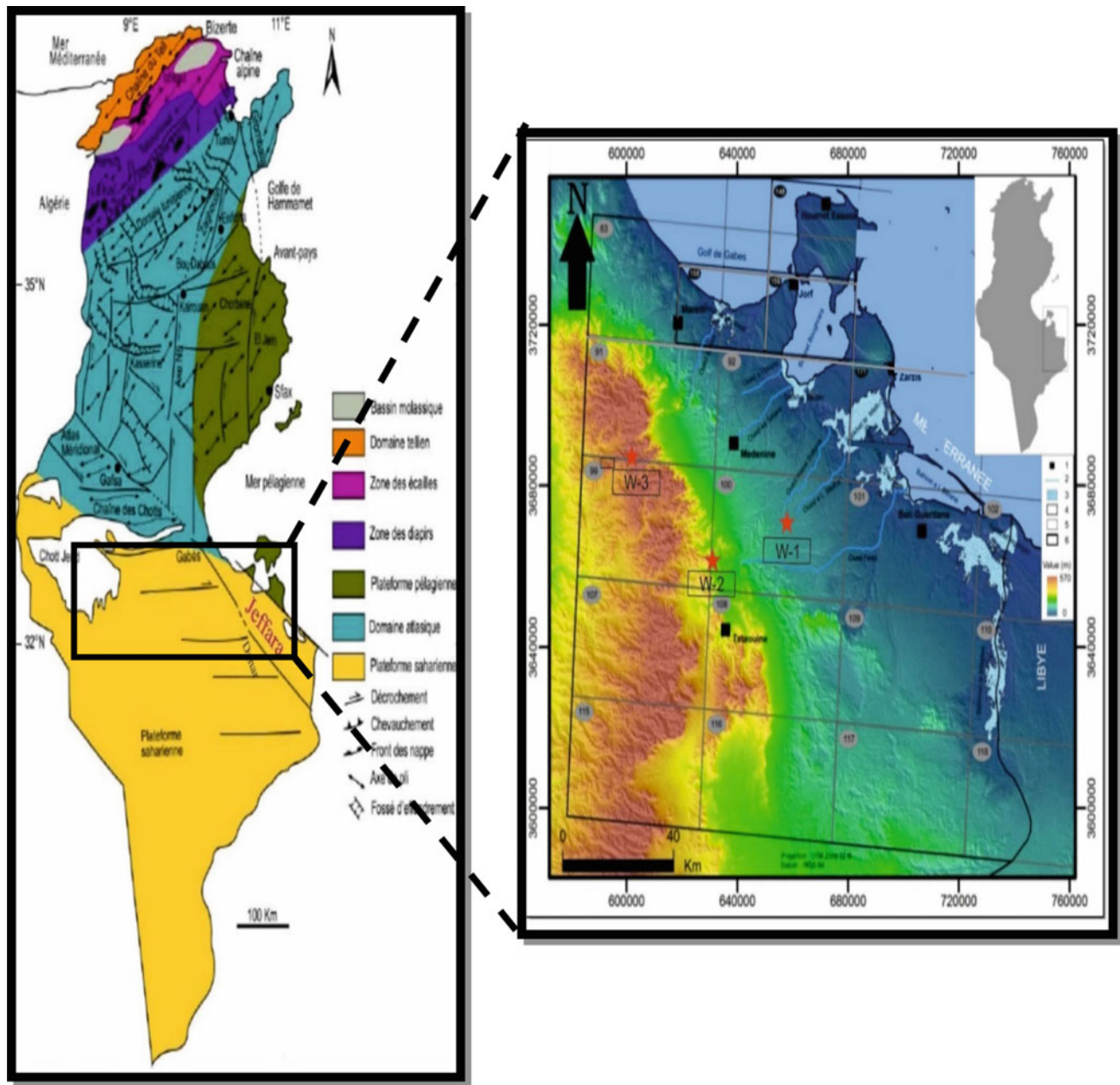


Fig. 1 Structural map of Tunisia showing the different structural domains (Kamoun et al. 2001)

Spectrometry (GC/MS). In addition, index samples from both wells were analyzed. The burial history and the thermal maturity of the potential layers were carried out using GENEx 1D.

3 Discussion

The Rock Eval pyrolysis results of the Permian samples, taken from the wells W-1 and W-2 of the Jeffara region (Tunisia), show that the Permian series crossed by the W-2

well is moderately-rich in predominantly type II organic matter (with a contribution of type III organic matter) [4] and can be retained as a potential source rock of oil (Fig. 2). The samples from the W-1 well are abnormally over-mature, probably due to a heat flux anomaly in this region (Della Vedova et al. 1995 in [2]).

Biomarker analyses using GC/MS have shown that Azzel and Fegaguira source rocks contain mature marine organic matter with a terrestrial input for W-2-2400 m, W-3-2372 m and W-2-2417 m that was deposited in a suboxic environment.

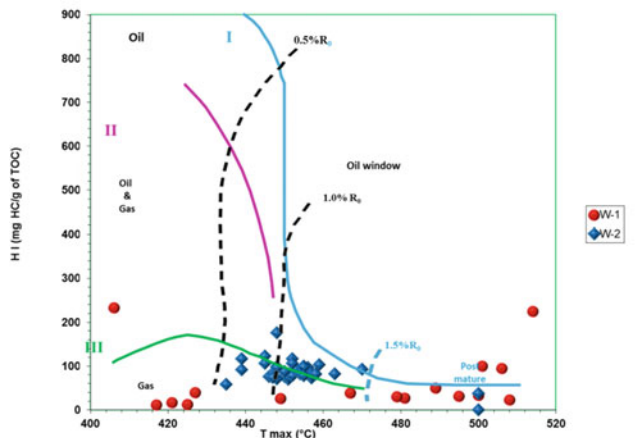


Fig. 2 Main Rock Eval results for the Permian analyzed samples

They seem to be generated from a marly/clay lithology source rock, rich in mainly marine organic matter (type II) with a continental contribution (type III), and which was deposited under a normal salinity in a suboxic-anoxic environment.

Oil-oil and source-rock geochemical correlations are among the most credible methods which are applied to determine the origin of oil. They are based on the principle of transmitting the chemical composition of the source rock to the expelled oil. It is essential to say that a negative correlation is a strong evidence of the lack of kinship between the samples and the source rock. While a positive correlation does not necessarily prove the origin of the sample, that is to say that an oil having the same chemical characteristics as the bitumen of a source rock, does not present any evidence but a guess about its origin [3].

The index-index correlation allowed the subdivision of oil into two distinct families. The first family includes the samples W-1-2271 m, W-1-2264 m and W-1-2753 m taken from the W-1 well, and the second family consists of the W-2-2550 m sample taken from the W-2 well.

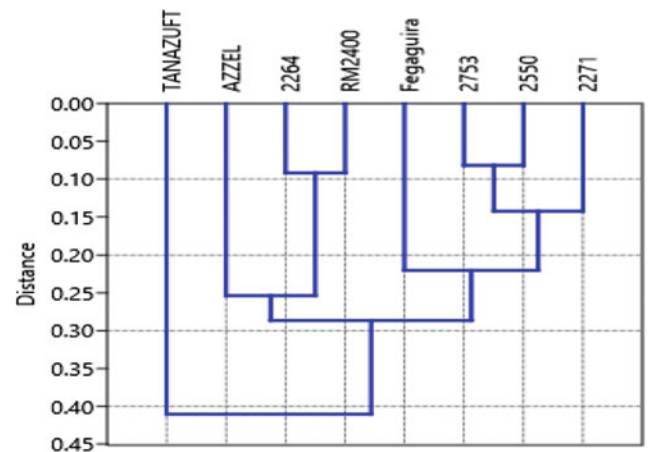
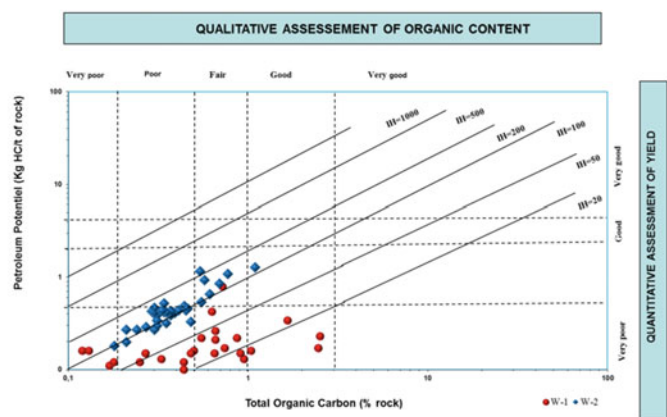


Fig. 3 Dendrogram of the hierarchical cluster analysis (HCA) of variable biomarker ratios showing index-source rock correlation

The index-source rock correlation shows a good agreement between the W-1-2271 m, W-1-2753 m and W-2-2550 m oil and the Fegaguira source rock, while the

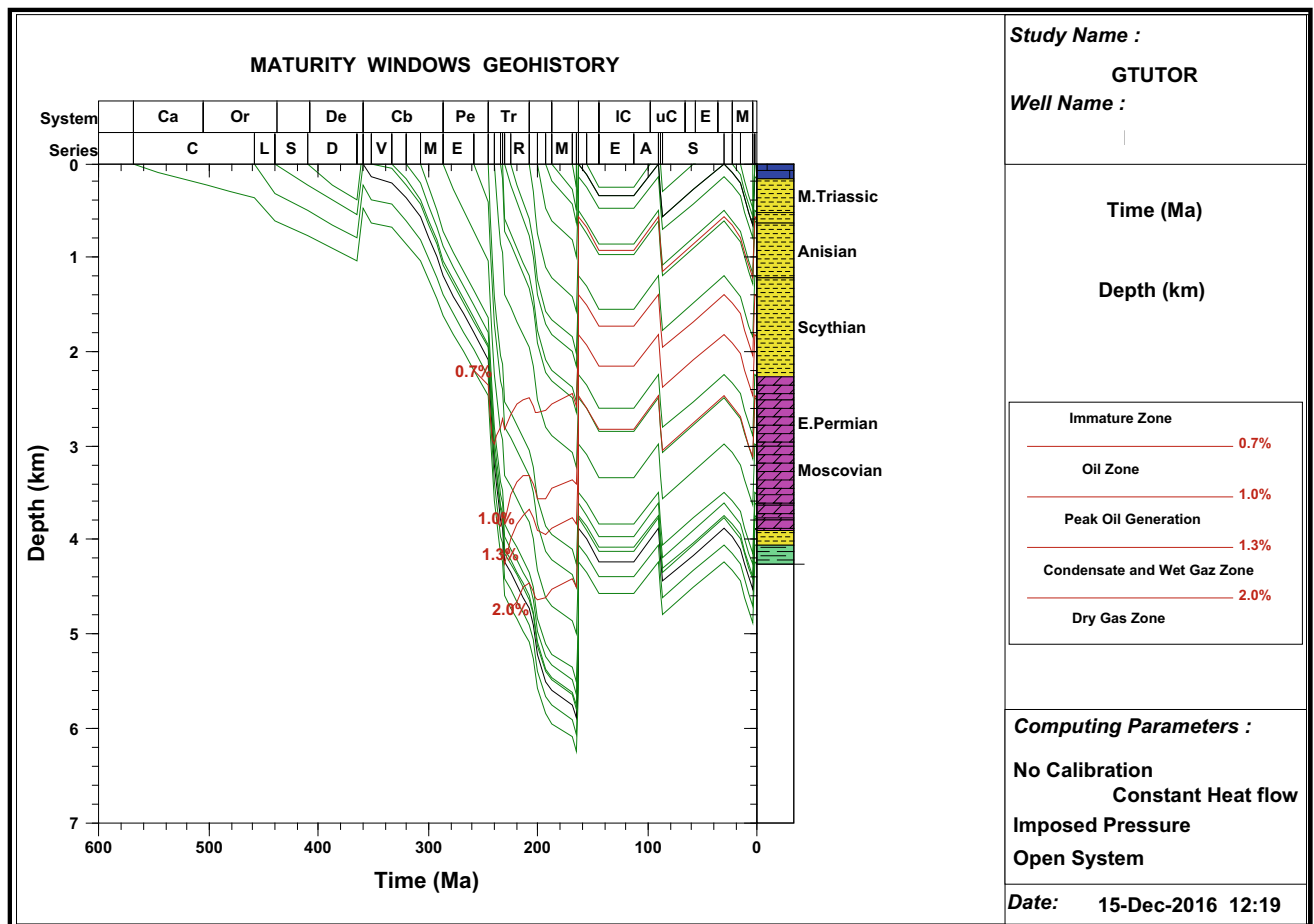


Fig. 4 Maturity history of source rocks in the W-1 well

W-1-2264 m oil is well correlated with the Permian source rock (Fig. 3).

The results of the numerical modeling, based on the data of the studied wells, show that the Permian source rock has reached the oil window ($R_0 = 0.7\%$) in the Lower Triassic (230 mA) in the W-1 well (Fig. 4). It has reached the maximum hydrocarbon generation ($R_0 = 1\%$) in the Late Triassic (218 Ma) and entered into the gas window area in the Jurassic.

It is believed that the Upper Permian source rock has already generated and expelled oils. In fact, oil generation began since the Late Permian to the Jurassic (Fig. 5).

Using geothermal parameters and a numerical modeling procedure, we tried to study the timing of oil expulsion in the study area. The hydrocarbon expulsion phase started since the Late Triassic (230 Ma) (Fig. 6).

Fig. 5 Hydrocarbon generation History of Permian series in the well 1

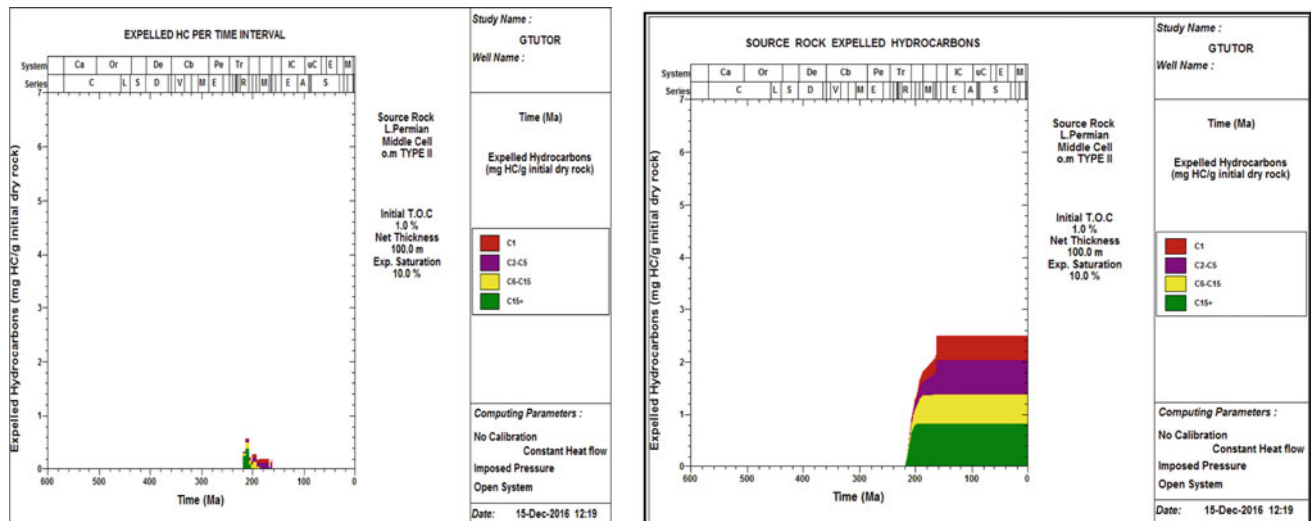
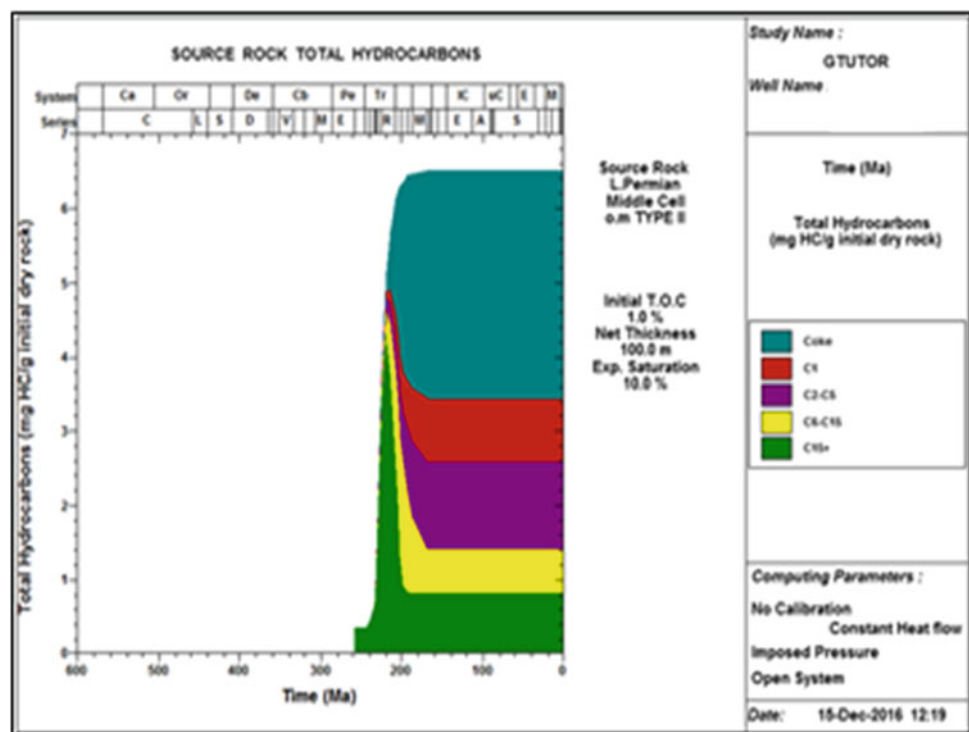


Fig. 6 Hydrocarbon expulsion History of Permian intervals at the W-1 well

4 Conclusions

The results of geochemical analyses performed on the Permian rock samples and on oil collected from wells W-1 and W-2 (Jeffara basin-Tunisia), indicate that the Upper part of the Permian series of the W-2 well is rich in organic matter and may constitute a good source rock of “Oil and Gas-prone”

quality. Index-index and index-source rock correlations indicate that the oil found in the upper part of the Permian series was generated, simultaneously, by the Permian source rock and the Paleozoic source rock (Azzel and Fegaguiria).

The 1D basin modeling results indicate that, overall, the hydrocarbon generation started in the Permian period (240 Ma), while oil expulsion took place during the Late Triassic period (230 Ma).

References

1. Ben Ferjani, A., Burolet, P.F., Mejri, F.: Petroleum Geology of Tunisia. Mem. ETAP N°1, Tunis, 194 p (1990)
2. Gabtni, H.: Deep characterization and geophysical modeling of the transition zones between the different structural blocks of central and southern Tunisia. Ph.D. thesis, University Tunis El Manar, 243 pp (2006)
3. Gurgy, K.: Correlation, alteration and origin of hydrocarbons in the GCA, Bahar, and Gum Adasi fields, Western South Caspian Basin: geochemical and multivariate statistical assessments. Mar. Pet. Geol. (20), 1119–1139 (2003)
4. Peters, K.E., Moldowan, J.M.: The Biomarque Guide, 363 p. Prentic Hall, Englewood Cliffs, NJ (1993)



Geopetroleum Evaluation of the Ordovician and Triassic Reservoirs in the Southern Part of Chotts Area (Southern Tunisia) and Maturity Modeling

Safa Kraouia, Amina Mabrouk El Asmi, Abdelhamid Ben Salem, and Moncef Saidi

Abstract

This study evaluates the geopetroleum assessment of the Ordovician series (El Atchane and El Hamra reservoirs) and the Triassic series (TAGI), in the Southern Chotts region, based on well logging data. The burial and thermal maturity history of the potential source rock Fegaguira Formation (Silurian in age) of the area, was accomplished using the BasinMod software. The generation and expulsion times of hydrocarbons in the region, as well as their quantities were also estimated. The Ordovician reservoirs (El Atchane and El Hamra) generally show the same petrophysical characteristics (the porosity of the two reservoirs varies between 5 and 12%) with a decrease in thickness from west to east until the total disappearance of the El Hamra Formation. This variation was related, on the one hand, to the bevelling of the Ordovician on the Telemzane arch and, on the other hand, to the erosive effects of the orogenic phases during Paleozoic (Taconic, Caledonian and Hercynian phases). The maturity history modeling of four wells in the south of the Chotts region shows that the Fegaguira source rock is mature and began generating hydrocarbons during the Early Cretaceous and expelled its hydrocarbons from the Paleogene in the wells 5 and 7 and from Cretaceous in the well 13 (at a SATEX of 10%). The Fegaguira source rock has not expelled in the well 19. The quantity of oil expelled by the Fegaguira source rock reached

36.3 bbl/acre ft rock and 33 bbl/acre ft rock in the wells 5 and 7 during Paleogene and 53.5 bbl/acre ft rock in the well 13.

Keywords

Southern Chotts • Petrophysical evaluation • Reservoir • El Atchane • El Hamra • TAGI • 1D modeling • Fegaguira • Expulsion

1 Introduction

The Chotts El Jerid basin is an intra-cratonic basin identical in appearance to the Ghadames basin. It constitutes a prolific hydrocarbon province for oil and gas production [1]. Several wells have already been proven productive in multiple fields of the region from two promising reservoir levels which are the Ordovician El Hamra reservoir and the Triassic TAGI reservoir.

As a result, there is a growing interest in this region for a better reservoirs and source rock levels characterization to enhance oil exploration and production.

The present paper targets the geopetroleum evaluation of the Ordovician series (El Atchane and El Hamra reservoirs) and the Triassic series (TAGI), based on well logging data. The burial and thermal maturity history of the potential source rock, Fegaguira Formation (Silurian in age) of the area, was accomplished using the BasinMod software. The generation and expulsion times of hydrocarbons in the region, as well as their quantities were also estimated.

2 Materials and Methods

The first aspect concerns the use of well logging data in order to better evaluate and characterize the Ordovician reservoirs (El Atchane and El Hamra) and the Triassic reservoir (TAGI). Various petrophysical parameters such as

S. Kraouia (✉) · A. Mabrouk El Asmi
Geology Department, Faculty of Sciences of Tunis, University of Tunis El Manar, University Campus, 2060 Tunis, Tunisia
e-mail: karouisafa@yahoo.fr

A. Mabrouk El Asmi
e-mail: amina.mabrouk@fst.utm.tn

A. Ben Salem · M. Saidi
Entreprise Tunisienne d'Activités Pétrolières,
avenue Mohamed V, Tunis, Tunisia
e-mail: abdelhamid.bensalem@etap.com.tn

M. Saidi
e-mail: saidi@etap.com.tn

porosity, water saturation and volume shale, using logging tools (GR, Neutron curves, density and sonic) and available records were estimated. This method is based on the determination of these parameters as well as the thickness and the depth of each reservoir, which subsequently made it possible to construct iso-thickness, iso-depth and iso-porosity maps.

3 Results and Discussion

3.1 Petrophysical Evaluation of Reservoirs in the Study Area

Using the final results of the logging interpretation, iso-thickness, iso-depth and iso-porosity maps were made. These maps show:

The Ordovician reservoirs (El Atchane and El Hamra)

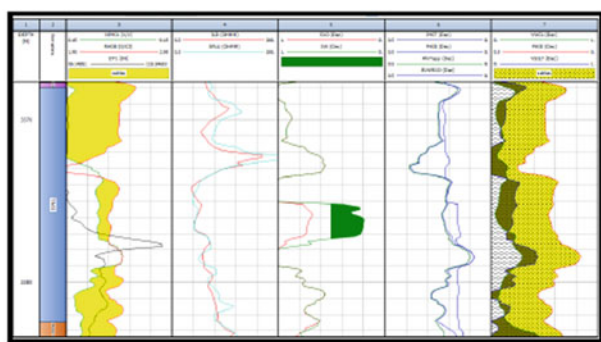
The Ordovician reservoirs (El Atchane and El Hamra) generally show the same petrophysical characteristics (the porosity of the two reservoirs varies between 5 and 12%) with a decrease in thickness from west to east until the total disappearance of the El Hamra Formation. This variation was related, on the one hand, to the bevelling of the Ordovician on the Telemzane arch and, on the other hand, to the erosive effects of the orogenic phases during Paleozoic (Taconic, Caledonian and Hercynian phases).

The Triassic TAGI reservoir

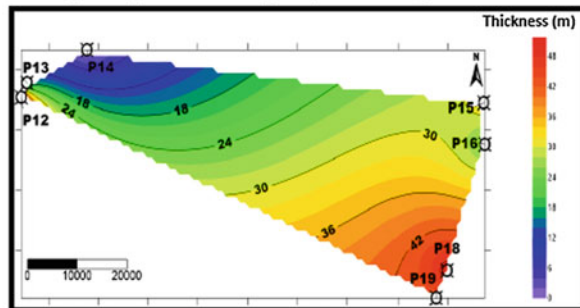
The TAGI reservoir is absent towards the west where it is totally replaced by volcanic material which took place through faulting during the Tethyan rifting. The TAGI occurs either below or above the volcanic body or may be completely absent. In the Chotts region, well reports even indicate the existence of the reservoir sandwiched with volcanic material above and below. This argues probably in favor of two volcanic phases during Triassic which are succeeded in time. Its porosity varies between 9.5 and 23.2% with the best porosities recorded at the well 13 (Fig. 1). In fact, in the latter well, the TAGI and the volcanism are characterized by good porosity ranging from 15.4 to 23.2% and hydrocarbon indices were found in the central and summit parts of the TAGI reservoir. This may be explained by two hypotheses:

- Volcanism did not affect the porosity of TAGI and the porosity of these two levels was improved by fracturing and diagenetic processes.
- Volcanism affected the porosity of the TAGI but later was improved by fracturing and diagenetic processes (for both levels).

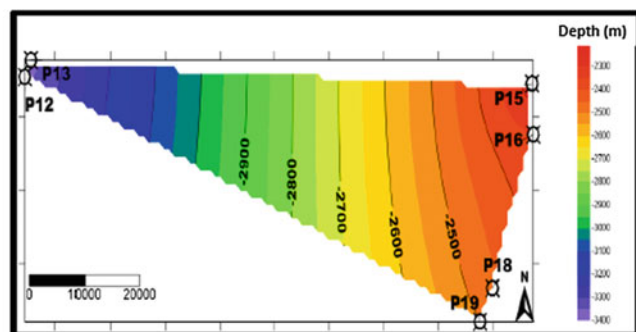
The Ordovician series and the Triassic series are good reservoirs in the southern zone of the Chotts and have the best characteristics towards the West of this zone.



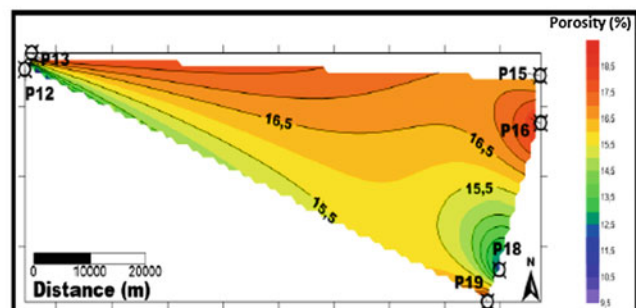
The different logging tools (GR, resistivity, Neutron, density, sonic and effective porosity) used for the petrophysical interpretation in the well 13



Iso-thickness of TAGI reservoir



Iso-depth of TAGI reservoir



Iso-porosity of TAGI reservoir

Fig. 1 Petrophysical evaluation of the Triassic TAGI reservoir

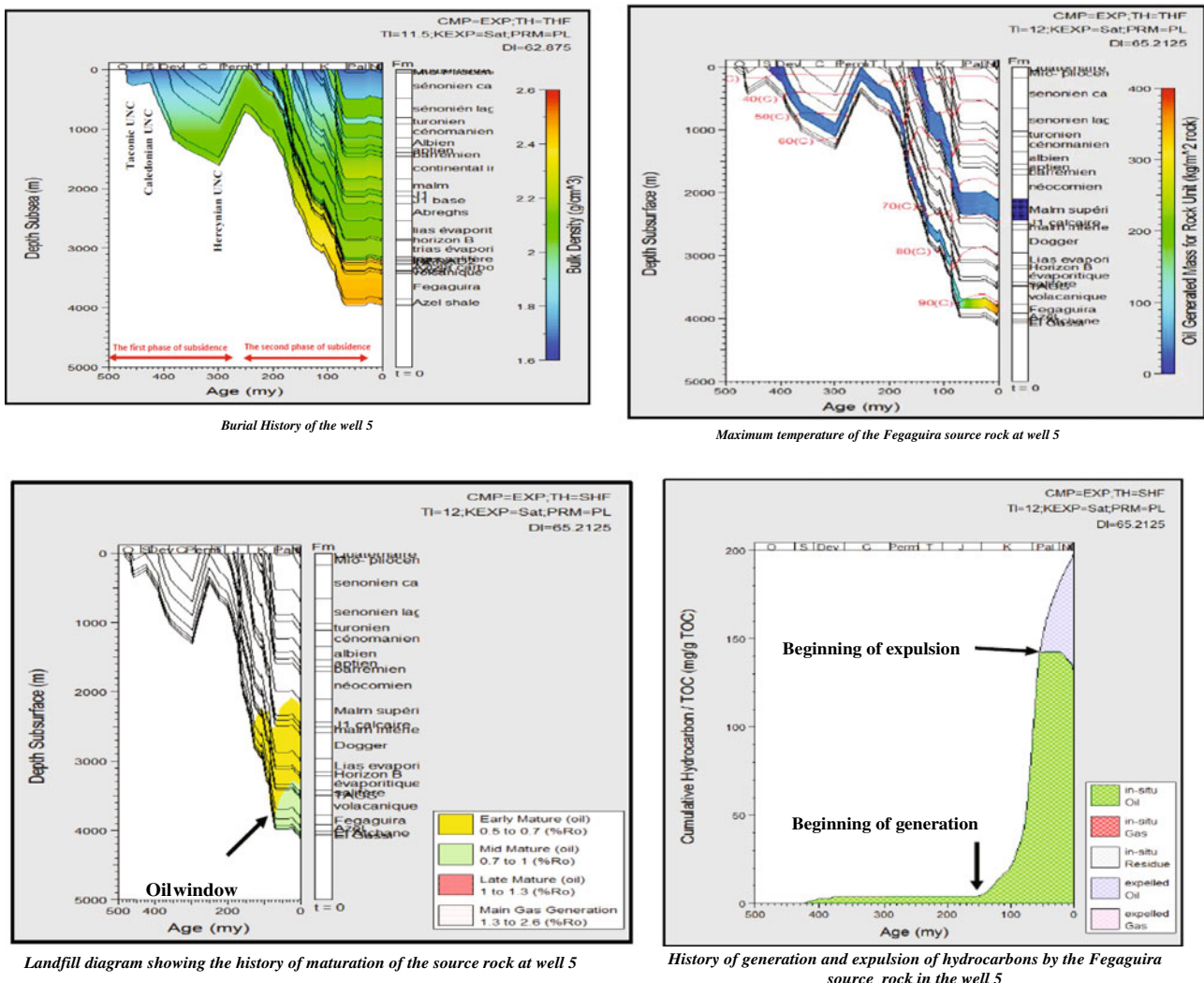


Fig. 2 1-D modeling results of the Fegaguira source rock in the well 5

3.2 1D Modeling of the Southern Region of the Chotts Basin

The second aspect of this study was to perform 1D modeling via the BasinMod software. This modeling allowed us to reconstruct the burial and thermal history and predict the timing of generation and expulsion of hydrocarbons. It also allowed us to calculate the quantities of hydrocarbons generated and expelled from 4 drilled wells (5, 7, 13 and 19) in the area. We have to note that the Fegaguira source rock is believed to have contributed to filling the candidate reservoirs of this region. It is considered a good to excellent source rock in North Africa [2] and it is interpreted to be the principal petroleum source rock in the Chotts basin and possible reservoir for shale gas and shale oil accumulations [1].

The modeling of the burial history of the basin in the study area shows two phases of subsidence which are interspersed by a compressive phase, the Hercynian phase

(290 Ma) which played a big role in sediment distribution. The erosion effect of this phase on the area is very important (900 m).

The first phase of subsidence occurred during the Paleozoic and the second phase during the Mesozoic age (Triassic–Cretaceous). The latter resulted in the deepest burial of sediments following the influence of the Tethyan rifting. The results of the modeling showed that the Fegaguira source rock was subjected to temperatures of 110 °C around 80 Ma in the well 13, 100 °C around 90 Ma in the well 7, 90 °C around 80 Ma in the well 5 and 80 °C around 80 Ma in the well 19.

The maturity history modeling of four wells in the south of the Chotts region shows that the Fegaguira source rock is mature and began generating hydrocarbons during the Early Cretaceous and expelled its hydrocarbons from the Paleogene in the wells 5 and 7, and since Early Cretaceous in the well 13 (at a SATEX of 10%).

The quantity of oil expelled by the Fegaguira source rock reached 36.3 bbl/acre ft rock and 33 bbl/acre ft rock in the wells 5 and 7 during Paleogene and 53.5 bbl/acre ft rock in the well 13 (Fig. 2).

4 Conclusions

This work focused on the Geopetroleum evaluation in the Southern part of Chotts area (southwestern Tunisia). Indeed, the Ordovician reservoirs (El Atchane and El Hamra) generally show the same petrophysical characteristics (the porosity of the two reservoirs varies between 5 and 12%) with a decrease in thickness from west to east until the total disappearance of the El Hamra Formation. This variation was related, on the one hand, to the bevelling of the Ordovician on the Telemzane arch, and on the other hand, to the erosive effects of the orogenic phases during Paleozoic (Taconic, Caledonian and Hercynian phases). However, the TAGI reservoir is absent towards the west where it is totally replaced by volcanic material which took place through faulting during the Tethysian rifting. Its porosity varies between 9.5 and 23.2% with the best porosities recorded at well 13. The TAGI and the volcanism are characterized by good porosity ranging from 15.4 to 23.2%. This may be explained by the fact that volcanism did not affect the

porosity of TAGI or it affected the porosity but was later improved by fracturing and diagenetic processes (for both levels).

1-D modeling results showed that the Fegaguira source rock was subjected to temperatures of 110 °C around 80 Ma in the well 13, 100 °C around 90 Ma in the well 7, 90 °C around 80 Ma in the well 5 and 80 °C around 80 Ma in the well 19.

The maturity history modeling of four wells in the South of the Chotts region shows that the Fegaguira source rock is mature and began generating hydrocarbons during the Early Cretaceous and expelled its hydrocarbons since the Paleogene in the well 7, and since the Early Cretaceous in well 13 (at a SATEX of 10%). The quantity of oil expelled by the Fegaguira source rock reached 36.3 bbl/acre ft rock and 33 bbl/acre ft rock in the wells 5 and 7, during Paleogene, and 53.5 bbl/acre ft rock in the well 13.

References

1. Belhaj Mohamed, A., Saidi, M., Soussi, M.: Organic Geochemistry of the Paleozoic Source Rocks in the Chotts Basin, Southern Tunisia. Society of Petroleum Engineers (2015)
2. Mejri, F., Burolet, P.F., Ben Ferjani, A.: Petroleum geology of Tunisia. A renewed synthesis. In: Memoir, vol. 22, 233p. ETAP (2006)

Hydrocarbon Source Rocks within the Western Flank of the South Caspian Basin (Azerbaijan): Geochemical Study and Petroleum System Modeling

Shalala Huseynova

Abstract

Five stratigraphic intervals in the Mesozoic–Cenozoic complex, which are distinguished as the source rocks within the western flank of SCB, are identified on the basis of geochemical study and petroleum system modeling: Eocene, Oligocene–Lower Miocene, Middle Miocene, Upper Miocene, and Lower Pliocene. Their hydrocarbon generation potential and maturity have been assessed. Retrospective analysis of the distribution of the hydrocarbon generation pots, at the different periods of geological time, shows that spatial distribution of HC generation pots is mosaic and corresponds to tectonic structure, lithological heterogeneity and generation potential of separate stratigraphic complexes, heterogeneity of heat and geobaric fields.

Keywords

South Caspian basin • Hydrocarbon • Organic matter
Petroleum system modeling • Pyrolysis
Hydrocarbon generation

1 Introduction

The South Caspian Basin (SCB) located in the central part of the Alpine-Himalayan folded belt. It is surrounded by the geostructural elements of the Greater Caucasus and Great Balkhan in the north, Elborz, Talish and the Lesser Caucasus in the south and Kopetdag in the east. The thickness of the Mesozoic–Cenozoic sedimentary cover in SCB reaches 30–32 km [1].

Oil and gas occurrences in the SCB are uncovered in a wide range of stratigraphic units from the Paleogene to the Upper Pliocene–Quaternary (see Fig. 1). The main reservoir

is the Lower Pliocene Productive Series (PS), containing about 90% of the explored oil and gas reserves. PS, with a thickness exceeding 8 km, consists of a deltaic sequence and is lithologically represented by sandstone and siltstone alternating with shale [2]. The wide stratigraphic intervals of Paleogene–Miocene and Middle Jurassic–Lower Cretaceous sediments are considered as the source rocks within the study area [3].

2 Investigation Methods and Database

Petroleum system modeling was applied for understanding the generation-migration and accumulation processes and evaluation of hydrocarbon potential of the sedimentary cover of SCB. The available geological, geophysical, thermobaric and geochemical database was analyzed and integrated into 2D modeling that was carried out along the several representative seismic-geological cross-sections (A-A', B-B', C-C', D-D') (see Fig. 1).

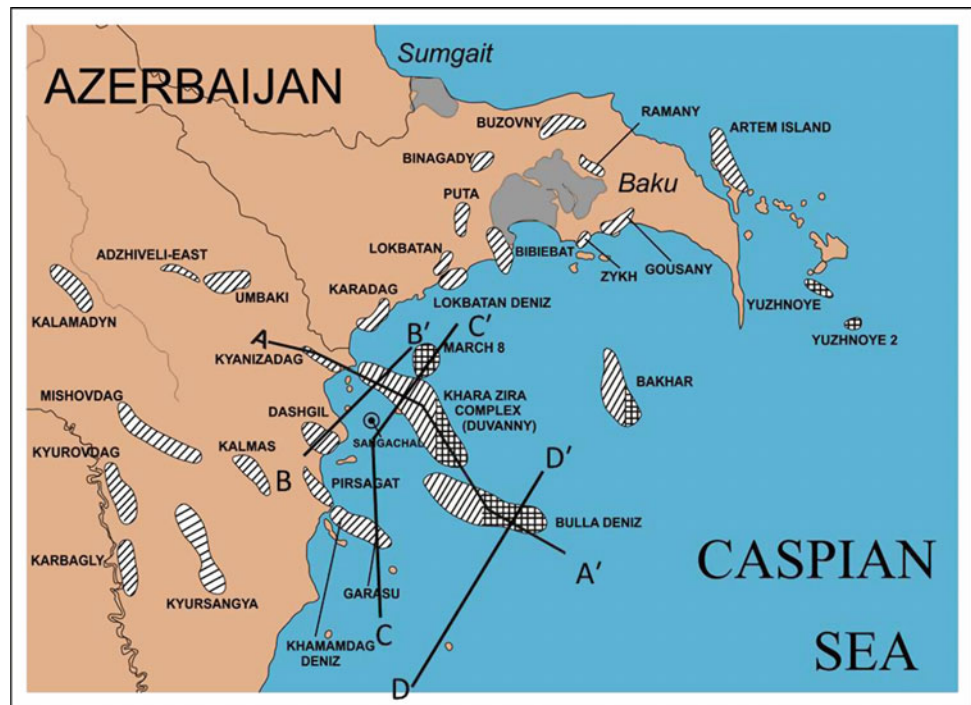
The quantitative and qualitative characteristics of organic matter in rocks and the oil-generation potential of the deposits were studied on the basis of pyrolytic analysis of core and mud volcano ejection samples, determined by pyrolysis.

3 Geochemical Study

One of the main conditions for the formation of oil and gas accumulations is the presence of rocks enriched with organic matter, that is the rocks with sufficient hydrocarbon generating potential. The hydrocarbon potential of sedimentary rocks was evaluated according to organic matter content and its quality. Paleocene deposits are the poorest in organic carbon content which constitutes one hundredths of a percent. Eocene deposits are characterized by a relatively high TOC varying from 0.57 to 2.8% [4]. The Oligocene–Lower Miocene (Maikop Series) sediments are characterized by the

S. Huseynova (✉)
Oil and Gas Institute of Azerbaijan National Academy of Sciences, 9, F.Amirov, Baku, AZ1000, Azerbaijan
e-mail: huseynova_shalala@yahoo.com

Fig. 1 Location map of oil and gas fields within the western flank of the South Caspian basin with lines of cross-sections for modeling



highest content of TOC, reaching 15.3%. The hydrogen index (HI) varies from 11 to 612 mgHC/gTOC. The kerogen corresponds to the types II and III [4]. Middle Miocene deposits (Chokrak-Spirialysis beds) are characterized by a satisfactory quality of OM: the TOC content varies within the range of 0.09–2.44%, and HI—73 to 541 mgHC/gTOC. The kerogen corresponds to type II, that indicates the possibility of generating liquid and gaseous hydrocarbons. The Upper Miocene deposits (Diatom suite) are characterized by a high TOC content—0.09 to 7.8% and HI—107 to 708 mgHC/gTOC. The kerogen of these formations mainly corresponds to type II. TOC content in the rocks of the Pontic Stage varies from 0.28 to 0.54%. Lower Pliocene deposits (PS) are very poor with TOC, except for the rocks of the lower section of the PS. In general, organic matter in the deposits of the lower and upper sections of the PS is characterized by a poor quality and is represented mainly by type III. TOC content is 0.02–2.71%, HI—15 to 334 mgHC/gTOC.

Pyrolytic analysis of Paleogene–Miocene clay rocks from the mud volcanoes shows their extremely high HC potential. The quantitative and qualitative composition of the OM improves from the Eocene to the Middle–Upper Miocene (Diatom) deposits. TOC content in mud volcano samples varies from 0.01% to 4.79–9.26% depending on the rock type, except for the samples of Eocene combustible shales with TOC reaching 24.1–30.0% [4]. According to T_{max}

values, OM content of the Paleogene–Miocene sediments is characterized by a low thermal maturity, decreasing from Eocene to Diatom sediments from 433 to 415 °C.

Thus, the quality and content of OM in Paleogene–Neogene deposits improve toward the center of the SCB. The source rocks are ranked as rich and very rich. It is supposed that they are able to generate hydrocarbons under favorable thermobaric conditions. The results of pyrolytic studies of the rocks of the mud volcanoes of the Paleogene–Miocene age show that, under conditions of relatively low heating, the rocks are not mature enough to generate hydrocarbons to a depth of 6 km.

4 Petroleum System Modeling

Paleoreconstruction of sedimentary covers of the western flank of SCB has been performed from Jurassic to Present time along the chosen seismic-geological cross-sections (see Fig. 1). 2D petroleum system modeling included simulations of burial history, structure forming, thermobaric conditions, hydrocarbon generation history, migration and accumulation. Models have been calibrated by temperatures, pressure, porosity, and vitrinite reflectance measured in wells.

Modeling of thermal history includes simulation of paleo and modern temperatures. Modeling of thermal history in

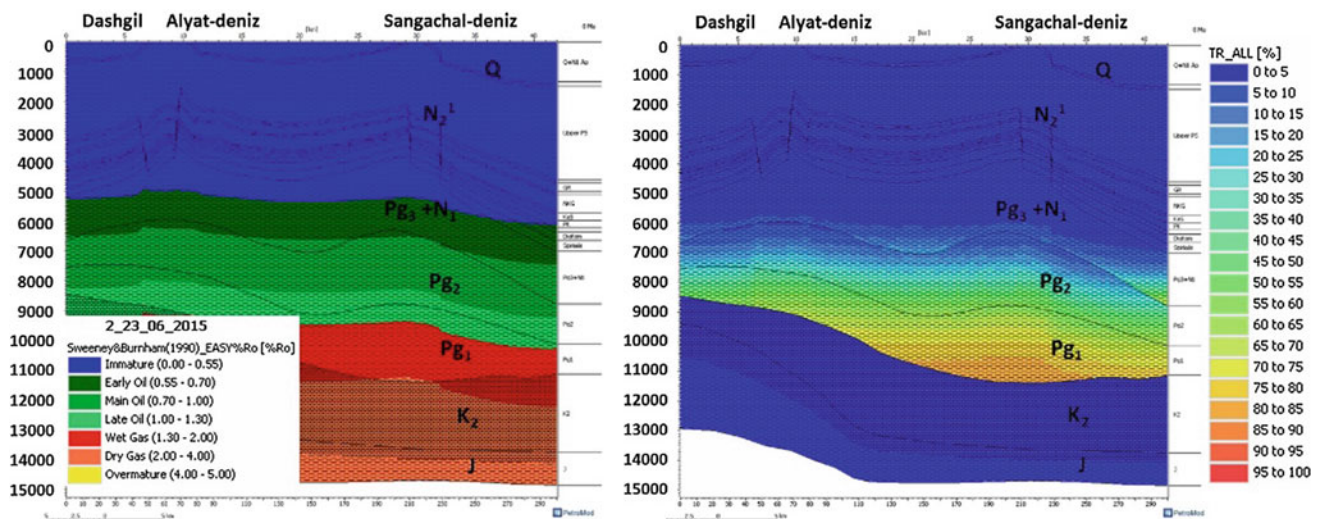


Fig. 2 Maturity (left) and transformation ratio (right) of organic matter of Mesozoic–Cenozoic deposits along the line CC': Oligocene–Miocene deposits are the main source rocks along the line CC'

space and time suggests the degree of heating and maturity of deposits in the different tectonic and stratigraphic complexes, at the different geologic periods and at present. The burial pattern and low thermal gradient suggest favorable conditions for the full zonation of HC generation, including the dry gas generation zone [5] (see Fig. 2, left).

Hydrocarbon generation interval is extremely extended [6]. The oil generation window begins at a depth of 5 km subsiding down to 6.5 km and corresponds to Oligocene–Miocene and Low Pliocene rocks. The gas window, located at a depth of 9.5–15 km at flank, and of 11–16.5 km in the subsided part of SCB, corresponds to Eocene–Cretaceous rocks. Mesozoic rocks are the most mature rocks. They are in the intensive gas generation zone at the flank and overmature in the subsided zone. Palaeogene–Miocene rocks are in the main oil and gas generation window. All the rocks younger than of Miocene age are immature, except for the lower horizons of the Low Pliocene Productive Series, which entered the early oil generation window.

Modeling of evolution of HC generation pots in space and time allowed the estimation of the degree of HC generation potential realization [7]. Eocene rocks realized 40–50 and 80–90% of their HC potential at the flank and at the subsided part, respectively. The degree of HC potential realization of Oligocene–Lower Miocene rocks is of 20% at the flank and reaches 60–70% with subsidence. Middle and Upper Miocene rocks realized only 20–25% of their HC potential (see Fig. 2, right).

5 Conclusions

The geochemical study and modeling of the Mesozoic–Cenozoic complex of the western flank of SCB gave an opportunity to assess their HC generation potential and to identify five individual intervals that can be considered as source rocks: Eocene, Oligocene–Lower Miocene, Middle Miocene, Upper Miocene, and Lower Pliocene. The modeling of HC generation history allowed to make a retrospective analysis of the distribution of the HC generation pots at the different periods of geological time. HC generation pots are migrating in the western direction. Spatial distribution of HC generation pots is mosaic and corresponds to tectonic structure, lithological heterogeneity and generation potential of separate stratigraphic complexes, heterogeneity of heat and geobaric fields.

References

1. Knapp, C., Knapp, J., Connor, J.: Crustal scale structure of the South Caspian basin revealed by deep seismic reflection profiling. Mar. Petrol. Geol. **21**, 1073–1081 (2004)
2. Gusejnov, D., Mirizade, S., Gusejnova, S.: Expansion features and properties of oil and gas reservoirs of the north-western slope of the South-Caspian basin. Oil Gas Geol. **2**, 55–66 (2015)
3. Guliyev, I., Mamedov, P., Feyzullayev, A., Kadirov, F., Aliyeva, E., Tagiyev, M.: Hydrocarbon Systems of the South Caspian Basin. Nafta-press, Baku (2003)

4. Feyzullayev, A., Guliyev, I., Tagiyev, M.: Source potential of the Mesozoic-Cenozoic rocks in the South Caspian basin and their role in forming the oil accumulations in the lower Pliocene reservoirs. *Petrol. Geosci.* **7**(4), 409–417 (2001) (EAGE/Geological Society of London)
5. Huseynova, S.: Modeling of geothermal conditions in Meso-Cenozoic sediments of Baku archipelago. *Azerbaijan Geol.* **3**, 29–37 (2015)
6. Huseynov, D., Huseynova, S.: HC generation and migration at the western flank of South Caspian basin: results of basin modeling. In: 76th EAGE Conference and Exhibition 2014 Proceedings, Th P12 05. EAGE, Amsterdam (2014)
7. Huseynova, S., Huseynova, G.: Hydrocarbon potential of the western flank of the South Caspian basin, Azerbaijan. In: 79th EAGE Conference and Exhibition 2017 Proceedings, Tu P5 02. EAGE, Paris (2017)



Organic Source Input, Thermal Maturity and Paleodepositional Conditions of Imo Formation in the Anambra Basin, Nigeria

Mutiu A. Adeleye and Damilola A. Daramola

Abstract

This investigation examines the samples of Imo Formation from Nzam-1 well, Anambra basin, to identify the source of organic matter, the depositional environment, thermal maturity and tectonic setting. The sediments consist of grey to dark grey, less gritty fissile shales, with no distinct grainy appearance or layered structure, and white to grey sandy shales with intercalations of fine grained sandstones. Biomarker results indicate short to middle chain *n*-alkanes, low to medium CPI values and narrow range of Pristane/Phytane ratio. Major oxides in the samples follow the trend: $\text{SiO}_2 > \text{TiO}_2 > \text{Fe}_2\text{O}_3$. Trace elements such as Sr, Ba, V, Ni, Co and Cr were identified. The biomarker results suggest thermally immature to early mature sediments deposited in anoxic to sub-oxic environment. The biomarkers of terpanes and steranes indicate derivation from a mixed marine algal source with minor contributions from terrigenous inputs. Trace element ratios also indicated oxic to dysoxic bottom water conditions, reflecting mixed terrigenous and marine conditions. Major oxide ratios indicated that samples were sourced from a passive continental margin under humid paleoclimatic conditions. Geochemical parameters (Cr/Ni, and Th/Cr ratios etc.) suggested a felsic dominated basement source.

Keywords

Imo Formation • Biomarkers • Trace elements
Organic source input • Thermal maturity

M. A. Adeleye (✉) · D. A. Daramola
Department of Geology, University of Ibadan, Ibadan, Nigeria
e-mail: mutiuadeleye@gmail.com

D. A. Daramola
e-mail: daramoladamilola93@yahoo.com

1 Introduction

The Anambra basin is characterized by undeformed and non-tectonised sediments with a relatively moderate temperature regime suitable for generation and accumulation of hydrocarbons [1]. Murat reported the structural relationships between the evolution of Anambra basin and Niger Delta with respect to the NE–SW trending Benue Trough. Imo Formation has been identified as one of the hydrocarbon source rocks in the Anambra basin [2, 3]. However, the Formation has received little attention despite its strong resemblance with the sediments of Akata Formation in the Niger Delta [4]. Imo Formation was reported as the outcropping lithofacies equivalent of marine Akata Formation in subsurface Niger Delta [5]. This study attempts to evaluate the source of organic matter, depositional environment, thermal maturity and tectonic setting of the Imo Formation from Nzam-I well in the Anambra basin.

2 Materials and Methods

Ditch cutting and core samples of Imo Shale Formation selected from a depth ranging from 525 to 600 m in the Nzam-1 well were examined for their lithology, color, and grain size among others. All the samples were finely pulverized, labeled and stored in vials. Selected samples were ultrasonically extracted using dichloromethane (DCM) and methanol (CH_3OH) as the solvent mixture in the ratio of (10:0), (5:5) and (0:10). All extractions were repeated three times and the extracts were pooled together. The extraction solvents were removed by evaporation and separated into the aromatics and saturate fractions. The saturate fractions were analyzed for biomarkers by Gas Chromatography Mass Spectrometry (GC-MS). Three samples were also demineralized by soaking 15–20 g each in 1 M HCl for 24 h, decanted and rinsed with distilled water. The supernatants were treated with 1 M HCl/10% HF for 5 days, decanted

and rinsed with distilled water till the pH of the water was 7 (neutral). The samples were oven dried at 40 °C, stored and subjected to Inductively Coupled Plasma-Mass Spectrometry (ICP-MS).

3 Results

The sediments of the Imo Formation encountered in Nzam-1 well consist of grey to dark grey, less gritty fissile shales with no grainy appearance, and white to grey sandy shales with intercalations of fine grained sandstones. The biomarker results of *n*-alkane, isoprenoid distribution, steranes and terpanes for the sample extracts are presented in Tables 1 and 2. The major oxides' results of the samples showed a dominance of SiO₂ (88.98–90.11%) and others as follows: Al₂O₃ (0.89–0.97%), Fe₂O₃ (0.98–2.31%), MgO (0.04–0.05%), TiO₂ (1.75–2.29%) etc. SiO₂, Fe₂O₃ and TiO₂ accounted for about >90% of the sediments while other oxides such as MnO, Na₂O, K₂O, Al₂O₃, P₂O₅ and Cr₂O₃ constituted <10%. Trace element concentrations of the Imo Formation showed that Ba, Sr, Mn, La, As and Ni contents are prominent with average values of 108.2, 15.07, 8.7, 7.7 and 7.5 ppm, respectively, while Cu, Pb, V, Co, and U have average values of 6.2, 4.8, 2.7, 2.5 and 0.2 ppm, respectively.

4 Discussion

4.1 Source of Organic Matter and Depositional Environment

The distribution of *n*-alkanes in oil and bitumen has been used to indicate the organic matter source [6]. The distribution of n-alkanes in Imo Formation samples reflects an organic matter derived from both marine and terrestrial environment [7]. Pr/Ph ratios were also proposed as an indicator for the redox conditions of depositional environment [8]. Pr/Ph ratios of the Imo Formation samples ranging from 0.41 to 0.97 suggest deposition in an anoxic environment [7, 9]. Closeness of some of the values to 1.0 also indicates sub-oxic conditions associated with marine sourced organic matter.

Pristane/nC17, Phytane/nC18 and carbon preference index (CPI) of *n*-alkanes are widely used as indicators of source rock types, depositional environment or condition and organic maturation [10]. Cross-plot of Pr/nC17 versus Ph/nC18 (Fig. 1) suggests that the organic matter in the Imo Formation samples were deposited in anoxic to sub-oxic environment or from mixed marine materials. The CPI values of the samples (0.31–1.12) indicate sediments from mixed marine organic matter or transition environment under relatively anoxic to sub-oxic depositional conditions.

Table 1 N-alkanes, isoprenoids and steranes data of the Imo Formation sample extracts

Depth (m)	Pr/Ph	Pr/nC17	Ph/nC18	CPI	OEP	TAR	20S/20S + 20R C29 steranes	$\beta\beta/(\beta\beta \alpha\alpha)$ C29 steranes	Results
595–600	0.97	0.21	0.24	0.98	0.92	0.16	0.40	0.57	Results
585–590	0.94	0.40	0.34	1.02	1.00	0.23	0.41	0.55	Results
575–580	0.96	0.30	0.26	1.02	0.94	0.23	0.40	0.55	Results
560–565	0.41	0.30	0.03	0.31	0.23	1.23	0.38	0.53	Results
540–545	0.93	0.37	0.35	1.12	0.76	0.04	0.37	0.55	Results
525–530	0.64	0.40	0.37	1.05	0.85	1.21	0.40	0.58	

Table 2 Terpanes data of the Imo Formation sample extracts

Depth (m)	C35ab (S)/ C34ab (S)	C35/C31– C35	C29H/C30H	C31R/C30H	Ts/Tm	Ts/Ts + Tm	C35HH/C30 + M Hopane	Mor/Hop	Results
595–600	0.94	0.07	0.87	0.71	0.71	0.41	0.28	0.19	Results
585–590	0.18	0.07	0.79	0.47	0.91	0.48	0.15	0.87	Results
575–580	0.21	0.04	0.65	0.98	0.75	0.43	ND	ND	Results
560–565	0.67	0.05	0.81	0.41	0.86	0.46	0.09	0.13	Results
540–545	0.17	0.03	0.61	1.38	0.82	0.45	ND	ND	Results
525–530	0.23	0.04	0.64	1.22	0.68	0.41	0.24	0.56	

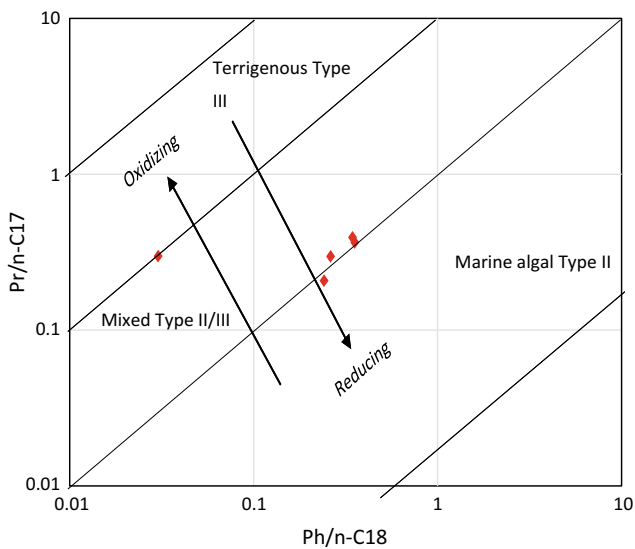


Fig. 1 Plot of Pr/nC-17 and Ph/n-C₁₈ for samples

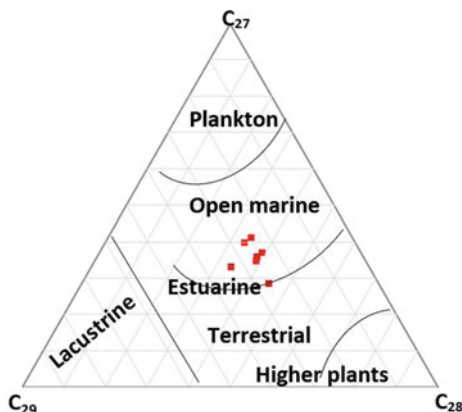


Fig. 2 Ternary diagram of regular steranes

A cross-plot of CPI versus Pr/Ph also supports anoxic to sub-oxic depositional environment. The ternary diagram of the steranes for shales of the Imo Formation shows contribution of marine organic source with significant concentration towards C₂₇, which means that the samples were deposited in an estuarine to marine environment (Fig. 2).

Trace element concentrations in sediments are also sensitive indicators for paleo-redox conditions [11, 12]. Range of V/Ni ratios for the Imo Formation samples (0.2–0.6) indicate predominantly terrigenous organic materials deposited under sub-oxic conditions [13]. Relatively low V/(V + Ni) ratios of 0.17–0.38 also denote oxic to sub-oxic conditions [14]. However, a cross plot of Vanadium and Nickel (Fig. 3) reflects organic matter from mixed marine and terrigenous source input deposited under oxic-dysoxic conditions.

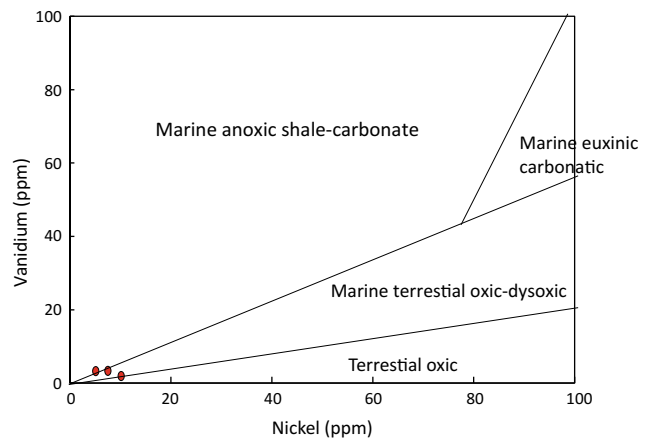


Fig. 3 Plot of V and Ni for the samples

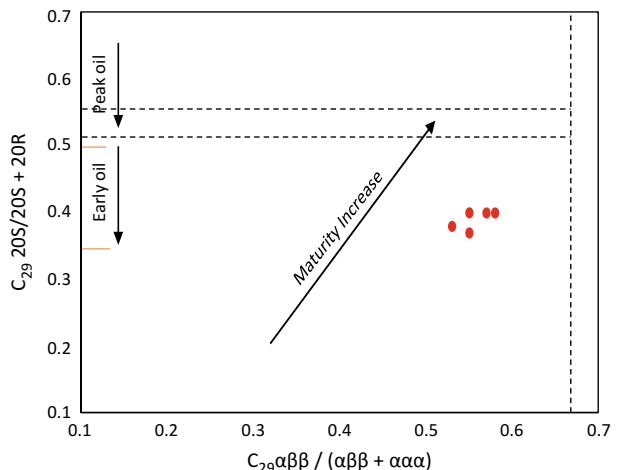


Fig. 4 Plot of steranes for the samples

4.2 Thermal Maturity

Alkane and Isoprenoids distribution, Pristane/n-C₁₇, Phytane/n-C₁₈, CPI and improved odd-even preference (OEP) are widely used as indicators of maturity [7, 9]. Low Pr/n-C₁₇ and Ph/nC-18 ratios in most of the studied samples suggest a reflection of the marginal maturity of the source rock. The CPI values of the Imo Formation samples (0.31–1.12) also reflect marginal maturity of the organic matter in the samples.

Sterane ratios are also widely used as parameters in oil and sedimentary organic matter [7]. C₂₉ (H)-sterane and 20S/(20S + 20R) ratio of Imo Formation samples, ranging from 0.37 to 0.41, reflects low to early mature source rocks for hydrocarbon generation. The maturity parameter based on ββ/(ββ + αα) ratio of Imo Formation in Nzam-1 well ranging from 0.53 to 0.58 indicates that the samples are early mature source rocks. The plot of 20S/(20S + 20R) and αββ/(αββ + ααα) for the C₂₉ steranes indicates samples within the early oil window (Fig. 4).

4.3 Tectonic Setting

Major oxides are useful indicators of a tectonic setting and paleoclimate [15, 16]. Plot of (K_2O/Na_2O) and SiO_2 indicates a passive continental margin setting for the sediments while the plot of SiO_2 and $(Al_2O_3 + K_2O + Na_2O)$ reveals humid paleoclimatic conditions for the samples. Average Al_2O_3/TiO_2 ratio (0.47) for the sediments suggests mafic igneous source. However, low Cr/Ni and Th/Cr ratios indicate that the sediments were derived from felsic dominated basement complex rocks.

5 Conclusions

Shales and sandy shales of Imo Formation from Nzam-1 well in the Anambra basin are composed of organic matter sourced from marine organic matter mixed with terrigenous organic matter deposited under anoxic to sub-oxic conditions. The sediments are marginal or early mature source rocks in early oil window. Trace element concentrations also reflected oxic-dysoxic bottom water conditions indicative of mixed terrigenous and marine deposition. Major concentrations of oxides revealed that the sediments were derived from a passive continental margin setting under humid paleoclimate.

References

- Murat, R.C.: Stratigraphy and paleogeography of the Cretaceous and lower tertiary in southern Nigeria. In: Dessauvagie, T.F.J., Whiteman, A.J. (eds.) African Geology, pp. 251–266. University of Ibadan Press, Nigeria (1972)
- Avbovbo, A., Ayoola, E.O.: Petroleum prospects of southern Nigeria's Anambra Basin. *Oil Gas J.* **79**, 334–348 (1981)
- Ekweozor, C.M., Gormly, J.R.: Petroleum geochemistry of late Cretaceous and early tertiary shales penetrated by the Akukwa-2 well in the Anambra Basin, Southern Nigeria. *J. Petrol. Geol.* **6**(2), 207–216 (1983)
- Short, K.C., Stauble, A.J.: Outline of geology of Niger delta. *AAPG Bull.* **51**, 761–779 (1967)
- Avbovbo, A.A.: Tertiary lithostratigraphy of the Niger Delta. *AAPG Bull.* **62**, 295–300 (1978)
- Duan, Y., Ma, L.H.: Lipid geochemistry in a sediment core from Ruogai Marsh deposit (Eastern Qinghai-Tibet Plateau, China). *Org. Geochem.* **32**, 1429–1442 (2001)
- Peters, K.E., Walters, C.C., Moldowan, J.N.: The Biomarker Guide, 2nd edn. Cambridge University Press, New York (2005)
- Didyk, B.M., Simoneit, B.R.T., Brassell, S.C., Eglinton, G.: Organic geochemical indicators of palaeoenvironmental conditions of sedimentation. *Nature* **271**, 216 (1978). (London)
- Peters, K.E., Moldowan, J.M.: The Biomarker Guide: Interpreting Molecular Fossils in Petroleum and Ancient Sediments. Prentice-Hall Inc., Englewood Cliffs, New Jersey (1993)
- Peters, K.E., Fraser, T.H., Amris, W., Rustanto, B., Hermanto, E.: Geochemistry of crude oils from eastern Indonesia. *AAPG Bull.* **83**, 1927–1942 (1999)
- Algeo, T.J., Maynard, J.B.: Trace-element behavior and redox facies in core shales of upper Pennsylvanian Kansas-type cyclothsems. *Chem. Geol.* **206**, 289–318 (2004)
- Mohialdeen, I.M.J., Raza, S.M.: Inorganic geochemical evidence for the depositional facies associations of the Upper Jurassic Chia Gara formation in NE Iraq. *Arab. J. Geosci.* **6**, 4755–4770 (2013)
- Galarraga, F., Reategui, K., Martínez, A., Martínez, M., Llamas, J.F., Márquez, G.: V/Ni ratio as a parameter in palaeoenvironmental characterisation of non-mature medium-crude oils from several Latin American basins. *J. Petrol. Sci. Eng.* **61**, 9–14 (2008)
- Lewan, M.D.: Factors controlling the proportionality of vanadium to nickel in crude oils. *Geochim. Cosmochim. Acta* **48**, 2231–2238 (1984)
- Roser, B.P., Korsch, R.J.: Determination of tectonic setting of sandstone mudstone suites using SiO_2 content and K_2O/Na_2O ratio. *J. Geol.* **94**, 635–650 (1986)
- Suttnar, L.J., Dutta, P.K.: Alluvial sandstone composition and palaeoclimate. 1. Framework mineralogy. *J. Sediment. Petrol.* **56**, 329–345 (1986)



Biodegradation of Hopanes, Steranes and Tricyclic Terpanes in Heavy Oils

Yang Li, Xiangchun Chang, Jinliang Zhang, and Youde Xu

Abstract

Nine heavy oils were analyzed to investigate the biodegradation of biomarkers. According to the characteristics of the presence of a fully developed series of 25-norhopanes and to the conspicuous depletion of hopanes, regular steranes and even tricyclic terpanes, the level of biodegradation of the samples were determined as ranging from PM 6 to PM 9. Among the samples, hopanes and regular steranes were biodegraded severely and the depletion of hopanes and of regular steranes increased with the increase of the biodegradation level. When the level of biodegradation reaches PM 8, the biodegradation of tricyclic terpanes begins. With the increase of biodegradation, the C_{21–22} steranes and diasteranes remain unaffected under the biodegradation level of PM 8, indicating that they can be used as conserved “internal standards” to evaluate the biodegradation of hopanes, regular steranes and tricyclic terpanes. However, the C_{21–22} steranes and diasteranes are degraded when the biodegradation level is over PM 9. Among the C_{19–26} tricyclic terpanes family, C₂₃ and C₂₁ tricyclic terpanes are the most readily degraded members, followed by C₂₀ tricyclic terpane, while the C₁₉, C₂₂ and C_{24–26} tricyclic terpanes seem more resistant to biodegradation.

Keywords

Biodegradation • Heavy oil • Biomarkers
Tricyclic terpanes

Y. Li · J. Zhang (✉)

Faculty of Geographical Science, Beijing Normal University,
Beijing, 100875, China
e-mail: jinliang@bnu.edu.cn

Y. Li · X. Chang

College of Earth Science and Engineering, Shandong University
of Science and Technology, Qingdao, 266510, China

Y. Xu

Research Institute of Petroleum Exploration and Development,
Shengli Oil Company, Sinopec, Dongying, China

1 Introduction

Biodegradation is one of the controlling factors of the formation of heavy oils [1, 2]. There is a consensus that with the increasing biodegradation, biomarkers are sequentially reduced, following the order *n*-alkanes > alkylcyclohexanes isoprenoids > bicyclic sesquiterpenes > hopane (with formation of 25-norhopanes) > regular sterane > hopane (without formation of 25-norhopanes) > tricyclic terpanes (TTs) > diasteranes > porphyrins [1, 3]. In most cases, the tricyclic terpanes were unaffected by biodegradation due to the resistance of these components to biodegradation [1–3]. However, when the biodegradation of oils becomes extremely severe, the biodegradation of tricyclic terpanes can obviously be seen [2]. In this study, all the selected samples were severely degraded, and some of the samples showed evidence of alteration of tricyclic terpanes. As a result, the biodegradation of hopanes, regular steranes and tricyclic terpanes was investigated. Meanwhile, the “internal standards” to evaluate the biodegradation of hopanes and regular steranes were determined and their applicability was discussed. Additionally, the time of tricyclic terpanes begins to decrease and the relative susceptibility of C_{19–26} tricyclic terpanes to biodegradation was illustrated.

2 Materials and Methods

The oil samples from the Carboniferous reservoirs were collected from wells in the eastern Chepaizi Uplift, Junggar Basin, NW China. The densities of the oil samples are greater than 0.92 g/cm³, indicating that all oils belong to heavy oils. And the biodegradation is the key factor for the formative mechanism of the heavy oils [2].

In order to investigate the characteristics of biodegradation of different biomarkers, a Gas chromatography–mass spectrometry (GC–MS) analysis of the aliphatic and aromatic fractions was performed.

3 Results and Discussion

3.1 Level of Biodegradation

Total ion current (TIC) diagrams of saturated hydrocarbons show a clear UCM peak and the loss of n-alkanes and isoprene alkanes is serious, indicating that crude oils have been severely degraded (Fig. 1).

Based on the relative abundance of various hydrocarbon classes, the levels of biodegradation of the oil samples were shown in Fig. 2 [1].

3.2 Biodegradation of Hopanes, Regular Steranes and Tricyclic Terpanes

As shown in Fig. 1, the abundances of C_{27-29} regular steranes were suddenly decreased when the level of biodegradation is higher than PM 7, while the C_{21-22} steranes and diasteranes were nearly unaffected with the increase of biodegradation. The ratios of regular steranes to C_{21-22} steranes and diasteranes show positive correlations with the level of biodegradation (Fig. 3a).

The fully developed series of $C_{29-C_{34}}$ 25-norhopanes of the selected oils can help determine the origin of 25-norhopanes [2]. The ratios of C_{29} 25-norhopanes to C_{30} hopanes (C_{29} 25-NH/ C_{30} H) show positive correlations with the level of biodegradation, indicating that 25-norhopanes originate by microbial demethylation of hopanes in this study (Table 1).

In this study, we selected three samples, of which the tricyclic terpanes were reduced in a different degree, to investigate the relative susceptibility of tricyclic terpane family. It is apparent that the ratios of C_{21} and C_{23} tricyclic terpanes to C_{27} diasterane decrease more sharply than those of the $C_{24-C_{26}}$ tricyclic terpanes (Fig. 3b). Thus, the C_{21} and C_{23} tricyclic terpanes are the most readily degraded members, while the C_{24-26} tricyclic terpanes seem more resistant to biodegradation. Abnormally, the ratios of C_{24-26} tricyclic terpanes to C_{21} sterane and C_{27} diasteranes increased with the level of biodegradation which increased to PM 9, indicating that even the C_{21} sterane and C_{27} diasteranes were biodegraded when the biodegradation was extremely severe (Fig. 3b and Table 1). The values of C_{19-26} TT/ C_{21} steranes remain stable with PM 7; however, the values sharply decrease when the level of biodegradation reaches PM 8.

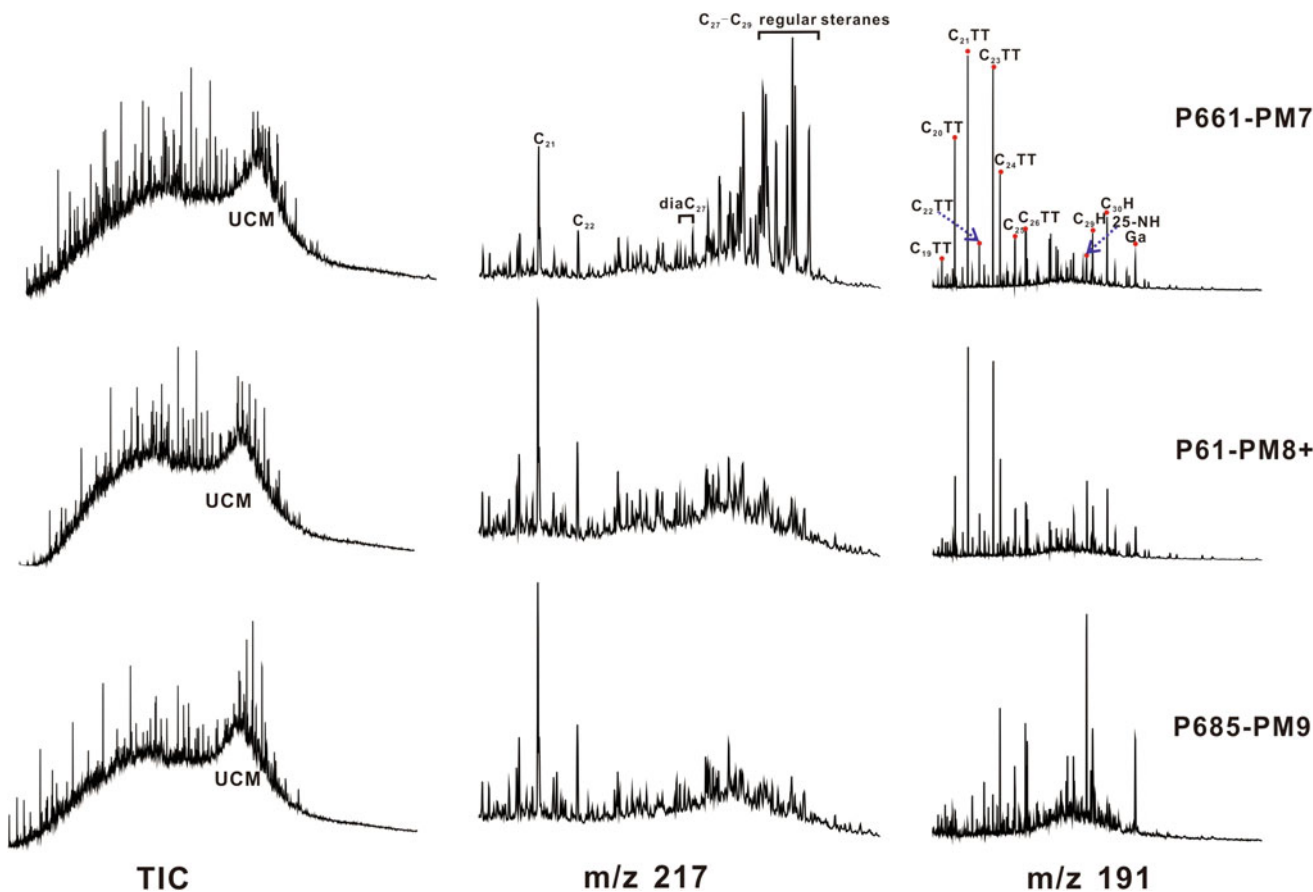


Fig. 1 Total ion chromatograms (TIC) of oils showing evident base line “humps” with a few detectable n-alkanes and distribution of steranes, hopanes and tricyclic terpane with the increase of biodegradation

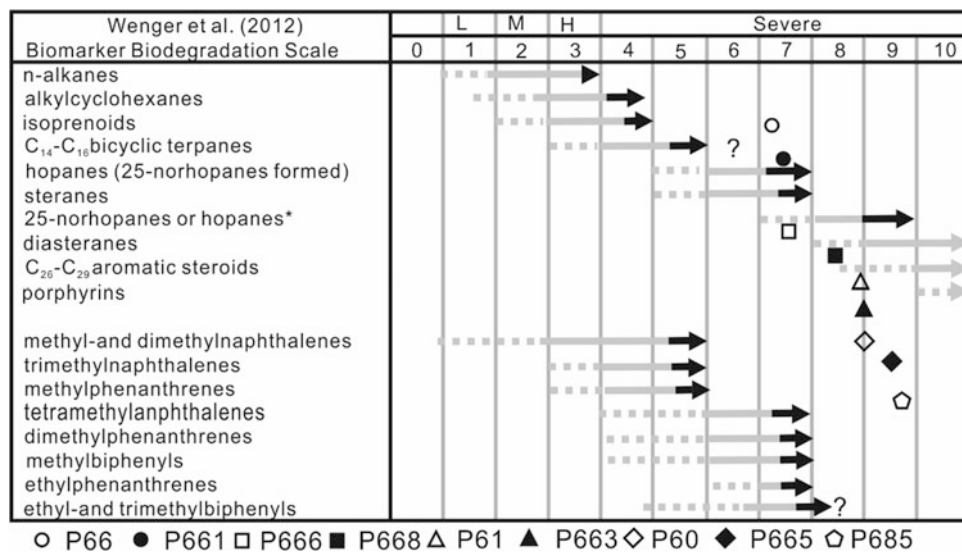


Fig. 2 The extent of biodegradation of oils can be ranked on a scale of 7–9 based on differing resistance of compound classes to microbial attack. Arrows indicate where compound classes are first altered (dashed lines), substantially depleted (solid gray), and completely

eliminated (black). The degree of biodegradation from Wenger et al. [4] reflects changes in oil quality (L, lightly biodegraded; M, moderately biodegraded; H, heavily biodegraded). *Hopanes degraded without the formation of 25-norhopanes

Fig. 3 Line charts showing biodegradation of C₂₇₋₂₉ regular steranes and C₁₉-C₂₆ tricyclic terpanes of the selected samples. TT: tricyclic terpane, 19–26: carbon number of tricyclic terpanes. The right Y-axis of plot A corresponds to the value of C₂₉ 25-NH/C₃₀H and the plot B was referred from Chen [3]

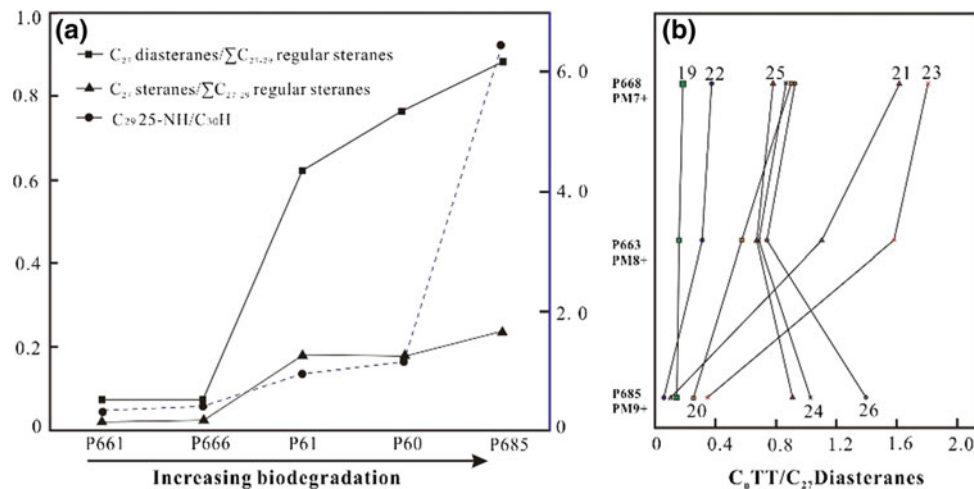


Table 1 The values of C₂₉ 25-NH/C₃₀H (a), C₁₉₋₂₆TT/C₂₁ steranes (b-i), LB = level of biodegradation

Well	LB	a	b	c	d	e	f	g	h	i
P66	7	0.31	0.31	1.69	2.43	0.48	2.41	1.23	0.98	1.21
P661	7	0.34	0.32	1.60	2.22	0.45	2.29	1.14	0.93	1.12
P666	7	0.42	0.27	1.40	2.24	0.44	2.25	1.10	0.92	1.10
P668	8	0.73	0.07	0.32	0.57	0.13	0.64	0.31	0.28	0.33
P61	8+	0.96	0.05	0.25	0.54	0.12	0.57	0.27	0.24	0.28
P60	8+	1.13	0.04	0.04	0.17	0.06	0.39	0.29	0.25	0.37
P663	8+	1.47	0.04	0.16	0.30	0.09	0.43	0.19	0.18	0.20
P665	9	5.49	0.04	0.08	0.04	0.02	0.10	0.26	0.23	0.37
P685	9	6.41	0.04	0.07	0.03	0.02	0.09	0.28	0.24	0.38

Thus, the biodegradation of tricyclic terpanes begins at the biodegradation level of PM 8.

4 Conclusions

1. The level of biodegradation of the heavy oils was subjected to biodegradation ranging from rank 6 to rank 9.
2. Hopanes and regular steranes were biodegraded more severely with the increase of biodegradation. The biodegradation of tricyclic terpanes begins when the level of biodegradation reaches PM 8.
3. The C_{21–22} steranes and diasteranes remain stable when the biodegradation level is lower than PM 8 and they can be used as conserved “internal standards” to evaluate the biodegradation of hopanes, regular steranes and tricyclic

terpanes. However, the C_{21–22} steranes and diasteranes are degraded when the biodegradation level is over PM 9.

4. Among the C_{19–26} tricyclic terpanes family, C₂₃ and C₂₁tricyclic terpanes are more susceptible to biodegradation than C_{24–26} tricyclic terpanes.

References

1. Peters, K.E., Walters, C.C., Moldowan, J.M.: *The Biomarker Guide. Biomarkers and Isotopes in the Petroleum Exploration and Earth History*, 2nd edn. Cambridge University Press, New York (2005)
2. Youde X.: Geochemistry of severely biodegraded oils in the Carboniferous volcanic reservoir of the Chepaizi Uplift, Junggar Basin, NW China. *Energy Explor. Exploit.*, 1–21 (2018)
3. Xiong, C.: Biodegradation of tricyclic terpanes in crude oils from the Bohai Bay Basin. *Org. Geochem.* **101**, 11–21 (2016)
4. Wenger, L.M.: Multiple controls on petroleum biodegradation and impact on oil quality. *SPE Reserv. Eval. Eng.* **5**, 375–383 (2002)



Detailed Hydrocarbon Analysis of Reservoir Fluids of Some Oil Fields of Upper Assam Basin (India)

Joyshree Barman, Subrata Borgohain Gogoi, and Debasish Konwar

Abstract

This study is an attempt to understand the role played by different formation water and crude oil samples in chemical enhanced oil recovery. The study pertains to the characterization of these samples in Agilent Gas Chromatography-Mass Spectrometry in order to determine the organics. The organics were further analysed in the library database of the National Institute Standards and Technology, to identify saturated and unsaturated compounds, organic alcohols and carboxylic functional groups in hydrocarbons. The presence of naphthenes and aromatics was also detected. Crude oil samples showed the presence of saturated and unsaturated hydrocarbons, with a predominance of –OH and –COOH functional groups in the hydrocarbons. While the formation water samples showed the presence of unsaturated hydrocarbons and hydrocarbons containing the –OH functional group with the predominance of saturated hydrocarbons. The presence of –COOH in the reservoir fluids, during the alkaline enhanced oil recovery, leads to the formation of in situ surfactant. The presence of –OH in the reservoir fluids leads to the reduction of wettability between the porous media and the oleic phase. The total acid number of the crude oil increases due to the presence of naphthenic acid, which is formed by the

reaction of naphthenes with the –COOH group. The predominance of –OH and –COOH functional groups in crude oil samples enhances the release of more oil from the negatively charged clay surfaces of the Upper Assam Basin.

Keywords

Reservoir fluids • Characterization • GC-MS EOR

Nomenclature

CO	Crude oil
FW	Formation water
RF	Reservoir fluid
E & P	Exploration and Production
NIST	National Institute of Standards and Technology
M.W.	Molecular weight
GC-MS	Gas Chromatography-Mass Spectrometry

1 Introduction

The crude oil (CO) and formation water (FW) were separated, and detailed characterizations of the hydrocarbon types were studied under Agilent Gas Chromatography-Mass Spectrometry. The importance of the study is focused in line with application of reservoir fluids data for EOR application [1, 2]. The –OH of formation water competes for the H from crude oil functional groups (–COOH), effectively breaking the hydrogen linkages that bound the oil to the clay. This means that if the formation water contains a large number of –OH, or high pH, the polar crude components might release more oil from the clay surfaces, which are mostly negatively charged leading to EOR [3]. The carboxylic acid components (–COOH) of crude oils are believed to be largely responsible for oil acidity, which is desirable for alkaline EOR [4]. The alkali generates in situ

J. Barman · S. B. Gogoi (✉) · D. Konwar
Department of Petroleum Technology, Dibrugarh University,
Dibrugarh, Assam 786004, India
e-mail: subrata@dbru.ac.in

J. Barman
e-mail: rs_joyshreebarman@dbru.ac.in

D. Konwar
e-mail: jrf_debasish@dbru.ac.in

surfactant by a reaction between the alkali and naphthenic acids, which also encourages alkaline EOR [5–8].

2 Materials and Methods

2.1 Materials

Table 1 showed the materials used for the study.

2.2 Methods

2.2.1 Separation of FW from CO by Gravity and Chemical Separation Methods

The CO and FW are separated from the RFs shown in Table 1 in a separating funnel, by adding 2–3 drops of de-oiler to RFs and shaking vigorously for half an hour and were then kept undisturbed for two days. FW separated from CO was carefully drained out from the separating funnel into a beaker without draining out the CO. Two or three pieces of CaCl_2 were added to the remaining CO and kept inside the water bath at a constant temperature of more than 60 °C. The setup was left for one day to ensure complete separation of FW from CO. After that, the separated FW was collected into a beaker.

2.2.2 GC-MS Experiments

Sample Preparation for GC-MS

The organic components in CO and FW were identified by GC-MS. The samples were prepared by dissolving in ethyl

acetate ($\text{C}_2\text{H}_5\text{COOCH}_3$) solvent until the solution was colourless.

Standard Reference Database Analysis in GC-MS

The prepared solution was then injected to the GC and GC peaks were obtained with retention time, the peaks were further characterized by the NIST standard reference database (library data) in the Agilent GC-7820A and Agilent MS 5920 [9].

3 Results

3.1 Organic Components Identified in FW-1, FW-2 and FW-3

The results of GC-MS are shown in Fig. 1. The identified peaks were further characterized by the NIST standard reference database from the Agilent Library data. Peak 1 of FW-1 is shown in (b) where Pentadecane, 2,6,10,14-trimethyl- is identified, indicating the presence of a paraffinic component. Peak 1 (FW-2) and peak 2 (FW-2) of FW-2 are shown in (d) and (e). Similarly, the peak 1 (FW-2) and peak 2 (FW-2) were characterized by the NIST standard reference database and the presence of Oxime-, methoxy-phenyl and Pentatriacontene, respectively, was highlighted. Peak 1 (FW-3) and peak 2 (FW-3) of FW-3 are also shown in (g) and (h) respectively. The peak 1 (FW-3) and peak 2 (FW-3) were characterized and the presence of Pentadecane, 2,6,10,14-trimethyl- and Octadecane, 3-ethyl-5-(2-ethylbutyl) was observed, respectively.

Table 1 Materials and instruments used

SN	Items	Specifications
1	RF-1	36° API
2	RF-2	22° API
3	RF-3	27° API
4	GC-MS	Make: Agilent, USA; Model: Agilent GC 7820 A and Agilent MS
5	Water bath	Make: Cannon Instrument Company, USA; Model: CT-500, Series II
6	Ethyl acetate ($\text{C}_2\text{H}_5\text{COOCH}_3$)	M.W. = 88.1 g/mol; Biochem Life Sciences, New Delhi
7	De-oiler	Oil E and P industries
8	Calcium chloride (CaCl_2)	M.W. = 110.98 mg/mol; Merck Specialties Pvt. Ltd., Mumbai

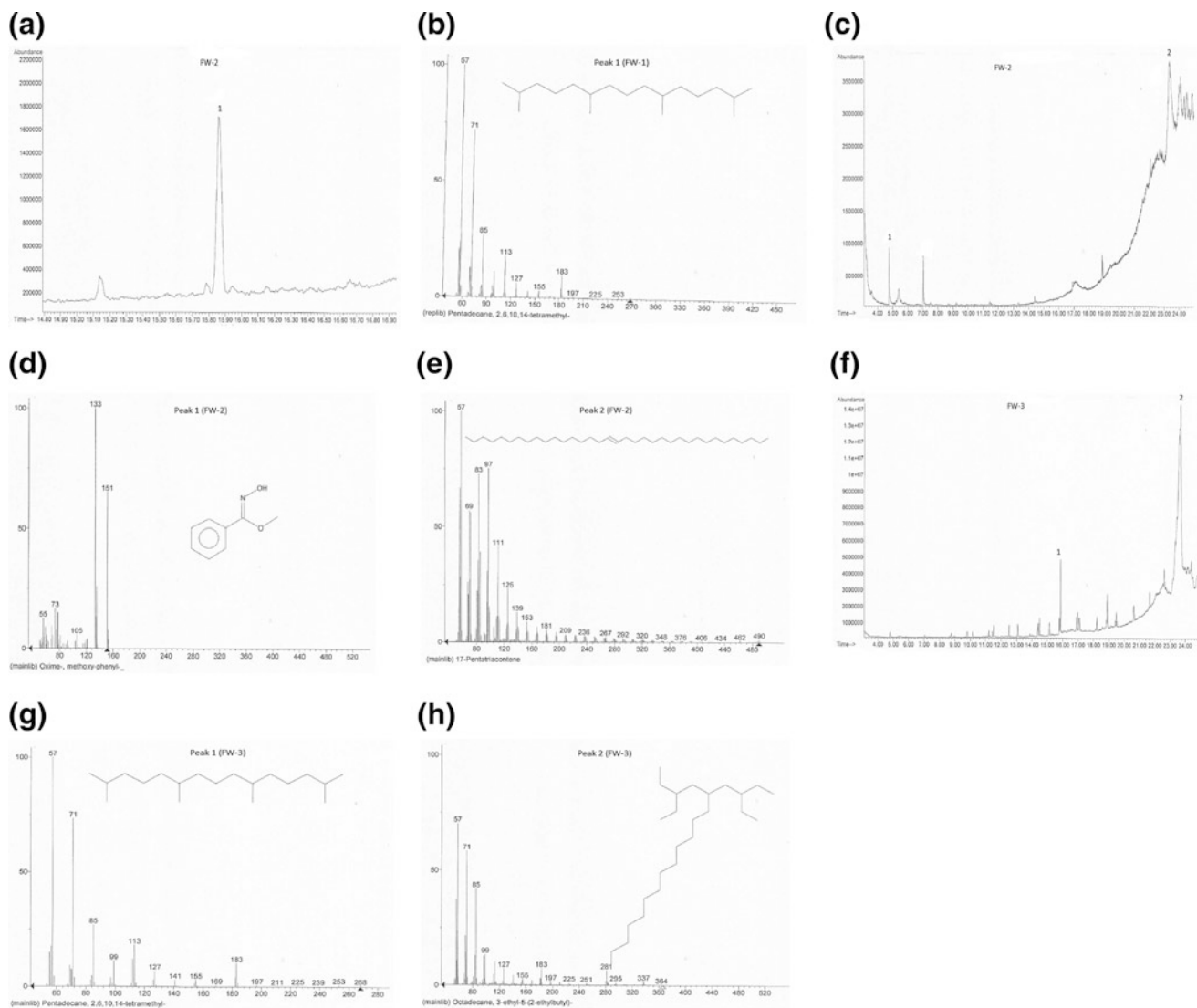


Fig. 1 GC finger prints of FW-1 (a); Pentadecane, 2,6,10,14-trimethyl- identified for peak1 of FW-1 (b); GC finger prints of FW-2 (c); Oxime-, methoxy-phenyl identified for peak 1 of FW-2 (d); 17-Pentatriacontene identified for peak 2 of FW-2 (e); GC finger

prints of FW-3 (f); Pentadecane, 2,6,10,14-trimethyl- identified for peak 1 of FW-3 (g); Octadecane, 3-ethyl-5-(2-ethylbutyl) for peak 2 of FW-3 (h)

3.2 Organic Components Identified in CO-1, CO-2 and CO-3

The results of GC-MS of crude oil samples are shown in Fig. 2. (i), (m), and (r) show CO-1, CO-2 and CO-3, respectively. The peaks found in CO's are identified by NIST library data. The identified peak 1 (CO-1), peak 2

(CO-1) and peak 3 (CO-1) of CO-1 are shown in (j), (k) and (l) respectively. Similarly, for CO-2, the identified peak 1 (CO-2), peak 2 (CO-2), peak 3(CO-2) and peak 4 (CO-2) are shown in (n), (o), (p) and (q), while, for CO-3, the identified peak 1 (CO-3), peak 2 (CO-3), peak 3 (CO-3) and peak 4 (CO-3) are shown in (s), (t), (u) and (v), respectively. The identified peaks are shown in Table 2.

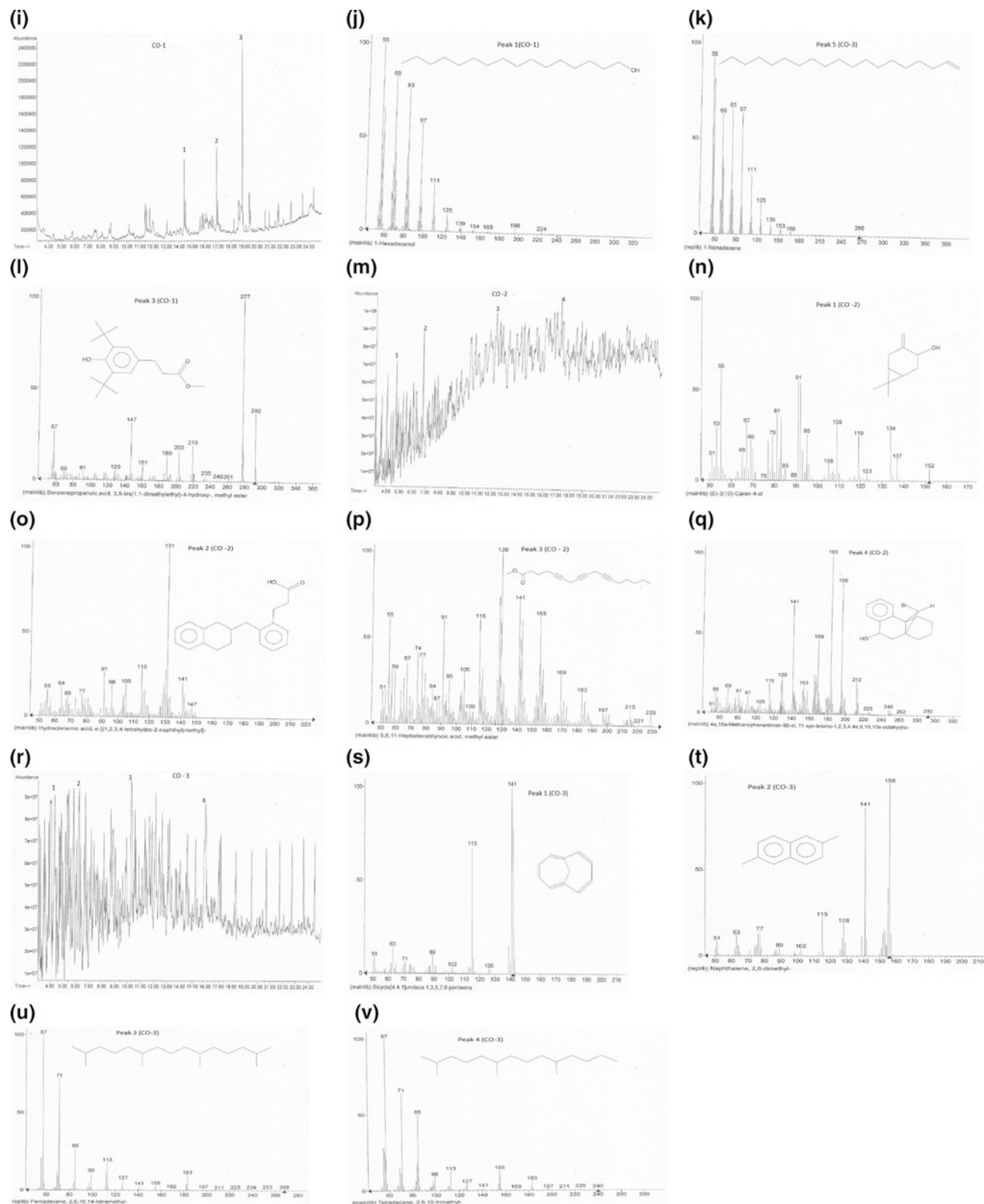


Fig. 2 GC finger prints of CO-1 (**i**); 1-Hexadecanol identified for peak 1 of CO-1 (**j**); Nonadecene identified for peak 2 of CO-1 (**k**); Benzene propanoic acid, 3, 5-bis (1,1-dimethylethyl)-4-hydroxyl-, methyl ester identified for peak 3 of CO-1 (**l**); GC finger prints of CO-2 (**m**); -3-(10)-Caren-4-ol identified for peak 1 of CO-2 (**n**); Hydrocinnamic acid, O-[1,2,3,4-tetrahydro-2-naphthyl] methyl identified for peak 2 of CO-2 (**o**); 5,8,11-Heptadecatrienoic acid, methyl ester

identified for peak 3 of CO-2 (**p**); 4a, 10a-Methanophenanthren-9β-ol, 11-syn-bromo-1,2,3,4,4a,9,10,10a-octahydro- identified for peak 4 of CO-2 (**q**); GC finger prints of CO-3 (**r**); Bicyclo [4.4.1] undeca-1, 3, 5, 7, 9-pentaene identified for peak 1 of CO-3 (**s**); Naphthalene, 2, 6-dimethyl- identified for peak 2 of CO-3 (**t**); Pentadecane, 2,6,10,14-tetramethyl- identified for peak 3 of CO-3 (**u**); Tetradecane, 2,6,10-trimethyl- identified for peak 4 of CO-3 (**v**)

Table 2 Identified organics in CO-1, CO-2 and CO-3

S. N.	CO	Peaks	Identified components
1	CO-1	Peak 1	1-Hexadecanol
		Peak 2	1-Nonadecene
		Peak 3	Benzenepropanoic acid, 3, 5-bis (1,1-dimethylethyl)-4-hydroxyl-, methyl ester
2	CO-2	Peak 1	-3-(10)-Caren-4-ol probable
		Peak 2	Hydrocinnamic acid, O-[1,2,3,4-tetrahydro-2-naphthyl)methyl
		Peak 3	5, 8, 11-Heptadecatrienoic acid, methyl ester
		Peak 4	4a, 10a-Methanophenanthren-9β-ol, 11-syn-bromo-1,2,3,4,4a,9,10,10a-octahydro-
3	CO-3	Peak 1	Bicyclo [4.4.1] undeca-1, 3, 5, 7, 9-pentaene
		Peak 2	Naphthalene, 2, 6-dimethyl-
		Peak 3	Pentadecane, 2,6,10,14-tetramethyl-
		Peak 4	Tetradecane, 2,6,10-trimethyl-

4 Discussions

Crude oil samples showed the presence of saturated and unsaturated hydrocarbons with the predominance of -OH and -COOH groups, especially naphthenic acids, indicating the formation of in situ surfactants when alkali/alkalis were introduced as an EOR slug or as a co-surfactant in surfactant alkali EOR or in Alkaline-Surfactant-Polymer EOR processes. The formation water samples showed the presence of phenols, naphthenic and aromatic components. The predominance of -OH and -COOH functional groups, in crude oil samples, releases more oil from the negatively charged clay surfaces under study.

5 Conclusions

The study conducted in GC-MS and supported by the NIST library database for crude oil and formation water samples concludes that Chemical EOR processes can be successfully implemented in the reservoirs of the Upper Assam Basin.

References

- Strand, S., Standnes, D.C., Austad, T.: New wettability test for chalk based on chromatographic separation of SCN- and SO₄²⁻. *J. Pet. Sci. Eng.* **52** (2006)
- Austad, T., Sharifpanahi, S.F., Strand, S., Black, C.J.J., Webb, C.J.J.: Conditions for a Low-Salinity Enhanced Oil Recovery (EOR) Effect in Carbonate Oil Reservoirs. *Energy Fuels* **26**(1), 569–575 (2012)
- <http://www.envsci.rutgers.edu/~gimenez/SoilsandWater07/Laboratories/Lab6.pdf>
- Rikka, P., Spectrometric identification of naphthenic acids isolated from crude oil. Master thesis of Texas State University-San Marcos (2007)
- Kumar, A., Mandal, A.: Characterization of rock-fluid and fluid-fluid interactions in presence of a family of synthesized zwitterionic surfactants for application in enhanced oil recovery. *Colloids Surf. A* **549**, 1–12 (2018)
- Mandal, A.: Chemical flood enhanced oil recovery: a review. *Int. J. Oil, Gas Coal Technol.* **9**(3), 241–264 (2015)
- Bera, A., Ojha, K., Mandal, A., Kumar, T.: Interfacial tension and phase behavior of surfactant brine oil system. *Coll. Surf. A: Physicochem. Eng. Aspects* **383**, 114–119 (2011)
- Barman, J., Gogoi, S.B., Sarmah, S.: Characterization of oil field formation water and its effect on tap water dilution for eco-friendly environment. *Int. J. Eng. Technol. Sci. Res.* **4**(8), 309–323 (2017)
- NIST library data from Agilent GC-7820A and Agilent MS 5920: 2007 Version

Geochemical Assessment of the Telisa Shale Gas Reservoir: A Case Study from the South Sumatra Basin, Indonesia

Abdul Haris, Aldo Hutagalung, and Agus Riyanto

Abstract

The geochemical assessment of a shale gas reservoir in the Telisa Formation in the South Sumatra Basin was carried out to identify the potential shale gas distribution. The objective of this paper is to characterize the core sample by analyzing the total organic carbon (TOC) content, kerogen type and thermal maturity of shale gas layers in terms of vertical resolution based on log data from four well log data. In addition, a seismic interpretation approach including a seismic attribute analysis and an inverted acoustic impedance is explored to spatially distribute the shale gas potential based on TOC values. Geochemical assessment of the Telisa shale gas reservoir revealed that the organic richness of the reservoir is classified as fair to good in quality. Kerogen type in the reservoir is considered a mixture of type II/III (oil/gas prone) to type III (gas prone). In terms of maturity, the Telisa shale gas reservoir is categorized as “in a mature stage”, representing an oil window up to a wet gas window. The prospective reservoir distribution is indicated by a shale lithology characterized by a high acoustic impedance range of 20,000–24,000 ft/s g/cc. In contrast, the organic richness of the Telisa shale reservoir is classified as “of fair quality”, with TOC in the range of 0.75–1 wt%.

Keywords

Geochemical assessment • Kerogen • TOC
South Sumatra basin • Indonesia

A. Haris (✉) · A. Riyanto
Geology and Geophysics Study Program, FMIPA Universitas
Indonesia, Depok, Indonesia
e-mail: abdharis@sci.ui.ac.id

A. Hutagalung
Reservoir Geophysics Program, Department of Physics, FMIPA
Universitas Indonesia, Depok, Indonesia

1 Introduction

The South Sumatra Basin province in Indonesia produces a large amount of both oil and gas each year. The province, as illustrated in Fig. 1, is a Tertiary basin overlying igneous and metamorphic rock, and is dominated by a clastic and carbonate sedimentary rock. For the Eocene up to the lower Oligocene, the sedimentary layer is composed of lacustrine shale of the Lahat/Lemat Formation. This laminated layer is overlain by lacustrine and deltaic coaly shale of the Talang Akar Formation, deposited during the Oligocene up to the lower Miocene [1]. The Lahat and Talang Akar Formations are believed to be the source rock in the South Sumatra Basin, and in some areas, are located in deep water [2]. However, the younger Baturaja and Gumai Formations also possibly serve as source rock [3].

The identified hydrocarbon potential in the South Sumatra Basin is predicted at around 4.3 Billion Barrel of Oil Equivalent (BBOE) [4], with the exploration cycle still continuing [5]. In this paper, we performed the geochemical assessment to characterize the core sample by analyzing the total organic carbon (TOC) content, kerogen type and thermal maturity of shale gas layers in terms of vertical resolution based on log data from four wells.

2 Method

The unconventional shale gas system in this study area indicates that the Telisa Formation is shale rock, which serves as both a source rock and a reservoir rock. Therefore, an accurate geochemical analysis and evaluation of this shale gas system is essential [6].

In the present study, we performed a geochemical assessment on the core sample by analyzing the total organic carbon (TOC) content, kerogen type and thermal maturity of shale gas layers in terms of vertical resolution based on log data from four well log data. Further, the vertical assessment

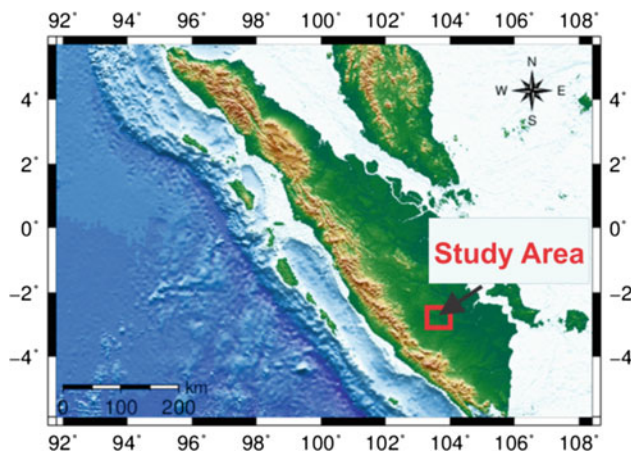


Fig. 1 Location of the study area in South Sumatra province

is combined by a lateral assessment, which is derived from seismic data. The most important characteristics of any shale gas reservoir are the quality and the quantity of organic richness contained in the deposited shale. This is typically assessed in terms of TOC and hydrogen content, which, when combined with thermal maturity data, are key to identifying the shale gas potential [7].

3 Results and Discussions

The geochemical assessment of shale core samples—obtained via core cutting for each well—included measurements of TOC, mineralogy, maximum temperature (T_{max}), and kerogen type. The following results are shown in different colors for each of the four wells, with green

representing Well-1, orange Well-2, yellow Well-3, and brown Well-4. Geographically, Well-1 is located some distance from Well-2, Well-3 and Well-4, which are clustered close to each other. Figure 2a shows the organic richness of the Telisa Formation based on data from the four wells, with quality ranging from fair to good.

In order to classify the prospect potential of the Telisa Formation in terms of hydrocarbon generation, a maturity level analysis was carried out by cross-plotting Ro versus T_{max} values. The potential value of the Telisa Formation greatly depends on whether it can be classified into an oil window, wet gas window, or dry gas window, and whether it is immature, mature, or over mature. Based on the obtained Ro values, the Telisa Formation can be classified into the range of an oil window to a wet gas window, with T_{max} analysis indicating maturity levels ranging from immature to mature. Figure 2b shows the maturity range of the Telisa Formation as represented by Ro as a function of depth. This figure shows that the top marker of Top 1 is defined at a depth of 8021 ft, Top 2 at 8250 ft, Top 3 at 8701 ft, and Top 4 at a depth of 8641 ft. In general, it can be seen that most of the data indicate an oil window at a depth of 8288 ft, with only a few values associated with a wet gas window at a depth of 10,720 ft.

Figure 3 displays the AI map of the upper Telisa Formation. The area indicated by the arrow represents a shale lithology associated with a high acoustic impedance range of 20,000–24,000 ft/s g/cc. In contrast, the shale lithology distribution also presents a low TOC range of between 0.75 and 1 wt%, as shown in Fig. 4. Higher TOC values correspond to a lower acoustic impedance, because a lithology with a higher organic material content is softer compared to

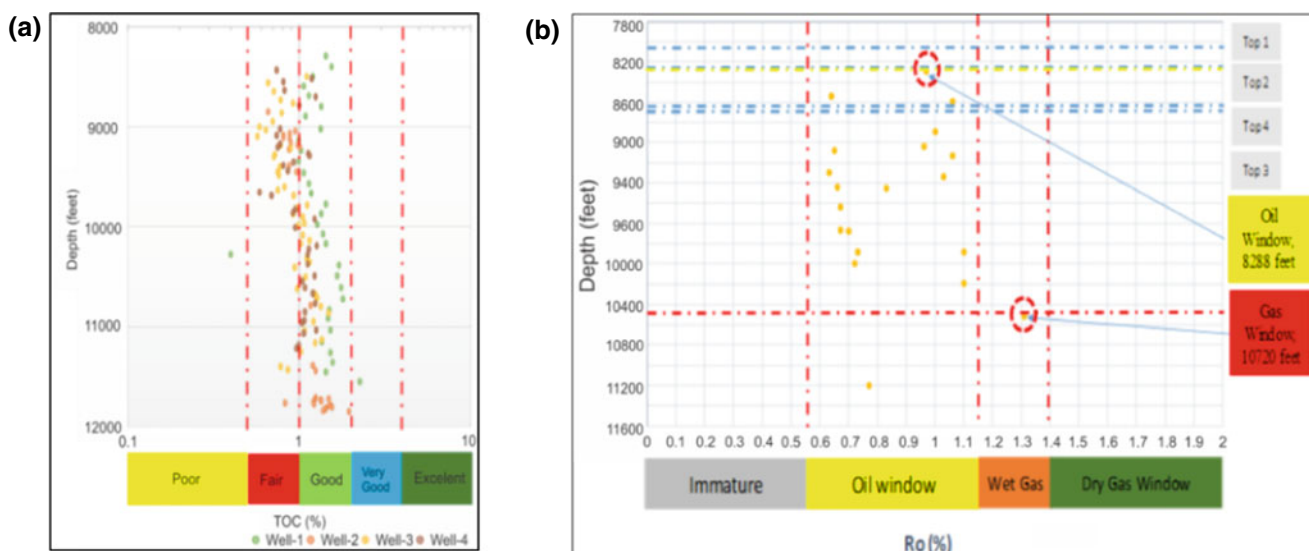


Fig. 2 Geochemical analysis of the organic shale Telisa Formation: **a** organic richness (TOC), and **b** maturity level in terms of vitrinite reflectance (Ro) as a function of depth

Fig. 3 Shale lithology distribution in terms of inverted acoustic impedance

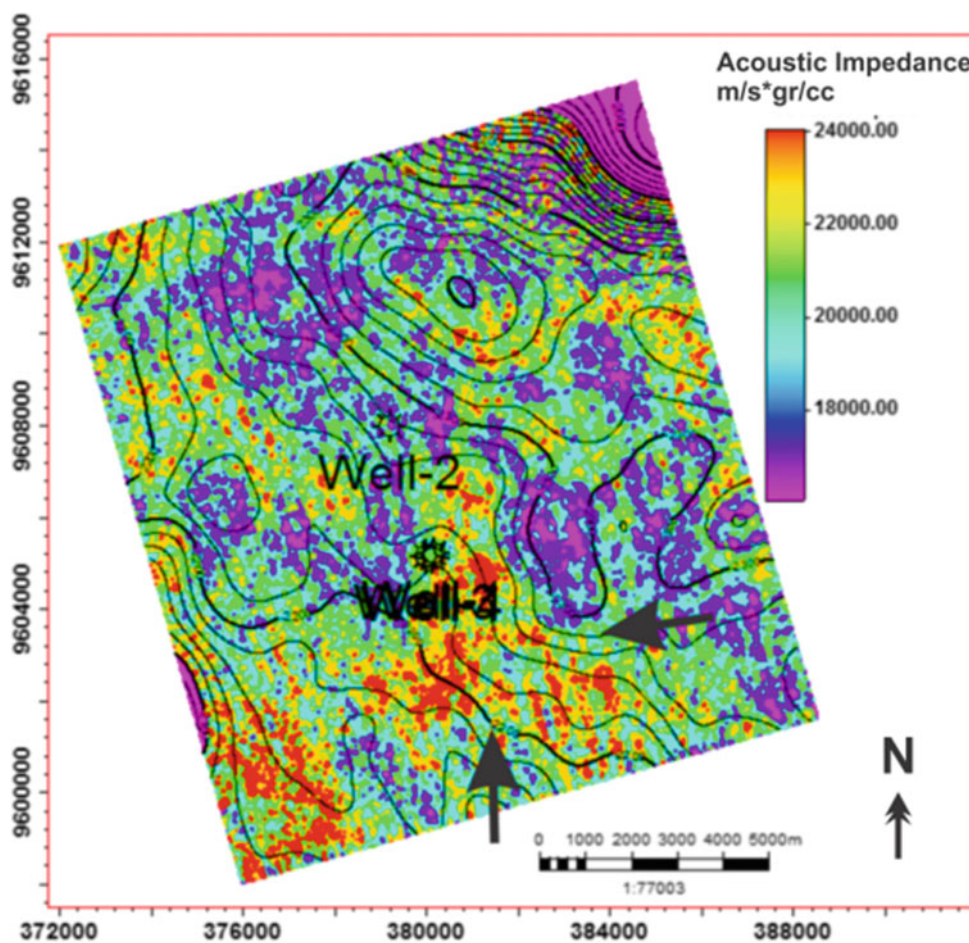
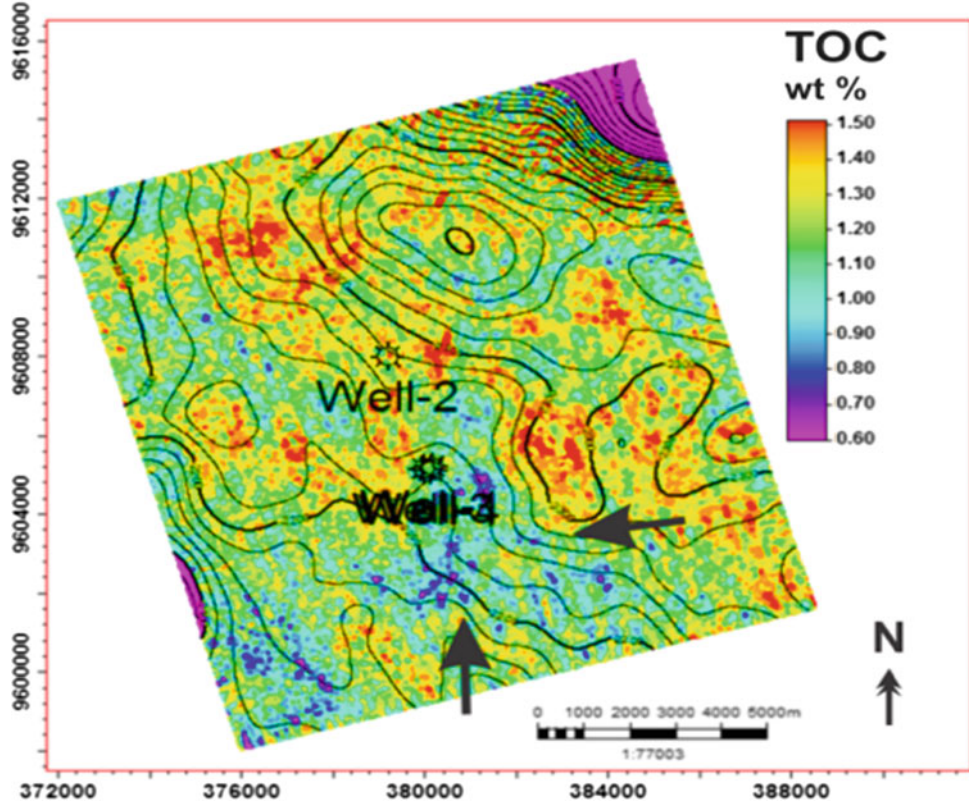


Fig. 4 Sweet spot of shale gas distribution in terms of TOC



surrounding rock. This figure indicates that the organic richness of the Telisa Formation can be classified as fair in quality across the entire study area.

4 Conclusions

Geochemical assessment was performed to identify the sweet spot of the shale gas reservoir within the Telisa Formation in the South Sumatra Basin, based on shale organic richness (TOC), level of maturity (Ro%), kerogen type, and gas content. Analysis of the organic richness of the Telisa shale Formation revealed quality levels ranging from fair to good. Kerogen within the Telisa Formation can be classified as type III, dominated by gas-prone kerogen but with a small part characterized by mixed oil and gas, with a high maturity level. The shale gas sweet spot was indicated by an AI range of 20,000–24,000 ft/s g/cc. In contrast, the sweet spot distribution reflects low TOC values ranging from 0.75–1 wt%, representing fair kerogen quality.

References

1. Rashid, H., Sosrowidjojo, I.B., Widiarto, F.X.: Musi platform and Palembang high: a new look at the petroleum system. In: Proceedings of the Twenty Sixth Annual Convention of the Indonesian Petroleum Association, Jakarta, May, pp. 265–276 (1998)
2. Argakoesoemah, R.M.I., Kamal, A.: Ancient Talang Akar deepwater sediments in South Sumatra basin: a new exploration play. In: Proceedings, Deepwater and Frontier Exploration in Asia and Australasia Symposium, Jakarta, p. DFE04-OR-009, Dec 2004
3. Sarjono, S., Sardjito: Hydrocarbon source rock identification in the South Palembang sub-basin. In: Proceedings of the Eighteenth Annual Convention of the Indonesian Petroleum Association, Jakarta, pp. 427–467, Oct 1989
4. Klett, T.R., Schmoker, J.W., Ahlbrandt, T.S.: Assessment hierarchy and initial province ranking. U.S. Geological Survey World Energy Assessment 2000—Description and Results. U.S. Geological Survey Digital Data Series—DDS-60, Chapter RH (2000)
5. Zeliff, C.W., Trollope, S.W., Maulana, E., Exploration cycles in the corridor block, South Sumatra. In: Proceedings of the Fourteenth Annual Convention of the Indonesian Petroleum Association, Jakarta, pp. 379–400, Oct 1985
6. Haris, A., Marbun, M.B., Bachtiar, A., Riyanto, A.: Geochemical analysis of shale gas reservoir based on well log and 3D seismic data in Pematang Formation, Central Sumatra Basin. In: Proceedings of the 2nd International Symposium on Current Progress in Mathematics and Sciences 2016, Depok. American Institute of Physics Conference Proceedings. 1862.1, 030176, pp. 1–4, 1–2 Nov 2017. <https://doi.org/10.1063/1.4991280>
7. Jarvie, D.M.: Geochemical assessment of unconventional shale gas resource systems. In: Rezaee, R. (ed.), Fundamentals of Gas Shale Reservoirs, pp. 47–69. Wiley, New York (2015). <https://doi.org/10.1002/9781119039228.ch3>

Part VI

Non-Conventional Energy Resources



Utilization of Abandoned Oil and Gas Wells for Geothermal Energy Production in Pakistan

Asif Mehmood, Jun Yao, Dong Yan Fan, Kelvin Bongole, and Ubedullah Ansari

Abstract

Geothermal energy is able to provide a cheap, safe and reliable approach to fulfill the energy requirement. Hot dry rock (HDR) geothermal energy can generate large scale energy on durable basis. To utilize this energy, enhanced geothermal systems (EGS) are used which evolve energy from deep seated (3–7 km) geothermal resources. The major cost in this type of power plant is that of drilling a bore-hole. The aim of this study is to utilize the already-drilled exploratory, dry and abandoned oil and gas wells of Pakistan. About 60% of total wells drilled in Pakistan are non-producing. Analyses of different zones are marked according to thermal range distribution, whereas the binary system power plant can be built on commercial scale. The current study also demonstrates the power-production system for economical electricity generation at three diverse source temperatures and concludes that a 12 in. borehole heat exchanger, at a depth of 3 km, can extract suitable energy to run a 3.2 MW turbine. The current study not only cures all the loss of petroleum industry but also proposes a method to overcome the required energy demands as well.

Keywords

Geothermal energy • Abandoned oil and gas wells • Hot dry rock

1 Introduction

The hot dry rock geothermal resources are much deeper than hydrothermal resources. Hot dry rock energy comes from a relatively water-free hot rock found at a depth of about 3000 m or more beneath the earth surface. One way to

A. Mehmood (✉) · J. Yao · D. Y. Fan · K. Bongole · U. Ansari
School of Petroleum Engineering, China University of Petroleum (East China), Qingdao, 266580, China
e-mail: asifupc@yahoo.com

extract the energy is by circulating cool water through man-made fractures in the hot dry rock. Cool water absorbs heat from the rock, which then can be extracted from the water at the surface for power generation, and the utilized cooled water is then reinjected through the fractures to pick up more heat, creating a closed-loop system [1].

Pakistan has several hydro-geothermal resources which are, nonetheless, difficult to exploit economically because they are not located near the urban areas [1]. As hot dry rock geothermal energy potential of Pakistan is high enough to be utilized commercially and economically [2], the current research focuses on the reuse of dry oil and gas wells in Pakistan, which could be utilized for the extraction of geothermal energy from HDR resources on an everlasting basis. Suitable planning is required to take this proposal which not only recovers the cost of the well from the petroleum industry but also minimizes the time and capital requirements of the HDR exploration project. An extensive temperature range (393–643 K) exists in different areas of Pakistan, subject to the geological setting of rocks [3]. Till date, various EGS projects have been initiated across the world, for instance in America, Japan, Australia, and Switzerland but no work has so far been carried out to utilize the HDR source potential of Pakistan [4].

Figure 1a shows the temperature distribution of different regions of Pakistan. Figure 1b is a satellite image of Pakistan on which the yellow circles show the drilled wells in different regions of Pakistan, while Fig. 1c reveals the exact location of maximum temperature spots and the clusters of wells. The data of these exploratory oil and gas wells are excellent research materials for the prediction of geothermal potential. Moreover, the HDR predictions in the western section of Pakistan were also confirmed by aeromagnetic surveys [1].

B1, B2 and B3 are base lines used to align the map with the satellite image by projecting upper, central, and bottom bases. P1, P2, P3 and P4 are the positioning configurations from map to satellite image for thermal fields 300–301 K, 301–302 K, 302–303 K, and 303–304 K, respectively. Statistical analysis of different areas projected over temperature fields of Pakistan are shown in Table 1.

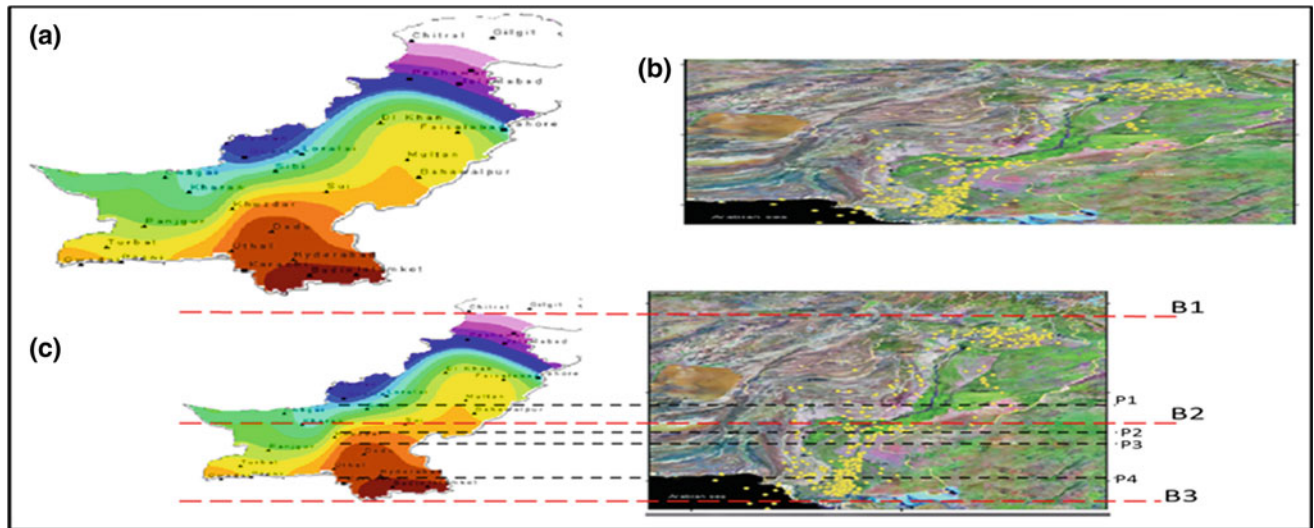


Fig. 1 Imaginary lines aligned on the map of Pakistan to demonstrate the division of oil and gas wells enclosed in various thermal regions

Table 1 Analytical statistics for different areas projected over the temperature fields of Pakistan

	Number of oil fields	Static areal expand	Well density in percentile	Thermal range
Area F B1-P1	62	30	<26	
Area E P1-B2	14	15	27	
Area D B2-P2	8	15	28	
Area C P2-P3	9	15	29	
Area B P3-P4	24	50	30	
Area A P4-B3	17	100	31	

The analysis indicates that Area A possesses nominal areal size but it is the one with the biggest number of wells. On the other hand, Area F which is spread on maximum areal extent possesses the lowest number of wells among all areas. Indeed, the second highest number of oil and gas wells falls in Area B. Actually, the concept of this research suggests that there is no need to allocate more budget for drilling the new wells because the already-existing wells can be utilized, especially that the area with maximum number of wells, Area A, lies in the maximum thermal magnitude range. The subsurface temperature range in Pakistan is naturally set in ascending order from north to south. Therefore, the installation of the suggested project has a more promising rate of success in the southern section of Pakistan.

2 HDR Geothermal Energy Extraction from Abandoned Oil and Gas Wells

With the introduction of the enhanced geothermal system (EGS) and borehole heat exchanger (BHE), it is now feasible to utilize deep geothermal energy. Therefore, this study presents the concept of using abandoned oil and gas wells for

geothermal energy production, which reduces the drilling cost and makes HDR resources more viable. There are large numbers of non-producing wells across the world [4]. However, in Pakistan, there are 1567 exploratory wells out of which 450 are abandoned and possess an estimated temperature range of 398–448 K [2]. Thus, an efficient and reliable technology is required to extract deeper geothermal energy. We followed the concept of using the double pipe heat exchanger developed by Davis and Michaelides [5]. In this model, organic liquid was used to convert the well to an annular heat exchanger.

A pipe designed with insulation is installed in the bore-hole as shown in Fig. 2. Organic fluid is injected down the annulus, as it flows downward it conducts heat from hot dry rocks in the wellbore vicinity, and the pressure of the fluid also increases due to gravity. The fluid then returns back towards the surface through the pipe, as it reaches the wellhead, the fluid's pressure decreases and the fluid converts into vapor form. These vapors can now be used as an energy source to run turbines. The factors influencing power-generation include pipe outer and inner diameters, injection pressure, vapor velocity, subsurface temperature and mass flow in the well.

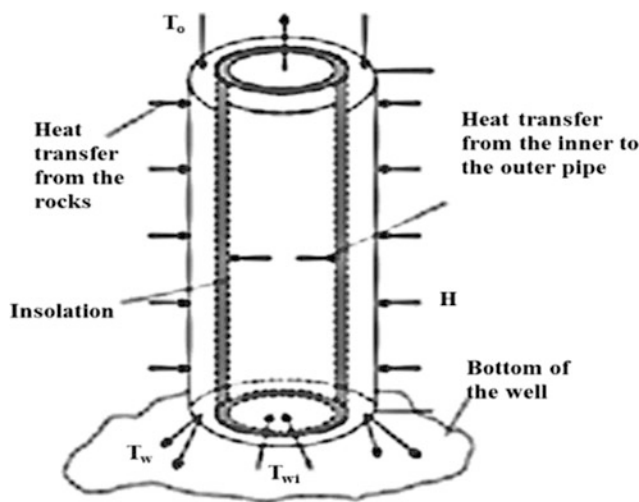


Fig. 2 Schematic diagram of the double-pipe heat exchanger for the use of deep well

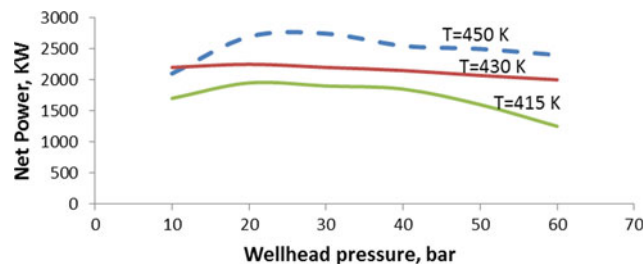


Fig. 3 Net power produced by an outer diameter (12") well as a function of organic fluid injection pressure and bottom-hole temperature [5]

According to Fig. 3, power production is dependent on the rate of heat exchange which is the function of fluid injection pressure and subsurface temperature. Thus, power is inversely dependent on wellbore temperature because of the difference of temperature flowing in and out. A 12 in. outer diameter well can give up to 2.5 MW of electricity on average and 3.2 MW at optimum conditions [5]. Indeed, at

450 K bottom hole temperature and pressure blow 10 bar, sudden power drop occurs due to blockage of well outflow.

3 Conclusions

The deep seated dry rocks are approached for HDR geothermal energy. These hot dry rocks get thermal energy from the earth's internal heat. The current study concludes that HDR geothermal energy can provide an alternate solution to defeat the energy crisis of Pakistan. The estimated resources are more than enough to balance the energy supply and demand. Moreover, these are cheaper, efficient and long-term energy resources. The installation of a binary system power plant is suggested, where a double pipe heat exchanger can produce profitable amounts of energy. The idea of using pre-drilled oil and gas wells for the extraction of geothermal energy can minimize the drilling cost. The access to the sub surface heat energy is provided through abandoned wells across the country. It is also suggested to launch the power production project in the southern section of Pakistan as it hosts a large number of abandoned wells in the region (A) with the highest temperature in the country.

References

1. Zaigham, N.A.: Geothermal energy resources of Pakistan. In: Proceedings of the World Geothermal Congress, Antalya, Turkey (2005)
2. Mehmood, A.: Geothermal energy potential of pakistan on the basis of abandoned oil and gas wells. In: J. Pet. Environ. Biotechnol. **8**(3) (2017)
3. Tahirkheli, R.K.: Geology of the Himalaya, Karakorum and hindukush in Pakistan. Geol. Bull. Univ. Peshawar **15**, 1–51 (1982)
4. Mehmood, A.: Future electricity production from geothermal resources using oil and gas wells. Open J. Yangtze Gas Oil **2**, 191–200 (2017)
5. Davis, A.P.: Geothermal power production from abandoned oil wells. Energy **34**(7), 866–872 (2009)



Determination of Deliverability Equation and IPR for Siba Gas Condensate Reservoir in (Iraq)—Case Study

Ghazwan Noori Saad Jreou

Abstract

A well deliverability equation is important to measure production capabilities under certain conditions of reservoirs' and bottom hole flowing pressures. Therefore, this work offered a gas deliverability equation for the Siba Gas Condensate Field in Iraq, particularly for the Yamama reservoir formation. The equation was obtained according to the methods of Houpert and Rawlins-Schellhardt for pressure-squared and pseudo pressure techniques. Results revealed that despite the lack of relevant information, the obtained deliverability equation was acceptable with mean absolute percentage errors (MAPEs) equal to 0.145053, 0.054328, 0.050463, and 0.046233, relative to available measured data. A generalized inflow performance relationship (IPR) from the literature was chosen for verification and comparison. Good and acceptable results were obtained with MAPEs equal to 0.001102726 and 0.001052612. A future IPR was derived to predict the flow behavior of the target reservoir production with a range of reservoir pressures no less than the current reservoir pressure of 8593 psia. The prediction was aimed at avoiding the loss of a significant amount of condensate in the reservoir because its measured dew point pressure is equal to 9021.35 psia. The constructed future IPR was compared with the generalized future IPR, and both showed good agreement with a MAPE equal to 5.234%.

Keywords

Gas condensate • Gas well deliverability • Siba gas condensate field—Iraq • IPR gas condensate • Gas condensate deliverability performance

G. N. S. Jreou (✉)

College of Engineering, University of Kufa, Kufa, Iraq
e-mail: Ghazwan.jreou@uokufa.edu.iq

1 Introduction

Despite their complex formation flow and thermodynamic behavior [1–8], gas condensate reservoirs as sources of hydrocarbons were recognized during the last decades of the previous century. Gas condensate reservoirs are classified as one type of gas reservoirs. Most gas condensate reservoirs are in a single phase at the time of discovery, but this state could no longer remain as it is. The lifetime of reservoirs can be changed under certain conditions of production, along with changes in pressure and/or temperature. These changes lead to the formation of liquid condensate from natural gas, especially when pressure drops below the dew point pressure under reservoir conditions, this mechanism of condensation formation, known as retrogradation, results in the buildup of a liquid phase region around the wellbore that exerts inverse effects on the gas flowing into the wellbore by decreasing the effective gas permeability of porous media and then gas production.

In the present work a deliverability equation for a gas production well in the Siba Gas Condensate Field was developed, particularly in the Yamama reservoir formation. The inflow performance relationship (IPR) for this gas condensate well is also established. Therefore, this is the first attempt to construct and assess natural gas condensate wells of the Siba gas condensate field in Iraq.

2 Determination of Deliverability Equation for the Siba Gas Condensate Reservoir

Data were collected from the available information [9–16] generated by the flow-after-flow test from the Siba_1 well to derive the deliverability equation for the Siba Gas Condensate Field—Yamama formation reservoir. This basic test method uses all stabilized data. The field and well data are taken from those references.

Part I

The traditional **Rawlins and Schellhardt** [17, 18] analysis requires a logarithmic graph (pressure-squared difference versus flow rate) with the best fit straight line passing through data points. Therefore, the deliverability curve from this plot is applicable. The n value (deliverability exponent) determined from the reverse of the slope equal to 0.5793. The flow coefficient C can be determined, when the deliverability exponent is determined with a point taken on the straight-line plot. Thus, the flow coefficient is equal to 1.791637065 Mscf/(psia²). The final deliverability equation in pressure-squared form according to the **Rawlins–Schellhardt** analysis approach is as follows:

$$Q_g = 1.791637065(Pr^2 - Pwf^2)^{0.5793} \quad (1)$$

Pseudo pressures are used for data analysis, for which the same approach is adopted, but the differences in pseudo pressures are plotted versus the flow rate. C and n values were determined, which are equal to 1.001660157 Mscf/D/(mmppsi_a/cp) and 0.55367, respectively. The final deliverability equation in pseudo pressure form according to the **Rawlins–Schellhardt** analysis approach is as follows:

$$Q_g = 1.001660157(Pp(Pr) - Pp(Pwf))^{0.55368491} \quad (2)$$

Part II

The same tests data are used in the analysis based on the **Houperf** method and pressure-squared and pseudo pressure approaches are employed. The deliverability equation can be developed after determining the deliverability coefficient accordingly.

$$(Pr^2 - Pwf^2) = 0.0146 Q_g + 194.23 Q_g^2, \quad (3)$$

$$(Pp(Pr) - Pp(Pwf)) = 0.0995 Q_g + 931.75 Q_g^2 \quad (4)$$

2.1 Determination of AOFP for the Siba Gas Condensate Reservoir

The AOFP for the Siba Gas Condensate Reservoir is determined by allowing the BHFP to be equal to the atmospheric pressure (14.65 psia) for the current average reservoir pressure of 8593 psia. Then, both calculation methods are used.

The AOFPs calculated by the **Rawlins–Schellhardt** method are 64.7163 MMscf/D from Eq. 1 and 22.7653 MMscf/D from Eq. 2, whereas those calculated by the **Houperf** method are 61.657602 MMscf/D from Eq. 3 and 35.88843 MMscf/D from Eq. 4.

These results demonstrate the differences in the calculated AOFP values based on pressure-squared and pseudo pressure approaches. The differences are attributed to the following.

1. The **Rawlins–Schellhardt** and **Houperf** methods differ because unlike the former, the latter has a theoretical base in its derivation and is thus not as theoretically rigorous. Nevertheless, the latter remains widely used in the gas industry.
2. The variation in the calculated AOFP values comes from the methodology of each approach. In the pseudo pressure approach, the pseudo pressure term depends on gas viscosity and gas deviation factor; the same is not true for the pressure-squared approach.
3. The pressure ranges covered by the pseudo pressure approach are wider than those of the pressure-squared approach, which are suitable for low pressures.

3 Results

3.1 Determination of IPR for the Siba Gas Condensate Reservoir

The second steps of this work are to construct an IPR for the Siba Gas Condensate Field–Yamama reservoir formation and to check the validity of the obtained relation in comparison with other results published in the literature, such as the generalized IPR developed by Hazim Al-Attar and Suleiman Al-Zuhai [19].

The obtained IPR curves are appropriate and consistent with the Vogel global standard form of IPR equations. The deliverability calculations must be facilitated when developing an IPR curve. Therefore, a rewritten constructed curve of this work is presented to easily estimate the gas flow rate at a given BHFP, especially after the determination of the AOFP.

3.2 Verification of Constructed IPR

The constructed IPR based on the available data from well Siba_1 and the calculation techniques of **Rawlins and Schellhardt** and **Houperf** for the Siba Gas Condensate Field–Yamama reservoir formation is compared with the generalized and published IPR.

The comparison between the constructed IPR and the generalized IPR is conducted for the pseudo pressure approach only because it can cover a wider range of pressure than the pressure-squared approach and it gives good results up to 2000 psia. The generalized IPR published in the form of pseudo pressure is shown below.

$$Y = -0.7193 X^6 + 0.6221 X^5 + 0.3037 X^4 - 0.6108 X^3 + 0.0756 X^2 - 0.6712 X + 1.0006, \quad (5)$$

where

$$Y = q/q_{\max} \quad \text{and} \quad X = P_{pr}/P_{pwf}.$$

The statistical error indicators present convergence values between them. The constructed IPR based on the **Houpert technique** is better than that based on the **Rawlins–Schellhardt technique** in terms of the derivation concept and the methodology of the calculation technique. Parameters **a** and **b** incorporate the reservoir characteristics rather than the **n** and **C** parameters derived from the **Rawlins–Schellhardt plot**, which is classified as an empirical method.

3.3 Prediction of Future IPR

IPR curves are usually useful in clarifying the relationship between the rates at which a well can be produced and the flow pressures at the bottom of the well under such rates. The deliverability exponent **n** in the present study is equal to 0.5793 according to the **Rawlins–Schellhardt technique**. This parameter is assumed to be constant in the production life. The following equation calculates $Q_{g,max,f}$ as

$$q_{g,max,f} = q_{g,max,p} \left[\frac{p_p(\bar{p}_{R,f})}{p_p(\bar{p}_{R,p})} \right]^{2n}. \quad (6)$$

A modified deliverability equation can be used to construct the inflow performance curve, especially when the new $q_{g,max}$ under the future reservoir pressure is determined as follows:

$$\frac{q_g}{q_{g,max}} = \left[1 - \left(\frac{p_{wf}}{\bar{p}_R} \right)^2 \right]^n, \quad (7)$$

Or

$$\frac{q_g}{q_{g,max}} = \left[1 - \frac{p_p(p_{wf})}{p_p(\bar{p}_R)} \right]^n \quad (8)$$

For the comparison step within the generalized future IPR, a calculation is performed by using pseudo pressure approaches according to the following equation:

$$Y = 10.436 * X^6 - 31.143 * X^5 + 33.876 * X^4 - 15.374 * X^3 + 1.4779 * X^2 + 1.7044 * X + 0.0234,$$

where

$$Y = Q_{g,max,f}/Q_{g,max,c}, \quad \text{and} \quad X = (P_p(Prf)/P_p(Prc)). \quad (9)$$

4 Discussion

The predicted AOPF values are 22765.08256 MMscf/D for the **Rawlins–Schellhardt technique** and 105835.0991 MMscf/D for the **Houpert technique**. These values are mainly acceptable and accurate from a practical standpoint compared with the general and superior IPRs of 22751.6667 and 105772.7287 MMscf/D.

The constructed IPR model in this work, based on Eqs. 1–4, presents accurate predicted deliverability values. The divergence of the predicted AOPF and other [18] flow values for Siba_1 reaches 13.41586 and 62.3704 MMscf/D, respectively. These advantages are attributed to the fact that the back pressure data of the well are probably from the transient flow period and that the constructed model assumes stabilized flow. Another reason is the use of pseudo pressure calculation approaches that depend on gas gravity and compositions. Therefore, the results of this part are consistent up to 2000 psia and confirm the applicability of using the P^2 ratio when dealing with more than 8000 psia, which makes us change the pseudo pressure ratio for the reservoir pressure of 8593 and higher.

The prediction of the future performance of the Siba_1 production well is also investigated in two ways. One way is the construction of future IPR with different reservoir pressures from the current pressure of 8593–9250 psia, including the dew point pressure of 9021.35 psia. The calculation result of this step indicates good agreements among the results despite their insignificant difference.

Another way is future calculation by the comparison between the constructed future IPR and the generalized IPR that was developed in 2009 for both 9000 and 9021.35 psia reservoir pressures. The results show an agreement with a mean absolute percentage error (MAPE) of 5.234%, which indicates that the constructed IPR model can also be used to predict the future gas well deliverability with confidence. A small discrepancy from 7000 to 14.75 psia. This difference causes some variation in $Q_{g,max,f}$. The difference is mainly attributed to the methodology of the constructed generalized future IPR, which fits large field data sets and covers a wide range of parameters included in the regression fit equation. Therefore, our considered case falls within such range with a MAPE of 5.234%.

5 Conclusion

This study establishes a gas well deliverability equation and predicts future IPR for the Siba Gas Condensate Field in Iraq, particularly the Yamama formation reservoir. The following conclusions are drawn from the obtained results.

1. An easy and new well form of the dimensionless IPR model is constructed for the Siba Gas Condensate Field to calculate the performances of gas condensate production wells from a flow-after-flow test under current reservoir conditions with an acceptable error percentage in comparison with measured data.
2. The constructed IPR can be used for gas deliverability calculations within an assumed range of bottom hole pressure considering turbulence effects. The IPR can be modified by adding a skin factor effect if necessary. Therefore, a rigorous IPR equation for the Siba Gas Field is recommended.
3. The constructed model is characterized as simple, applicable, and accurate relative to the published generalized IPR model. It also shows the same trend as that of the published IPR in the literature.
4. The calculation techniques of Houpert and Rawlins and Schellhardt are accurate at reservoir pressures below 2000 psi when the pressure-squared approximation is used. This conclusion is consistent with published phenomena in the literature.
5. The constructed IPR model for current and future deliverability conditions presents a MAPE of 5.234%.

References

1. Craft, B.C., Hawkins, M.F.: Applied petroleum reservoir engineering, 2nd edn. Prentice Hall Inc., Upper Saddle River (1991). ch4
2. Mc Cain, W.D., Jr.: The Properties of Petroleum Fluids, 2nd edn (Chap. 5). Penn Well Publishing Company (1990)
3. Bruno, R.: Gas condensate well test analysis. M.Sc. thesis, Stanford University, June 2001
4. Ahmed, T.: Reservoir Engineering Handbook, 3rd edn. (2006)
5. Shi, C.: Flow behavior of gas—condensate wells. Ph.D. Dissertation, Stanford University (2009)
6. Fevang, Ø.: Gas condensate flow behavior and sampling. Ph.D. dissertation. The Norwegian Institute of Technology, University of Trondheim, Oct 1995
7. Lol, R.R.: Well testing in gas-condensate reservoir. M.Sc. thesis, University of Stanford, June 2003
8. Mott, R.: Calculating well deliverability in gas condensate reservoirs. EAGE—10th European Symposium on Improved Oil Recovery, Brighton, UK, 18–20 Aug 1999
9. Naji, M.A., Hadi, A.E.: The Oil Industry in Iraq, Mar 2009, printed in Iraq Arabic version
10. A review of geological study for Siba gas Field (Yamama Formation), Petroleum Exploration Company, Iraq (2000)
11. Ahmed, K.K.: Mathematical modeling of Yamama reservoir—Siba field. M.Sc. thesis, University of Baghdad (2015)
12. Principal well results siba_1 Baghdad 10th July 1969 (ERAP IRAK _BRANCH)
13. A technical report for development of yamama formation in Siba field, reservoir and development Directorate, Ministry of Oil, Jan 1990
14. A geological study for yamama formation—Siba field. Petroleum Exploration Company, Iraq Oct 1993
15. A reservoir study for evaluation of c and D units of Yamama reservoir formation—Siba field, Reservoir and Development Directorate, Ministry of Oil, Iraq (1994)
16. A detailed study of Yamama reservoir formation, Reservoir and Development Directorate, Ministry of Oil, Iraq Mar 2004
17. Chaudhry, A.U.: Gas Well Testing Handbook. Gulf Professional Publishing is an imprint of Elsevier Science. Copyright © 2003
18. Johnston, J.L., Lee, W.J., Blasingame, T.A.: Estimating the stabilized deliverability of a gas well using the Rawlins and Schellhardt method: an analytical approach. In: SPE 23440 (1991)
19. Al-Attar, Hazim, Al-Zuhair, Sulaiman: A general approach for deliverability calculations of gas wells. *J. Petrol. Sci. Eng.* **67**, 97–104 (2009)

Stimulation-Based Recovery Enhancement Feedback of Oil-Rim Reservoirs

Afshin Davarpanah

Abstract

Oil-rim reservoirs are considered as some of the unconventional reservoirs in which a thin oil layer, a thick gas cap and an aquifer layer are involved. The economic prosperity of drilling this type of reservoirs, involves novel enhanced oil recovery techniques to produce more oil volume. Production from oil-rim reservoirs would be a particular challenge due to their unique characterization. In this comprehensive study, we simulate six different scenarios with drilling new wells horizontally or vertically on the oil recovery enhancement for selecting the optimum technique which has more compatibility with the reservoir characteristics. Moreover, another objective of this study is to investigate the dominant influence of simulation procedures in each scenario on the key parameters of gas/oil ratio, water cut and, pressure drop. The drilling of a horizontal well (and its potential contact with the reservoir) results in the best performance among other scenarios, and scenarios of drilling new vertical wells have yielded excellent results for commencing the production operation.

Keywords

Oil-rim reservoirs • Enhanced oil recovery
Horizontal well • Oil production • Economic prosperity

1 Introduction

Oil-rim reservoirs are unconventional thin oil reservoirs associated with an underground aquifer and a big gas cap. This kind of unconventional reservoirs is typically categorized according to the structural location of the gas cap layer. The mobility differentiation between the current

A. Davarpanah (✉)
Department of Petroleum Engineering, Science and Research
Branch, Islamic Azad University, Tehran, Iran
e-mail: Afshin.Davarpanah@srbiau.ac.ir

phases in the reservoir (e.g., oil and gas) has made a driving force to the oil thinning layer by a downward gas movement to build an inverse pattern for the contact of gas/oil (henceforth, GOC) around the horizontal wellbore [1–4]. In order to enhance the recovery factor of oil-rim reservoirs, some of the traditional field production performances are:

- Oil production development regarding the negligible volume of gas production (primarily by the GOR control) and further development of gas cap after the production of an ultimate possible volume of oil. This issue could lead to significant delays in gas production.
- Oil production development regarding the negligible volume of gas production (primarily by the GOR control). In such cases, reservoirs need a gas supply to increase the recovery factor.
- Oil and gas development requires the precise management of reservoir accessibility to the maximum volume of oil and gas, however, it has a particular limitation in the primary production owing to the presence of gas.
- The developmental plan of a gas cap without oil development. This technique is preferable when the thickness of the oil layer is extremely thin, and the economic viability of this technique is not feasible [5–8].

2 Methods

2.1 Simulation Procedure

The studied field is located in the southwest of Iran. It extends over an area of 74,131.6 acres. According to the API, the oil of this reservoir (higher than 40° API) is considered as light crude oil and the initial reservoir pressure and temperature at the datum depth of 1968.5 ft (below sea level) have been recorded at 2147 psi and 140 °F, respectively. The cumulative oil field production by the end of 2003 was between the average rate of 9217.130 ft³/day and,

17.6573 MMft³, and the gas storage was at an average rate of 1,301,451.4 ft³/day, 5932.864 MMft³. It should be noted that in this field there is only one production well. The purpose of the history-matching phase of the reservoir is to adjust the input information to the model (geological and reservoir data) in an acceptable range so that the output information from the model (output pressures and flows) can match the actual data of the reservoir. This part of the simulation of the reservoir may be time-consuming and, ultimately, has no precise or absolute results. Therefore, even with full information, there can be no point-to-point matching, in particular with well pressure. Due to the uncertainty in the parameters of fractures and considering that in a split reservoir, the main path of production is a gap, the fracture characteristics were recognized as the matching parameters of the history. These parameters include porosity, absolute permeability, DZMATRIX, SIGMA and fracture transfer coefficient. Furthermore, due to the availability of reservoir drain, despite the unavailability of the data on the production of water, the attempt was made to compare the relative compliance with the time of increasing water production in the reservoir history, and information on water supply such as porosity, permeability, connections to the reservoir and thickness as Matching parameters were considered. In this study, by constructing several different models, we tried to approximate the behavior of the simulator model with the real behavior of the reservoir. In this regard, by changing the matching parameters in acceptable ranges and by adjusting these values in the Eclipse 100 simulation model, we tried to capture the history of oil production and pressure of well 1 in this field. The logical ranges for matching are as follows:

- The field oil production should be fully adapted.
- Oil pressures up to a maximum of ± 50 psi can be regarded as acceptable pressures.
- Qualitative water quality matching.

3 Results and Discussion

As can be seen in Fig. 1, at the first period of production, there was a gradual decrease in the oil production. Oil production increased dramatically and it reached its maximum value (about 9200 STB/Day) in the year 2003. The reason for this enhancement is the simultaneous gas and water injection. After that, it decreased slightly. Furthermore, scenario 1 and scenario 2 have experienced a substantial oil production decline. Among the five simulations, the results of scenarios 4 and 5 displayed the highest oil production

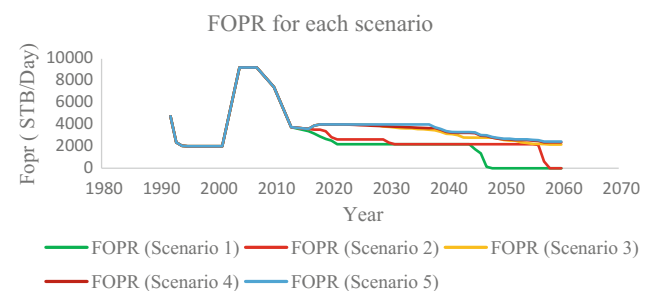


Fig. 1 Field oil production rate (FOPR) for each scenario

rates. Scenarios 3 and 5 have experienced a slight decrease in the oil production, without reaching zero value.

4 Conclusions

Production from oil-rim reservoirs is challenging because of their specific characterization which makes electing the best injection scenario for oil and gas production a significant concern for engineers. The main conclusions of this extensive simulation are:

- Based on the simulation results for the studied field, scenarios 4 and 5 represent the best and optimum technique for the recovery enhancement; it is evident that after drilling new wells, the production rate has experienced a constant decline never reaching the zero value.
- The necessary facilities for producing oil with high GOR are required to reach a production rate higher than 4000 barrels per day.
- Considering the application of horizontal wells for a better utilization coefficient and production of vertical fractures in this project, the horizontal well was also included in the model due to relatively similar results of vertical wells (because of the absence of vertical fractures).
- In general, it can be concluded that although the simulation results are optimum in the fifth and sixth scenarios, the fifth scenario in which we have three vertical wells is the most preferable scenario in the field because of the high expenditures of drilling horizontal wells, which are outrageously expensive and time-consuming.

References

1. Aggoun, R.C., Tiab, D., Owayed, J.F.: Characterization of flow units in shaly sand reservoirs—Hassi R'mel oil rim, Algeria. *J. Petrol. Sci. Eng.* **50**(3–4), 211–226 (2006)

2. Al-Hadhrami, H.S., Blunt, M.J.: Thermally induced wettability alteration to improve oil recovery in fractured reservoirs. In: SPE/DOE Improved Oil Recovery Symposium. Society of Petroleum Engineers (2000)
3. Carpenter, C.: Smart-horizontal-well drilling and completion for thin-oil-rim reservoirs in Malaysia. *J. Petrol. Technol.* **67**(05), 103–107 (2015)
4. Chan, K.S., et al.: Smart horizontal well drilling and completion for effective development of thin oil-rim reservoirs in Malaysia. In: International Petroleum Technology Conference (2014)
5. Civan, F.: Near Wellbore Damage and Remediation (1997)
6. Dilib, F.A., et al.: Closed-loop feedback control in intelligent wells: application to a heterogeneous, thin oil-rim reservoir in the North Sea. *SPE Reservoir Eval. Eng.* **18**(01), 69–83 (2015)
7. Eaton, A.N., et al.: Real time model identification using multi-fidelity models in managed pressure drilling. *Comput. Chem. Eng.* **97**(1), 76–84 (2017)
8. Maree, J.P., Imsland, L.: Performance and stability for combined economic and regulatory control in MPC. In: World Congress (2014)



Electrochemical Studies of Porphyrin and Its Metal Complexes

Bechki Lazhar, Kadri Mohamed, and Lanez Touhami

Abstract

This study aims to establish a group of heterogeneous organic compounds of porphyrin and derived compounds. This is useful for many medical fields such as phototherapy or industrial therapy, namely dyes and OLED screens. On this basis, we assembled a group of six compounds and a group of their compounds with different metals (Zn, Co, Cu, Fe and Pd) and studied their properties by spectral methods. We conducted an electrochemical study through the voltmeter ring to study the effect of alternatives and of the metal quality on the oxidation for a group of six porphyrin compounds, which enabled us to study future applications for vehicles obtained and developed in OLED, organic light emitting Diodes technology.

Keywords

Porphyrin • Complex • Hack and Suzuki
Non-covalent effects • Corrosion • Inhibitor

1 Introduction

Electrochemistry studies the chemical substance reactions occurring in a remedy at the user interface of the electron and/or ionic conductor, through the use of an exterior potential difference over the interface, and by calculating the associated current response. The difference can also be

documented as a function of the applied current. A good example of an electrochemical process is oxidation and/or reduced amount of an electroactive varieties at a good electrode. The electrochemical methods used in this thesis include cyclic voltammetry, linear sweep voltammetry, amperometry and potentiometry [1].

In this publication, the redox habit of porphyrins has been thoroughly investigated for their relevance to many biological procedures and lots of book reviews have been published in this field.

Metalloporphyrins containing flat iron and cobalt have been used as a model of chemical substances for hemoproteins and vitamin B12, nickel porphyrins have served as models for coenzyme F430, while other metalloporphyrins have been used to study natural reactivity and function associations. A large number of metalloporphyrins has been looked into during the previous three decades. These include: compounds with a huge selection of different porphyrin macrocycle, a dozen of different coordinated axial ligands and nearly 80 metals ions [1].

The majority of metalloporphyrins electrochemistry entails either the central metallic ion or the conjugated π system; which means that the electrochemistry of metalloporphyrins can be explained from two points of view: the type of central metallic ion and the type of macrocycle. However, the electrochemistry of metalloporphyrins can be affected by the structural factors related to the quantity and the kind of substituents mounted on the macrocycle or even to the number of axial ligands destined to the central metallic ion [2].

Within the reviews released by Kadish, Felton [3], Davis [4], and Buchler [5], the authors talked about the electrochemistry of octaethylporphyrin (OEP) and tetraphenylporphyrin (TPP) derivatives. The chemical substances of the two series will always be used as comparison chemical substances against ideals of other recently synthesized metalloporphyrins.

Although lots of hydroporphyrin complexes have been synthesized, their poor yield, balance and purity highly

B. Lazhar (✉) · K. Mohamed
VPRS Laboratory, University of Ouargla, PO Box 511
30000 Ouargla, Algeria
e-mail: lbechki1@gmail.com

L. Touhami
University of El Oued, El Oued, Algeria

limited the electrochemical and spectroscopic studies of the complexes. The electrochemical studies of some free-base [5] and iron hydroporphyrin complexes [6] have included the measurements of the redox potentials, and little information is known about the facts of electron transfer.

On this basis, the voltmeter ring was used to study the effect of alternatives and the quality of the metal on the oxidation for a group compounds and enabled us to study future applications on vehicles obtained and developed in OLED, organic light emitting Diodes technology.

2 Methods and Materials

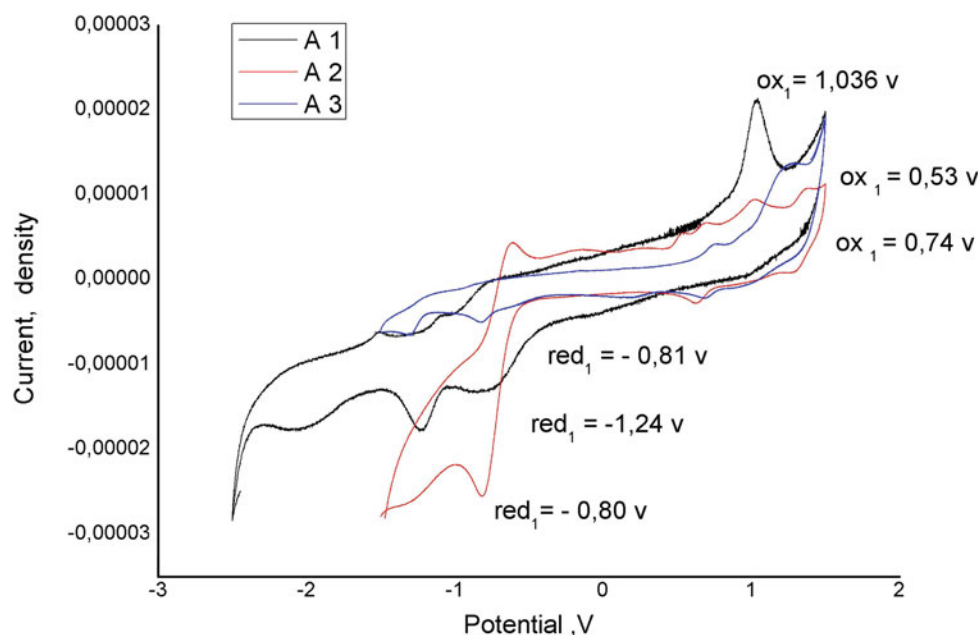
All solvents were “Aldrich” grade unless stated otherwise. The following solvents were distilled prior to use (under argon): propionic acid; dichloromethane, aldehyde, pyrrole and MgSO₄.

The UV-Vis spectrophotometer (UV-2450, Shimadzu) was used.

The Analytical thin-layer chromatography (TLC) was performed on Merck Silica Gel 60 F254 TLC plates. Preparative column chromatography was performed on silica gel (40–63 µm) which was purchased from Qingdao Haiyang Chemical Co. Ltd. China.

H, DQF COSY and NOESY NMR experiments were recorded on an Avance Bruker 400 spectrometer at 400.155 MHz. All samples were prepared in CDCl₃. Spectra were referenced to CHCl₃ at 7.26 ppm.

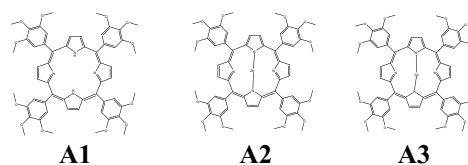
Fig. 1 Cyclic voltammogram for (A1, A2, A3) in CH₂Cl₂ (0.1 M Bu₄NBF₄) at a glassy carbon working electrode. Scan rate = 100 mV s⁻¹



3 Results and Discussion

3.1 Electrochemical Study Comparison of Compounds (A1, A2, A3)

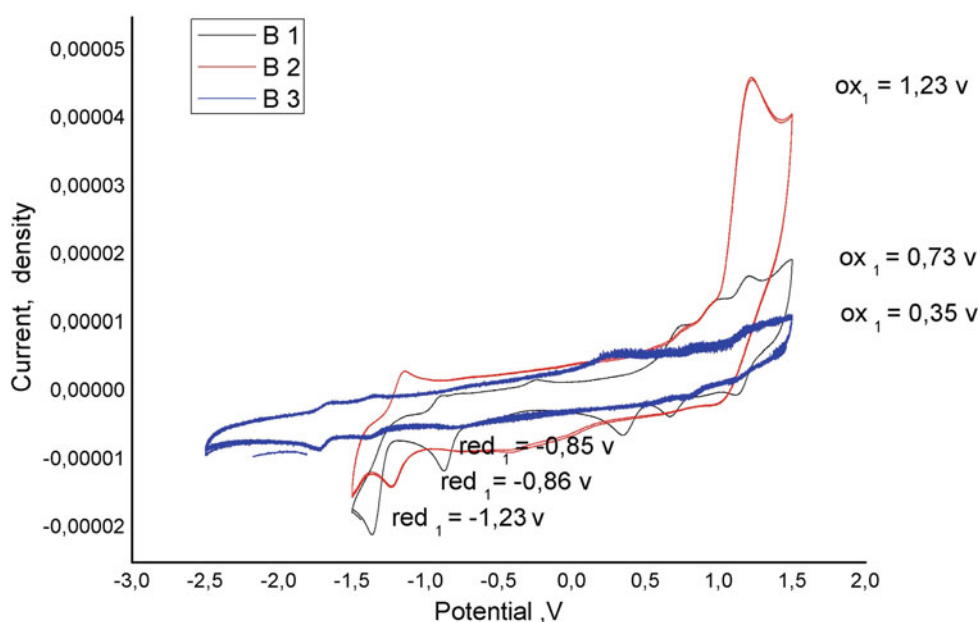
The redox behavior of A1, A2, A3 was measured by cyclic voltammetry in dry CH₂Cl₂ using 0.1 M Bu₄NBF₄ as a background electrolyte. The cyclic voltammogram (Fig. 1) reveals redox processes associated with the porphyrin. On the oxidation side of the CV, a clear irreversible wave is observed at A1 (Ox₁ = 1.03 V) A2 (Ox₁ = 0.53 V, Ox₂ = 1.01 V, Ox₃ = 1.36 V) A3 (Ox₁ = 0.74 V, Ox₂ = 1.28 V). On the reduction side of the CV, a clear irreversible and quasi-reversible wave is observed at A1 (Red₁ = -0.76 V, Red₂ = -1.23 V) A2 (Red₁ = -0.8 V) A3 (Red₁ = -0.81 V, Red₂ = -1.29 V). Value differences ΔI Red₁ – Ox₁ I on the order were A1 = 2.27 V, A2 = 1.33 V, A3 = 1.56 V.



3.2 Electrochemical Study Comparison of Compounds (B1, B2, B3)

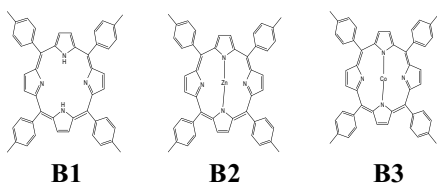
The redox behavior of B1, B2, B3 was measured by cyclic voltammetry in dry CH₂Cl₂ using 0.1 M Bu₄NBF₄ as a

Fig. 2 Cyclic voltammogram for (B1, B2, B3) in CH_2Cl_2 (0.1 M Bu_4NBF_4) at a glassy carbon working electrode. Scan rate = 100 mV s⁻¹



background electrolyte. The cyclic voltammogram (Fig. 2) reveals redox processes associated with the porphyrin. On the oxidation side of the CV, a clear irreversible wave is observed at B1 ($\text{Ox}_1 = 1.23 \text{ V}$) B2 ($\text{Ox}_1 = 0.73 \text{ V}$, $\text{Ox}_2 = 0.86 \text{ V}$) B3 ($\text{Ox}_1 = 0.35 \text{ V}$, $\text{Ox}_2 = 0.98 \text{ V}$, $\text{Ox}_3 = 1.2 \text{ V}$). On the reduction side of the CV, a clear irreversible and quasi-reversible wave is observed at B1 ($\text{Red}_1 = -1.23 \text{ V}$) B2 ($\text{Red}_1 = -0.85 \text{ V}$, $\text{Red}_2 = -1.38 \text{ V}$) B3 ($\text{Red}_1 = -0.86 \text{ V}$, $\text{Red}_2 = -1.35 \text{ V}$).

Value differences $\Delta I \text{ Red}_1 - \text{Ox}_1$ I on the order were B1 = 2.46 V, B2 = 1.2 V, B3 = 1.59 V.



4 Conclusions

We have studied electrophoresis by an electrochemical study through comparing a group of porphyrins to the effect of the tug, donor groups and the quality of the metal on the properties of oxidation and regression. The two-phase comparison was made between the compounds (B1 B2 B3) (A1 A2 A3)

based on different metals. Based on different functional substitutions in (A1 A2 A3), the value of ($\text{RED}_1 - \text{OX}_1$) was in the following order 2.27, 1.33, 1.56. The difference between the first reaction and the first oxidation decreases in the compound containing the zinc metal and then the cobalt, after that the compound without metal.

It can be concluded that in the case of the mesomeric group tug, the value of the difference between the oxidation and the first return of the compound, whether metal or non-metal, increases compared with the donor group.

References

1. Felton, R.H.: The Porphyrins. In: Dolphin, D. (ed.) vol. 5, pp. 53–115. Academic Press, New York (1978)
2. David, D.G.: The Porphyrins. In: Dolphin, D. (ed.) vol. 5, pp. 127–150. Academic Press, New York (1978)
3. Felton, R.H.: The Porphyrins. In: Dolphin, D. (ed.). Academic Press, New York (1978)
4. Davis, D.G.: The Porphyrins. In: Dolphin, D. (ed.). Academic Press, New York (1978)
5. Buchler, J.W.: Porphyrins and Metalloporphyrins. In: Smith, K.M. (ed.). Elsevier, New York (1975)
6. Flits, W.: Adv. Heterocyclic Chem. **43**, 73 (1988); Scheer, H.: The Porphyrins. In: Dolphin, D. (ed.) vol. 2, chap. 1. Academic Press, New York (1978)